Low-Temperature Physics

U. S. Department of Commerce

National Bureau of Standards

Circular 519

UNITED STATES DEPARTMENT OF COMMERCE • Charles Sawyer, *Secretary*
NATIONAL BUREAU OF STANDARDS • A. V. Astin, *Director*

Low-Temperature Physics

Proceedings of the NBS Semicentennial Symposium on
Low-Temperature Physics
Held at the NBS on March 27, 28 and 29, 1951

National Bureau of Standards Circular 519
Issued October 6, 1952

For sale by the Superintendent of Documents, U. S. Government Printing Office
Washington, 25, D. C. : Price $1.75 Buckram

Foreword

The Low Temperature Symposium was the first of twelve symposia held during 1951 as part of the scientific program of the National Bureau of Standards in the year 1951, which marked the fiftieth anniversary of its establishment. The subjects of the symposia represent scientific fields in which there is considerable current interest and in which the Bureau is active.

Low temperature research at the Bureau was begun early in its history with establishment of facilities for liquefying air and hydrogen. In 1931 helium was successfully liquefied here for the first time in this country, for use in superconductivity research. Research was also carried forward on the properties of hydrogen and deuterium. In recent years research has been conducted in several fields, including the properties of liquid helium, superconductivity, calorimetry, thermometry, and liquefier development.

No discussion of low temperature research in this country would be complete without an acknowledgment of the generous support given by the Office of Naval Research during the years following the war. It has been the custom to hold periodic meetings, under the auspices of the ONR, for representatives of the various laboratories engaged in ONR-sponsored low temperature research. By agreement with ONR it was decided that this Symposium would be substituted for the usual ONR Conference. This symposium was organized by J. R. Pellam and E. Maxwell, with the assistance of the Bureau's Low Temperature Symposium Committee. The cooperation of the ONR in making possible the symposium series is gratefully acknowledged.

A. V. Astin, *Director*,
National Bureau of Standards.

Contents

Contents

1. Theory of the Superconducting State[1]

by H. Fröhlich[2]

The main problem in finding a theory of the superconducting state, it seemed to me, was to find an interaction of the correct magnitude. Once this was discovered one might hope that it also would lead to the observed electromagnetic properties. I had noticed many years ago that the energy ms^2(m=electron mass, s=velocity of sound), which is of a very small magnitude, plays a role in some questions of conductivity. Much later it occurred to me that Bloch's[3] description of the interaction of electrons in crystals with the lattice vibrations is one aspect of a field theory which must lead to an interaction between electrons. In fact, according to Bloch, electrons can move freely through ideal crystals, but are scattered when deviations from the strict periodicity occur. Of particular interest here are the deviations due to the thermal vibrations. When quantized, their interaction with electrons can be described in terms of emission or absorption of single quanta. Similar to radiation theory one should then expect that an interaction between electrons follows that can be described in terms of virtual emission and reabsorption of quanta. At first sight, it might seem that the analogy with radiation theory is not very far reaching because in our case free electrons of sufficient energy will spontaneously emit vibrational quanta. In radiation theory spontaneous emission of quanta by free electrons is not possible in general. However, in our case the electrons move with a velocity, v, which is very large compared with the velocity, s, of sound. The corresponding case in radiation theory would be a charged particle moving with a velocity larger than the velocity of light. Although this is not possible in vacuum, it can occur in media with a refractive index larger than unity. The corresponding radiation has in fact been discovered and is known as Čerenkov radiation.

Let us follow the analogy with radiation theory a step further. The interaction between particles at rest is uniquely described in terms of their distance in ordinary space. This is not so for moving particles whose interaction also depends on velocity. The influence of the velocity dependent terms increases as the velocity of light (of sound in our case) is approached. It may be expected than that when $v \gg s$, the velocity dependent terms predominate. In fact, it will be shown presently that in our case where $v/s \simeq 10^3$ the interaction is best described in momentum space.

In elaborating the above-mentioned ideas one is at once faced with the difficulty that the conventional theory of metals is based on the free electron hypothesis, which has never been derived theoretically, nor has it been stated in exact terms. This hypothesis implies that the Coulomb interaction between electrons can be replaced by an effective periodic potential, so that the problem of many electrons

---

[1] Proc. Phys. Soc. (London) **63** [A] 778 (1950); Phys. Rev. **79**, 845 (1900); Proc. Phys. Soc. (London) **64** [A] 129 (1951).

[2] Department of Theoretical Physics, Liverpool University, Liverpool, England.

[3] F. Bloch, Z. Physik **52**, 555 (1928).

reduces to one-electron problems. Deviations from a strictly periodic potential will then act as a perturbation. However, the above hypothesis is never used for all electrons but only for those near the top of the Fermi distribution. Let $f_0(k)$ be the Fermi distribution at the absolute zero of temperature; $h\mathbf{k}$ is the momentum of a free electron and

$$\epsilon_k=\frac{h^2k^2}{2m} \tag{1}$$

its energy, assuming the influence of the periodic field to be negligible. Consider then states in which the electrons are distributed according to a function $f(k)$ and in which n_w vibrational quanta of wave number w are excited. The free-electron hypothesis then demands that the energy of the above state differs from the state where $f=f_0$ and $n_w=0$ by three terms: (1) the kinetic energy $\sum\limits_w \epsilon_k[f(k)-f_0(k)]$ of the electrons, using eq (1), (2) the energy of the quanta, $\sum\limits_w n_w hws$, where s is the empirical velocity of sound, (3) the difference in interaction between electrons and lattice vibrations from the state f_0, $n_w=0$. It is proposed to calculate this energy difference with the help of second-order perturbation theory and to find the distribution $f(k)$ leading to the lowest energy by variation of f.

This last term is thus given by (M_w-matrix element for the emission of a quantum; $\mathbf{q}=\mathbf{k}-\mathbf{w}$)

$$\sum_k\sum_w\frac{|M_w|^2[f(k)(1-f(q))-f_0(k)(1-f_0(q))]}{\epsilon_k-\epsilon_q-\hbar ws} \tag{2}$$

It can be split into two terms:

$$E_1=\sum_k[f(k)-f_0(k)]\sum_w\frac{|M_w|^2}{\epsilon_k-\epsilon_q-\hbar ws}, \tag{3}$$

$$E_2=\sum_k\sum_q\frac{f(k)f(q)-f_0(k)f_0(q)}{\epsilon_k-\epsilon_q-\hbar ws}. \tag{4}$$

In E_1 the sum over w is again a function of k, say y_k. This term is therefore given by

$$E_1=\sum_k y_k[f(k)-f_0(k)], \tag{5}$$

i. e., it is of the same form as the kinetic energy in zero order, replacing ϵ_k by ϵ_k+y_k. The second term, however, is of great interest. There we have replaced the sum over w by a sum over q. It is then seen that E_2 would be zero if $s=0$, i. e., if the perturbation of the electrons by the lattice vibrations were replaced by a static perturbation leading to the same matrix element. Hence we can also write

$$E_2=\sum_k\sum_q\psi(k,q)[f(k)f(q)-f_0(k)f_0(q)], \tag{6}$$

where

$$\psi(k,q)=\frac{\hbar ws}{(\epsilon_q-\epsilon_k)^2-\hbar ws};\ w=|\mathbf{q}-\mathbf{k}|. \tag{7}$$

From a formal point of view this energy E_2 can be considered as due to an interaction between electrons in momentum space; $\psi(k, q)$ is thus the energy of interaction between two electrons with momentum k and q.

From (7) it follows that the interaction energy E_2 is positive when the zero order energies of the two electrons are nearly equal; it is negative for larger energies, roughly speaking when the velocities differ by more than the velocity of sound. This interaction thus tends to shift electrons from the top of the Fermi f_0 distribution to higher values. This tendency is opposed by the increase in kinetic energy connected with such a shift. Two cases must then be distinguished, depending on whether the magnitude of E_2 is or is not sufficient to overcome the increase in kinetic energy.

If $|E_2|$ is sufficiently large then $f_0(k)$ is no longer the distribution with the lowest energy but is replaced by another the $f_1(k)$ distribution. In k-space this distribution is obtained from the spherical f_0 distribution by shifting from the surface a shell of width $\Delta k \sim ms/\hbar$, by about Δk. When this f_1 distribution is stable then the metal is proposed to be a superconductor. For in contrast to the f_0 distribution E_2 interaction energy has now to be spent to deform the f_1 distribution in k-space. It has been shown by F. London that this is required to derive the London equations that describe phenomenologically the magnetic behavior of superconductors. The energy difference of a stable f_1 distribution from the normal f_0 distribution is of the order m/M ev (m=electronic mass; M=atomic mass) per electron. It is thus of the correct magnitude. Moreover, as this energy is proportional to $1/M$, it accounts quantitatively for the isotopic effect predicted by the theory. Finally, it may be remarked that the condition for the stability of the f_1 distribution can be expressed in terms of the high-temperature resistivity of metals. This leads to a selection of superconductors in fair agreement with observations.

2. Superconductivity and Lattice Vibrations

by J. Bardeen [1]

The isotope effect, discovered independently by E. Maxwell [1] [2] of the National Bureau of Standards and by Reynolds, Serin, Wright and Nesbitt [2] of Rutgers University, indicates that superconductivity arises from interactions between electrons and lattice vibrations. Both groups found a pronounced dependence of transition temperature, T_c, of mercury on isotopic mass, M. The Rutgers group showed that T_c varies approximately as $M^{-1/2}$ and this result has since been confirmed as well from measurements on separated tin isotopes [3].

The mean square amplitude of zero-point motion of the atoms of the crystal also varies as $M^{-1/2}$. These experiments therefore indicate that there is an intimate connection between superconductivity and lattice vibrations. A theory of superconductivity based on electron-vibration interactions has been given by Fröhlich [4], and the writer [5] has independently given a somewhat different theory based on the same general idea. Fröhlich's theory is based on interactions between electrons arising from the field of phonons, whereas we have used a model based on wave functions and energies of the individual electrons as affected by the vibrations. Later developments indicate that the theories are not so far apart as they first appeared. However, there are difficulties with both approaches. Fröhlich used an expression based on second-order perturbation theory in a range where its validity is uncertain. As we shall see, there are also difficulties with our model.

We shall first discuss the nature of the wave functions and energies for electrons in superconductors and then show how the theory leads to the London phenomenological equations and thus explains the electromagnetic properties of the superconducting phase.

Figure 2.1 shows the nature of the interaction between electrons and lattice vibrations. The normal modes of vibration of a crystal lattice are waves; here is shown a longitudinal wave with a period equal to twice that of the lattice. The coordinate q represents the displacement from the equilibrium position. The lattice wave gives a varying potential which an electron sees, as indicated by the interaction potential above. When the ions are close together, the potential is more positive, giving a lower energy for the electrons. Where they are farther apart, the potential is higher. During the next half cycle, when q changes sign, the sign of the interaction potential is reversed. The ions in the lattice are continually in motion, even at the absolute zero, so that the electrons see a fluctuating potential. One might expect to get a lower energy if the electrons could follow the motion of the ions, giving a higher than normal density when the fluctuating potential is low and a low density where the potential is high. This requires that the wave functions for the electrons depend on the vibrational coordinates.

The complete Hamiltonian for the metal can be written as a sum of three terms, one for the electrons with the ions in their equilibrium

---

[1] Bell Telephone Laboratories, Murray Hill, N. J. Present address, University of Illinois, Urbana, Ill.

[2] Figures in brackets indicate the literature references on p. 10.

positions, H_e, one for the lattice vibrations, H_L, and a term, H_I, representing the interaction between the two:

$$H = H_e + H_L + H_I. \tag{1}$$

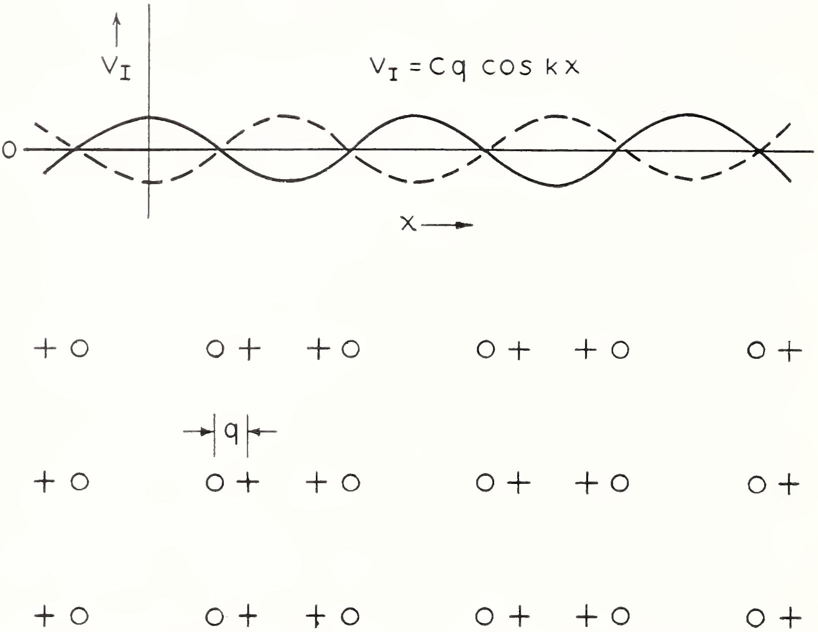

FIGURE 2.1. *Schematic diagram of interaction V_I, between electrons and lattice vibrations.*

Usually one considers the interaction terms only in connection with scattering and resistance. We are here concerned with their effect on the wave functions and energy. We have taken the interaction terms into account by using a wave function for the complete system of the form:

$$\Psi = \varphi_e(x_i, q_r) Q(q_r). \tag{2}$$

The wave function for the electrons, φ_e, which involves the vibrational coordinates, q_r, parametrically, is approximated by Slater-Fock determinantal wave functions in which the wave functions of the individual electrons are of the form:

$$\Psi_k = a_k(q_r)\Psi_k + \Sigma_{k'} a_{kk'}(q_r)\psi_{k'}, \tag{3}$$

where ψ_k is the Bloch function for wave vector $\boldsymbol{k}$. In calculating the energy of the lattice vibrations, one must remember to take derivatives of φ_e with respect to the vibrational coordinates, q_r,

In the ideal case, with no interaction, the one-electron wave functions are the Bloch functions, ψ_k. Most of the interaction energy occurs in the normal phase; there is only a small additional energy decrease in going to the superconducting phase. In the normal metal one may take the interaction terms into account by adding to ψ_k a sum over the various states $\psi_{k'}$ with which ψ_k interacts via the lattice vibrations. For a Fermi distribution of electrons at temperature T the first order correction to the wave functions is [3]

$$\Psi_k=\psi_k+\Sigma_{k'}\frac{m_{kk'}q_{kk'}\psi_{k'}}{\epsilon_k-\epsilon_{k'}+\hbar\omega_{kk'}\coth[(\epsilon_k-\epsilon_{k'})/2kT]}. \tag{4}$$

Here $m_{kk'}q_{kk'}$ is the matrix element for the vibration whose wave vector connects the states k and k'. We have indicated explicitly that the matrix element is proportional to the displacement, $q_{kk'}$. In the denominator there is in addition to the energy difference between the Bloch states, $\epsilon_k-\epsilon_{k'}$, a term proportional to the phonon energy, $\hbar\omega_{kk'}$, which comes from the derivatives of φ_e with respect to $q_{kk'}$. The hyperbolic cotangent comes from use of the Fermi distribution function appropriate to a temperature T.

The energy is changed in the second order:

$$E_k=\epsilon_k+\Sigma_{k'}\frac{|m_{kk'}q_{kk'}|^2}{\epsilon_k-\epsilon_{k'}+\hbar\omega_{kk'}\coth[(\epsilon_k-\epsilon_{k'})/2kT]}. \tag{5}$$

The interaction energy does not depend very strongly on the wave vector $\boldsymbol{k}$ nor on the distribution of electrons in $\boldsymbol{k}$-space. The interaction terms are of the sort expected for the normal phase; they give a small decrease in energy of the electrons but no appreciable change in effective mass nor in the electrical properties.

Superconductivity presumably arises from interactions for which the energy denominators are small and for which the second-order perturbation theory is not valid. The condition

$$\Sigma_{k'}|a_{kk'}|^2>\sim 1 \tag{6}$$

requires first that the temperature be sufficiently low, otherwise the hyperbolic cotangent is large, and second that the matrix elements be sufficiently large compared with $(\hbar\omega_{kk'})_{AV}$. The second of these conditions is approximately

$$N(E)|m_{kk'}q_{kk'}|^2_{AV}>(\hbar\omega_{kk'})_{AV}, \tag{7}$$

where $N(E)$ is the density of states in energy at the Fermi surface. This condition is essentially equivalent to the criterion for superconductivity of Fröhlich as modified by the author. It is a fairly reliable criterion for distinguishing those metals that are superconductors.

The interactions important for superconductivity are those for which the energy denominators are small and for which the Bloch states have energies close to the Fermi surface:

$$\epsilon_k\cong\epsilon_{k'}\cong E_F. \tag{8}$$

The energy differences $|\epsilon_k-\epsilon_{k'}|$ are presumably of the order of kT_c. It has been proposed that these interactions give a decrease in energy of the electrons with energies near E_F as illustrated in figure 2.2.

The conditions under which such an energy reduction can be expected to occur are still uncertain. We have used wave functions of the form

$$\Psi_k=N_k(q_r)(\Psi_k+\Sigma_{k'}b_{kk'}q_{kk'}\Psi_{k'}) \tag{9}$$

---

[3] The derivation is given in Rev. Mod. Phys. **23**, 261 (1951).

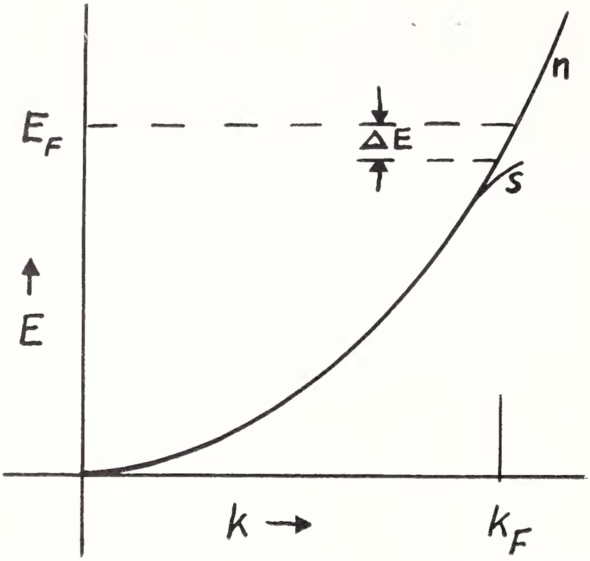

FIGURE 2.2. *Schematic plot of energy versus wave vector for normal and superconducting phases.*

where the sum is over k' such that $|\epsilon_{k'}-\epsilon_k|<\Delta E$. Normalization is given by the factor $N_k(q_r)$, the $b_{kk'}$ are chosen to give a minimum energy, and the $\psi_{k'}$ are Bloch functions modified as in (4) to include the interactions for which $|\epsilon_{k'}-\epsilon_k|>\Delta E$. The minimum is now obtained when k' runs only over the unoccupied states. These wave functions give an energy reduction of the desired sort, but the theory is nevertheless unsatisfactory.

If, as previously assumed, the interactions in (9) do not occur in any way in the normal phase, the calculated energy difference between the normal and superconducting phases is too large. This suggests that these interactions do occur in the normal phase, but in such a way that the effective mass is not altered. Further, the dynamic nature of the interaction, which is undoubtedly important, does not play a role in this formulation. An adequate theory requires more powerful methods of approach.

With wave functions of the form (9), the energy decrease per electron is proportional to $(q_{kk'}^2)_{AV}$ and thus varies as $M^{-1/2}$, in agreement with the isotope effect. The fractional number of states affected is $\sim\Delta E/E_F$, so that the energy difference between the normal and superconducting phases is of the order of

$$W_n-W_s=H_c^2/8\pi\sim n(\Delta E)^2/E_F, \tag{10}$$

where n is the number of conduction electrons per unit volume. The critical field, H_c, varies in the same way with isotopic mass as the critical temperature.

The effective mass, being inversely proportional to the curvature of E versus $\boldsymbol{k}$, is very small for electrons with energies near the Fermi surface in the superconducting phase:

$$m_{eff}=[\hbar^2\partial^2E/\partial k^2]^{-1}\sim\Delta E/E_F. \tag{11}$$

As $\Delta E \sim kT_c \sim 10^{-3}$ ev and E_F is of the order of several electron volts, m_{eff} is of the order of $10^{-4}m$. As the configuration is similar to that of an almost filled band, the properties are similar to those of a metal with $\alpha 10^{-4}$ hole per atom with an effective mass $\sim 10^{-4}m$.

The states involved in the superconducting transition lie in a thin shell of ***k***-space with thickness of the order of

$$\Delta k \sim (\Delta E/E_F)k_F \sim 10^{-4} \times 10^{8} \sim 10^{4} \text{ cm}^{-1}. \tag{12}$$

The smallness of the range Δk means that the wave functions extend over large distances in real space. The uncertainty relation

$$\Delta k \Delta x \sim 1 \tag{13}$$

gives a lateral extent $\Delta x \sim 10^{-4}$ cm.

The large Δx and small m_{eff} are, of course, related. A small effective mass means that it takes considerable energy to confine the wave function to a small volume. It is this property that leads to the explanation of the magnetic properties of the superconducting phase.

There are two aspects to superconductivity. First, the infinite conductivity, most strikingly shown by a persistent current in a ring, and second, the perfect diamagnetism, or Meissner, effect; a superconductor excludes a magnetic field. These two aspects are closely related. Either one almost, but not quite, gives the other. Both follow from the London phenomenological theory, which is based on the idea that it is the diamagnetic property that is the fundamental one. According to this view, all superconducting currents are diamagnetic in origin, and are always associated with a magnetic field. The present theory leads to the London equations, and is thus also based on the idea that the fundamental property of a superconductor is the Meissner effect and that those aspects usually associated with infinite conductivity are secondary and follow as a consequence.

The recent experiment of Houston and Muench [6] on the damping of an oscillating sphere in a magnetic field is good evidence that this is the correct view.

It is believed that superconductivity in a sense can be considered to be an extreme case of diamagnetism of the London-Peierls type. If an ordinary metal is placed in a magnetic field, electrons describe orbits which are analogous to the classical circular orbits of electrons moving in a magnetic field. The diamagnetic currents are confined to a thin surface layer. Near the surface, current from electrons in interior orbits is balanced to a large extent by electrons in boundary orbits. In the classical theory the compensation is perfect; there is no net current and no diamagnetism. Landau showed that quantum effects give a small net diamagnetism which is inversely proportional to the square of the electron mass. Peierls showed that in real metals one should use an appropriate effective mass rather than the true electron mass.

In a superconductor, the effective mass is very small and the diamagnetic effects very large; so large in fact that the magnetic field is confined to a thin layer corresponding to the penetration depth of the London theory. One must reexamine the theory and it is found that if the effective mass is sufficiently small there are no orbits corresponding to either the circular orbits in the interior or to the boundary orbits. The magnetic field vanishes in the interior and the field at the surface is insufficient to provide a quantum state. The wave functions of the electrons are only slightly modified by the magnetic field. The approach is essentially that of F. London [7], who has shown some years ago that the phenomenological equations follow if the wave functions in the superconducting state are such that they are not modified very much by a magnetic field. The small effective mass and consequent great exaggeration of quantum effects give this property. Thus the London equations are a consequence of the theory.

The following qualitative aspects of the theory appear to be fairly well established: (1) Superconductivity arises from interactions between electrons and lattice vibrations, (2) the important interactions are those between electrons with energies close to the Fermi surface, (3) it takes considerable energy to confine the wave functions to a small volume. This property is described in our model by the small effective mass of the electrons, (4) the wave functions are not modified very much by an applied magnetic field. This leads to the London phenomenological equations according to the approach of F. London. All of these aspects are also true for Fröhlich's version of the theory.

The exact conditions under which superconductivity should occur are still uncertain. Whether or not the interactions are such as to give a "shell" distribution as in Fröhlich's theory or whether they simply lower the energies of electrons near the Fermi surface as in figure 2.2, remains to be determined. An adequate theory of the way the properties vary with temperature awaits a better picture of the state at absolute zero.

---

[1] E. Maxwell, Phys. Rev. **78,** 477 (1950).

[2] C. A. Reynolds, B. Serin, Wright, and L. B. Nesbitt, Phys. Rev. **78,** 487 (1950).

[3] See the papers presented at this Symposium by C. A. Reynolds, B. Serin, and L. B. Nesbitt; E. Maxwell, D. Shoenberg, and K. Mendelssohn.

[4] H. Fröhlich, Phys. Rev. **79,** 845 (1950).

[5] J. Bardeen, Phys. Rev. **79,** 167 (1950); **80,** 567 (1950); **81,** 829 (1951). Rev. Mod. Phys. **23,** 261 (1951).

[6] W. V. Houston and N. Muench, Phys. Rev. **79,** 967 (1950).

[7] F. London, Proc. Roy. Soc. (London) [A] **152,** 24 (1935). Phys. Rev. **74,** 562 (1948).

3. On the Nature of the Superconducting Transition[1]

by L. Tisza[2]

Introduction

The heuristic ideas advanced recently concerning the nature of the superconducting state [1][3] have been conceived before the discovery of the isotope effect and before the theories of Fröhlich [2] and Bardeen [3] came to my attention. Starting from the assumption that superconductivity cannot be accounted for in terms of a free electron theory and in view of the well-known difficulty of a many electron problem, it seemed reasonable to inquire into the symmetry properties of many-electron wave functions and attempt to obtain a type exhibiting the characteristic superconducting properties. It was left for a later time to provide a quantitative derivation of such wave functions from quantum mechanics.

In view of the experimental and theoretical progress achieved in the course of the last year, it is pertinent to ask whether these considerations are still of interest. Indeed, Fröhlich and Bardeen have unexpectedly extended the scope of the free electron theory toward an explanation of superconductivity, and their work in conjunction with the isotope effect made it obvious that the lattice dynamics had an important part in this phenomenon. This feature was absent in [1].

Nevertheless, it would seem that an affirmative answer can be given to the above question, and in particular the following points should be made.

1. In spite of its success, the free electron theory has its limitations. For example, it has so far failed to account for the fact that the normal-superconducting transition occurs at a sharp transition temperature even without an external field and hence in the absence of a supercurrent. In other words, we get no answer to the questions: What sort of long-range order parameter characterizes this process, the sudden onset of which is obvious from the entropy curve? It is possible that this shortcoming is connected only with mathematical difficulties; yet, we will advance arguments in favor of the view that at this point we have reached the inherent limitations of the model.

2. The potential generality of the symmetry considerations of [1] was impaired by the assumption of a fixed, rigid lattice. We will outline in the sequel how this procedure can be generalized by characterizing the lattice with dynamic parameters. As a result, we obtain a general framework into which the detailed calculations of Fröhlich-Bardeen can be fitted in a natural fashion. At the same time, this framework is more comprehensive and provides an answer concerning the nature of the superconducting phase transition. It

---

[1] This work was supported in part by the Signal Corps, the Air Matériel Command, and the Office of Naval Research.

[2] Department of Physics and Research Laboratory of Electronics, Massachusetts Institute of Technology, Cambridge, Mass.

[3] Figures in brackets indicate the literature references given on p. 20.

has also a heuristic value in suggesting ways of approach for a future quantitative theory.

3. In order to achieve these results one has to take a more fundamental attitude than is usually the case in the theory of solids—one has to consider the crystal as a collection of nuclei and electrons and investigate the applicability of the socalled adiabatic method developed by Born and Oppenheimer [4] for molecules, to the case of crystals. That the understanding of superconductivity requires a critical reconsideration of the fundamental assumptions of the theory of solids may well prove to be its most interesting theoretical aspect.

It is obvious that it will be some time before the program here formulated can be developed in detail. The following account should be considered as a progress report.

The Adiabatic Approximation

The results of the adiabatic approximation that are relevant to the present problem may be summed up as follows.

Consider an electrically neutral system of nuclei and electrons. In the first approximation assume the nuclear mass to be infinite and solve the electronic eigenvalue problem at fixed nuclear positions (many-center problem), whereby the eigenvalue $U(R)$ and the eigenfunction $\phi(r;R)$ will contain as parameters the nuclear configuration R. The electronic coordinates are represented by r.

Of special interest are the configurations $R^{(0)}$, for which the electronic energy is a minimum:

$$\frac{\partial U}{\partial R_i}=0 \quad i=1,2,\ldots, \tag{1}$$

and

$$U(R)=U(R^{(0)})+\frac{1}{2}\sum_{i,k} u_{ik}(R_i-R_i^{(0)})(R_k-R_k^{(0)})+\ldots, \tag{2}$$

with

$$u_{ik}=\frac{\partial^2 U}{\partial R_i \partial R_k},$$

the "stiffness matrix" being positive definite.

In second approximation the wave function of the molecule is

$$\psi(r,R)=\phi(r;R)\chi(\xi), \tag{3}$$

where χ is a wave function corresponding to a coupled vibration of the nuclei in the potential provided by the quadratic terms in (2). (The coulomb repulsion of the nuclei is supposed to be included in U). The ξ are normal coordinates describing the small deviations of the nuclei from their equilibrium positions. In the same approximation the total energy $U_{tot.}$ is additive in the electronic and the vibrational energies

$$U_{tot.}=U+U_{vib}. \tag{4}$$

Mixed terms would appear in higher approximation.

These results depend essentially on the assumption that the electronic levels are well separated compared to the spacing of nuclear levels. In particular, the electronic level should not be degenerate. As a rule, these conditions are satisfied for molecules. There are exceptional cases, however, in which the expression (1) has to be replaced by a sum

$$\Psi=\sum_{l,m} c_{lm}\phi_l(r;R)\chi_{lm}(\xi). \tag{5}$$

The coefficients c_{lm} have to be determined by perturbation or variational methods. A problem of this sort has been calculated by Renner [5] for the case of linear molecules. For a short account of these more subtle aspects of the adiabatic approximation we refer to the review article of Sponer and Teller [6].

In the case of crystals it has been usual to state that these are nothing but big molecules and accept the above results, in particular the simple formulation (3) without further scrutiny.

Actually, the condition concerning the spacing of the electronic levels is satisfied only for the electronic ground state of insulators. In case of metals there is a practically continuous distribution of electronic levels close to the ground state. Hence one should discuss wave functions of the type (5), the cumbrousness of which is obvious if one notes that r and R stand for all the electronic and nuclear coordinates.

Counteracting this complication is the fact that the crystal symmetry brings about simplifications by allowing the introduction of special coordinates characterizing the unit cell of the crystal. This procedure will be demonstrated in the discussion of insulators. This should serve as an introduction to our main topic, the discussion of normal and superconducting metals.

Nonmetallic Crystals at Absolute Zero

It may appear somewhat surprising that we have no satisfactory proof that the Schrödinger equation possesses spatially periodical solutions. Actually, the root of the trouble may be that this would be asking for too much. Exactly periodical solutions are not required for the quantum mechanics of solids, and they may not be realized even at absolute zero because of the zero-point vibrations. We will advance an assumption expressing the crystal periodicity in a formal way that is at the same time less sweeping and more fertile in conclusions than the one commonly used.

As a preparation, we introduce coordinates particularly adapted to the problem.

Consider a fundamental domain of N unit cells containing n atoms each, and apply the usual periodical boundary conditions. We introduce a number of coordinates $X_1, X_2, \ldots X_r$ characterizing the ideal lattice. The first six, $X_1 \ldots X_6$, should specify the size and shape of the unit cell and the next $3(n-1)$ determine the relative position of the atoms in the base. In addition, we have $3Nn-r$ normal coordinates ξ describing the small deviations of the atoms from the equilibrium positions.

We will call the X macrocoordinates, the ξ microcoordinates. The former are invariants of the translation group, the latter are elastic waves that are multiplied by a phase factor for every translation operation of the crystal. (It is clear from this distinction that, differing somewhat from current usage, we set apart the zero wave vector end of every optical branch among the X.)

The macrocoordinates may be directly measured by X-ray methods, whereas the ξ can be approached only statistically.

In terms of these coordinates, we can express the fundamental assumption of crystal physics as follows:

The lowest solution ϕ $(r; R)$ of the many-center problem (fixed nuclei) of an extended system of nuclei and electrons (electricall. neutral and of the proper stoichiometric composition) is periodical

Consequently, the $3Nn$ equilibrium conditions of the form (1) can be replaced by the r equations

$$\frac{\partial U}{\partial X_i}=0 \quad i=1, 2, \ldots r. \tag{6}$$

Likewise, the stability condition is expressed in terms of an r by r stiffness matrix.

We assume in this section that we are dealing with an insulator, hence this electronic state is supposed to be nondegenerate and well separated from the higher levels.

Releasing the nuclei from their fixed position, the second approximation wave function is

$$\Psi(r, X, \xi)=\phi(r;X)\chi(\xi;X) \tag{7}$$

Here ϕ is a function of r and χ a function of ξ, but both contain X as a parameter.

The use of (7) implies the assumption, which we explicitly formulate, that the zero-point vibration does not destroy the translational symmetry. This excludes helium from our considerations where this is what actually happens and the lowest state is not crystalline.

The state represented by (7) is then periodical in the sense that the mean deviation of the nuclei from the sites of an ideal lattice is small compared to the lattice constant and constant over space.

On the other hand, the parameters X of this ideal lattice will be slightly shifted as a function of the nuclear mass in much the same way as the nuclear equilibrium positions in molecules do not exactly coincide with the minima of the potentials.

So far we have considered only the lowest state, which implied among other things that the crystal is not under an external stress. This discussion can be easily extended to include the case of stress. Then the condition of equilibrium is

$$\frac{\partial U}{\partial X_i}=P_i^{(0)} \quad i=1, 2 \ldots 6, \tag{8}$$

where the X_1 represent the components of strain multiplied by the volume of the fundamental domain, and the $P_i^{(0)}$ are the components of the external stress.

Equation (8) has, of course, no analogue in case of molecules. Similar relations take care of the case of external electric and magnetic fields, which we shall not explicitly consider.

In such a way we have subdivided the macroscopic coordinates into two classes—those which do and those which do not have a conjugate external force. Together with the microcoordinates, we have now three different types of coordinates. This distinction is implicitly contained, e. g., in a paper by M. Born [7]. The importance of this classification of the coordinates for the theory of phase transitions has been pointed out by the author [8]. The macrocoordinates with and without conjugate forces have been called there thermodynamic and quasithermodynamic coordinates, respectively.

At the present point this terminology is justified more by analogy, since up to the present we have not introduced any thermodynamical or statistical idea, and our theory is purely quantum mechanical, referring to absolute zero. Nevertheless, as we are going to show, our formalism contains all the essential ingredients for phase transitions of both of the first and of the second kind.[4]

We will outline how the main aspects of the theory of phase transitions follow from our results. The rest of this section, and the following as well, parallels closely the discussion in [8], to which we refer for details.

Obviously, for a crystal under stress the energy need no longer be a minimum, as it is indicated also by the relation (8).

It is convenient to introduce the function

$$U[P^{(0)}]=U-\sum P^{(0)}X, \tag{9}$$

where the summation is taken over all the nonvanishing external forces.

The condition of equilibrium in the presence of the external forces is that $U[P^0]$ should be a minimum, i. e.,

$$\frac{\partial U[P^{(0)}]}{\partial X}=0 \tag{10}$$

for all the macrovariables. The condition of stability is again the positive definiteness of the stiffness matrix evaluated at the state in question.

It is an interesting point that the set of coordinates $X_1 \ldots X_r$ is by no means fixed and several competing crystal structures described in entirely different types of coordinates, as, e. g., diamond and graphite may have to be considered. Although one of these states will be the lowest, the $U[P_0^{(0)}]$ curves, or hypersurfaces may intersect and we have a phase transition. Hereby no entropy change, hence no latent heat is involved. The melting process of helium under pressure and superconducting-normal transitions in a magnetic field, both near absolute zero show that such transitions are indeed observed. Of course in most cases these transitions would not be observable, since the time rate of the transition would be negligibly small.

In addition to these phase transitions of the first kind (or first order), we may have also transitions of the second kind (critical points). For details we have to refer to [8]; here we will be satisfied

---

[4] The fundamental reason for this is that the assumption of a system with translational symmetry, and and hence the possibility of introducing macrocoordinates, implies in principle the filling of the entire space. Thus we are dealing with asymptotic laws of quantum mechanics whereby the limiting process is one over space. This limiting process leads to results that are rather analogous to the limiting process of statistical mechanics, which is a limiting process in time carried out over the sequence of microstates of the system. However, the spatial limiting process (the volume tends to infinity at constant density) is of importance even in the theory of condensation. Cf. B. Kahn and G. E. Uhlenbeck, Physica **5**, 399 (1938).

to give a short summary of the characteristic features of these transitions. They are defined by the fact that on varying a parameter, e. g., a component of the stress, the discriminant of the stiffness matrix vanishes:

$$D=|u_{ik}|=0. \qquad (11)$$

The inverse of the stiffness matrix which may be called the compliance matrix becomes singular, its elements show the typical λ-shaped anomalies. It may be noted that the elements of this singular matrix are of the form $(\partial X_i/\partial P_k)_{P_j}$, where the index P_j indicates that the stresses are kept constant on differentiation.

As to the mechanism of the transition the following may be said: $D=0$ brings the system as close to instability as possible, and true instability is avoided by changing the number of macroparameters. For example, imagine a pseudocubic crystal which is distinct from its mirror image. Suppose that on varying the stress the two pseudocubic forms come gradually close to each other in order to merge into a single cubic form at the critical point. Let us call Y the macroparameters measuring the deviation from the cubic form. In the cubic form with $Y=0$ the symmetry is higher, in the pseudocubic from, with $Y\neq 0$, the symmetry is lowered, and new superstructure lines appear in the X-ray spectrum. The parameter Y may actually represent a whole set of coordinates [8].

The importance of a change in symmetry elements at λ-points has been first emphasized by Landau for the case of order-disorder transformations [9].

It should be finally emphasized that in the present case the transformation involves no change in order. In fact, both phases have zero entropy and are completely ordered. Transitions of this type have been called in [8] "displacive transformations."

Nonmetallic Crystals at Finite Temperatures

The theory of phase transitions outlined in section 3 has the peculiarity that it refers to pure quantum states and applies only to systems at absolute zero. A comparison with [8] shows that these results can be generalized to systems at finite temperatures by the simple device of adding the entropy ($X_0=S$) to the thermodynamic variables with the temperature ($P_0=T$) as the conjugate force. All we said above about transitions of the first and second kinds can be repeated with these variables added, and indeed for practical purposes, temperature is the preferred parameter for bringing about these transitions.

This method of introducing thermodynamics into our quantum mechanical discussion yields quick results and is dictated here by limitations of space. However, we wish to dispel the impression that the purely quantum mechanical discussion requires the injection of extraneous phenomenological elements. As will be shown elsewhere, by further expanding the line of reasoning of this paper, one can provide thermodynamics with a novel type of quantum mechanical foundation. In fact, thermodynamics may be said to be the quantum mechanics of spatially extended atomic systems; or rather that part of the quantum mechanics of such systems which can be obtained from the consideration of the integrals of motion. The presence of the macrovariables in our equations which are not thermodynamical (quasithermodynamic variables) shows that our results have a wider scope than traditional thermodynamics, chiefly because of the existence of quantum mechanical integrals having no classical analogue. In the case of crystals, the invariants of the translation group provide such integrals.

As an interesting application for the use of such quasithermodynamic variables we consider now the problem of order-disorder transformations. Up to this point it was assumed that the nuclei would carry out small oscillations around the sites of the ideal lattice. In addition, however, the equilibrium positions themselves may be displaced. One has lattice defects, dislocations, and order-disorder phenomena. Only the last phenomenon will be our concern here.

This phenomenon is very well known, and a few hints will suffice to show how it integrates into the present framework.

The essential point is that the number of sites available for a type of atom (or atomic group) exceeds the number of atoms to be placed. A simplified but typical system would be the socalled Ising model, in which every unit cell contains a "dipole" capable of two orientations. Each pair of parallel neighbors contributes a positive constant and each pair of antiparallel neighbors a negative constant to the total energy of the system.

A complete specification of the orientations of all dipoles constitutes a microparameter, whereas the socalled long-range-order parameter

$$Z=\frac{N_+-N_-}{N_++N_-} \tag{12}$$

is a macrovariable. N_+ and N_- represent the numbers of dipoles in each orientation. If the "dipole" is an electric or magnetic dipole, then Z is a thermodynamic parameter. Otherwise (e. g., an NH_4 tetrahedron) Z is a quasithermodynamic parameter. It plays exactly the same role in producing a critical point of the order-disorder type as the parameter Y does for a "displacive" type critical point (section 3).

The classical theory of order-disorder is applicable to real cases only under special conditions. According to quantum mechanics there is a resonance between states of equal energy, contributing a resonance energy to the configurational energy of the system. The classical theory assumes that this contribution is negligible. In particular, the resonance between the ordered states $+Z$ and $-Z$ is negligible, except perhaps if Z is still close to zero. On the other hand, the resonance between degenerate states should be effective for the establishment of equilibrium.

Normal and Superconducting Metals

Reviewing the crystals of the elements with an unprejudiced mind, one may feel surprised why there are so many insulators among them. Apart from the rare gases all atoms contribute incomplete shells to the crystal which should lead to highly degenerate electronic states, at least if the crystals were highly symmetrical as close-packed or cubic. Actually the crystals of the insulators are generally of lower symmetry, and the atoms are displaced so as to form groups characteristic of their column in the periodic table, complete their shells and thus get rid of their degeneracy. This may be conceived as an analogue of the Jahn-Teller effect in molecules [6].

Proceeding to the left in the periodic table a point is reached where this is no longer possible because even in the most advantageous nuclear configuration there are more electronic orbits than electronic states. We have again the situation of an order-disorder transformation, but in contrast to the classical case the resonance energy is not negligible compared to the configurational energy. Indeed the standard band theory starts from Bloch functions giving up any idea of a localized electron configuration.

We will outline the assumptions under which this procedure can be justified within the adiabatic method. Usually these assumptions are made unwittingly.

We have to start now from a wave function of the form (5). In terms of the coordinates introduced in section 3 we have

$$\Psi(r;X^{(av)})=\sum_{l,m} c_{lm}\phi_l(r;X^{(l)})\chi_{lm}(\xi;X^{(l)}) \tag{13}$$

The important point is that different electronic functions may depend on different macroparameters which we symbolize by the superscripts. Likewise, the elastic frequency spectrum and hence the functional form of the χ is different for the various electronic states. Of course, it may be presumed that the variation in X is not too drastic and the function Ψ will be characterized by some average value $X^{(av)}$.

In order to arrive at the band approximation, one has to make a series of assumptions.

In the first place, one assumes that the electronic function depends only on the average nuclear positions and vice versa.

Hence we have

$$\Psi(r;X^{(av)})=\sum_{l} c_l\phi_l(r;X^{(av)})\sum_{m} c_m\chi_m(\xi;X^{(av)}). \tag{14}$$

Here $X^{(av)}$ represents a set of fixed parameters, hence we have a complete separation of electronic and nuclear motions. In particular, the energies are additive.

$$U=U^{(el)}+U^{(n)}. \tag{15}$$

As a next step the electronic wave function is constructed from single-particle functions. The details of this procedure are not relevant in the present connection.

This is the basis for the discussion of the normal metal, or what might be called a theory of the disordered state. The entropy connected with this disorder is considerably reduced because of the Fermi-Dirac degeneracy.

The occurrence of superconductivity shows that in a number of metals there is a competing ordering process that sets in at a sharp transition temperature. It is plausible to connect this phenomenon tentatively with those terms of eq (13) that have been lost on the transition to (14). A single term of this sort would be of the form

$$\varphi_1(r;X^{(1)})\chi(\xi;X^{(1)}), \tag{16}$$

where $X^{(1)}$ differs somewhat from $X^{(av)}$ and producing a lowering of the crystal symmetry. Actually, we do not have to assume that (16) factorizes and may replace it by the more general expression

$$\Phi_1(r, \xi; x^{(1)}). \tag{17}$$

The translation operation corresponding to the symmetry of $X^{(av)}$ will give rise to, say ω terms equivalent to (17). In contrast to the classical theory of order-disorder transformations, we are not neglecting the quantum resonance between equivalent states and we obtain that the simplest possibility for the wave function of an "ordered" state is

$$\Psi=\sum_{l=1}^{\omega} c_l\Phi_l(r, \xi; X^{(l)}). \tag{18}$$

Certain qualitative features of (18) can be obtained on the basis of symmetry considerations. We are dealing with a modulation of the original lattice symmetry whereby the electronic and nuclear modulations are closely coupled.

The function (18) is in a certain sense the generalization of the wave function of [1], and of those of Fröhlich and Bardeen as well. The analogy with the resonating electron lattice of [1] is obvious, but the present functions involve also the distortion of the ion lattice.

Thus an important defect of [1] is removed. In that paper the electronic eigenfunctions were obtained through symmetry considerations, and it was shown that the superconducting properties would follow for $\omega \geqq 3$. The dynamic stability of the electron superlattices was not investigated. We see now that this stability is a consequence of a deformation of the ion lattice, a many-electron analogue of the "self-trapping" of electrons [10].

On the other hand, the general framework here considered is compatible with the calculations of the electron-lattice interaction by Fröhlich and Bardeen. According to Fröhlich (p. 853, reference 2), the lattice interaction "leads to an alteration of the distance correlation of two electrons in ordinary space." Moreover, ". . . one electron can benefit from the lattice deformation produced by another one if it remains sufficiently close (in ordinary space) to it." The difference is, however, that according to the present paper the above-mentioned correlation presents a long-range order in contrast to the short-range order of Fröhlich and Bardeen. Or, in other words, in the present theory one particular elastic wave of the wavelength ω times the lattice constant plays a particular role in the superconducting state. The importance of a single quantum state is an essential feature of London's phenomenological theory and is important also in the case of helium II. It is responsible for the sharp λ-temperature and for the existence of a zero-entropy state.

What determines the number ω, or the wave length, of the elastic wave thus singled out of the spectrum? The answer is, the ratio of the number of electrons to the available low energy orbits in the cystal. (See section 4, reference 1). The same thing can be expressed also in terms of the band theory—A modulation of the lattice leads to the splitting of the original band. A particularly advantageous state will be obtained if the number of electrons is just sufficient to fill a "subzone" thus obtained [11].

A quantitative investigation of this question is under way along with a number of related questions. For example, it seems very likely that the Fröhlich-Bardeen condition of superconductivity is essentially identical with our general requirement that the discriminant of the stiffness matrix should vanish. This is made likely by a recent calculation of Wentzel [12], who finds that Fröhlich's condition implies the vanishing of the sound velocity, i. e., the vanishing of one of the stiffness moduli.

Finally, a remark about the case $\omega=2$. It was shown in [1] that the lowest state is now that of an insulator. There is no deformation of the lattice (one should think of the symmetry of NaCl), hence there is no macroparameter to produce a critical point. Thus in this case one should expect a gradual increase of the resistivity for $T\rightarrow 0$.

Summary and Discussion

A half phenomenological theory is presented that seems to provide a comprehensive qualitative framework for the quantum mechanics of solids. It is essentially based on two asumptions. In section 3 the first was called the fundamental assumption of crystal physics. It is unlikely that this assumption should be seriously challenged.

On this basis the formalism provides definite conditions for the phase transitions of the first and second kinds. These conditions seem to be applicable to practically all transitions. Our second assumption is that they are relevant also for the case of superconductivity. Although rather plausible, at the present juncture it seems safer to consider this only as a working hypothesis. At any rate, this assumption leads to a virtually unique electronic mechanism for superconductivity. The picture thus obtained incorporates the the basic idea of the Fröhlich-Bardeen theory ascribing superconductivity to the electron-lattice interaction. On the other hand, the use of free-electron wave functions seems to be justified only above the transition temperature. The superconducting state itself is given more nearly by the resonating superstructures of [1] stabilized by the closely coupled deformations of the lattice.

The theory is characterized by a high degree of consistency. It is suggestive of more specific investigations, which we hope to follow up.

From the experimental point of view, the superstructures here postulated should be observable in the X-ray spectrum. The scanty experiments carried out so far were not appropriate to decide this question in either way.

References

[1] L. Tisza, Phys. Rev. **80**, 717 (1950).
[2] H. Fröhlich, Phys. Rev. **79**, 845 (1950).
[3] J. Bardeen, Phys. Rev. **80**, 567 (1950).
[4] M. Born and R. Oppenheimer, Ann. Physik **84**, 457 (1927).
[5] R. Renner, Z. Physik **92**, 172 (1934).
[6] H. Sponer and E. Teller, Rev. Modern Phys. **13**, 90 (1941).
[7] M. Born, Rev. Modern Phys. **17**, 245 (1945).
[8] L. Tisza, On the General Theory of Phase Transitions, in Smoluchowski, Mayer, and Weyl, Phase Transformations in Solids (John Wiley & Sons, Inc., New York, N. Y., 1951). Also M. J. Klein and L. Tisza, Phys. Rev. **76**, 1861 (1949).
[9] L. Landau and E. Lifshitz, Statistical physics, p. 200 (Oxford 1938).
[10] H. Fröhlich, H. Pelzer, and S. Zienau, Phil. Mag. **41**, 221 (1950).
[11] Cf. J. C. Slater, Phys. Rev. **84**, 179 (1951).
[12] The author is indebted to Prof. Wentzel for communicating his unpublished note.

4. Field Theoretic Description of Interactions in a Superconductor

by M. Dresden [1]

Abstract

In a recent paper, Tomonaga [2] developed a description of a nonideal Fermi gas, which appears eminently suited for application to problems in superconductivity. Effectively it is shown that under certain conditions—such as long-range forces, relatively low excitations—any system of interacting Fermi particles can be described by a density field, which then is to be quantized according to Bose statistics. The Hamiltonian of this density field is identical with the Hamiltonian of an infinite set of coupled harmonic oscillators. It is well known that the interaction of the electrons and the lattice in a solid can be described in terms of emission and absorption of vibrational quanta, or equivalently in terms of an interaction of the electrons with a "phonon" field. Hence, if one uses the Tomonaga representation of the nonideal electron gas, one can describe all interactions in a superconductor by two interacting, scalar Bose fields. As one usually restricts oneself to single emission and absorption processes, the interaction between the fields is to be bilinear. The field theoretic problem thus stated can be solved exactly for any value of the coupling parameter. The lowest state of this system can be studied without difficulty; it reveals many of the properties usually associated with the superconductive state.

---

[1] University of Kansas. Lawrence, Kans.
Tomonaga, Progress of Theoretical Physics **5**, 544 (1950).

5. Determinantal Eigenfunctions for the Theory of Superconductivity[1]

by William Band[2]

In this report we point out some hitherto unrecognized but inescapable consequences of the Pauli exclusion principle when applied rigorously to an electron assembly as a whole. When these are combined with some physical ideas about phase coherence among the zero-point Debye modes previously reported[3] we are led to make some speculations towards a theory of superconductivity that appears to be highly promising.

To ensure complete conformity with the Pauli principle it is necessary to describe an assembly of N electrons by an eigenfunction that is antisymmetrical in all the electrons. Consider a determinant formed from any N one-particle free-electron wave functions, specified by a "spectrum" of N wave numbers or $\boldsymbol{k}$-vectors. It can be proved without trouble that the totality of such determinants formed from all conceivable spectra of N $\boldsymbol{k}$-vectors in the whole of $\boldsymbol{k}$-space, forms a closed orthogonal set of determinantal eigenfunctions. These basic determinantal eigenfunctions are solutions only for a free electron gas, but because of this closure theorem the solution for any other problem with N electrons can always be expressed as a linear combination of these basic determinants.

Consider first a small perturbation by a periodic rigid lattice-type potential, and start with the zeroth-order eigenfunction of lowest energy whose spectrum just fills a sphere in $\boldsymbol{k}$-space. First-order resonance occurs with every other determinant with a $\boldsymbol{k}$-spectrum that differs from the zeroth order spectrum by one and only one pair of $\boldsymbol{k}$-vectors if these vectors satisfy the familiar Bragg reflection relation with the lattice. No determinants can occur in first order resonance with more than one electron taking part in the resonance simultaneously, without violating the exclusion principle. This has two consequences that appear at first sight erroneous from the point of view of one-electron formalism but which nevertheless appear to be inescapable results of the full application of the exclusion principle.

First, there is no energy gap in the neighborhood of the top of a Bloch zone; the resonance energy has a maximum negative value at the surface but does not change sign for larger energies. Second, the resonance energy is not proportional to the number of electrons in the assembly, and for a given density per unit volume it is proportional only to the square root of the volume. Negative resonance energy therefore favors breaking up the assembly into a number of separate exclusive subassemblies, each having its own smaller volume in space.

Phonon excitation of the lattice introduces additional resonance with exchange of energy between lattice and electrons, opening holes in the $\boldsymbol{k}$-spectrum near the Fermi surface even at absolute zero of temperature. Under suitable conditions this restores the energy gap at

---

[1] This work was sponsored by the Office of Naval Research.

[2] Department of Physics, The State College of Washington, Pullman, Wash.

[3] W. Band, Phys. Rev. **79**, 739 and 1005 (1950).

the top of a Bloch zone and yields positive resonance energy if the assembly overlaps slightly into the next zone. This positive resonance energy is still proportional only to $V^{\frac{1}{2}}$ and so favors coherence of the assembly in one single unit throughout the lattice.

Neglecting all magnectic effects it can be proved that the state of lowest energy is always one of zero net current: resonance energy, with or without phonon exchange, is insufficient to stabilize a spontaneous current.

The probability current in general, calculated with the determinantal eigenfunctions, contains a direct and an exchange part, both of which vanish everywhere when the $\boldsymbol{k}$-spectrum is symmetrical. With an asymmetrical $\boldsymbol{k}$-spectrum the direct current is definite, and the exchange currents break up into loops flowing round the lattice cells; each loop has self-inductance, and neighboring loops have mutual inductance. Qualitatively this is just what is needed to understand the Meissner effect. It is generally agreed that an explanation of the Meissner effect is necessary and sufficient to understand superconductivity. It is not generally realized that the Meissner phenomena include more than the diamagnetic effects observed in large superconductors, and that they are necessarily associated with the ovserved ability of the supercurrent to jump over lattice imperfections even in noninductive linear superconductors that are too thin to show any diamagnetic effects. The supercurrent must in fact have not only magnetic stability sufficient to absorb and therefore nullify the magnetic field inside the superconductor, but also sufficient inertia of "supermomentum" [4] to jump across the residual resistance due to lattice defects. In the present picture both these are provided for: mutual inductance between the exchange current loops stabilize (by means of magnetic energy) a state in which surface currents prevent penetration of a magnetic field with respect to any state in which a field penetrates the specimen. The self-inductance of the exchange current loops provides extra inertia or supermomentum.

If the lattice potential is too large to be treated as a small perturbation, it is insufficient to start as above with a single basic determinantal eigenfunction in zeroth approximation. To give even a zeroth order approximation of the lowest state it becomes necessary to include a linear combination of a number of basic determinants, some at least of which must have spectra corresponding to excitation of one or more electrons from $\boldsymbol{k}$-vectors far too small to yield resonance with the lattice. First-order resonance then induces a family of $\boldsymbol{k}$-spectra from each $\boldsymbol{k}$-spectrum appearing in the zeroth approximation, but in general can cause no transitions between the spectra in the zeroth approximation. Each family of $\boldsymbol{k}$-vectors can be thought of as corresponding to a single state of the assembly. The lowest of these states is essentially the same as the one just described for small perturbations, with a spectrum that just fills a sphere in $\boldsymbol{k}$-space; it has the same properties and contributes the same stability and inertia through its exchange currents. The assembly is in this lowest state only a fraction of the time because it has to be combined with the other relatively excited states to give the full description of the assembly. We thus have a situation agreeing with the phenomenological picture of F. London. Whereas we have a lowest state occupied a fraction of the time by all the electrons, the phenomenological picture has a

---

[4] Max von Laue, Theory of superconductivity (Springer, Berlin, 1949).

proportion of the electrons in the superconducting state all of the time.

First-order resonance within one family or state cannot cause electric resistance, the scattering due to such resonance is completely symmetrical in the sense that there is no loss of energy with time, and as much scattering occurs into any **k**-vector as there is out of it. Electric resistance arises only from transitions between the different families or states of the whole assembly, and these occur only through lattice imperfections and misfits.

Elsewhere we have advocated the view (see footnote 3) that residual resistance near 0° K is due to phase misfits between phase-coherence domains of the zero-point Debye modes of the lattice, and that an order-disorder transition among these phase domains is essentially responsible for the transition into the superconducting state, and explains Maxwell's isotope effect. We may combine this idea with the above finding (pages 23, 24) that positive resonance energy favors coherence. It is in fact suggested that each phase-domain is a proper region over which to consider the electrons as a single assembly to which the exclusion principle may be applied. An order-disorder transition into a coherent condition would be assisted by positive resonance energy, opposed by negative resonance energy; the temperature of the transition increased by positive and lowered by negative resonance energy. If it can be proved—and this has not yet been attempted—that a magnetic field would increase the negative resonance energy, the destruction of superconductivity by a magnetic field and the fact that this occurs as a first order phase change, can be well understood in terms of this picture.

This theory still contains a number of speculative features already emphasized, but for the present it apparently has one major advantage over other recent theories in that it does not rely upon unreasonably great lattice interactions to stabilize the supercurrent, but instead provides both the stability and the inertia of the supercurrent through magnetic forces among exchange currents, that could exist even with very small lattice interactions.

Qualitatively the theory leads essentially to the same criteria for the occurrence of superconductivity as the other theories. To provide positive resonance energy through phonon exchange, the conduction electron assembly must only just overlap into the conduction band, so that there are comparatively few conduction electrons.[5] Also the energy of misfit between phase domains must be comparatively great to give a high enough transition temperature to be observable; and this means that a large residual resistance favors superconductivity. It is only in the ordered state where the residual resistance has nearly vanished that the supermomentum is sufficient to maintain the supercurrent.

---

[5] W. Band, Proc. Cambridge Phil. Soc. **42**, 311 (1946).

6. Superconductivity of Isotopes of Mercury and Tin[1]

by C. A. Reynolds, B. Serin, and L. B. Nesbitt[2]

The measurements of the critical-field–temperature relations for various isotopes of mercury already reported[3] have been extended down to 1.37° K. The critical field is a parabolic function of temperature within the experimental error over the whole range of temperature. The data for each isotope (average mass number M) was fitted to a parabolic relation by the method of least squares. As is well known, Kok[4] has shown that a parabolic form of the critical-field curve follows from a difference in specific heat per unit volume between the normal and superconducting states of the form $\gamma T + KT^3$, where T is the absolute temperature. Thus, the values of γ and K, as well as the critical field at absolute zero, H_0, for each isotope, were computed from the least-squares parabola. These data, as well as the critical temperatures, T_c, are summarized in table 6.1.

Table 6.1.

M	H_0	T_c	γ	K	K/M
	Oersteds	°*K*			
199.5	420	4.185	1,600	273	1.37
200.7	419	4.175	1,600	275	1.37
202.0	417	4.160	1,600	278	1.375
203.2	414	4.146	1,590	278	1.37

It is fairly clear from table 6.1, that γ, the term coming from the electronic specific heat in the normal state, is constant for the different isotopes, whereas K is proportional to the mass. However, the differences in the critical fields between the various isotopes are quite small; and these conclusions, while valid, are just within the limits imposed by experimental error. Thus, further measurements were made with tin, where the differences in critical fields are much greater.

The measurements with tin were made on each of two isotope samples and two samples of natural tin, at 70 temperatures between the critical temperature and 1.27° K. The isotope samples were somewhat impure, $M=113.6$ being 99.5 percent tin, and $M=123.8$ being 99.8 percent tin. The natural samples were prepared from 99.995 percent pure Johnson-Mathey tin. The characteristics of the two samples of natural tin were identical over the whole range of temperature.

The critical-field–temperature curves are parabolic below 2° K, but deviate considerably from this form at higher temperatures. The critical fields are higher than would be expected from fitting the low-temperature data to a parabola. However, it was found that the quantity H/H_0 was the same function of T/T_c for all the samples. (H is the critical field at temperature T.) The fields H_0 were obtained

---

[1] This work has been supported by the Office of Naval Research, by the Rutgers University Research Council, and by the Radio Corporation of America.

[2] Physics Department, Rutgers University, New Brunswick, N. J.

[3] B. Serin, C. A. Reynolds, and L. B. Nesbitt, Phys. Rev. **80**, 761 (1950).

[4] J. A. Kok, Physica **1**, 1103(1934).

by extrapolation. The occurrence of this universal form shows that γ is constant for the different isotopes.

The data for tin are summarized in table 6.2.

TABLE 6.2.

M	T_c	H_0	H_0/T_c
	°*K*	*Oersteds*	
113.6	3.805	312	82.0
118.7	3.732	304	81.5
123.8	3.659	298	81.4

Fitting the critical-temperature–mass relation to a form $M^\alpha T_c=$ constant gives $\alpha=0.46\pm0.02$. The slope of the critical-field curves at the critical temperature is 146 oersteds/°K. These results agree with those reported by Shoenberg [5] for isotopes of different average mass numbers.

---

[5] D. Shoenberg, et al., Nature **166**, 1071 (1950); see also K. Mendelssohn, et al. on the same page.

7. Recent Work at the National Bureau of Standards on the Isotope Effect[1]

by E. Maxwell[2]

Measurements of the critical fields and transition temperatures of tin and thallium isotopes are in progress, and some preliminary results are available. The measurements are made by observing magnetic transitions by means of a direct-current method of flux measurement. The apparatus and method will be described in detail in a later publication [1].*

The isotopic materials were obtained from the United States Atomic Energy Commission in the form of SnO_2 and Tl_2O_3 and reduced to the metallic form by E. L. Weise of the Chemistry Division of National Bureau of Standards. The specimens were in the form of capillary wires approximately 0.3 by 50 mm that had been cast in vacuum, sealed off in Pyrex capillaries, and later recrystallized under a temperature gradient to form single crystal.

The original interest in thallium stemmed from a suggestion, advanced soon after the discovery of the isotope effect in mercury, that the phenomenon might be an indirect consequence of the isotopic dependence of atomic volume on the atomic mass.[3] Such an atomic-volume dependence is to be expected from the anharmonicity of even the zero-point vibrations of the lattice. Previous results [2, 3] on tin, indium, and tantalum had shown that the transition temperature, and in fact the entire critical-field curve, are shifted toward higher temperature when the atomic volume is increased by the application of external tension and toward lower temperature when the atomic volume is decreased by applied hydrostatic pressure. Some later experiments [4] on thallium, however, had revealed a pressure dependence of the opposite sign, i. e., application of hydrostatic pressure raised the transition temperature. Accordingly, if there were a simple relation between the volume effect and the isotope effect, one might expect a reversal in sign of the isotope effect for thallium. This, however, was found not to be the case.

Measurements were made on thallium samples of masses 203.3 and 205.0, as well as on natural thallium, mass 204.4. The isotope shift was observed and was found to be normal in sign, i. e., the sample of heavier mass had a lower transition temperature. Consequently, the possibility of a simple correlation between the volume and isotope effects is ruled out.

Quantitative results on thallium are not yet available. Due to some secondary effects, not yet fully understood, the critical-field curves for the different samples are slightly shifted from run to run, although the internal consistency and precision in any one experiment is good. This may be caused by the thallium sticking to the walls of the Pyrex capillaries and being put under strain due to differential thermal expansion.[4] This problem is receiving further investigation.

---

*Figures in brackets indicate the literature references on p. 30.

[1] Supported by the Office of Naval Research.

[2] National Bureau of Standards, Washington, D. C.

[3] The theoretical treatments of Fröhlich and Bardeen had not yet appeared.

[4] Note added May 31, 1951. It appears that the difficulty was due to the supercooling of the specimens. The degree of supercooling was not the same in different experiments when the specimens had been warmed up to room temperature between times.

In making these measurements it was necessary to keep track of the helium level and correct the apparent temperature for the hydrostatic head of the helium in the Dewar. If this precaution was omitted, the apparent temperatures above the λ point were too high. This source of error is not present below the λ point, as there can be no thermal gradients in He II.

Isotopically enriched specimens of tin of mass 116.8, 118.1, 119.8, and 123.1, as well as natural tin (118.70), have been measured in weak fields (up to about 20 oersteds) and both the transition temperature and $(dH_c/dT)_{T_c}$ observed (fig 7.1). The zero field transition temperatures are given tin table 7.1. The slope $(dH_c/dT)_{T_c}$ is 146 oersteds/°K for all samples. From a plot of mass-temperature data in logarithmic form the best value of the slope was found to be 0.50, with a standard deviation of 0.03, in agreement with the theoretical predictions of Fröhlich [5] and Bardeen [6] and the earlier observations of Serin, Reynolds, and Nesbitt [7] on mercury.

These measurements are being extended to lower temperatures.

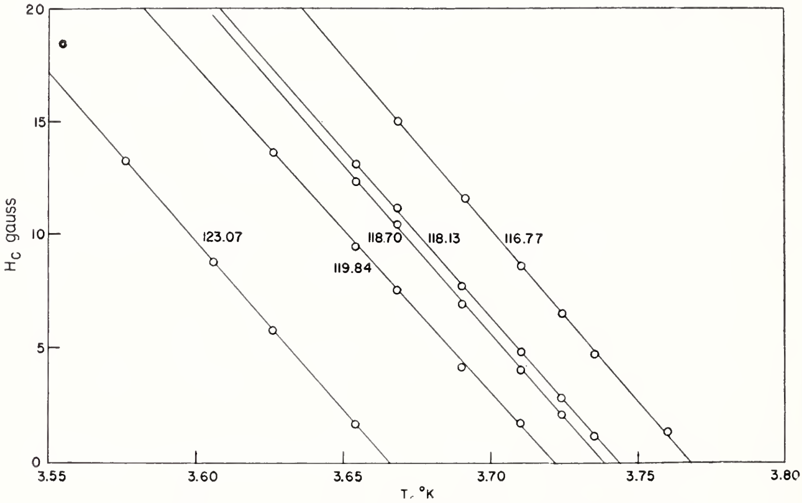

Figure 7.1. *Critical field—temperature curves for* Sn *isotopes.*

Table 7.1. *Transition temperatures of* Sn *isotopes*

Mass	*Tc*
	°K
116.77	3.7680
118.13	3.7438
118.70 (nat)	3.7384
119.84	3.7202
123.07	3.6658

---

[1] Phys. Rev. **86**, 235 (1952).

[2] G. J. Sizoo and H. K. Onnes, Leiden Comm. No. 180b (1925).

[3] N. Alekseyesky, J. Phys. (USSR) **3**, 443 (1940).

[4] L. S. Kan, B. G. Lazarev, A. I. Sudovstov, Doklady Akad. Nauk SSSR **69** (No. 2) 173 (1949).

[5] H. Fröhlich, Proc. Phys. Soc. [A] **63**, 778 (1905); Phys. Rev. **79**, **845**, (1950).

[6] J. Bardeen, Phys. Rev. **79**, 167 (1950); **80**, 567 (1950).

[7] B. Serin, C. A. Reynolds, L. B. Nesbitt, Phys. Rev. **78**, 813 (1950).

8. Superconductivity of Tin Isotopes[1] [2]

by J. M. Lock, A. B. Pippard, and D. Shoenberg [3] [4]

Detailed measurements have been made of the transition temperatures and critical magnetic fields of isotopes of tin electromagnetically separated at the Atomic Energy Research Establishment, Harwell. The samples studied had mean atomic weights of 116.2±.05, 119.9±.05, and 123.75±.1, and two specimens of each sample were investigated, using Shoenberg's [2] ballistic method for magnetic-moment measurement. By the use of thin wires cast in silica tubes the demagnetizing coefficient of the specimens was reduced as far as possible, so that sharp magnetic transitions were obtained.

The width of the temperature transition in a small magnetic field (2 gauss) varied from one specimen to another, but there was no significant difference between the transition temperatures of two specimens of the same atomic weight. Two specimens, one of isotope 116 and the other of isotope 124, showed particularly sharp transitions, enabling the difference in their transition temperatures in zero field, ΔT_c, to be accurately determined as $0.108 \pm 0.001°$ K. The absolute values of T_c, on the 1949 scale, for the three samples were determined as 3.767° K for isotope 116, 3.712° K for isotope 120, and 3.659° K for isotope 124, but these values may be systematically in error by a few thousandths of a degree on account of uncertainties in the estimation of the correction to be applied for the hydrostatic head of liquid helium. This error is not significant in the determination of ΔT_c as both specimens were measured simultaneously and were subject to the same correction.

The two specimens that showed sharp temperature transitions also showed very sharp magnetic transitions at constant temperature, and their critical fields, H_c, and the difference in critical fields, ΔH_c, were measured at a number of temperatures between the transition temperatures and 1° K. Values of ΔH_c could be determined within 1/20 gauss. The importance of an accurate determination of the variation with temperature of ΔH_c is that it provides a sensitive test of the similarity in shape of the critical-field curves of two isotopes. Thus, if the critical-field curves were truly parabolic, ΔH_c should be a linear function of T^2. In fact, a graph of ΔH_c against T^2 shows that it is not quite linear, but this is accounted for by the departure of the critical-field curves from the exact parabolic shape. If it be assumed that the curves are of similar shape, in the sense that they may be represented by an equation of the form $H_c/H_0 = f(T/T_c)$, where H_0 is the critical field at 0° K, with the additional condition that H_0/T_c takes the same value for all isotopes of the same metal, it is a simple matter to calculate from one critical-field curve how ΔH_c should vary with T. This calculation has been carried out, and the predicted curve is in very good agreement with the experimental points over the whole temperature range. This curve will

---

[1] Preliminary results have already been published [1].

[2] Figures in brackets indicate the literature references on p. 32.

[3] Royal Society Mond Laboratory, Cambridge, England.

[4] Presented by D. Shoenberg

be included in a detailed account of the investigation, which will be published shortly [3], and will not be reproduced here. The assumption made above, that H_0/T_c is the same for different isotopes, is verified within the limits of experimental error. A sensitive test is provided by a comparison of $\Delta H_0/H_0$ with $\Delta T_c/T_c$, where H_0 and T_c refer to isotope 116. The experimental values are as follows:

$$H_0=307.5 \text{ gauss}, \; T_c=3.767^\circ \text{ K for isotope 116}$$

$$\Delta H_0=8.90\pm.05 \text{ gauss}, \; \Delta T_c=.108\pm.001^\circ \text{ K}$$

$$\frac{\Delta H_0}{H_0}=(2.894\pm.016)\times10^{-2}, \quad \frac{\Delta T_c}{T_c}=(2.867\pm.027)\times10^{-2}.$$

There is thus good evidence for the geometrical similarity of the critical-field curves of different isotopes.

One consequence of this is that the electronic specific heat of tin is independent of isotopic mass, as may be shown by a simple thermodynamic argument, on the assumption that the specific heat of a superconductor varies at very low temperatures more rapidly than that of a normal metal. On account of the limits of experimental accuracy, it is not possible to show decisively that the coefficient γ in the normal electronic specific heat, γT, is entirely independent of isotopic mass, M, but the experiments indicate that if $\gamma \sim M^m$, then m is probably less than 0.02. This is in agreement with theoretical expectations.

A more important consequence of the constancy of H_0/T_c is that the theoretical prediction of Fröhlich [4] and Bardeen [5], that $H_0 \sim M^{-1/2}$, may be tested, as has previously been assumed without experimental confirmation, by measurements of T_c rather than H_0. The present results show that the theoretical prediction is very nearly substantiated by experiment; for instance, if a relation of the form $T_c \sim M^{-n}$ be assumed, then n must have the value 0.462±.014, which is close to the predicted 0.5. The fact that nearly the predicted variation is found in both tin and mercury [6] provides strong support for the idea that the occurrence of superconductivity is intimately dependent on interactions between electrons and the crystal lattice. The small numerical disagreement, which it is believed is too large to be a consequence of experimental error, is not so great as to cause serious doubt as to the essential correctness of the ideas of Fröhlich and Bardeen, but is probably to be explained by inexactitudes of the theory in matters of detail, which may be disposed of in more comprehensive treatments.

---

[1] W. D. Allen, R. H. Dawton, J. M. Lock, A. B. Pippard, and D. Shoenberg, Nature **166,** 1071 (1950).
[2] D. Shoenberg, Phys. Soc. Cambridge Conference Report II, p. 85 (1947).
[3] J. M. Lock, A. B. Pippard, and D. Shoenberg, Proc. Cambridge Phil. Soc. **47,** pt. 4, 811 (1951).
[4] H. Fröhlich, Phys. Rev. **79,** 845 (1950); Proc. Phys. Soc. [A] **63,** 778 (1950).
[5] J. Bardeen, Phys. Rev. **80,** 567 (1950).
[6] E. Maxwell, Phys. Rev. **78,** 477 (1950). C. A. Reynolds, B. Serin, W. H Wright, and L. B. Nesbitt, Phys. Rev. **78,** 487 (1950).

9. Superconductivity at the Clarendon Laboratory[1]

by K. Mendelssohn [1]

In the field of superconductivity the three main lines of study at the Clarendon Laboratory were the isotope effect, the mechanism of the transition, and the heat conductivity in the superconductive state and in the normal state.

The discovery that the transition temperature of a superconductor depends on the mass of the metal ion made by Maxwell in Washington and by Reynolds and Serin at Rutgers University has received further importance by the prediction that such an effect should exist according to the theories of Fröhlich and Bardeen. When, therefore, Allen and Dawton of the Atomic Energy Research Establishment at Harwell made available to us tin specimens with a high degree of isotopic separation, it was decided to make a close examination of the transition points and the critical fields. As all experiments so far carried out on isotopes were measurements of the magnetic susceptibility, and as the same tin isotopes were to be investigated also by this method at the Royal Society Mond Laboratory in Cambridge, it seemed of interest to carry out measurements of the electric resistance. Although it was likely from previous experience that resistance measurements may differ from those of the susceptibility at higher fields, agreement was to be expected at lower field strength. The chief advantage of our method is that it yields direct determinations in zero field, where the susceptibility measurements have to rely on extrapolation and that it furnishes an independent measurement of the purity of the sample by the value of the residual resistance. This latter check is of considerable importance as the effect to be determined is rather small and as it is well known that the transition temperature is very sensitive to impurities. Indeed, only those samples of commercially available metals that are spectroscopically pure will yield reliable values of the transition points. In the case of separated isotopes where the preparation of metallic samples had to rely on very small amounts of substance, it was therefore of considerable value to be able by an independent method to separate the effect produced by the mass difference from impurity effects. The following values were obtained on four samples, including one of natural tin:

M	116.2	118.7	120.0	123.6
T_c	3.764	3.727	3.710	3.653
$T_cM^{0.5}$	4,057	4,061	4,064	4,061
R_4/R_{90}	$5\text{x}10^{-3}$	$2.5\text{x}10^{-3}$	$1.5\text{x}10^{-3}$	$2\text{x}10^{-3}$

M is the isotopic mass, T_c the transition point in zero field, and the product $T_cM^{0.5}$ is the quantity that, according to theory, should be a constant. The experiments show that this is indeed the case. It is likely that in this work the determination of the transition tempera-

---

[1] Clarendon Laboratory, Oxford, England.

ture is at least as accurate as that of the isotopic mass of the samples. R_4/R_{90} represents the ratio in resistivity between helium temperatures and 90° K. The values for this ratio, which indicates the purity of the sample, are the same for the three separated isotopes as for the natural tin of weight 118.7, which was a spectroscopically pure specimen. It can therefore be assumed that the effect found is indeed due to variation of the mass of the tin atom.

Experiments on the transition of the electric resistance in magnetic fields in the case of lead, tin, and mercury had shown that these metals all showed a tendency toward lower temperatures to have the transition spread over a finite interval of temperature. This is different from the change in the susceptibility, which was found (for the completely longitudinal case) to be confined to a sharply defined field and temperature. In order to investigate this problem further, experiments on the simultaneous determination of resistance and susceptibility have been carried out, using an a-c method. The results so far obtained were, however, more complex than expected and have as yet not led to a clear separation of the resistive and magnetic effects.

Another aspect of the transition on which experiments are in progress is the change of a persistent current at constant temperature by the variation of an external magnetic field. Earlier experiments on a torus had established the figure of the magnetization curve. Work carried out at the Clarendon Laboratory before the war had suggested that the time effects occasionally observed in the superconductive transition are due to the slow change of currents on the boundary surface between superconductive and normal material. If this concept were true, one would expect the magnetization curve of a torus to consist of three regions showing different behavior. At low fields, currents are induced in the outer surface of the ring only. At high fields the body of the torus will split up into the intermediate state consisting of small regions of superconductive and normal metal. In neither case should we expect the occurrence of time effect as no large regions of superconductive and normal material are coexistent. However, in between these two cases there exists a region of intermediate fields where, in equilibrium, the ring is completely superconductive but where any change in the external field strength requires a change in the magnetic flux passing through the hole of the torus. Nothing can be said a priori about the mechanism of this change, but it would seem likely that owing to some small inhomogeneity in the shape of the torus a tube of flux may enter it at this place and then pass through the body of the ring. In this process certain parts of the ring will be rendered temporarily nonsuperconductive. As the tube of flux must be sheathed in currents that will have to travel with it through the material of the ring, we can expect this process to require some time, and one might therefore expect time effects to occur in the magnetic induction. Careful measurements of the induction of a torus that should elucidate this question were therefore started before the war but had to be discontinued at its outbreak. However, these preliminary observation had given already evidence of the occurrence of time effects in the predicted region.

Somewhat different experiments on the same problem have now been started. Instead of measuring the total induction of the torus, the passage of magnetic flux is recorded by coils above and below the ring, having equal diameter with it. Using this arrangement, time effects have now indeed been observed in the region of medium fields where they were expected. These time effects were absent in low and high fields. The actual range of fields at which the flux in the hole of the torus can be expected to change depends on the ratio of the total diameter of the ring to the diameter of the wire which forms it. So far only one ratio has been investigated. Besides the detailed information on the mechanism of the transition provided by this work, the observation of the actual passage of flux through the body of the ring opens some interesting thermo-dynamical questions, an answer to which can probably be obtained by calorimetric measurements in this region of fields and temperatures.

The largest proportion of the work in superconductivity has been concerned with the thermal conductivity. From measurements before the war it was known that in a pure metal the heat conductivity of the superconductive phase is smaller than that of the normal. This can be accounted for by the fact that the superconductive electrons have zero entropy and cannot therefore contribute to the transport of thermal energy. The position is much more complex in metals containing impurities and in superconductive alloys. We have shown recently that while a lead-tin alloy will behave exactly like a pure metal as regards its heat conductivity, an alloy of lead, containing 10 percent of bismuth, exhibits quite different effects. Here the heat conduction is much larger in the superconductive than in the normal phase, and there are very complex effects occurring in the transition region. In order to investigate these phenomena further, we have now measured the heat conductivity of a whole series of lead-bismuth alloys of compositions varying between 0.02 and 10 percent of bismuth (see fig. 9.1). As the results show, the alloys with

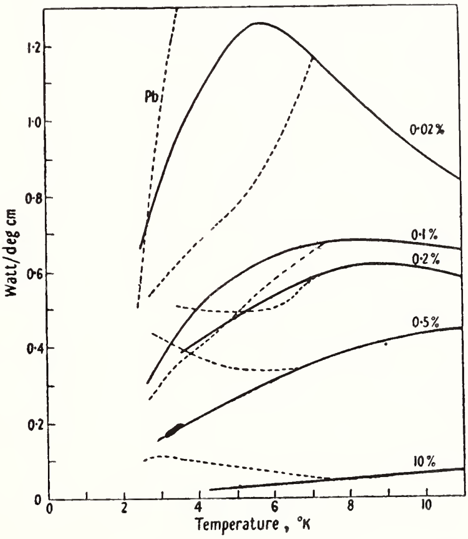

FIGURE 9.1. *Heat conductivity of* Pb–Bi *alloys.*
———, Normal state; - - - - - superconductive state.

lower bismuth contents (0.02 and 0.1%) show a behavior similar to pure lead, but the two curves for the superconductive and the normal metal approach gradually as the impurity content is increased. The alloy with 0.2 percent of bismuth is of particular interest, because it exhibits a crossing over of the curves at a temperature below the transition point. Another interesting feature is the gradual shift with increasing percentage of bismuth of the maximum in the thermal conductivity to higher temperatures. This is, of course, what one would expect from the theory of thermal conductivity of normal metals.

10. Heat Transfer in Superconducting Alloys

by J. K. Hulm [1]

Introduction

Recent experiments [1, 2] [2] on the thermal conductivity of pure metals at liquid-helium temperatures have led to two notable conclusions: first, that in this temperature range the behavior of normal metals is in qualitative agreement with predictions of the electron theory of metals, and second, that the behavior of superconducting metals is at least roughly described by an empirical scheme in which each term in the normal heat conductivity, associated with a given transport and a given scattering mechanism, is modified in its own characteristic manner on transition to the superconducting state. It is obviously of interest to know whether these conclusions are also valid for metallic alloys, but in this question it must be borne in mind that the free electron theory of thermal conductivity in normal alloys, due to Sommerfeld and Bethe [3] and Makinson [4], only applies directly to homogeneous solid solutions, and does not allow for such complications as several phases, inhomogeneities, small grain structure, and high internal strains, which are often present in actual alloys. Unfortunately, hardly any data exist for alloy specimens in which the above complications are definitely known to have been avoided. Indeed, in the few previously reported mesaurements of the thermal conductivity of alloys at low temperatures, little information is given about the metallurgy of the specimens. These considerations led us some time ago to undertake heat-conduction measurements on carefully prepared samples of the binary system indium-thallium, which forms solid solutions from zero up to about 50 atomic percent of thallium, and has superconducting transition temperatures convenient for the liquid-helium range. The specimens were provided by J. W. Stout and L. Guttman, who have previously studied the magnetic and electrical properties of the same alloy system [5]. Thermal-conductivity measurements were made with an improved form of the differential gas-thermometer arrangement described elsewhere [2]. The present paper gives experimental data for a very uniform composition, single-crystal specimen containing 10 atomic percent of thallium, the highest composition to which the heat conduction measurements have so far been extended.

Results

Typical data obtained by Stout and Guttman (lower curves) and the author (upper curve) for the isothermal magnetic-field variation of the magnetic induction, B; the electric resistivity, ρ; and the thermal conductivity, K, of the 10 percent specimen are shown in figure 10.1. It is at once evident that the magnetic field necessary to

---

[1] Institute for the Study of Metals, University of Chicago. Chicago, Ill.

[2] Figures in brackets indicate the literature references on p. 41.

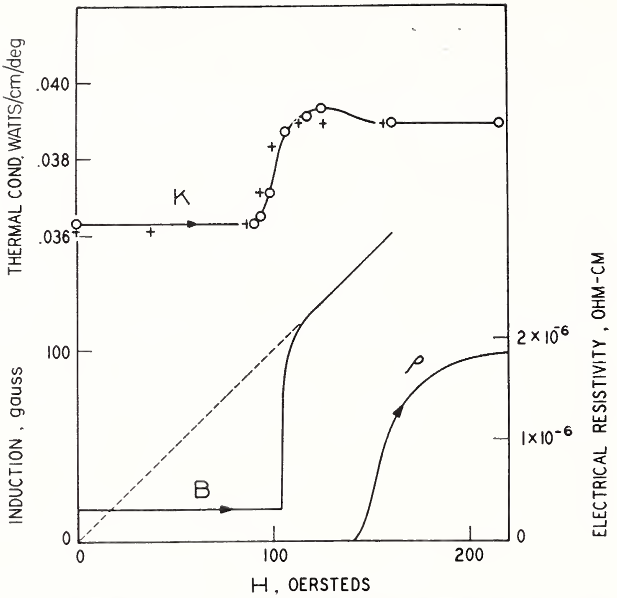

Figure 10.1. *Magnetic-field variation of magnetic induction, electric resistivity, and thermal conductivity of indium plus 10 percent of thallium at 2.6° K.*

○, Increasing field; + decreasing field.

restore the electrical resistance is considerably higher than that required for almost complete penetration of the field into the specimen, a phenomenon already well known for alloys [6]. The conclusion must be reached that although nearly all of the specimen passes from the superconducting to the normal state in the neighborhood of 100 gauss, where K and B rise steeply, the latter to the value H, a very small fraction of the whole bulk of the specimen remains superconducting at higher field strengths and provides a path of zero or low resistance for the current used in measuring ρ for applied fields up to about 220 gauss. This raises the problem of how small regions of abnormally high critical field may exist in an apparently homogeneous, strain-free, single crystal. A clue is given by the fact that the curve of thermal conductivity in figure 10.1 drops slightly as the field is increased beyond 120 gauss, before a steady value characteristic of the normal state is reached. A similar drop in K was observed in all transition curves for the 10 percent specimen, and probably indicates that the thermal conductivity of the abnormal regions decreases considerably when their superconductivity is destroyed. Such a decrease may perhaps be due to a local thallium content greater than 10 percent, the grounds for this view being, first, that the data for the main bulk of the specimen suggest that the value of K in the superconducting state, K_s, will exceed that in the normal state, K_n, for a sufficiently high thallium content (see later discussion), and second, that other workers [7, 8] have found K_s greater than K_n in certain high-concentration alloys. As small regions with greater than average thallium content would probably be overlooked in the chemical test of the homogeneity of our specimen, the presence of such regions is at least a possibility.

The temperature dependence of K_s and K_n for the 10-percent specimen is compared in figure 10.2 with that for an indium specimen containing only 0.1 percent of impurity. It should be mentioned that although the former results are assumed to apply to a homogeneous 10 percent alloy, the data was taken directly from a family of curves of the type of figure 10.1, neglecting the effect of small regions of abnormally high critical field. This may involve a error of an few percent in K at the lowest temperatures, but unfortunately the correction cannot be derived accurately from the available data.

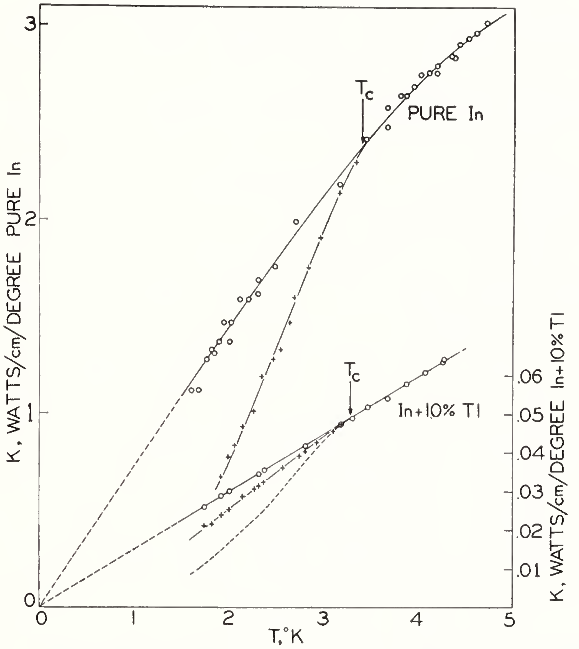

FIGURE 10.2. *Temperature variation of thermal conductivity of indium plus 10 percent of thallium and pure indium (0.1 percent of impurity) in superconducting and normal states.*

O, Normal; +, superconducting.

Discussion

According to the electron theory of metals [3, 4], the normal thermal conductivity of a single crystal of indium containing 10 percent of thallium in homogeneous solid solution is of the form

$$K_n=(L_0/\rho_0)T+aT^2 \tag{1}$$

at liquid helium temperatures. The first term on the right-hand side is the conductivity, K_{en}, due to heat transfer by electrons with scattering by impurities, L_0 being the Lorenz constant, $\frac{1}{3}(\pi k/e)^2$, and ρ_0 the residual electric resistivity. The second term is the conductivity, K_{gn}, due to heat transfer by lattice waves with scattering by electrons, 'a' being a constant of the alloy equal to 4.93 $K_\infty/\Theta^2N_a^2$, where Θ is the Debye temperature, N_a is the number of conduction electrons per atom, and K_∞ may be taken to a good approximation as the thermal conductivity of pure indium at room temperature. Of the above terms, K_{en} appears to be dominant for the 10-percent specimen, since the observed K_n in figure 10.2 is almost exactly proportional to temperature, with a coefficient, 1.49 x 10^{-2} watt cm^{-1} deg^{-2}, which is in rough agreement with the value 1.30 x 10^{-2} watt cm^{-1} deg^{-2} derived from the observed ρ_0. This conclusion is supported by the fact that estimates of the coefficient a, based on theory and on liquid-hydrogen data, both yield values close to 1 x 10^{-4} watt cm^{-1} deg^{-3}, from which K_{gn} is only about 3 percent of K_n at 4° K.

Although no detailed electronic theory of K_s has so far been proposed, we have recourse for the present discussion to an empirical scheme [2] based partly on previous experiments and partly on qualitative arguments, which assume the existence of normal and superconducting electron phases within a superconductor. The first suggestion is that K_s, like K_n, involves the sum of an electronic term, K_{es}, and a lattice term, K_{gs}. For an alloy specimen with normal terms of the type shown in eq (1), the superconducting terms are assumed to have the form

$$K_s = f(T/T_c)\cdot(L_0/\rho_0)T + h(T/T_c)\cdot aT^2, \tag{2}$$

where f and h are functions of reduced temperature, which tend to unity as the transition temperature, T_c, is approached. If the superconducting electron phase plays no part in heat transfer, either in transport or in scattering processes, it is evident that owing to the reduced number of normal electrons, f and h should be less than and greater than unity respectively in the superconducting range. Previous experiments have confirmed this view, although it must be pointed out that while f was shown to be roughly of the form $2(T/T_c)^2/1+(T/T_c)^4$ for tin and indium, the meagre available data did not lead to a definite form for h.

According to eq (1) and (2), K_{es} may be estimated for the 10-percent specimen by multiplying the observed K_n, which is very nearly equal to K_{en}, by an appropriate function f. Taking f as the ratio K_s/K_n for the pure indium specimen,[3] one obtains for K_{es} the lowest, dotted curve in figure 10.2. This curve lies well below the observed superconducting curve for the 10-percent alloy, indicating that besides K_{es}, K_s contains an extra conductivity component, which increases steadily as the temperature is reduced. It seems reasonable to identify this component with the lattice term, K_{gs}, in which case the ratio K_{gs}/K_{gn} or h varies roughly as $(T/T_c)^{-5}$. Although the exponent of T/T_c is somewhat sensitive to the value of a, which is only roughly known, there seems little doubt that K_{gs}/K_{gn} exceeds unity, in agreement with previous experiments. As already pointed out [2], this is probably at least partly due to the fact that superconducting electrons do not scatter the lattice waves.

Finally, it should be noted that $(K_s - K_{es})$ for the 10-percent specimen is by no means definitely known to be of lattice origin. As small regions of abnormally high critical field are present in the specimen, this extra component in K_s may perhaps be of the circula-

---

[3] For the pure indium specimen, $K_n = K_{en}$, with dominant impurity scattering; the slight curvature of K_n in the upper part of the temperature range is due to a small lattice vibration scattering term which does not, however, affect the present considerations.

tion type proposed by Mendelssohn and Olsen [8]. In view of these possibilities, it is worth pointing out that lattice and circulation components should react differently to substantial changes in the total thallium content of the specimen. Assuming that h only depends upon T/T_c, it is evident that the lattice component K_{gs} or haT^2 is not affected, to the first order, by changes in the concentration of thallium. In the circulation process, however, as the fraction of the specimen volume with abnormally high critical fields increases rapidly with increasing thallium content [5], a circulation component of K_s should also vary rapidly during such a change. It is hoped that owing to this difference in behavior, experiments on specimens with thallium content greater than 10 percent will reveal the true nature of the (K_s-K_{es}) term.

References

[1] W. J. de Haas and A. Rademakers, Physica **7,** 992 (1940); A. Rademakers, Physica **15,** 849 (1949).
[2] J. K. Hulm, Proc. Roy. Soc. [A] **204,** 97 (1950).
[3] A. Sommerfeld and H. Bethe, Handbuch der Physik Springer, Berlin, 2d ed. **24,** pt. 2, p. 545, 1933).
[4] R. E. B. Makinson, Proc. Camb. Phil Soc. **34,** 474 (1938).
[5] J. W. Stout and L. Guttman, page 51 in these proceedings.
[6] D. Shoenberg, Superconductivity, p. 81 (Camb. Univ. Press, 1938).
[7] W. J. de Haas, and H. Bremmer, Commun. Kamerlingh Onnes Lab., Univ. Leiden, 220 c (1932), 243 c (1936).
[8] K. Mendelssohn and J. L. Olsen, Proc. Phys. Soc. [A] **63,** 2 (1950).

11. Experiments on the Magnetic Transition from the Superconducting State to the Normal State[1]

by M. P. Garfunkel and B. Serin [2] [3]

The critical magnetic field for the transition from the superconducting state to the normal state is usually defined in terms of the properties of an ideal cylinder, infinite in length and of large diameter, placed in a longitudinal, uniform magnetic field. All actual experiments, of course, are performed with finite cylinders; where, because of the nonzero demagnetization of the ends, the transition is initiated with the formation of an intermediate state at the ends of the cylinder. Thus, the transition of the bulk of the cylinder to the final normal phase, can take place by growth from an already established nucleus of that phase present at the ends of the sample.

The experiment to be described was an investigation into normal-superconducting-state transition under such conditions that the transition occurred without the creation of an intermediate state. This was accomplished by the application of a small, constant, uniform, longitudinal magnetic field, h, over a small central section of a long cylinder, while the sample as a whole was carried through the transition by the application of an additional uniform, longitudinal magnetic field, H, over its entire length.

The samples were made from Johnson-Matthey tin, cast in glass tubes 0.15 cm in diameter and 8 cm long. They were grown into single crystals and left in the glass. Field h was provided by a solenoid wound on the glass tube. The coil had 560 turns over a length of 5 cm, with taps every centimeter. This arrangement permitted one to apply field h to different parts of the sample and to varying lengths of sample. Field H was produced by a solenoid on the outside of the helium flask. The earth's magnetic field was cancelled by Helmholtz coils to give a net field over the sample of less than 0.02 oersted.

The state of the sample in any given magnetic field was determined by measuring its magnetic susceptibility by a method similar to the method developed by Shoenberg.[4] A coil was lifted clear of the sample and then permitted to drop over it. The electromotive force induced in the coil was proportional to the magnetic moment of the sample. This electromotive force was detected by a photoelectric cell galvanometer amplifier.

The usual type of longitudinal magnetic field transition ($h=0$) for a sample is shown in figure 11.1 (a). The transition is quite sharp, having a total width of about 0.2 oersted. There is no detectable hysteresis in this transition.

No appreciable change is made in the transition by the application, in the direction to add to H, of a constant magnetic field, h, of 1

---

[1] This work has been supported by the Office of Naval Research, the Rutgers University Research Council, and the Radio Corporation of America.

[2] Physics Department, Rutgers University, New Brunswick, N. J.

[3] Presented by B. Serin.

[4] Shoenberg, Phys. Soc. London, Report of an international conference on fundamental particles and low temperatures, **II**, Low temperatures, p. 85 (1946).

oersted over a 1-cm length at the center of the sample. The transition to the normal state occurs very close to the same value of field H as in the case $h=0$. There is no indication that the central section goes into the normal state when the total field over that portion exceeds the critical field.

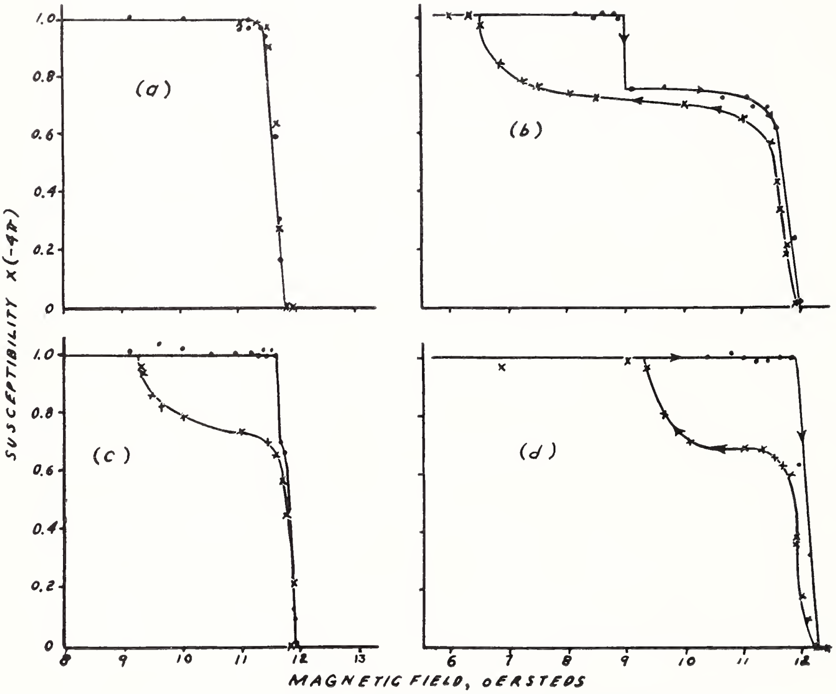

FIGURE 11.1. *Curves of susceptibility versus magnetic field.*

a, Field in sample coil=0; b, field in sample coil 2=5.40 oersteds; c, field in sample coil 2=2.70 oersteds; d, field in sample coil 3=2.70 oersteds.

NOTE ADDED MAY 26, 1951

The remaining parts of figure 11.1 show the results obtained with larger values of the magnetic field, h, in such a direction as to add to H. In figure 11.1 (b), $h=5.40$ oersteds. The dotted points were observed with H increasing and the crosses with H decreasing. We note in figure 11.1 (b), that when H is increasing, the field over the central section reaches 14.4 oersteds (even though the critical field for the sample is 11.8 oersteds from figure 11.1 (a), before that section makes an abrupt transition into the normal state. The parts of the sample over which $h=0$ remain in the superconducting state until field H reaches the critical value, and then the whole sample passes into the normal state. On decreasing H, the sample, with the exception of the central section, returns to the superconducting state when H reaches the critical value. The transition of the central section, however, now is delayed until the total field over that section is reduced to the critical value. Thus, there is an appreciable hysteresis in the transition. Figure 11.1 (c) and 11.1 (d) show the transitions with a smaller value of the magnetic field, h, applied over different parts of the sample.

It has proved possible to explain these results in terms of the surface energy at the boundary between normal-conducting and superconducting metal and detailed considerations of the thermodynamics of the growth of the final phase.

12. New Experiments on the Superconductivity of Metal-Layers Condensed at Low Temperatures

by Rudolf Hilsch [1]

Abstract

The transition temperatures of pure superconducting metals, if condensed at helium-temperatures from the vapor-state, were found to be quite different from the well known values of the normal bulk metals. So far the effect for Sn, In, Tl, Al, Pb, and Hg has been studied. The deviations are of the order of one degree Kelvin and seem to be in connection with the Debye characteristic temperatures. In all cases the normal transition point appears when the condensed layers are annealed once to room-temperature. Lattice distortions are to be responsible for the abnormal values. The influence of the condensation temperature on the transition temperature has been specially measured for layers of tin.

A new method of producing unknown alloys has been worked out by condensation of two different metals at the same time. The system tin-copper has been investigated in this new atomic-disperse state. A Transition temperature of 7° K can be reached. The superconducting properties of a number of systems show a remarkable effect. The normal transition point of 3.7° K for tin is for instance reduced to 1.5° K if only 10^{-4} chromium is added by simultaneous condensation at low temperatures.

This method results in a system of substances in a quenched state and is applicable in numerous cases. So it was for instance possible to realize a content of 10 percent "Farbzentren" in a system like KCl+K.

---

[1] Physikalisches Institut der Universität Erlangen, Erlangen, Germany.

13. Kinetics of the Superconducting Phase Transition

by T. E. Faber [1] [2]

This work is principally concerned with two macroscopic aspects of the process whereby a rod of tin in a longitudinal magnetic field becomes superconducting. The transition involves the growth of one phase at the expense of the other, and the two problems are, first, to decide what governs the field strength at which this growth is just able to start, and, second, in what direction and how fast it then proceeds. The specimens used are about 20 cm long and between 1 and 4 mm in diameter. They are surrounded by a number of regularly spaced coils, some of which are search coils used to follow the phase growth through the flux changes that accompany it. The rest are little solenoids with which the field strength can be varied locally if desired.

These specimens all "supercool", that is, the transition does not start even when the field is reduced some way below the critical value, H_c. It can be shown, by reducing the field locally rather than over the whole specimen, that different regions will stand quite different amounts of supercooling. Measurements have been made on short sections of each of several specimens of the limiting field (H_L) at which the supercooling does eventually break down, and typical results are presented in figure 13.1. Here the quantity $(H_c^2-H_L^2)/H_c^2$ (denoted by ϕ) is plotted against temperature for three sections of a single specimen. Values of ϕ were reproducible in separate experiments, between which the specimen had warmed to room temperature.

It has been suggested [3] that supercooling is due to the difficulty of forming a small nucleus of the superconducting phase in a normal matrix owing to the existence of an interphase surface tension. Now in fact, if one accepts for the magnitude of this surface tension the value suggested by intermediate state measurements,[4] it can be shown that even in a highly supercooled specimen the formation of such a nucleus should be so difficult as to be impossible. It would demand an increase in the total Gibb's function of the order of 10^8 kT. It therefore seems necessary to assume that there are flaws in the specimens where the surface tension is reduced, probably to such an extent that it becomes negative. Here there will exist seeds of the superconducting phase, which, when the field is low enough, expand and infect the surrounding metal where the surface tension is large. Analysis of this model leads to the equation

$$\phi=\frac{\Delta}{Z}+n, \tag{1}$$

where $\Delta=8\pi/H_c^2\times$(surface tension), Z is a length characteristic of the size of the particular flaw concerned, and n a factor characteristic of its shape.

---

[1] Royal Society Mond Laboratory, Cambridge, England.
[2] Presented by D. Shoenberg.
[3] H. London, Proc. Roy. Soc. [A] **152,** 650 (1935).
[4] M. Désirant and D. Shoenberg, Proc. Roy. Soc. [A] **194,** 63 (1948), and E. R. Andrew and J. M. Lock, Proc. Phys. Soc. [A] **63,** 13 (1950).

According to this theory the three graphs in figure 13.1 may be interpreted as being due to three separate flaws of different size and shape. The temperature variation of ϕ, which is much the same in all cases, is controlled by the temperature variation of Δ. As this known (see below), it is possible to check eq (1) by plotting ϕ against Δ, with temperature as a variable parameter. Figure 13.2 demonstrates that the agreement is satisfactory. The values deduced for Z and n show that the flaws are from 1 to 15×10^{-4} cm in width and are probably rather elongated.

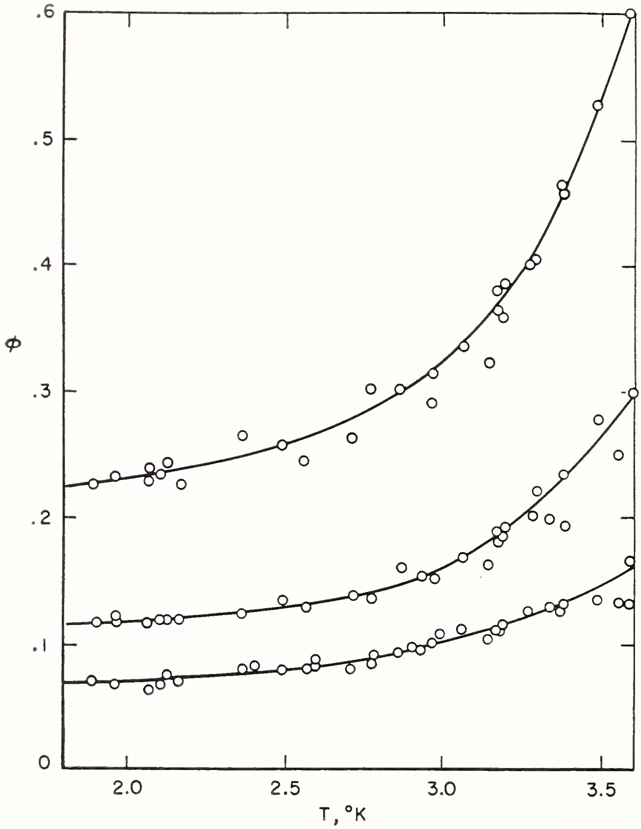

Figure 13.1.

In order to study the problem of phase growth the transition is deliberately set off at one end of a specimen that is only slightly supercooled, and the voltage pulses that are produced in the search coils, one after another down the specimen, are then recorded photographically. Each pulse is found to take the form of an initial sharp peak followed by a long, irregular tail, i. e., a quite small fraction of the total flux is expelled promptly, the rest taking a matter of minutes to escape. The reason for this appears to be that the superconducting phase propagates most readily along the surface, and it therefore tends to form a superconducting sheath that practically locks in the flux in the interior. The thickness of the sheath can be gaged from the area of the peak in the voltage pulses, and it is found to be proportional to $(H_c - H)^{-1}$. In addition, from the time separating the pulses from two search-coils, one can determine the velocity of forward growth of this sheath as it establishes itself. This velocity v is of the order of centimeters per second and is proportional to $(H_c - H)^2$ (fig. 13.3).

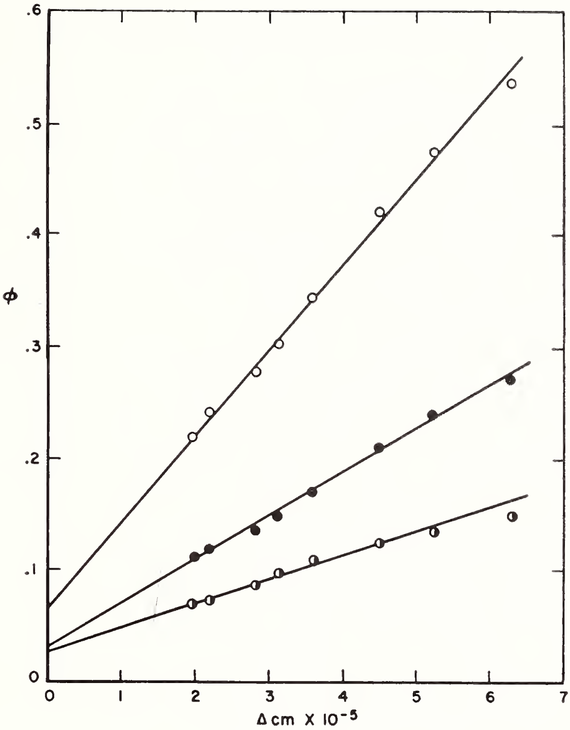

FIGURE 13.2.

Eddy currents set up in the normal metal have been suggested as a factor slowing down the rate of phase propagation (see, in particular, Pippard),[5] and they will account for the present results provided that surface tension is considered as well. Briefly, the supercooled transition makes available a certain amount of free energy per unit volume, and this can be equated to the sum of the increase in surface free energy and the energy dissipated by eddy currents, the latter depending on v. Thus, for a superconducting layer at the surface of thickness d growing forward with velocity v, we have

$$\frac{H_c^2 - H^2}{8\pi} \cdot d = \frac{H_c^2}{8\pi} \cdot \Delta + C \cdot H^2 d^2 \sigma v, \tag{2}$$

where σ is the conductivity of the normal metal, and C is a dimensionless constant whose magnitude can be roughly estimated. There is

---

[5] A. B. Pippard, Phil Mag. **41**, 243 (1950).

reason to suppose that d will adjust itself to make v a maximum, in which case

$$d=\Delta\left(\frac{H_c-H}{H_c}\right)^{-1}, \tag{3}$$

and

$$v=\frac{8\pi C}{\sigma\Delta}\left(\frac{H_c-H}{H_c}\right)^2. \tag{4}$$

It will be seen that this theory predicts the observed variation of both d and v with (H_c-H). Further, it shows how information concerning Δ can be extracted from the experiments; owing to the uncertainty in C and the difficulty of measuring d the magnitude of Δ is left in some doubt, but its temperature variation can be fairly reliably derived. This information, which is in fair agreement with the intermediate state results, has been used in the plotting of figure 13.2.

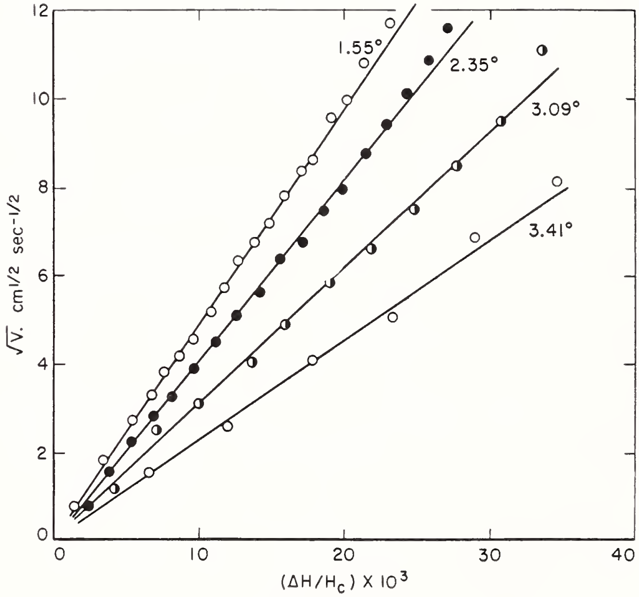

FIGURE 13.3.

However, doubt has recently been cast on the theory by preliminary experiments on impure specimens, which show that v varies more slowly with $1/\sigma$ than eq (4) suggests. Evidently the treatment requires modification, perhaps by a consideration of mean free path effects.

14. Superconducting Properties of Indium-Thallium Alloys

by J. W. Stout and Lester Guttman [1]

Previous work on the superconducting properties of alloys [1] [2] has indicated that, in contrast to the behavior of pure metals, alloy specimens are characterized by an absence of the Meissner effect [2], broad transitions extending over a range of temperature in zero field, and at constant temperature a broad range of field strength over which the magnetic flux penetrates into the specimen. Furthermore, the magnetic field necessary to restore electric resistance is greater, often by as much as a factor of 10, than the field at which substantially all of the flux has penetrated into the specimen. These properties have been explained [1] by assuming that in an alloy there is a sponge structure so that different parts of a specimen have different critical temperatures and critical field strengths. Upon the application of a magnetic field, at constant temperature, the superconductivity of parts of the specimen is assumed to be destroyed first, leaving a network of fine filaments of superconducting material. Because of the finite penetration depth the critical field of a very small filament is higher than that of a large piece and so, if the filaments are fine enough and numerous enough, the field necessary to restore electric resistance may be considerably higher than that needed to obtain practically complete penetration of the flux.

In an alloy consisting of two or more solid phases one would expect that the physical and chemical inhomogeneities would account for a variation in superconducting properties throughout the specimen. However, for a pure, single-phase, intermetallic compound there is no evident reason why the specimen cannot be completely homogeneous. Shoenberg [3] has found that a carefully prepared specimen of the compound Au_2Bi exhibits superconducting behavior similar to that of a pure metal, and in recent experiments [4] on the compound MgTl we have noticed a similar behavior. A physically and chemically homogeneous metallic solid solution would be disordered on an atomic scale, but on a scale comparable to that of penetration depths (10^{-5} cm) it would be uniform. In order to investigate the behavior of a solid solution we chose the system indium-thallium, which was thought at the time this investigation was begun to have a continuous range of solid solutions from pure indium to 40 atom percent thallium [5]. This system has the advantage that the solutions melt at a convenient temperature, so single crystals can readily be grown and both components are "soft" superconductors, exhibiting ideal behavior. In an X-ray examination of specimens in the supposedly continuous solid-solution range one of us [6] found that there occurs a transformation from a face-centered tetragonal to a face-centered cubic structure. However, there is no evident separation into two phases of different composition upon passing through the transforma-

---

[1] Institute for the Study of Metals, University of Chicago, Chicago, Ill.

[2] Figures in brackets indicate the literature references on p. 60.

tion, and the transition is probably one of the second order [7]. The phase diagram as given by Guttman [6a], is reproduced in figure 14.1.

The samples used in this work were in the range from 0 to 20 percent thallium and consequently are face-centered tetragonal at low temperatures. The single-crystal samples were in the form of cylinders 6 mm in diameter and 15 cm long. They were grown from the melt in precision-bore 6.3-mm-inside-diameter Pyrex tubing. An alloy of the appropriate composition was first made by melting the components together under an atmosphere of nitrogen with vigorous stirring and then casting the liquid in a graphite mold. The cast sample, usually about 19 mm in diameter, was then swaged down

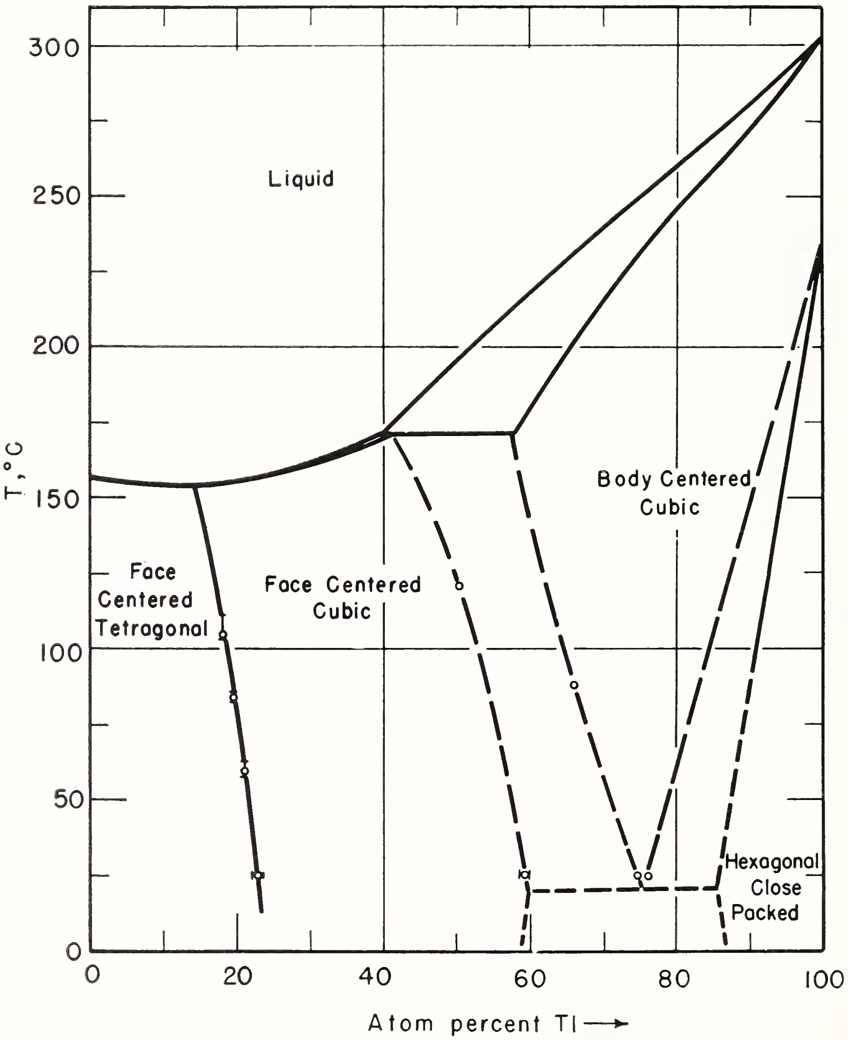

FIGURE 14.1. *Phase diagram of indium-thallium system.*

until it would fit into the glass crystal-growing tubes. The glass tubes were lubricated by washing them with a solution containing 0.01 percent of mineral oil in carbon tetrachloride, draining off the solution, and then evaporating any remaining solvent under vacuum. This procedure left a very thin film of oil on the inside of the glass, which prevented sticking of the metal. If too much oil remains, small bubbles appear on the surface of the specimens. The swaged samples were inserted in the glass tubes, which were then evacuated to 10^{-5} mm mercury and sealed off. The tubes were placed in the single-crystal furnace, which was heated to a temperature sufficient to melt the samples and controlled at this temperature. The sample tubes were then lowered, at a rate of 13 mm/hr, through the temperature gradient of the furnace, so that the solid grew from the bottom. The crystals could usually be removed from the tubes by gentle tapping, but as this method produced deformation, some samples were removed by dissolving the tubes in a concentrated HF solution, which did not appreciably attack the alloys. The samples, as removed from the tubes, were about 30 cm long. A region 15 cm long, of a single crystallographic orientation, was cut from each specimen by a saw consisting of a glass string passing through a solution of concentrated nitric acid and over the sample. This saw cuts by the chemical action of the nitric acid and therefore does not deform the single crystal. The specimens employed for the superconductivity measurements were essentially single crystals, although some had small regions where slip had occurred in handling. The 20 percent thallium specimen had transformed from cubic to tetragonal during cooling to room temperature after solidification, and there were transformation markings on its surface similar to but on a much large scale than those described by Guttman [6a] for polycrystalline samples. The sample was probably a single crystal when it solidified from the melt, but upon passing through the transformation it broke down into a set of tetragonal crystals having fixed orentations [6b] relative to the original cubic axes. The energy of the interfaces between these various orientations of the tetragonal crystals, as is the case with boundaries between crystallographic twins, is apparently very small compared to that of ordinary grain boundaries in a polycrystalline specimen, and we observed nothing in the superconducting properties that we could ascribe to the presence of these boundaries.

Samples for analysis were taken from the regions near the cut ends of the specimen. The results [3] are listed in table 14.1.

Table 14.1. *Composition of indium-thallium single-crystal specimens.*

Atom percent thallium		
Nominal	Top	Bottom
5	5.04	5.05
10	10.07	10.07
15	14.91	15.26
20	19.35	20.43

The 5- and 10-percent specimens are uniform within the accuracy of the analysis, but the other two are definitely richer in thallium at

---

[3] We are indebted to R. E. Fryxell for these analyses.

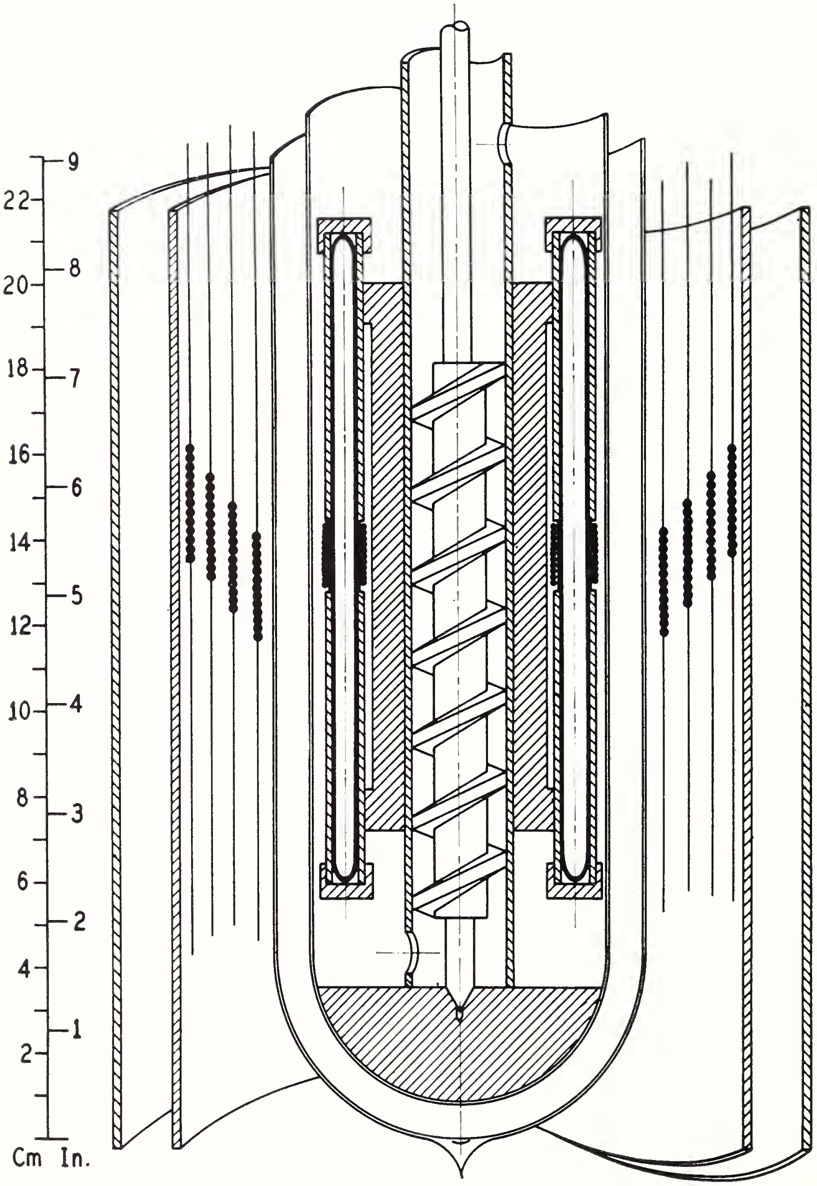

Figure 14.2. *Apparatus for induction measurements of superconductors.*

the bottom end. The reason for this may be seen by reference to figure 14.1. For the 5- and 10-percent specimens the liquid is richer in thallium than the solid in equilibrium with it. The first solid to freeze at the bottom of the tube leaves behind thallium-rich liquid. As the crystallization proceeds, a steady state will be reached where the solid freezing out has the over-all composition of the original melt, and there is a composition gradient in the liquid from the thallium-rich material in contact with the solid to the original liquid composition. As the more dense liquid is below, it is stable against convection, and the length of the gradient zone is determined by the rate of diffusion in the liquid and the rate of lowering of the tube. For the 15- and 20-percent specimens, on the other hand, the situation is reversed. Convection therefore continually stirs up the liquid, and a steady state cannot be maintained. It would be possible to grow single crystals from the top down, provided there were a reservoir of material to keep the liquid forced up against the solid. In this case it should be possible to set up a steady state undisturbed by convection and produce single crystals of very uniform composition in the range to the right of the melting-point minimum in figure 14.1.

The apparatus used for the magnetic-induction measurements is shown in figure 14.2. The samples were held in Lucite tubes, on each of which was wound a two-layer coil, 16 mm long, of about 300 turns of No. 40 Formex insulated copper wire. The Lucite tubes were turned to a thickness of 0.25 mm beneath the coils in order to minimize leakage flux. Five specimen holders, containing the four samples described above and a single crystal of pure indium (about 99.9% purity), were mounted symmetrically about a central Micarta tube, which served as a housing for the stirrer, a screw driven by a variable-speed motor. Slots were cut in the Lucite tubes to insure

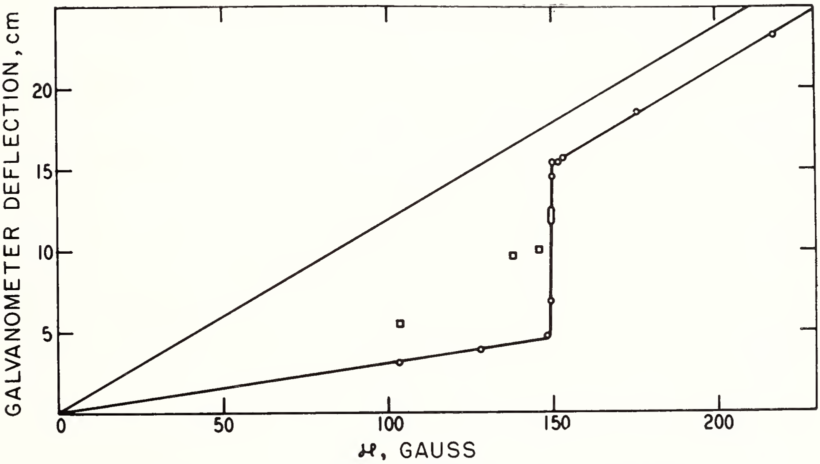

FIGURE 14.3. *Galvanometer deflection versus applied field.*

5% Tl, 95% In; T=2.737° K; 82% Meissner effect.

contact between the samples and the liquid-helium bath. A uniform longitudinal magnetic field was provided by a solenoid mounted in the nitrogen bath surrounding the helium Dewar. The solenoid consisted of four layers, each 40 cm. long, of No. 16 Formex insulated copper wire, each layer being wound in an accurately turned groove on a Micarta tube. The precision of the machining was such that the field could be calculated to within 0.1 percent from the dimensions of the solenoid and the current.

The coils on the Lucite sample holders were connected through a selector switch to a ballistic galvanometer. The procedure of measurement was to change the magnetic field rapidly and to observe the galvanometer deflection corresponding to the change in magnetic induction through the coils. A typical series of data is shown in figure 14.3 for the 5 percent specimen and in figure 14.4 for the 20-percent specimen. When the sample is completely superconducting the galvanometer deflection is small and is due to the leakage flux between the sample and the coil. As the magnetic field is increased beyond the critical field the flux penetrates into the sample with a sudden increase in galvanometer deflection. In figures 14.3 and 14.4 the straight line through the origin represents the galvanometer deflection for a sample of unit permeability (above the zero-field

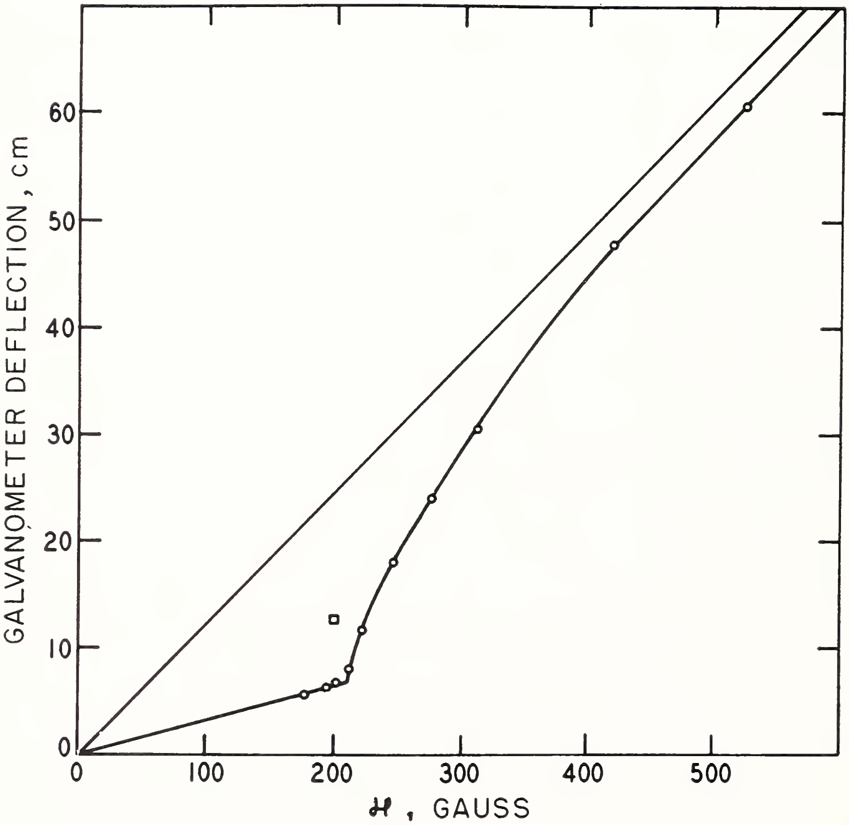

FIGURE 14.4. *Galvanometer deflection versus applied field.*
20% Tl, 80% In; T=1.286° K; H_c=211.0 gauss; 81% Meissner effect.

superconducting transition temperature). At high fields the points for the galvanometer deflection on a superconducting specimen lie on a parallel line displaced downward by an amount corresponding to the flux remaining in the superconducting specimen in zero field. It was found that the flux change in going from field zero to field $\boldsymbol{H}$ was the same (for a nonvirgin sample) as for the reverse step, and if the change was made in several steps, the sum of the galvanometer deflections equaled that for a single total change. The points indicated by circles are obtained by applying a field equal to the abscissa of the point and then measuring the deflection when the field is quickly reduced to zero. The smoothness of the curve through these points is evidence that once a large field is applied, the flux trapped in zero field remains constant. The points indicated by squares in figures 14.3 and 14.4, however, are evidence for hysteresis of the following kind: These data were obtained by increasing the applied field to a value where penetration was complete, then slowly reducing to an intermediate value, and finally observing the galvanometer deflection obtained when the intermediate field was removed by interrupting the current. The flux present at a given field is greater if it is reached from high fields in this way, than if it is approached from zero field.

From data such as those in figures 14.3 and 14.4 one can calculate the flux of induction, B, through the sample. In figures 14.5 and 14.6. are plotted values of the induction divided by the critical field, $\boldsymbol{H}_c$, as a function of the ratio of the applied field to the critical field. Such a plot was found to vary only slowly as the temperature (and consequently $\boldsymbol{H}_c$) changed, so it could be used to compare the behavior of different specimens of the same alloy. The critical field is taken as that where flux penetration begins.

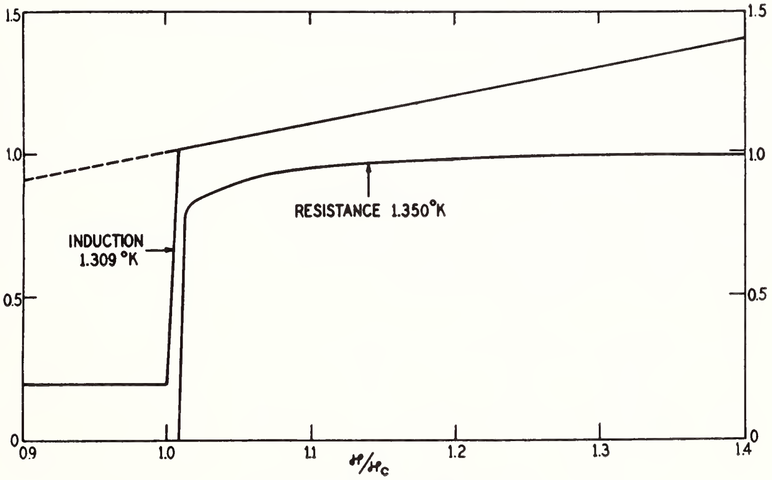

FIGURE 14.5. *B-H curves.*
5% Tl, 95% In.

Resistance measurements were made on the same single-crystal samples used for the induction measurements. For this purpose, current and potential contacts were made with small split copper rings held onto the samples with brass screws kept under tension by spring washers of phosphor bronze. The resistance transition curves

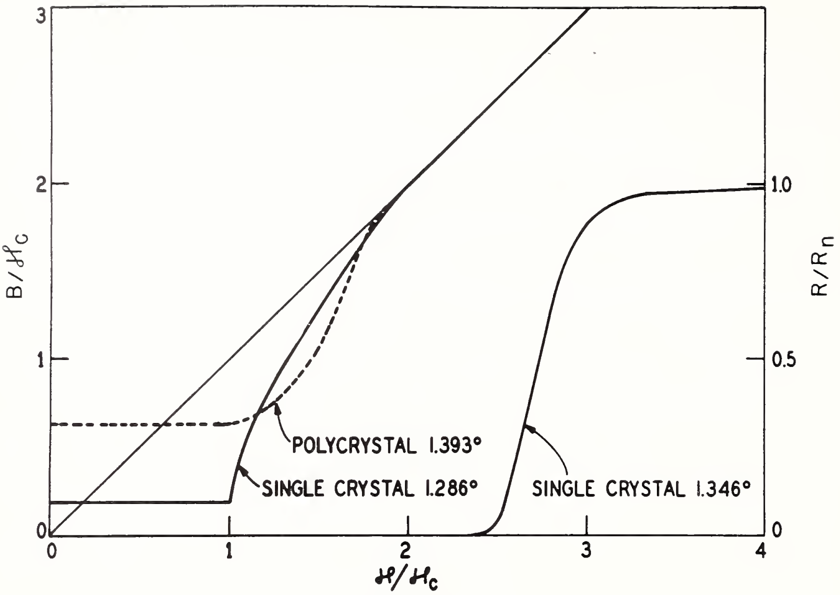

FIGURE 14.6. *B–H curves.*
20% Tl, 80% In.

of the five specimens in zero field are shown in figure 14.7. The transition is quite sharp, and there is only a slight increase in breadth in going from the pure indium sample to the 20-percent alloy. The appearance of resistance upon the application of a magnetic field was measured at various temperatures for all the specimens. Typical data are shown in figures 14.5 and 14.6. For the 5-percent specimen the resistance rose sharply at a field about 1 percent higher than that at which flux penetration began. For the 20-percent specimen, on the other hand, resistance reappeared at a field over twice that of the

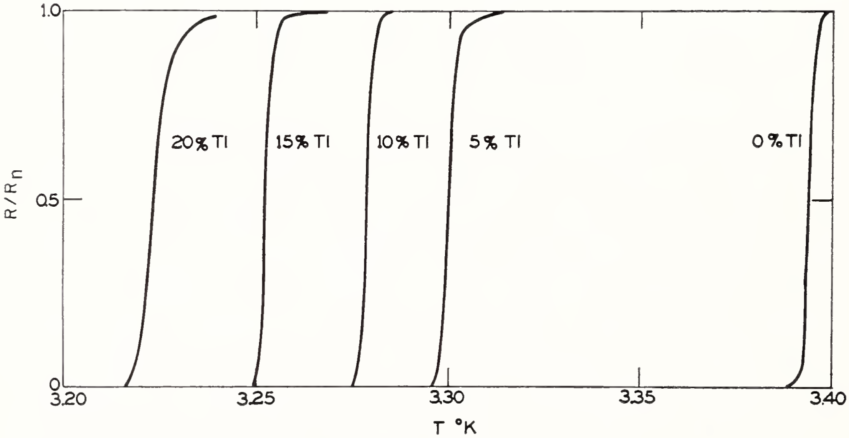

FIGURE 14.7. *Resistance transition curves of indium-thallium alloys in zero magnetic field.*

beginning of flux penetration. The behavior of the 10- and 15-percent specimens was intermediate between the 5- and 20-percent specimens.

It was thought that the broadness of the magnetic transition in the 15- and 20-percent specimens might be due to the composition gradients shown in table 14.1, and consequently two new specimens of these compositions were prepared. These were polycrystalline samples prepared by strain-annealing of cast samples that had previously been reduced in area by a factor of nine by swaging. This technique insures very good chemical homogeneity, as verified by analysis. During the annealing the crystal grains grew to an average size of from 1 to 2 mm. The results of the measurement on the 20-percent sample are shown in figure 14.6 (dashed curve). The principal effect is an increase in the amount of trapped flux (reduced Meissner effect), and although the shape of the transition curve is somewhat different, its breadth is about the same.

The critical magnetic fields corresponding to the beginning of flux penetration were fitted by least-squares analysis to equations of the form $\boldsymbol{H}_c=\boldsymbol{H}_0(1-T^2/T_0^2)$, where $\boldsymbol{H}_0$ is the critical field at $T=0$ and T_0 is the critical temperature at $\boldsymbol{H}=0$. The observed critical fields deviated significantly from the simple parabolic relationship, particularly at the higher temperatures, and the extrapolation of curves through the actual data to $\boldsymbol{H}=0$ gave values of T_0 in good agreement with those shown by the resistance measurements (fig. 14.7). However, the assumption of the parabolic relationship permits a calculation of the coefficient, γ, of the linear term in the heat capacity of the normal metal, which is ascribed to the electrons. The values of $\boldsymbol{H}_0$ and T_0 from the least-squares equations and the maximum deviations from the actual data are listed in table 14.2. Also presented are the values of γ calculated from the relation $\gamma=\boldsymbol{H}_0^2/2\pi\ T_0^2$.

TABLE 14.2. *Values of $\boldsymbol{H}_0$ and T_0 for indium-thallium alloys for best fit to expressions $\boldsymbol{H}_c=\boldsymbol{H}_0(1-T^2/T_0^2)$*

Composition (atom percent thallium)	$\boldsymbol{H}_0$	T_0	Maximum deviation	γ
	Gauss	°*K*	*Gauss*	*cal deg*$^{-2}$ *mole*$^{-1}$
0	285. 4	3. 376	1. 8	4.3×10^{-4}
5	277. 4	3. 283	2. 3	4. 3
10	285. 3	3. 257	1. 7	4. 6
15	281. 7	3. 254	1. 5	4. 6
20	253. 0	3. 225	1. 8	3. 8

The present work shows that for carefully prepared single-crystal specimens of alloys consisting of solid solutions of up to 20 atom percent of thallium in indium the Meissner effect is large (about 85% expulsion of flux), and the resistance transition curve in zero field is sharp. In these respects the alloys behave like pure metals. For the 5 percent alloy the penetration of flux on the application of a magnetic field occurs at a sharply defined field, and the restoration of resistance appears at almost the same field strength. As the thallium content increases to 20 percent, the penetration of the magnetic field takes place over a gradually increasing range, and the ratio of the field corresponding to the appearance of resistance to that for the beginning of flux penetration continually increases.

---

[1] (a) K. Mendelssohn, Rep. Prog. Phys. **10,** 358 (1946); (b) D. Shoenberg, Superconductivity, chap. VI (Cambridge University Press, London, 1938).
[2] W. Meissner and R. Ochsenfeld, Naturwiss. **21,** 787 (1933).
[3] D. Shoenberg, Nature **142,** 874 (1938).
[4] L. Guttman and J. W. Stout, These Proceedings, page 65.
[5] M. Hansen, Aufbau der Zweistofflegierungen, p. 827 (J. Springer, Berlin 1936).
[6] (a) L. Guttman, J. Metals (Trans. AIMME) **188,** 1472–77 (1950); (b) J. S. Bowles, C. S. Barrett, and L. Guttman, 1478–85.
[7] J. W. Stout, Phys. Rev. **74,** 605 (1948).

15. Investigation of Superconductivity in Lead Compounds, Gold Alloys, and Molybdenum Carbide

by R. P. Hudson and K. Lark-Horovitz[1]

In 1933 Meissner, Franz, and Westerhoff[2] made electric-resistivity measurements on lead sulfide down to 1.3°K and concluded that the very pure substance is a semiconductor, whereas the occasional appearance of superconductivity in specimens showing a metallic characteristic must be due to small amounts of excess lead. Dunaev and Maslakovitz[3] have worked with specimens containing small amounts of lead impurity (carrier concentration of the order $10^{19}/\text{cm}^3$) and find a metallic behavior below 450° C but no superconductivity down to 2.15°K.

Quite recently Darby, Hatton, and Rollin[4] reported superconductivity in PbS, PbSe, and PbTe all at about 5°K, as measured by a magnetic method. The materials were prepared by fusion together of the constituents in a vacuum; no X-ray investigation was made, apparently, to look for excess lead. The value 5°K is most interesting, being relatively far removed from the normal lead transition temperature of 7.3°K.

It is now generally accepted that chemically very pure lead sulfide behaves as a semiconductor. If it should become superconducting at low temperatures, this would be the only known case of such behavior, and would be of great interest in view of the present picture of superconductivity being due to some kind of rearrangement of electrons at the surface of the Fermi sphere.[5]

We have investigated the problem, using the ballistic-throw magnetic method of detection; this enables one to distinguish most readily between a bulk effect and an impurity effect. The specimen under investigation is enclosed in the bulb of a gas thermometer, which is surrounded by a vacuum case immersed in a bath of liquid helium. It was hoped to perhaps reproduce the results of Darby, et al. and then to show that the specimens were impure, but we were unable to obtain a 5-deg transition, and the results are essentially a confirmation of Meissner's work.

Pure lead sulfide may be prepared in the form of a fine powder by precipitation from solutions of, for example, lead acetate and sodium sulfide. Care must be taken in the method of fusing together lead and sulfur, for the reaction is strongly exothermic and some of the sulfur is vaporized. This difficulty may be overcome by heating the mixture in a graphite crucible inside an evacuated, sealed-off quartz tube. After the reaction has taken place, the temperature of the furnace is raised to the melting point of the sulfide (1,120°C) and held there for a time before cooling again. Ingots may also be pre-

---

[1] Department of Physics, Purdue University, Lafayette, Ind.

[2] W. Meissner, H. Franz, and H. Westerhoff, Ann. Physik **17**, 593 (1933).

[3] U. A. Dunaev and U. P. Maslakovitz, J. Theoret. Exptl. Phys. (USSR) **17**, 901 (1947).

[4] J. Darby, J. Hatton, and B. V. Rollin, Proc. Phys. Soc. [A] **63**, 1181 (1950).

[5] H. Fröhlich, Phys. Rev. **79**, 855 (1950).

pared by using the precipitated powder instead of the lead-sulfur mixture.

We have made measurements on ingots prepared by fusion and on the precipitated powder both finely divided and sintered. In most cases no transition could be observed down to 1.3°K, and the X-ray photographs contained only PbS lines. In a few specimens a very small (partial volume) effect was found at 7.3°K, the normal lead transition temperature, and the X-ray patterns for these specimens included a very weak extra line, presumably due to excess lead.

Crystals of natural lead sulfide (galena) and of the pure commercial product also gave negative results. A fusion sample of lead telluride became superconducting at 7.3°K, the magnitude of the effect indicating that it was confined to a small fraction of the total volume of the specimen, and the presence of lead was confirmed by X-ray. A single crystal of lead telluride (kindly supplied by R. Smith of T. R. E., Malvern) showed no transition down to 1.3° K.

These experiments, in essentially reproducing Meissner's results—and extending them in the case of lead telluride—strongly suggest that these lead compounds are not superconductors. We feel that the results of Darby, et al. may be explained by the presence of excess lead in their specimens (a possibility admitted by the authors) as their transition temperatures and critical field curves are nearly the same for the three different compounds. A few percent of excess lead could easily form a superconducting network of lead veins that would give an apparently complete volume effect,[6] and the stated procedure of rapidly cooling the melt to room temperature might result in internal strains sufficient to alter the transition temperature appreciably. Alternatively, one might suspect a consistent error in their temperature measurement, details of which are not given.

Fröhlich (see footnote 5) has suggested that gold-palladium and gold-platinum alloys containing more than 60 atomic percent of gold might become superconducting. The aim is to form an alloy between a monovalent metal and a transition metal in such a way that most of the electrons of the monovalent metal will be used to fill up the incomplete shell of the transition metal. The theory indicates that to make a normal metal superconducting, one should reduce the number of free electrons per atom, if this can be done without greatly changing other parameters.

We have investigated specimens of the following compositions, with negative results down to 1.3°K:

Au	Pd	Pt
%	%	%
60	40	------
70	30	------
80	20	------
85	------	15

Meissner [7] reported superconductivity in molybdenum carbide (Mo_2C) measured by the electrical method, the transition being considerably extended, i. e., between 2.5° and 3.1°K. We investigated

---

[6] R. P. Hudson, Phys. Rev. **79**, 883 (1950).

[7] W. Meissner, Z. Physik **65**, 45 (1930).

a specimen of Mo_2C by the electrical method from room temperature down to 1.3°K and by the magnetic method between 4.2° and 1.3°K, finding no transition. On a suggestion of J. K. Hulm we extended the magnetic measurements above 4.2°K and found a small (partial volume) effect spread out between 4.6° and 5.0°K. This transition was presumably obscured in our electric-resistivity measurements by the absence of a continuous superconducting path through the specimen, or by a contact resistance. The structure was checked by X-ray investigation and apart from the Mo_2C pattern, two very weak "foreign" lines were evident, which may be due to MoC. The latter becomes superconducting at 7.9°K according to Meissner (see footnote 7), and it is therefore possible that pure Mo_2C is not a superconductor, but that the presence of a small amount of MoC gives rise to a superconducting transition at a temperature that depends on the concentration of MoC in the Mo_2C. The Meissner curve is suggestive of the transition taking place in two partly overlapping stages, which would hardly be observed if the specimen were homogeneous.

16. Superconductivity in MgTl and LiBi

by Lester Guttman and J. W. Stout[1]

Intermetallic compounds, i. e., ordered intermediate phases with compositions close to simple atomic ratios, frequently have metallic properties, and some have been shown to be superconducting as well. By studies of isomorphous series of compounds, one might gain some insight into the effect of electron concentration, and hence, of zone filling, on the transition temperature and critical magnetic field strength. Furthermore, as is well known, when the critical field has a "parabolic" dependence on temperature, one can evaluate the heat capacities of the metal in the normal and superconducting states, assuming them to be proportional to T and to T^3, respectively.

A large number of binary phases have the cesium-chloride structure. If we consider only those with the ideal composition AB, and exclude those containing a ferromagnetic element, or in which both elements are known nonsuperconductors, there remain HgLi, HgMg, LiTl, MgTl, CaTl, SrTl, LaTl, MgLa, AgLa. Of these MgTl seemed easiest to prepare.

The calculated quantities of magnesium (sublimed) and thallium (impurity about 0.1%) were melted together in a graphite crucible under a commercial magnesium melting flux. The first product was remelted in a helium atmosphere to free it of flux and oxide, and allowed to solidify slowly in a cylindrical graphite mold 6.2 mm in diameter. The final specimen was about 85 mm long, with roughly conical ends. A chemical analysis for both components gave 51.4 to 54.2 atomic percent Tl, depending on the location and method of computation; the excess over MgTl was presumably present as essentially pure Tl.[2] The product oxidized rapidly in air.

For the measurements, the rod was sealed into a closely fitting glass tube containing helium at 1 atmosphere. The central portion of the tube has been ground externally to reduce the wall thickness, and on this portion was wound a coil of No. 40 copper wire, in two layers of about 215 turns each. The measurements, carried out in the cryostat and solenoid magnet described elsewhere by Stout and Guttman,[3] gave the results collected in table 16.1. The critical field has been taken to be that at which flux penetration began in increasing field. Penetration was complete at a field that was 5 percent higher at 2.56° K and 7 percent higher at 1.29° K. The fraction of flux remaining in zero field increased in the same temperature range from 27 to 76 percent of that which would have been present had field penetration been complete at the point where it began. These features are apparent in figure 16.1, where the magnetic induction, B, and applied field, $\boldsymbol{H}$ are plotted on a reduced scale, in which the unit for both is the critical field. The sharpness of transition and expulsion of field are in marked contrast to typical "alloy behavior" [3] [4], although no great pains were

---

[1] Institute for the Study of Metals, University of Chicago, Chicago, Ill.

[2] M. Hansen, Aufbau der Zweistofflegierungen, p. 875 (J. Springer, Berlin, 1936).

[3] Paper 14 in this volume.

[4] K. Mendelssohn, Rep. Prog. Phys. **10**, 358 (1946); D. Shoenberg, Superconductivity, chap. VI (Cambridge University Press, London, 1938).

taken to prepare a sample free of grain boundaries and uniform in composition.

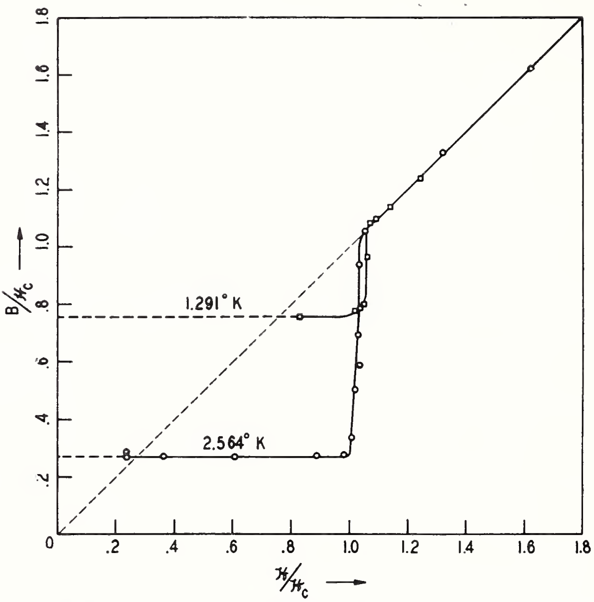

FIGURE 16.1. *Magnetic induction versus applied magnetic field for* MgTl *at two temperatures.*

TABLE 16.1. *Critical magnetic fields of* MgTl

Temperature	Critical magnetic field	
	Observed	Calculated
°K	*Gauss*	*Gauss*
1.291	169.3±2%	171.2
2.083	93.8±2%	93.4
2.422	48.3±1%	48.8
2.509	35.2±2%	36.3
2.564	28.2±1%	28.2

The critical field is quite linear in T^2, as shown in figure 16.2, where the solid line has the equation

$$H_c=220.0[1-(T/2.745)^2],$$

from which were calculated the values in column 3 of table 16.1. From the equation

$$\gamma=\frac{H_0^2}{2\pi T_0^2}$$

and the observed[5] lattice parameter, $a_0=3.628$ A, we compute $\gamma=3.51\times10^{-4}$ cal/deg^2 for 1/2 g atom of MgTl. The corresponding

---

[5] E. Zintl and G. Brauer, Z. phys. Chem. **B20**, 245–71 (1938).

value for Tl, 3.20×10^{-4} cal/deg^2 g atom, is only slightly less, although both $\boldsymbol{H}_0$ and T_0 are less for the latter.

It is planned to repeat the measurements on a specimen prepared more carefully, and to extend them to as many as possible of the isomorphous compounds listed above.

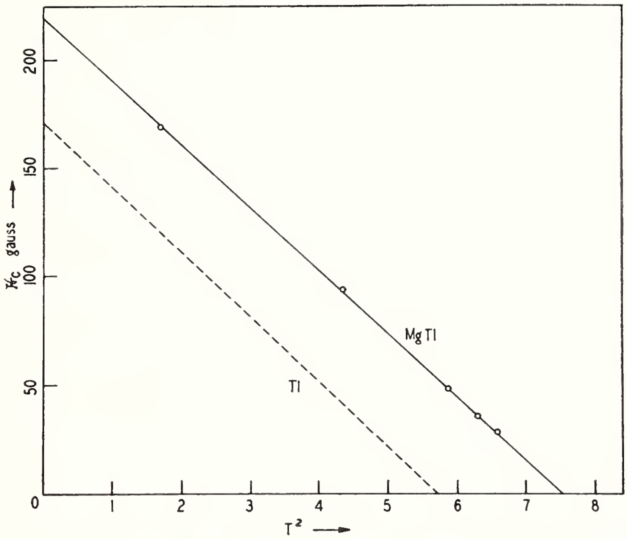

FIGURE 16.2. *Temperature dependence of critical magnetic field for* MgTl.

The compound α–LiBi has also been found to be superconducting, but the sample exhibited broad transitions, due partly, at least, to the fact that it was in the form of a short cylinder. From only two points, assuming a parabolic relation, the zero-field transition temperature is estimated at 2.47° K, greater than the value 2.23° K reported [6] for the isomorphous NaBi, although the threshold fields seem to be considerably lower than for NaBi. These measurements too will be repeated with a better sample.

---

[6] J. M. Reynolds and C. T. Lane, Phys. Rev. **79**, 405–6 (1950).

17. New Superconducting Compounds

by B. T. Matthias and J. K. Hulm [1]

In an attempt to throw further light on the conditions necessary for the occurrence of superconductivity, we have recently studied a number of binary compounds of elements that are apparently not superconducting by themselves. The compounds so far investigated fall into two groups, first, intermetallic compounds with bismuth, and second, borides and nitrides of molybdenum.

Meissner expresses the opinion [1] [2] that a cubic modification of bismuth would probably be superconducting. As quite a number of cubic bismuth compounds are now known to be superconducting, this assumption seems to be quite well founded. The known superconducting compounds include Au_2Bi, several alkali-metal-bismuth compounds, Rh-Bi and Bi_3Ni. In 1948 Alekseyevsky [2] reported $CaBi_3$ to become superconducting at 1.7° K, and it therefore seemed logical to extend the investigation to the strontium and barium-bismuth systems.

The phase diagram of Ba-Bi has been studied by Grube and Dietrich [3], who find a compound of the form $BaBi_3$, which, according to etching pictures, is cubic. The Sr-Bi system does not appear to have been previously investigated.

No special difficulties were encountered in preparing $SrBi_3$ and $BaBi_3$ in an inert atmosphere. Both compounds are formed as silvery cubes, $SrBi_3$ being somewhat more stable in air than $BaBi_3$. The latter begins to decompose in a few minutes under the action of humidity.

From measurements of their magnetic susceptibilities, both compounds were found to be superconducting, $SrBi_3$ at about 5.5° K and $BaBi_3$ slightly above 6° K. These transition temperatures are the highest known for bismuth compounds with nonsuperconducting elements.

Molybdenum, which according to Shoenberg [4] does not become superconducting above 0.3° K, was found by Meissner [5] to form superconducting carbides. We have extended the number of known superconducting molybdenum compounds by investigating the borides and nitrides. Of these, Mo_2B, Mo_2N, and MoN are all superconducting, whereas the other borides of molybdenum and Mo_2P are apparently not superconducting above 1.3° K. MoN has an unusually high transition temperature at about 12.0 K. More detailed results for molybdenum compounds have been published elsewhere [6].

[1] W. Meissner, Handbuch der Exp. Physik. [2] **11,** 221 (1935).
[2] N. Alekseyevsky, Russ. J. Phys. **9,** 350 (1945).
[3] G. Grube and A. Dietrich, Z. Electrochem. **44,** 755 (1938).
[4] D. Shoenberg, Proc. Cambridge Phil. Soc. **36,** 84 (1940).
[5] W. Meissner, H. Franz, and H. Westerhoff, Z. Phys. **75,** 521 (1932).
[6] J. K. Hulm and B. T. Matthias, Phys. Rev. **82,** 273 (1951).

---

[1] Institute for the Study of Metals, University of Chicago, Ill.

[2] Figures in brackets indicate the literature references.

18. Occurrence of Superconductivity Below 1° K

by B. B. Goodman[1] [2]

Various pure metals have been cooled to about 0.1° K, using a method already described by Mendoza [1].[3] From magnetic observations, ruthenium and osmium were found to become superconducting [2] below 1°K. The critical fields of these superconductors and also of aluminium, cadmium, gallium, and zinc were measured [3]. A number of metals were found to remain normal down to the lowest temperature tried.

The very low temperatures were produced by the adiabatic demagnetization of a pill of paramagnetic salt, usually potassium chrome alum. Thermal contact between the metal specimen and the salt was through a copper rod hard-soldered to copper foils embedded in the salt. The metal specimens were usually gripped in a copper cup at the end of this copper rod. Two separate mutual inductances surrounding the salt tube were used in conjunction with a 40 c/s a-c bridge to make independent magnetic observations on the salt and on the metal; the absolute temperatures were deduced from the magnetic measurements on the salt. Values of the critical magnetic field of a superconductor were obtained by studying its alternating field susceptibility in various steady magnetic fields.

Accurate critical-field measurements were made on aluminium, cadmium, gallium, and zinc, using annealed ellipsoids of spectroscopically pure metal having axial ratios of about 3:1. By making the measurements under different conditions, it was possible to prove that the temperature of the specimen was given by the temperature of the salt. The results could be accurately represented by relations of the form $H_c = H_0\ (1-(T/T_c)^2)$; the values of H_0 and T_c for these metals shown in table 18.1 are probably accurate to about 1 percent. These results are in fair agreement with previous work [4, 5, 6], but a detailed examination suggests that the present results are probably more accurate.

Table 18.1.—*Summary of results*

[A guide to the quality of the specimen is provided by the ratio of the resistance of the normal metal at T_c to the resistance at 273° K denoted by ρ/ρ_{273}.]

Element	ρ/ρ_{273}	T_c	H_0	γ cal mole^{-1} deg^{-2}	
				Calculated from present results	Calorimetric measurements
		°K	*Gauss*		
Aluminum	18×10^{-4}	1.197	106.0	2.95×10^{-4}	[1] 3.48×10^{-4}
Cadmium	3.1	0.560	28.8	1.28	
Gallium	1.0	1.103	50.3	0.91	
Zinc	14	0.905	52.5	1.16	[2] 1.25 [3] 1.50
Ruthenium	150	.47	46	3.0	
Osmium	400	.71	65	2.7	

[1] Kok and Keesom [7].
[2] Keesom and van den Ende [8], recalculated by Silvidi and Daunt [9].
[3] Silvidi and Daunt [9].

---

[1] Royal Society Mond Laboratory, Cambridge, England.
[2] Presented by D. Shoenberg.
[3] Figures in brackets indicate the literature references given on p. 72.

Superconducting transitions were observed for the first time in ruthenium and osmium. McLennan, Allen, and Wilhelm [10] reported a transition in ruthenium at 2.04° K, but they later found it was due to a surface layer of tungsten carbide. It may be mentioned that ballistic measurements on the ruthenium rod revealed appreciable hysteresis, and suggested a value of H_0 of order 20 percent lower than the value in table 18.1 obtained by the alternating-field method. The values of H_0 and T_c for osmium may also differ appreciably from the true thermodynamic values. A superconducting transition in spectroscopically pure rhenium powder beginning at 2.2° K confirmed the earlier discovery by Aschermann and Justi [11].

In the experiments on nonsuperconductors a small mass of paramagnetic salt that could be cooled only by conduction through the metal specimen was usually used to estimate the lowest temperature reached by the metal. Special arrangements were used in mounting the alkali metals. The specimen of cobalt was a closed wire loop to ensure that a superconducting transition would not be masked by possible changes in its ferromagnetic properties. The following metals were not superconducting down to the temperatures indicated: lithium (0.08° K), sodium (0.09° K), potassium (0.08° K), barium (0.15° K), yttrium (0.10° K), cerium (0.25° K), praseodymium (0.25° K), neodymium (0.25° K), manganese (0.15° K), cobalt (0.12° K), palladium (0.10° K), iridium (0.10° K), platinum (0.10° K).

In table 18.1 estimates of the electronic specific heats of the superconductors derived from the critical field measurements are compared with calorimetric measurements. It may be noted that the estimates of γ for the superconductors ruthenium and osmium are low in comparison with the values of γ for the five elements Fe, Co, Ni, Pd, Pt in group VIII of the periodic table, which range from 12×10^{-4} cal mole^{-1} deg^{-2} to 33×10^{-4} cal mole^{-1} deg^{-2}.

---

[1] E. B. Mendoza, Ceremonies Langevin-Perrin (Paris, 1948).
[2] B. B. Goodman, Nature **167,** 111 (1951).
[3] B. B. Goodman and E. B. Mendoza, Phil. Mag. **42,** 594 (1951).
[4] N. Kurti and F. E. Simon, Proc. Roy. Soc. [A] **151,** 610 (1935).
[5] D. Shoenberg, Proc. Cambridge Phil. Soc. **36,** 85 (1940).
[6] J. G. Daunt and C. V. Heer, Phys. Rev. **76,** 1324 (1949).
[7] J. A. Kok and W. H. Keesom, Physica **4,** 835 (1937).
[8] W. H. Keesom and J. N. van den Ende, Proc. Roy. Acad. Amsterdam **35,** 143 (Leid. Comm. 219b) (1932).
[9] A. A. Silvidi and J. G. Daunt, Phys. Rev. **77,** 125 (1950).
[10] J. C. McLennan, J. F. Allen, and J. O. Wilhelm, Trans. Roy. Soc. Can. [III] **23,** 283 (1929); [III] **25,** 13 (1931).
[11] G. Aschermann and E. Justi, Phys. Z. **43,** 207 (1942).

19. Penetration of a Magnetic Field into Thin Superconducting Films[1]

by J. M. Lock[2]

The penetration depth, λ, of a magnetic field into a superconductor can conveniently be studied by measuring the magnetic susceptibility of a superconducting specimen of very small dimensions. Hitherto such measurements have been restricted to colloidal specimens of mercury[3] and to thin superconducting cylinders,[4] and both methods suffer from disadvantages that prevent absolute values of λ from being obtained. The use of thin superconducting films, however, enables one dimension of the specimen to be made sufficiently small (a few times greater than λ) to give an appreciable change in susceptibility, and at the same time makes it possible to use specimens of sufficient volume to give reasonable accuracy in the measurements.

Specimens of tin, lead, and indium were prepared by evaporating the metal in a vacuum onto thin mica sheet. The average thickness of the films was found by direct weighing before and after deposition. They were then cut without deforming the metal film, and a large number of layers were stacked in order to get a sufficient volume of the metal into a small specimen holder. The magnetic moment of each specimen was measured ballistically with a uniform magnetic field applied parallel to the plane of the films. Magnetization curves were plotted for a number of different temperatures, and from their initial gradients the susceptibility of the superconducting film could be derived. A typical set of magnetization curves is shown in figure 19.1, from which it is seen that the diamagnetic susceptibility decreases as the temperature is raised, a result to be expected from the rise in penetration depth as the transition temperature is approached. The susceptibility also decreases as the thickness of the film is reduced, and the most important feature of the results is the close agreement between the experimental variation of susceptibility with thickness and that predicted on the basis of the phenomenological theory of F. and H. London (1935). This is shown in figure 19.2, in which the values of $-4\pi\chi$ for a number of tin films are plotted against $a\lambda_0/\lambda$, where $2a$ is the thickness of the film. It is assumed that the temperature variation of λ/λ_0 follows the law

$$\lambda/\lambda_0 = 1/\sqrt{(1-(T/T_c)^4} \tag{1}$$

for which there is a good deal of evidence.[5] The full curve in figure 19.2 is a plot of the theoretical variation of $-4\pi\chi$ for a flat superconducting plate, namely,

$$-4\pi\chi = 1-\frac{\lambda}{a}\tanh\frac{a}{\lambda}, \tag{2}$$

---

[1] Presented by D. Shoenberg See also J. M. Lock, Proc. Roy. Soc. [A] **208**, 391 (1951).

[2] Royal Society Mond Laboratory, Cambridge, England.

[3] D. Shoenberg, Proc. Roy. Soc. [A] **175**, 49 (1940).

[4] M. C. Desirant and D. Shoenberg, Proc. Phys. Soc. **60**, 413 (1948).

[5] J. G. Daunt, A. R. Miller, A. B. Pippard, and D. Shoenberg, Phys. Rev. **74**, 842 (1948).

which follows directly from the London equation

$$\nabla^2 H = H/\lambda^2. \tag{3}$$

The values of λ_0, the penetration depth at absolute zero, derived from these measurements are $5.0 \pm 0.1 \times 10^{-6}$ cm for tin, $3.9 \pm 0.3 \times 10^{-6}$ cm for lead, and $6.4 \pm 0.3 \times 10^{-6}$ cm for indium. The magnetization curves are found to become more rounded as the film thickness is

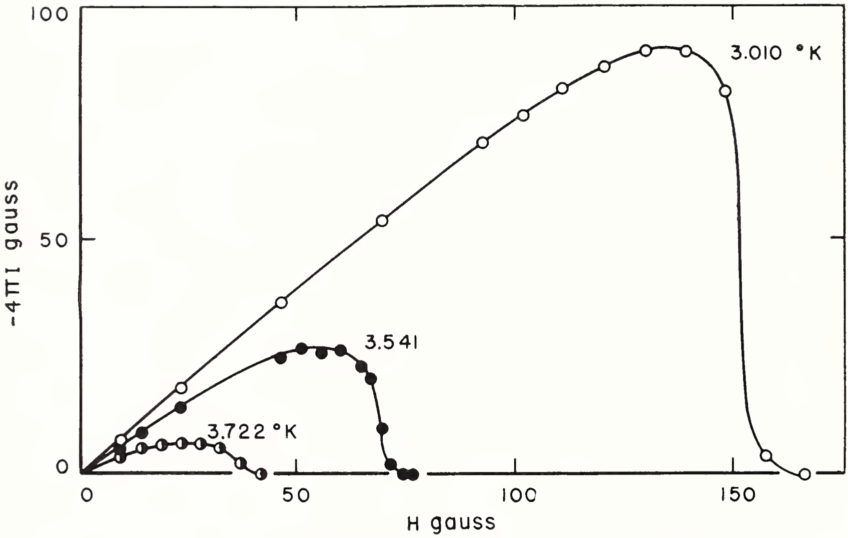

FIGURE 19.1. *Typical magnetization curves for thin film.*

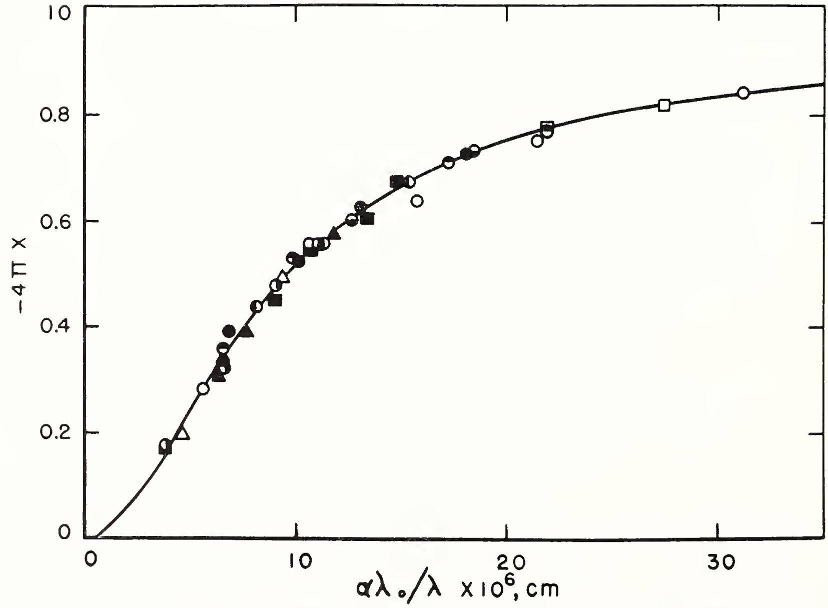

FIGURE 19.2. *Susceptibility of tin films as a function of the parameter $a\lambda_0/\lambda$.*

reduced, and it has been pointed out by Pippard that the area under the curve never differs greatly from the value $H_c^2/8\pi$ for a thick specimen. This lends support to the idea that the surface energy per unit area between the normal phase and an insulator differs only very slightly from that between the superconducting phase and an insulator. The fact that the magnetization curves of the thinnest films are considerably rounded explains why the critical fields of these films are higher than would be the case if the magnetization curves were linear up to the critical field.

No evidence has been found for a nonlinearity of the magnetization curves of the type predicted by the theory of Heisenberg [6] and Koppe,[7] increasing markedly at the lowest temperatures. The strongest evidence against this idea is derived from some of the lead films, which gave perfectly linear magnetization curves at a temperature of only 0.14 T_c.

---

[6] W. Heisenberg, Two lectures (Cambridge University Press, 1949).

[7] H. Koppe, Ergeb. exakt. Naturw. **23**, 283 (1950).

20. Magnetic Properties of a Hollow Superconducting Lead Sphere

by Julius Babiskin [1]

Measurements have been made to determine the nature of the equatorial magnetic-field distributions inside and outside a hollow superconducting lead sphere (2 in. in diameter, 3/16 in. wall thickness) in a uniform applied magnetic field. Previous experiments studied the magnetic field outside solid and hollow tin spheres, [1, 2, 3] [2] inside a canal bored through a solid tin sphere,[2] and in the space between two tin hemispheres [1, 4]. The magneto-resistance of nine calibrated bismuth probes (.011 in. thick, .16 in. long) in fixed positions was utilized to determine the magnetic fields as in the previous experiments. Lead was chosen for these experiments rather than tin in order to take advantage of the combination of the higher critical fields (H_c) for lead and of the increased sensitivity of the magneto-resistance of bismuth at higher magnetic fields.

All experiments were performed at 4.2°K, where $H_c \simeq 540$ gauss for lead. The uniform applied magnetic field (H_A) was obtained from a solenoid immersed in liquid nitrogen. The error in H_A is $\sim 1/2$ percent. The measured magnetic field (H_M) as determined from the calibration curves of a bismuth probe is a weighted mean average of the absolute value of the magnetic field over the dimensions of the bismuth probe. When H_M is homogeneous and normal to the bismuth probe, the error of H_M is ~ 1 percent. When H_M is inhomogeneous over the dimensions of the bismuth probe, the error of H_M could be large and indeterminate depending upon the degree and structure of the inhomogeneity. The hollow lead sphere (99.996% pure) was made by welding together two hemispherical shells with the previously calibrated bismuth probes in fixed positions on the equatorial plane of the hollow sphere with respect to H_A.

Figure 20.1 shows the results for bismuth probes in the hollow section of the sphere. The hollow sphere is a perfect magnetic shield along OA up to $H_A=382$ gauss at A. In the intermediate state along AB, a time-dependent increase [5] of H_M at constant H_A was observed. In all cases where a time dependence was observed, H_M was measured until the time dependence became negligible, so that all plotted points in figures 20.1 and 20.2 are time-independent equilibrium values of H_M at constant H_A. H_M was greater for Bi III than for Bi I along AB. The hollow sphere went completely into the normal state at B, and $H_M=H_A$ along BC. A time-dependent decrease of H_M at constant H_A was observed along BD. H_M was greater for Bi I than for Bi III along BD. The straight lines branching from BD at $H_A=0$ show that the observed frozen-in field at $H_A=0$ is completely shielded up to $H_A=120$ gauss. Upon the reversal of H_A along BD, the curves for all internal bismuth probes converge to a uniform distribution of $H_M=0$ at $H_A=-390$ gauss at point D. Upon the removal of H_A along

---

[1] Naval Research Laboratory, Washington, D. C.

[2] Figures in brackets indicate the references on p. 79.

DO, the internal uniform distribution of $H_M=0$ is completely shielded to point *O* and the cycle *OABCBDO* could be repeated. Thus, the initial conditions for superconductivity at point *O* were restored in the hollow section of the sphere, although a small frozen-in field remained outside the hollow sphere. The symmetric hysteresis cycle *CBDEFGBC* could also be repeated.

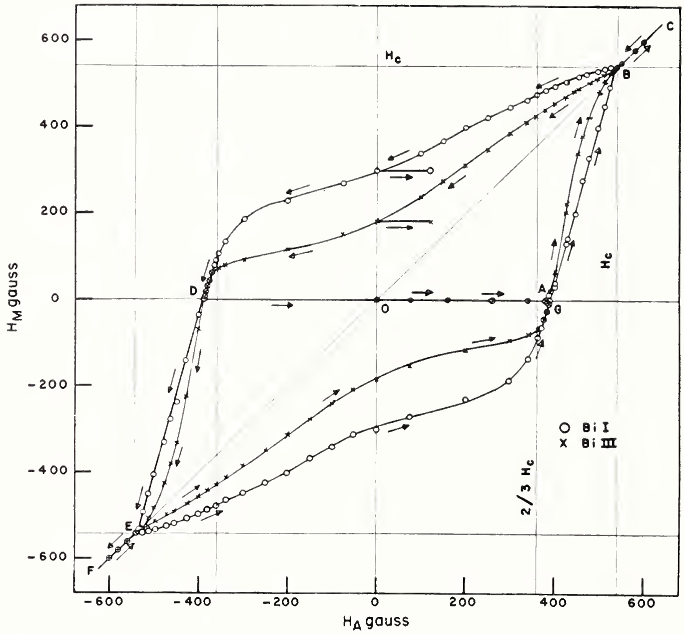

FIGURE 20.1. *H_M versus H_A for bismuth probes on the equitorial plane inside the sphere;* Bi I *at the inside edge;* Bi III *at the center.*

Figure 20.2 shows the results for a bismuth probe outside the sphere. The slope of $OA=1.45$ and $H_M=H_c$ at $H_A=374$ gauss at *A*. Along *AB* for an increment of H_A, an initial jump of H_M to a value slightly greater than H_c and then a time-dependent decrease of H_M at constant H_A until $H_M=H_c$ again were observed. This time-dependent decrease of H_M outside the sphere occurred simultaneously with the time-dependent increase of H_M inside the sphere. A time-dependent increase of H_M at constant H_A was observed along *BD*. The discontinuity in *BD* is due to a high inhomogeneity of H_M over the dimensions of the bismuth probe. The dashed line, which crosses the discontinuity in *BD*, is an approximation of the average H_M in this region. The frozen-in field at $H_A=0$ along *BD* was opposed to the original direction of H_A. Upon the removal of H_A from point *D* at $H_A=-374$ gauss to $H_A=0$ gauss, the curves for all external probes converged to point 0. In this way the frozen-in field has been eliminated outside the sphere. The cycle *OABCBDO* in figure 20.2 as well as the symmetric hysteresis cycle can be repeated. Thus the initial conditions for superconductivity have been restored outside the sphere, although a small frozen-in field remained inside the sphere. It is therefore seen that the initial conditions for superconductivity

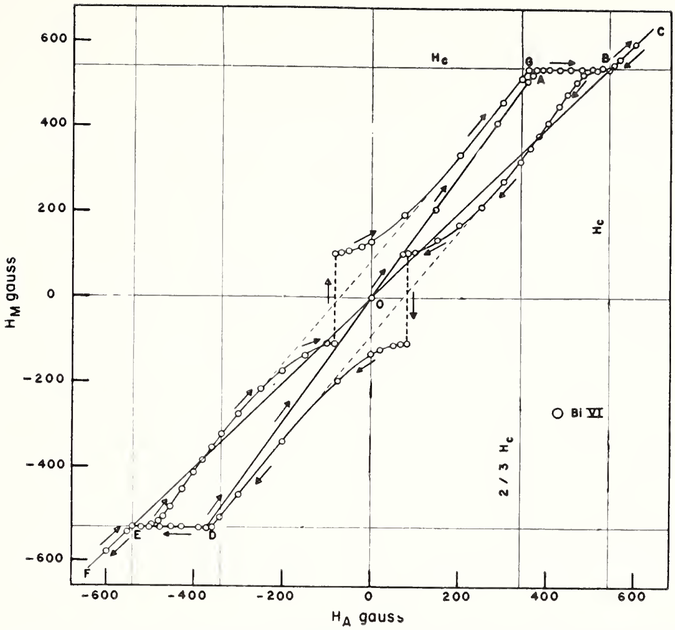

FIGURE 20.2. *H_M versus H_A for a bismuth probe outside the sphere very close to the equator.*

were restored either inside or outside the sphere, but not simultaneously.

Further hollow-sphere experiments are planned and more detailed results will be published. Acknowledgment is due J. de Launay and R. L. Dolecek for having suggested this experiment and to the members of the Cryogenics Branch at the Naval Research Laboratory for profitable discussions and suggestions.

---

[1] W. J. deHaas and A. Guinau, Physica **3,** 182, 534 (1936).
[2] A. Shalnikov, J. Phys. (USSR) **6,** 53 (1942).
[3] K. Mendelssohn and J. Babbitt, Proc. Roy. Soc. (London) [A] **151,** 316 (1935).
[4] A. Shalnikov, J. Phys. (USSR) **9,** 202 (1945).
[5] W. J. deHaas, A. Engelkes, and A. Guinau, Physica **4,** 595 (1937).

21. Studies on Oscillating Superconducting Spheres

by R. H. Pry, A. L. Lathrop, and W. V. Houston [1]

In the course of the last few years at the Rice Institute Low Temperature Laboratory, a series of studies has been made on the properties of superconducting spheres oscillating in the presence of an external magnetic field. These studies have been undertaken in order to reexamine closely the adequacy of the London-von Laue formulation of the electromagnetic forces on a superconductor.

In the ordinary formulation of a force exerted by a magnetic field on a conductor oscillating with its axis perpendicular to the field direction, the electrons in the conductor set up eddy currents by induction to resist the change in field relative to a set of axes fixed to the body. The external magnetic field then exerts a force on this current, which, because of the strong interaction between the current and the ion lattice, can be computed in terms of the force exerted on the body itself.

In a superconductor oscillating similarly in a magnetic field there exists a supercurrent which, through the London theory, exerts only an inward tension on the surface of the body of magnitude $\frac{1}{2}\lambda I_s^2$, where I_s is the supercurrent density, and λ is the London superconducting constant. The normal currents are present also, to some extent, in the superconductor, but they are reduced by an amount proportional to the penetration of the magnetic field. Except for the effect of these small normal currents, then, there should be no force acting tangent to the superconducting surface.

To test this conclusion, Houston and Muench [2] constructed the apparatus shown in figure 21.1 consisting of a torsion fiber of 3-mil tungsten wire, on the end of which is suspended a 1-in.-diameter sphere of tin. Actually, the sphere is separated from the fiber by a Pyrex tube in order that the fiber is not subjected to low temperatures. On the top of this tube a four-sided mirror is attached so that the oscillations of the system can be observed by means of a beam of light and a scale. The horizontal magnetic field in the region of the sphere could be varied from 10^{-4} gauss to 100 gauss by means of the Helmholtz coils shown. The sphere was first cooled with liquid helium to a temperature of 4.2° K, then to 3 deg and 2 deg below the superconducting transition, and measurements were made of the period and damping of the system as a function of the external magnetic field in the normal and superconducting states. These measurements were made for numerous values of the horizontal field in the normal state up to about 1 gauss and in the superconducting state up to 45 gauss.

---

[1] The Rice Institute, Houston, Tex.

[2] W. V. Houston and Nils Muench, Phys. Rev. **79**, 967 (1950).

Normal conduction theory shows that there will be a field-dependent torque exerted on the sphere of magnitude

$$L=-\frac{2\pi B_0^2R^3}{\mu_0}\left\{1-\frac{3(\sinh x-\sin x)}{x(\cosh x-\cos x)}\right\}\theta-\frac{2\pi B_0^2R^3}{\mu_0 w}\left\{\frac{3(\sinh x+\sin x)}{x(\cosh x-\cos x)}-\frac{6}{x^2}\right\}\dot{\theta},$$

where $x=(2w\mu_0R^2/\tau)^{\frac{1}{2}}$, R is the radius of the sphere, τ is the specific resistivity, w is the angular frequency, and μ_0 is necessary here because of the use of rationalized mks units. As this torque contains terms in both the angular displacement and velocity of the sphere, both a restoring and damping torque will exist, dependent on the square of the applied horizontal magnetic field. Figure 21.2 is a graph of the calculated damping and restoring torque plotted against the parameter x. As can be seen, as the conductivity or angular frequency of the sphere is increased, the restoring torque increases steadily to a max-

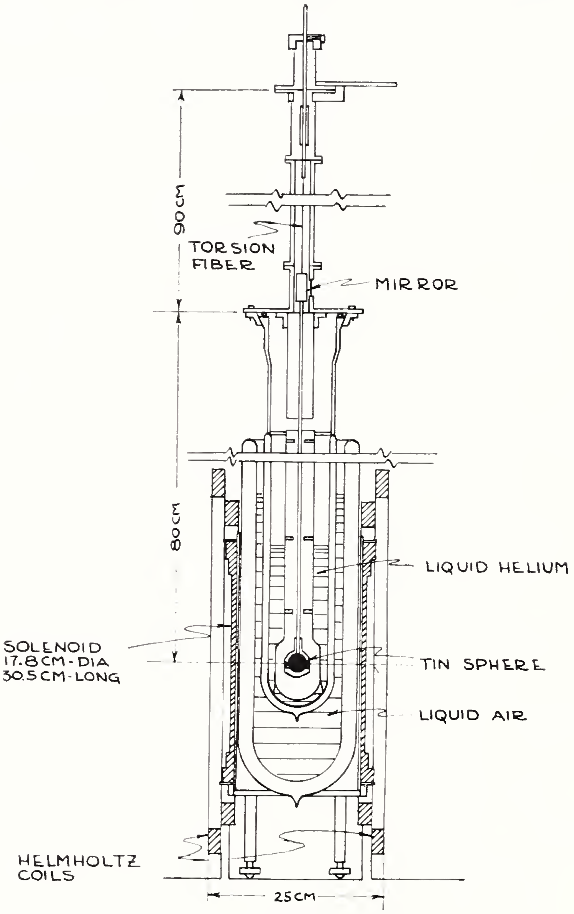

FIGURE 21.1. *Diagram of apparatus.*

imum value, but the damping torque increases to a maximum and then decreases again to zero.

The most recent data obtained from this experiment checks very closely with the above theory in that the field-dependent torques were, in the normal state, dependent on the square of the applied field and gave a reasonable value for the conductivity of the tin sphere at 4.2° *K*, a value that is consistent with both the period and damping measurements to within the experimental error.

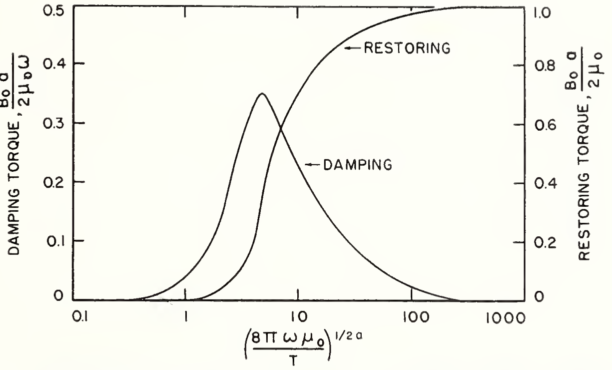

FIGURE 21.2. *Damping and restoring torque as a function of the specific resistivity of a normal conducting sphere.*

In the superconducting state, no field dependent damping was observed in excess of 6×10^{-7} of that observed in the normal state, and no field dependent restoring torques were observed that could not be attributed to a frozen-in moment or some ellipticity in the sphere, and therefore dependent on the sphere orientation, in excess of 10^{-5} of that in the normal state. If the sphere had become perfectly conducting, no field-dependent damping torque would have been observed, but the graph of the torques shown in figure 21.2 indicates that the eddy currents set up would create a large restoring torque, which was not observed.

A rough estimate made from the London-von Laue theory indicates that, indeed, the torques exerted in the superconducting state should be of the order of magnitude of 10^{-12} of that in the normal state so that it can be said that this experient in no way contradicts the London formulation and again points to the difference between perfect and superconductivity.

There is another way, however, that superelectrons may apparently exert a force on a spherical superconductor that is tangent to the surface. If a vertical magnetic field is suddenly applied to the torsion pendulum described above, an electric field will exist in the sphere during the change in magnetic field so as to produce an electron and positive-ion current in opposition to the increase in the magnetic field. As the electrons cannot interact with the ion lattice, one then observes a torque on the body as a whole corresponding to the positive ion current. Such a torque is explainable through momentum considerations in the London theory, is of a magnitude proportional to *m/e* of the electrons, and is in the direction opposite to the direction of the electron current. As this torque is very small, it can be most readily observed by subjecting the sphere to a vertical oscillating magnetic field with the same frequency as the natural frequency of the torsion system and thus drive the system to a resonance amplitude.

In 1940 Kikoin and Gubar[3] reported the results of an experiment of this type on a superconducting lead sphere, but the analysis of their result was based upon a microscopic mechanism similar to the gyromagnetic effect in ferro- and paramagnetism and further they left some doubt in their report as to the sign they obtained for the torque produced. In 1948 Meissner[4] reanalyzed the results of this experiment from the standpoint of the London theory, as mentioned above, and found these results consistent in magnitude with the theory if the free-electron mass is used to compute the result, but there still remained some doubt as to the sign of the experimental effect.

Because of the importance of this result, we have undertaken to repeat this experiment. The apparatus is again as shown in figure 21.1. The Helmholtz coils are used to compensate the horizontal component of the earth's field, and the solenoid, capable of producing 130 gauss, is used to produce the vertical oscillating magnetic field. To be assured that one does not obtain an effect due to a small frozen-in moment or due to some ellipticity in the sphere, great care must be taken to eliminate as completely as possible all horizontal steady fields and any horizontal component of the vertical oscillating field.

The preliminary results for this experiment indicate that, even though the magnitude of the gyromagnetic effect is not yet determined to better than 15 percent, due to the above disturbing effects, it is in accord with the momentum treatment based on London's equations.

It is important to emphasize, in view of Bardeen's recent articles on superconductivity, which involve an effective superelectron mass of 10^{-4} of the free-electron mass, that if the mass of an electron in a superconductor is measured in the way described here, one obtains a result that is of the same order of magnitude as the free-electron mass.

---

[3] I. K. Kikoin and S. W. Gubar, J. Phys. (USSR) **III**, 333 (1940).

[4] W. Meissner, Sitz. Bayerische Akad. Wiss. 321, (1948).

22. Eddy Currents and Supercurrents in Rotating Metal Spheres at Liquid-Helium Temperatures

by P. B. Alers, J. W. McWhirter, and C. F. Squire [1]

For some time we have known that a solid sphere of superconducting metal shows a perfect Meissner effect if the following experimental steps are taken: (a) Rotate the sphere rapidly in the normal conducting state, (b) cool the sphere slowly through the superconducting transition temperature while still rotating, and (c) stop the rotation. Experimental investigation shows that the sphere has undergone a perfect Meissner effect. These findings were first published by Love, Blunt, and Alers.[2] The present investigation has put some quantitative understanding behind the effects, both from the experimental and theoretical sides.

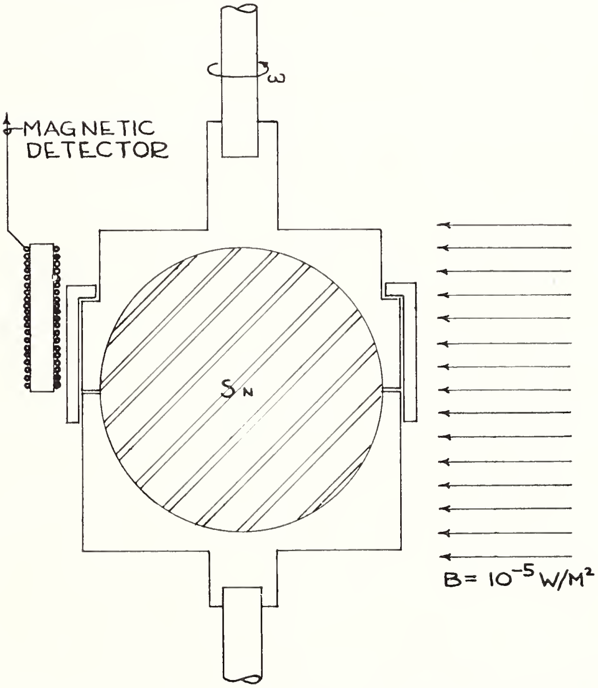

Figure 22.1. *Simplified sketch of the experimental apparatus.*

Figure 22.1 of this section shows schematically the sphere of tin housed in Textolite, so that rotation at speeds, ω, may be obtained through a driving torque on the shaft extending upward and out of the liquid-helium bath. A magnetic detector (saturable core reactor) is shown in figure 22.1, and this is located close to the rotor in such a

---

[1] The Rice Institute, Houston, Tex.

[2] W. F. Love, R. F. Blunt, and P. B. Alers, Phys. Rev. **76**, 305 (1949).

way that any changes in the vertical magnetic-field component results in a steady signal on a meter. Most of the vertical-field component of the earth was removed by use of compensating Helmholtz coils placed external to the Dewar flasks. The horizontal component of the earth's field is shown in figure 22.1.

At 4.2° K the electric conductivity of tin is very high, 4×10^{10} mhos/m, so that if the sphere shown in figure 22.1 is rotated at this temperature, the eddy currents are enormous. At the very modest speed of 2.5 rps the eddy currents are so large that the magnetic field is removed from most of the interior of the sphere and can only penetrate into a small skin depth of about 0.82 mm at the surface of the metal. This shows up on the magnetic detector because the magnetic-flux lines are forced over and around the rotating sphere and thus produce a strong vertical component of the magnetic field. We may rotate the sphere some five times faster, but the detector indicates very little further change in the field distribution. That is to say, once the angular velocity is great enough to produce eddy currents of a size to remove the magnetic flux from the bulk of the sphere, further increase in the speed of rotation achieves little more in this sense. Quite slow speeds of rotation produce such small eddy currents that the external field penetrates most of the sphere. Quantitative results have been obtained on the speed of rotation as a function of the size of the eddy currents, i. e., the degree to which the magnetic field is removed from the interior of the sphere. At higher temperatures, say 20° K, the electric conductivity is smaller, so that one must use much higher speeds of rotation in order to produce large eddy currents. Figure 22.2 shows these studies at both 4.2° K and at 20° K. The ordinate is plotted as the ratio of the size of the eddy current induced in the sphere to the size of the superconducting current that the sphere possesses when in the superconducting state and showing the complete Meissner effect. This plot brings out clearly the similarity between the intensity and distribution of the eddy currents and the superconducting surface currents that produce the Meissner effect. Experi-

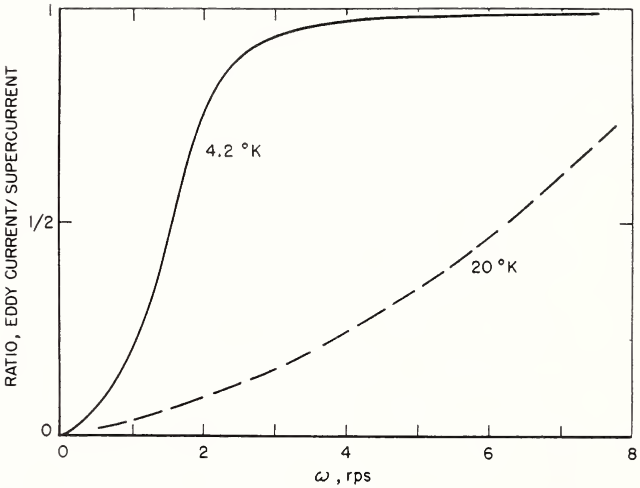

FIGURE 22.2. *Ratio of eddy current to supercurrent as a function of the speed of rotation.*

mentally, this is established by observing no change in the field distribution at the detector when the sphere is cooled while rotating into the superconducting state. When the tin sphere is cooled slowly in this way and the rotation stopped, again no change in the detector signal is observed. Thus the eddy currents have the same distribution as the superconducting Meissner currents. The superconducting currents maintain their intensity whether the sphere is rotating or not.

We may use classical theory to describe the magnetic-field distribution around a sphere of metal that is rotating in the manner shown in figure 22.1. A simple change of coordinate system will allow the sphere of metal to stay fixed and the magnetic field to rotate around. The equation to be satisfied is

$$\nabla^2 B - j\omega\mu\sigma B = 0,$$

where ω is the angular velocity, μ the magnetic permeability, and σ the electric conductivity. The polar-coordinate description of the field gives a radial component, which is

$$B_r = B_0 \left\{ 1 + \frac{D}{r^3} \right\} \cos\theta,$$

where $p = \omega\mu\sigma$ gives a depth of penetration in the skin $1/\sqrt{2p}$, and

$$D = -a^3 \left\{ 1 - \frac{3}{\sqrt{2p}a} \frac{\sinh\sqrt{2p}a - \sin\sqrt{2p}a}{\cosh\sqrt{2p}a - \cos\sqrt{2p}a} \right\}$$

$$- ja^3 \left\{ -\frac{3}{pa^2} + \frac{3}{\sqrt{2p}a} \frac{\sinh\sqrt{2p}a + \sin\sqrt{2p}a}{\cosh\sqrt{2p}a - \cos\sqrt{2p}a} \right\},$$

where the distance $r \geq a$, and where a is the radius of the sphere, The eddy currents are distributed over the surface to a depth $1/\sqrt{2p}$. and from outside the sphere these eddy currents produce a dipole at the center of magnitude, D. The imaginary component of the dipole is the out-of-phase component, and at 4.2 K its magnitude is only one-tenth that of the real part for an $\omega = 2.5$ rps. For infinite conductivity or for infinite angular velocity, the imaginary component of the complex dipole moment vanishes.

The London theory for a sphere in a magnetic field and for the metal in the superconducting state with perfect Meissner effect gives the equation.

$$\nabla^2 B - \frac{\mu}{\lambda} B = 0,$$

where $\lambda = m/ne^2$ is determined by the number, n, the mass, m, and charge, e, of the superconducting electrons. The skin depth $1/\sqrt{(\mu/\lambda)} = 1.6 \times 10^{-5}$ mm. The radial component of the field exterior to the sphere, which by the way is not rotating, is given by

$$B_r = B_0 \left\{ 1 + \frac{M}{r^3} \right\} \cos\theta,$$

and the magnitude of the pure real dipole moment is

$$M=-a^3\left\{1-\frac{3}{\sqrt{\frac{\mu}{\lambda}}a}\coth\sqrt{\frac{\mu}{\lambda}}a+\frac{3}{\frac{\mu}{\lambda}a}\right\}.$$

Comparing this with the dipole set up by the eddy currents, one sees that they are equal in the limit of very fast speeds of rotation, with high conductivity. Indeed, experimentally they are indistinguishable at speeds of $\omega=2.5$ rps for tin at 4.2 K.

It is well known that for tantalum the Meissner effect is practically nonexistent because the metal freezes in all of the existing flux when it becomes superconducting. We looked into this and found that pure tantalum in bulk quantity has been made by sintering together the small flakes or grains. Sound pulses are found to scatter very badly on passing through tantalum metal.[3] Thus from a physical point of view, the metal is not homogeneous, and one can understand that the Meissner effect might not be realized by a metal of this physical make up. We have found that our specimen of pure tantalum was of this sort, but that we could force it to have a complete Meissner effect through the technique of rotating the specimen in the normal state and, while still rotating, cooling it into the superconducting state. The cooling must be done very slowly, otherwise some frozen-in flux will result. We shall report on the critical magnetic-field curve for tantalum in a subsequent report.

---

[3] W. C. Overton, Jr., Thesis, The Rice Institute (May 1950).

23. Atomic Heat of Indium at Liquid-Helium Temperatures

by J. R. Clement and E. H. Quinnell*

One of the principal phenomena that must be explained by any theory of superconductivity is the difference in the specific heats of a material in the normal and the superconducting states. Of all the 20 known superconducting elements, there exist calorimetric measurements sufficiently accurate to determine this quantity for only three; namely, tin, thallium, and tantalum. The results on these do not make completely clear what a theory must explain. For this reason, the low-temperature calorimetry program at the Naval Research Laboratory has been initially directed toward obtaining information on the specific heat of superconducting elements in both the normal and the superconducting states.

We shall report here some calorimetric measurements on indium. There are several reasons why indium was chosen to be measured. It has a low melting point, so the sample was easy to prepare. Critical-field measurements have been made by Daunt and collaborators [1] and by Misener,[2] so one is able to compute specific heat differences by using these results and the thermodynamics of superconductors.[3] It is a soft superconductor and therefore can be maintained in the normal state with a magnetic field of a few hundred gauss. Finally, we could find no calorimetric data in the literature below about 50° K.

Before discussing the results obtained, we shall outline briefly the calorimetric technique used. The fundamental definition of heat capacity, $C=dQ/dT$, gives

$$C=\frac{dQ}{dT}=\frac{dQ/dt}{dT/dt}=\frac{\dot{Q}}{\dot{T}}. \tag{1}$$

At any time, and, in particular, when the sample under investigation is being heated, one can measure the true time rate of temperature change, $\dot{T}$, provided there exists thermal equilibrium between the sample and the thermometer. The other quantity in the equation, $\dot{Q}$, the rate at which heat is being added, is not directly measurable. However, we know that

$$\dot{Q}=JI^2R+\dot{Q}_L, \tag{2}$$

where JI^2R is the heat being added by the heater and/or thermometer, J being the mechanical equivalent of heat, and $\dot{Q}_L$ is the heat being added to the sample because of incomplete thermal isolation. We also know that

$$\dot{Q}_L=C\dot{T}_L, \tag{3}$$

---

*Naval Research Laboratory, Washington, D. C.

[1] J. G. Daunt, A. Horseman, and K. Mendelssohn, Phil. Mag. 27, 754 (1939)

[2] A. D. Misener, Proc. Roy. Soc. [A] 174, 262 (1940).

[3] C. J. Gorter and H. B. G. Casimir, Physica 1, 306 (1934).

where $\dot{T}_L$ is the rate of change of temperature caused by incomplete thermal isolation. From (1) and (3) we get for the heat capacity of the sample

$$C=\frac{JI^2R}{\dot{T}-\dot{T}_L}. \tag{4}$$

There are several possible methods for applying this result to the reduction of data. One may use the actual derivatives that appear in eq (4), or one may calculate integrals over time intervals sufficiently small to obtain an average value of the specific heat over a small temperature range. For the actual determination of the derivatives (or integrals), one may secure temperature-time curves either before and after the heating period only, during heating only, or before, during, and after the heating period. Our technique requires knowledge of the time-temperature curves only during heating, the sole heat source being the thermometer itself. From the temperatures obtained by extrapolating these curves to the beginning and end of the heating periods, we take for $\dot{T}_L$ for the nth heating period.

$$\dot{T}_L=\frac{1}{2}\left[\frac{T_f^{n-1}-T_i^n}{\Delta t_{n-1}^n}+\frac{T_f^n-T_i^{n+1}}{\Delta t_n^{n+1}}\right]. \tag{5}$$

Equation (5) shows $\dot{T}_L$ is the average of the rate of change of temperature between the beginning of the heating period under consideration and the end of the preceding one, and the rate of change of temperature between the end of the heating period under consideration and the beginning of the following one.

Let us consider now the sources of error in specific-heat data so obtained. The numerator of eq (4) is JI^2R, and the errors in this quantity are determined by the accuracy of the ammeter and voltmeter used and can be reduced to extremely small quantities without difficulty. So far as the two terms in the denominator are concerned, they are both subject to errors because of inaccuracies in thermometry. In our technique the first is subject to direct measurement, whereas the second is implied according to eq (5). We have found that we can determine $\dot{T}_L$ to within 5 to 20 percent, depending on the degree of thermal isolation maintained during an experiment. This means that if we are aiming for an accuracy of 1 or 2 percent in our final results, we must have $\dot{T}$ 5 to 20 times as large as $\dot{T}_L$. This condition has been found a feasible one in most of the experiments carried out so far.

From eq (4) we can deduce the well-known fact that errors in low-temperature specific-heat measurements are due primarily to inaccuracies in thermometry. Therefore, we shall describe the thermometer used in the measurements. Some years ago at NRL we investigated the electric resistance-temperature curves for a number of composition resistors of the type ordinarily used in radio and electronic circuits. One type [4] gave very consistent and reproducible results, not only during a single experimental run in liquid helium, but also from one run to another, the resistor having warmed to room temperature between runs. This particular brand also had an extremely large sensitivity, over 100 percent per degree in the liquid-helium

---

[4] One watt, 180 ohm type, manufactured by Allen-Bradley Co., 118 W. Greenfield Ave., Milwaukee 4, Wis.

region. We found that these resistors very nearly fit a theoretical equation for semiconductors: [5]

$$R = AT^{-1/4}e^{\alpha/T}. \tag{6}$$

For our purposes A and α are undetermined constants. In particular, the resistor that was put in the indium sample fits this equation exactly between 1.6° and 4.2° K. Equation (6) can be written in another form giving a linear relationship, thus simplifying the task of testing whether a resistor obeys eq (6),

$$\log R + \tfrac{1}{4}\log T = \log A + \alpha/T. \tag{7}$$

Figure 23.1 shows $\log R + \frac{1}{4}\log T$ plotted against $1/T$ for the resistor in the indium sample. The points plotted give an indication of the reproducibility of this resistor as the measurements with a magnetic field were taken some weeks after those without a magnetic field. They also show that the calibration was not affected by magnetic fields up to 250 gauss.

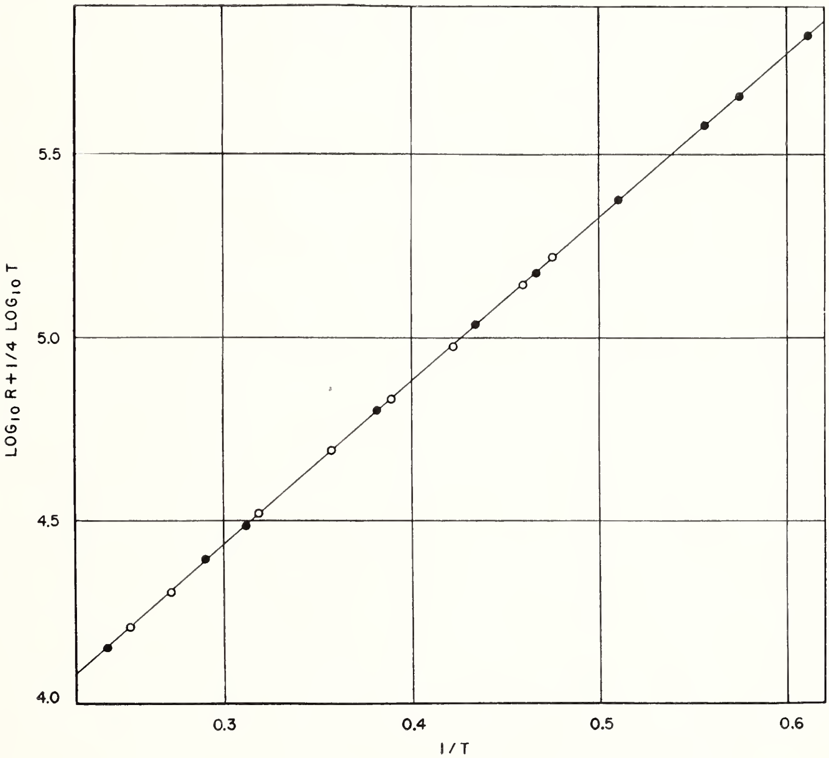

FIGURE 23.1. *Calibration of carbon resistor in indium sample 1.*

○, No applied magnetic field; ●, applied magnetic field=250 gauss; voltage across resistor=0.75 volt.

Figure 23.2 shows a cross section of the vacuum calorimeter and a sample with the resistor in position. The sample is in the form of a cylinder, with the resistor placed along the axis and in the geometric

---

[5] See Seitz, Modern theory of solids, p. 191 (McGraw-Hill Book Co., Inc., New York, N. Y. (1940)).

center of the sample. A bridge[6] operated at constant voltage is used to measure the resistance of the thermometer-heater. The application of constant voltage to the bridge makes the calculation of the power developed by the resistor a relatively simple problem.

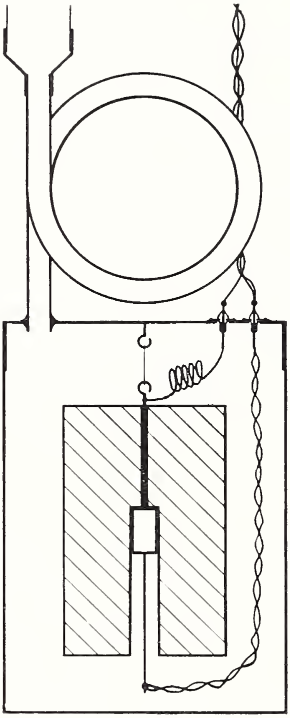

FIGURE 23.2. *Calorimeter assembly.*

Using the method outlined here for measuring specific heats, we made a few measurements on tin to see whether our method gave results in agreement with those previously obtained at Leiden[7,8,9] and at the same time to investigate sources of error in our method. During the course of these experiments we found a large error in the resistance versus time data. To reduce this error we replaced the clock and galvanometer that we first used with a recording galvanometer. Figure 23.3 shows all the results obtained, including the original ones with the clock and galvanometer. Only the three points at 3.935°, 4.027°, and 4.054° K were obtained using the recording galvanometer. The smooth curves were determined by plotting C/T versus T^2 for all existing data and drawing what appeared to be the best smooth curve through these data. The NRL results are in good agreement generally with those obtained at Leiden by somewhat different methods.

Measurements were also made on an indium sample, with a stated purity of 99.9+%, the principal impurity being thallium. The sample weighed 122.1 g. Figure 23.4 shows the results obtained with

---

[6] A description of this bridge can be found in Roberts, Heat and thermodynamics, p. 23 (Blackie & Son, Ltd. (1940).

[7] W. H. Keesom and J. N. van den Ende, Proc. Amst. Roy. Acad. **35**, 143 (1932).

[8] W. H. Keesom and J. A. Kok, Proc. Amst. Roy. Acad. **35**, 743 (1932).

[9] W. H. Keesom and P. H. van Laer, Physica **5**, 193 (1938).

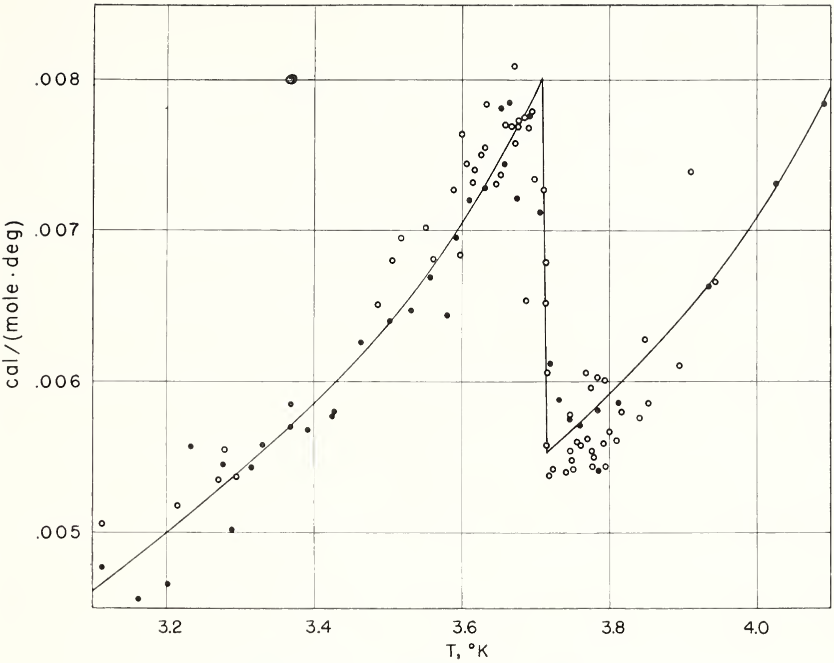

Figure 23.3. *Atomic heat of tin.*

○, Leiden results; ●, NRL results.

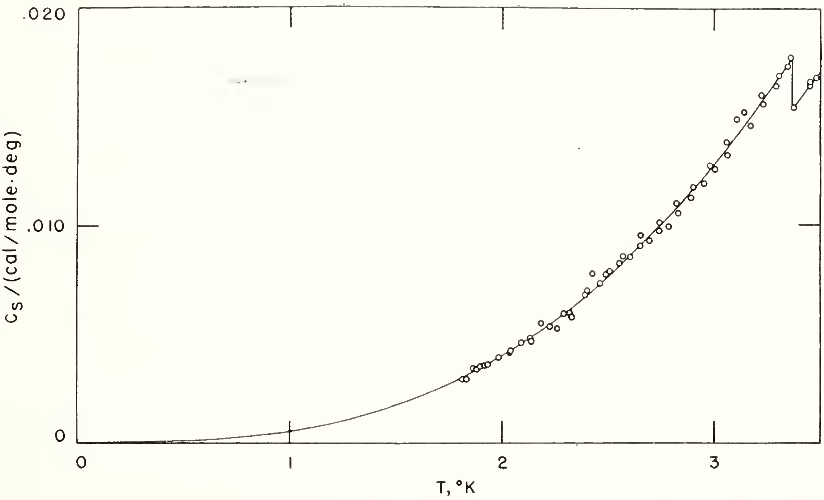

Figure 23.4. *Atomic heat of superconducting indium.*

no magnetic field applied to the sample, that is, for superconducting indium. Data from four separate experimental runs are included, although they are in no way differentiated in the figure. The maximum deviation of any point from the smooth curve is about 6 percent.

The heating curves show that the jump at the superconducting transition occurs within less than 0.01° K.

Figure 23.5 shows the results obtained on normal indium. Again, results from three separate experiments are included without differentiation. For these data the maximum deviation of any point from the smooth curve is less than 2 percent.

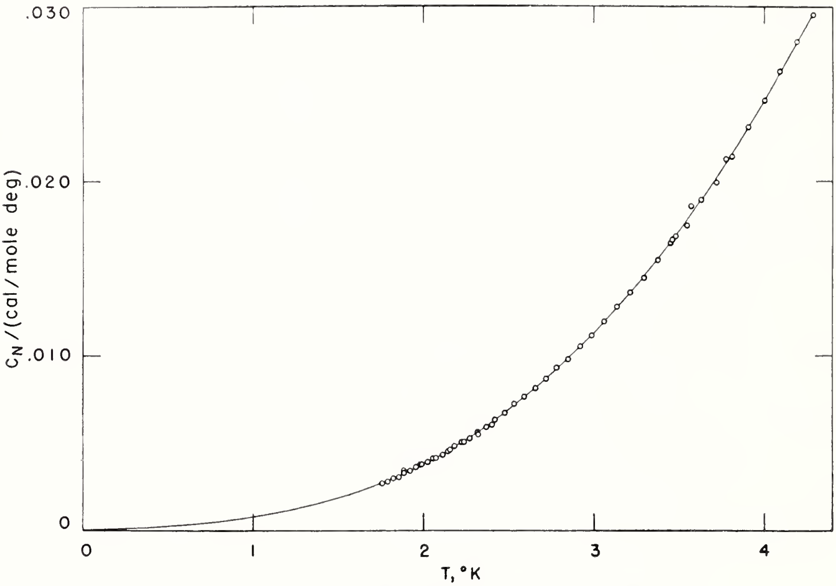

FIGURE 23.5. *Atomic heat of normal indium.*

Part of these data and some preliminary conclusions are reported elsewhere.[10] However, since that time, further data have been obtained, and the tentative conclusions then stated have changed somewhat.

Figure 23.6 shows C_N/T versus T^2. The intercept of this curve, and therefore the value of γ, was determined by calculating by least squares the best curve of the form

$$C_N = AT^3 + \gamma T \qquad \left(T < \frac{\Theta_D}{50}\right) \tag{8}$$

in accordance with Blackman.[11] The value of the Sommerfeld electronic specific-heat coefficient that we obtain in this manner is $\gamma = 3.23 \times 10^{-4}$ cal/mole·deg.^{2} The Debye characteristic temperature, Θ_D, that we find is about 106° K. From measurements of critical magnetic fields, Daunt, et al. (see footnote 1) found $\gamma = 3.5 \times 10^{-4}$, and Misener (see footnote 2) found $\gamma = 3.6 \times 10^{-4}$ cal/mole·deg.^{2}

---

[10] J. R. Clement and E. H. Quinnell, Phys. Rev. **79**, 1028 (1950).
[11] M. Blackman, Proc. Roy. Soc. [A] **149**, 117 (1935).

Figure 23.7 shows a similar plot for the superconducting data. For tin such a diagram gives a curve very nearly linear and appearing to pass through the origin of the coordinates. In other words, it indicates that the specific heat of tin in the superconducting state can be closely represented by a T^3 law and no linear term. It seemed impossible to do this for the indium data. The smooth curve in figure 23.7 is intended to have no significance other than to show that a simple T^3 law appears insufficient. It is not considered conclusive evidence that a linear term is necessary in the superconducting state.

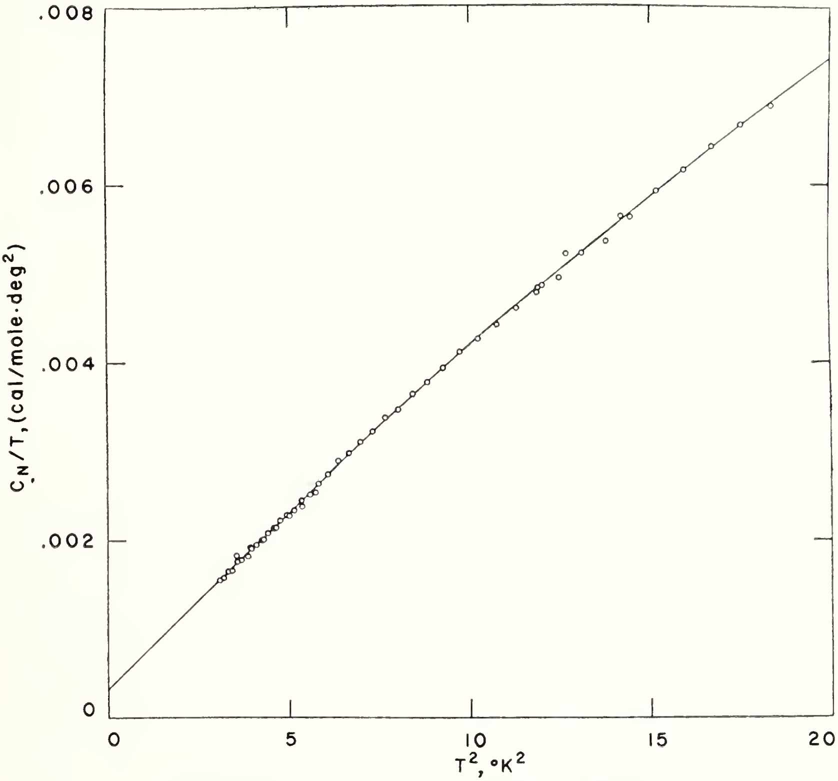

FIGURE 23.6. *C/T versus T^2 for normal indium.*

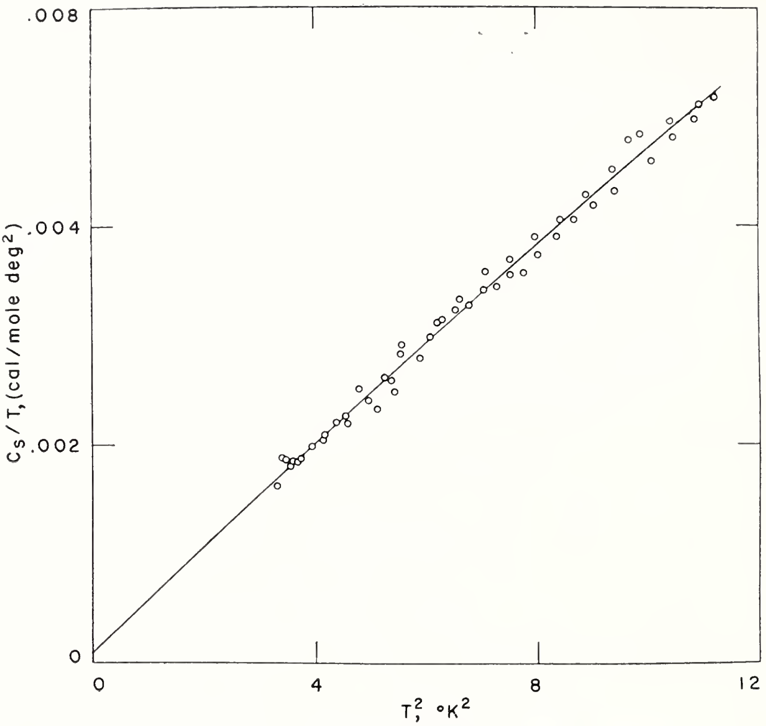

FIGURE 23.7. *C/T versus T^2 for superconducting indium.*

Figure 23.8 shows values of $C_S - C_N$ plotted in the form $\Delta C/T$ versus T^2. This figure compares the values calculated by Daunt, Horseman, and Mendelssohn (see footnote 1) and by Misener (see footnote 2) from critical magnetic field measurements with the values obtained from this calorimetric data. The calorimetric values were determined by taking the difference between the actual measured values in the normal state and the value in the superconducting state as obtained at the same temperature by interpolating linearly the C_S/T versus T^2 curve between the two nearest temperatures at which actual data were available. The agreement between the critical-field results and the calorimetric results is fairly good over the region of measurement. The great spread in the calorimetric data is due to the fact that the specific-heat differences are so small compared to the actual specific-heat values being subtracted that errors become very large. The straight line in this figure again has no special significance. It is the curve obtained by subtracting the smoothed and extrapolated curves of figures 23.6 and 23.7.

Finally, we point out that due to the large lattice specific heat and the relatively low transition temperature of indium, the results would be more conclusive if the data could be extended to lower temperatures. Although we can consistently reach 1.3° or 1.4° K by pumping the particular apparatus used in the calorimetric experiments reported here, we have been unable to obtain data below about 1.8° K.

We hope to solve this difficulty in the near future and may then extend the data for indium to lower temperatures. We also plan to make some calorimetric measurements on mercury. These would be very interesting in view of the widely varying values of γ and Θ_D obtained by other methods.

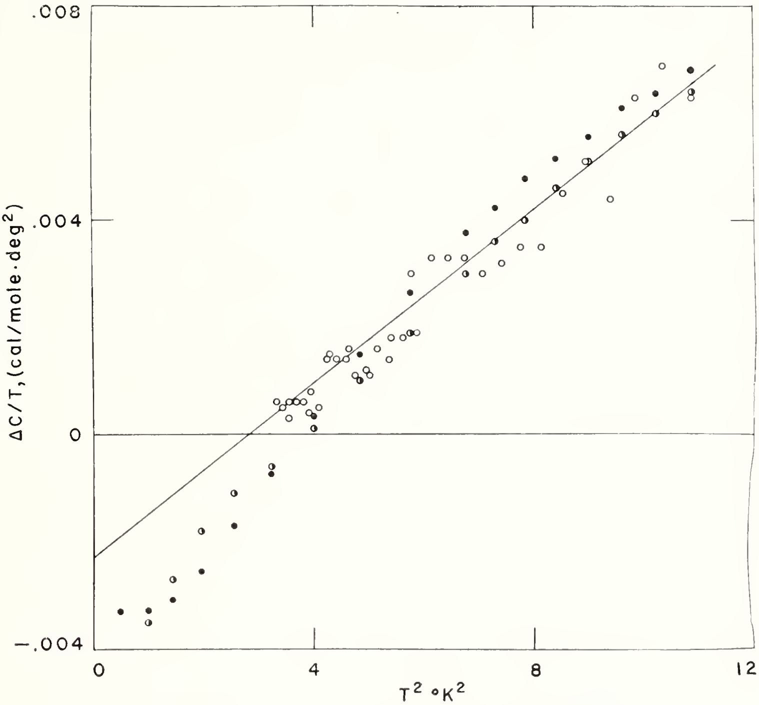

FIGURE 23.8. $(C_S - C_N)/T$ *versus* T^2 *for indium.*

○ From calorimetric data; ◑, Daunt, et al., from critical field; ●, Misener from critical field.

24. Specific Heat of Niobium at Various Temperatures[1]

by A. Brown,[2] M. W. Zemansky,[2] [3] and H. A. Boorse [2] [4]

Introduction

Previous experimental work on the superconductivity of niobium has involved the determination of the H versus T curve. Recent work by Cook, Zemansky, and Boorse [5] gives a zero-field transition temperature of 8.65° K and a value of $\gamma=375\times 10^{-4}$ calories/mole deg [2] (where γ is the coefficient of the linear term in the specific heat of the normal state). More recent work by H. Preston-Thomas [6] at Bristol led to neither a unique value of the transition temperature, nor a unique H versus T curve. Earlier measurements by Daunt and Mendelssohn [7] in the liquid helium temperature range give transitions to the normal state at considerably smaller field strengths than those found by Cook, Zemansky, and Boorse, and thus a smaller value of γ. In all cases the value of γ, which is calculated from the H versus T curves by the use of thermodynamic formulas, is larger than the known value for any other element.

Some of the suggested causes of discrepancies in the magnetic data are impurities in the niobium, dependence on the past history of any individual sample, and the possibility that the thermodynamic formulas may not be applicable in all cases. Cook, Zemansky, and Boorse, for example, state that a tantalum impurity of 0.2 percent or less cannot be detected by spectroscopic analysis. They find, however, that the transitions measured by an a-c method were reversible, whereas the other investigators find some appreciable "frozen in" flux. All the above difficulties in the calculation of the specific heat and the value of γ may be circumvented by the use of calorimetry.

A direct experimental measurement of the heat capacity of niobium will determine whether the linear term is unusually large for this element, and in addition it is possible to see if there is a nonzero value of the linear term in the superconducting state. The small amount of data available on vanadium indicates a situation similar to niobium, and it is planned to investigate this element also. The specific heat of a superconductor at very low temperatures has been described by the relations

Normal state.................. $C_n=\gamma T+464.4\,(T/\theta_n)^3$
Superconducting state.......... $C_s=464.4\,(T/\theta_s)^3$

Thus, if these relations are used, the values of γ, θ_n, and θ_s can be directly obtained. It is to be noted that θ_s is not necessarily the same as θ_n, and thus θ_s is not a true Debye characteristic temperature in the usual sense of the term.

---

[1] Assisted by Office of Naval Research and Linde Air Products Co.

[2] Pupin Physics Laboratory, Columbia University, New York, N. Y.

[3] The City College of New York, New York, N. Y.

[4] Barnard College, Columbia University, New York, N. Y.

[5] D. B. Cook, M. W. Zemansky, and H. A. Boorse, Phys. Rev. **80**, 737, (1950).

[6] H. Preston-Thomas, The University, Bristol, England (dissertation).

[7] J. G. Daunt and K. Mendelssohn, Proc. Roy. Soc. [A] **160**, 127, (1937).

Calorimeter

An adiabatic calorimeter was constructed for the measurements outlined above. The experimental space (15 inches long and 1.1 inches in diameter) can be entirely surrounded by a bath of liquid helium or other refrigerant, except for an opening to a high-vacuum pumping line. This experimental space contains an aluminum thermal dam or radiation shield, inside of which the niobium sample is suspended by two nylon threads. All electric leads to the sample are first wound around the shield and held in thermal contact with it by means of clear glyptal lacquer.

The sample itself is provided with a resistance thermometer, a separate heater of constantan, and an Au-Co versus Cu difference thermocouple between it and the shield. The shield has a separately controlled heater in order to keep it at the same temperature as the sample, and thus insure adiabatic conditions. A pair of mutual-inductance coils used with a ballistic galvanometer is also provided in order to determine the state of the sample.

Results at Liquid Nitrogen Temperatures

For initial measurements in the superconducting state a phosphor-bronze resistance thermometer was insulated from and secured to the niobium sample by means of clear glyptal lacquer. The lacquer was considerably thinned before it was used and was baked at 110° C after application. The weight of one complete coat of glyptal was found to be 0.03 g, whereas the weight of the niobium (in the form of a cylinder ½ inch in diameter and 2 inches long) was 52 g.

It was found that this phosphor-bronze thermometer was sufficiently sensitive at liquid-nitrogen temperatures to give reliable measurements of the heat capacity. In the liquid-helium temperature range the phosphor-bronze thermometer had a resistance of approximately 4 ohms at 4° K, and 2 ohms at 2° K. In addition, the thermometer was found to be completely reproducible from run to run.

The specific heat of niobium in the liquid-nitrogen temperature range is shown in figure 24.1. The results plotted on the graph repre-

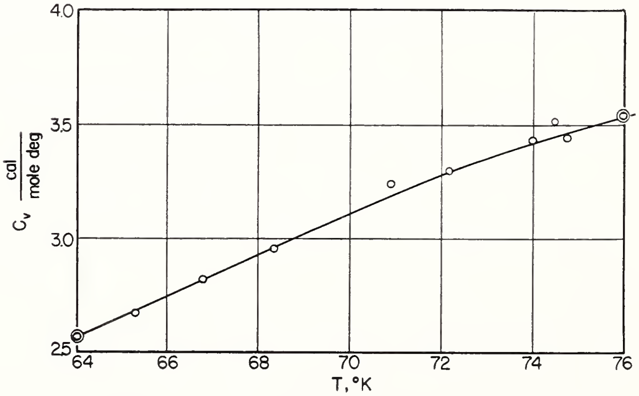

Figure 24.1. *Specific heat of niobium from 64° to 76° K.*

sent data taken on different days, with various resistance-thermometer currents, and with various heater currents. Data were taken by measuring a long "before-period" with the heater off and the temperature essentially constant, a few check points during the short heating period, and a long "after-period," with the temperature again essentially constant. The data showed an abrupt and discontinuous change in the slope of the thermometer resistance versus time curve at the instants of turning the heater on and off. No evidence of overheating was seen when the heater was turned off. The precision of these results is estimated to be plus or minus 5 percent.

Figure 24.2 shows the value of the Debye characteristic temperature from 64° to 76° K. This curve is obtained directly from the specific-heat data shown in figure 24.1 by means of the Debye formula. No correction for the linear term was included. The conversion from the measured C_p to C_v is in the order of 0.5 percent or less. It is to be noted that (except for the linear term) this is Θ_n, the Debye characteristic temperature for the normal state, and also that, as is pointed out by Blackman, it is not expected to be a constant. In fact, the value of Θ_n at helium temperatures may be quite different.

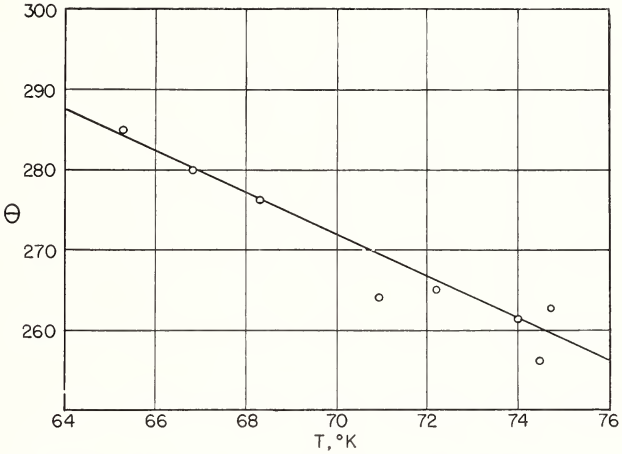

Figure 24.2. *Debye characteristic temperature of niobium from 64° to 76° K.*

Results at Liquid-Helium Temperatures

Measurements of the specific heat of niobium in the normal and superconducting states at liquid-helium temperatures are now underway. Some preliminary results have indicated the value of Θ_s to be approximately 160° K, which is to be compared with the value of 69° K of Cook, Zemansky, and Boorse. The specific heat anomaly at the zero-field transition temperature has been observed.

25. High-Frequency Resistance of Tin, Lead, and Indium

by C. J. Grebenkemper and John P. Hagen [1]

The surface resistance of several metals has been measured, using a resonant cavity of cylindrical shape operating in the lowest mode. The effect of surface finishes has been studied. The cavity chosen for our experiments is cylindrical in shape, of circular cross section, and operates in the TE_{111} mode, which is the lowest mode for a cavity of that geometry. It is a transmission-type cavity, and coupling is made through a small hole accurately located in the center of each end plate. The cavity is constructed of two pieces and joined along a line that is the center of the cylindrical section. If symmetry is maintained, no current should cross the junction. Coupling is made to the cavity by means of two stainless steel waveguide sections through small coupling holes in the cavity itself. One of the waveguide sections goes to the transmitting oscillator, the other to the receiver. Mica windows are placed on one end of the waveguide section and the other end soldered to the cavity. The cavity is then evacuated.

The rapid and accurate measurement of very high Q's at microwave frequencies presents a difficult problem Our measurement procedure is to use a decay method in which the resonator is excited by a pulse of r-f energy and the decay of energy in the cavity is observed after the oscillator is shut off.[2] Even with this means one must use a stable oscillator as a generator, but it is not necessary to achieve a stability of a few hundred cycles in 10,000 megacycles to obtain good measurements of Q. The receiver used is a superheterodyne type, and the generator is a reflex klystron. With this system the coupling to the cavity can be made very light. Consequently, the corrections for the radiation loss through the coupling holes can be made quite small. Several hole sizes were used, ranging in size from 0.078 inch in diameter to 0.099 inch in diameter. Calculations show the radiation, Q, for the smallest hole to be about 60×10^6, for the largest hole about 8×10^6. The unloaded Q of the cavity is obtained from the measured loaded Q corrected for the radiation Q.

Various types of surface treatments were given to the inner surfaces of the cavities. Some cavities were cast in carbon molds and then turned in a lathe. Various types of polishing were tried. Electrodeposited surfaces were investigated. One specimen was formed by cold-pressing a block of tin with a hydraulic press. The purity of the tin used in our experiments was of 99.994 percent.

The normal surface conductivity just above the transition temperature was considerably below the value expected by classical theory, which is in agreement with numerous other experiments and the Reuter-Sondheimer theory of the anomalous skin effect.[3] The pressed-tin specimen yielded the poorest conductivity in the normal region, being about 117 ohm^{-1}. This compares very favorably with

---

[1] Naval Research Laboratory, Washington, D. C.

[2] J. P. Hagen, Decrement (Q) Measurements of low loss cavities (URSI General Assemoly 1948).

[3] G. E. H. Reuter and E. H. Sondheimer, Proc. Royal Soc. [A] **195.** (1948).

Fairbank,[4] who gives a value of 115 ohm^{-1}. The cast-tin specimens, whose inner surfaces were turned in a lathe, yielded a figure of 133 ohm^{-1}. The best mechanical-polished specimen yielded a figure of 160 ohm^{-1}. Pippard in his experiments with single crystals of tin quotes values of 148 ohm^{-1} to 220 ohm^{-1}, dependent on the crystal orientation with current flow.[5]

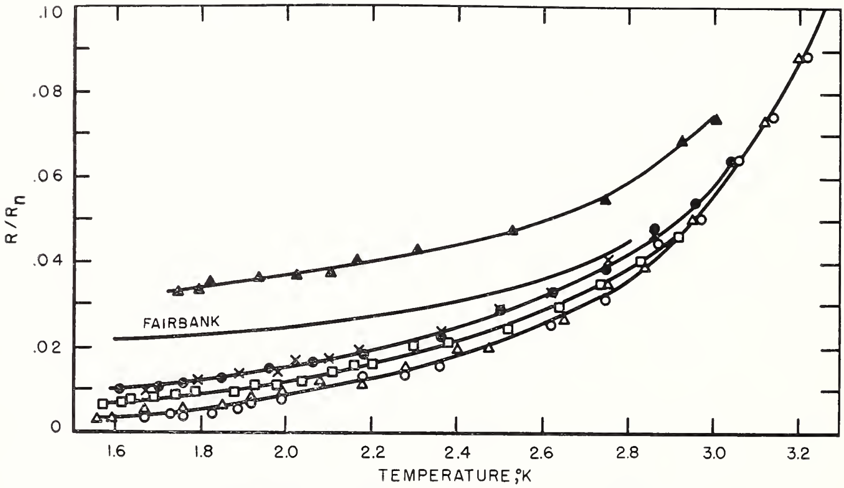

FIGURE 25.1. *Normalized surface resistance versus temperature for tin.*

▲, March 5, 1951: Pressed tin, $f=9$, 105 Mc/sec; ●, February 8, 1950: Cast-tin machine finish, $f=9{,}155$ Mc/sec; ×, April 11, 1950: Electroplated tin, $f=9$, 160 Mc/sec: □, September 29, 1950: Cast-tin mechanically polished, $f=9$, 160 Mc/sec; △, August 4, 1950; ○, August 8, 1950; Electroplated tin polished, $f=9$, 145 Mc/sec.

Figure 25.1 shows the results obtained for the different types of surface finishes. Normalized surface resistance is plotted against temperature. The temperature scale used is the 1937 Leiden scale. Only the lower part of the curves are shown in figure 25.1 as all the curves are in essential agreement near the transition temperature and start to diverge only at about 3.2° K. The pressed-tin surface yielded the highest resistance, being somewhat higher than that obtained by Fairbank. The agreement in the normal region was very good. This difference in the lower temperature region may be due to differences in measurement techniques.

The machined-surface cast-tin specimen yielded a somewhat intermediate value, being considerably better than the pressed surface. The crosses indicate experimental points for an electrodeposited tin surface. The tin was deposited on a brass base from an acid tin bath at a relatively slow rate. Experimental evidence indicates good agreement between these two very different methods of surface preparation. The effects of mechanical polishing on the cast-tin specimen is also shown in figure 25.1. This specimen is the same one used above, except now it has been mechanically polished by placing a number of random-sized steel balls inside the cavity and then rotating it in a lathe for several hours. A considerable improvement in the conductivity has been effected by this process. The bottom curve in figure 25.1 is for an electroplated tin surface after it had been mechanically

---

[4] W. M. Fairbank, Phys. Rev. **76**, (1949).

[5] A. B. Pippard, Nature **162**, (1948); Physica **15**, (1949); Proc. Roy. Soc. (London) [A] 203, (1950)

polished and then etched with hydrochloric acid and a light tin plate deposited over the polished surface. The normalized surface resistance, R/R_n, is extrapolated to 0° K in terms of a function of temperature in a manner first suggested by Pippard. In figure 25.2, $f(T)$ is

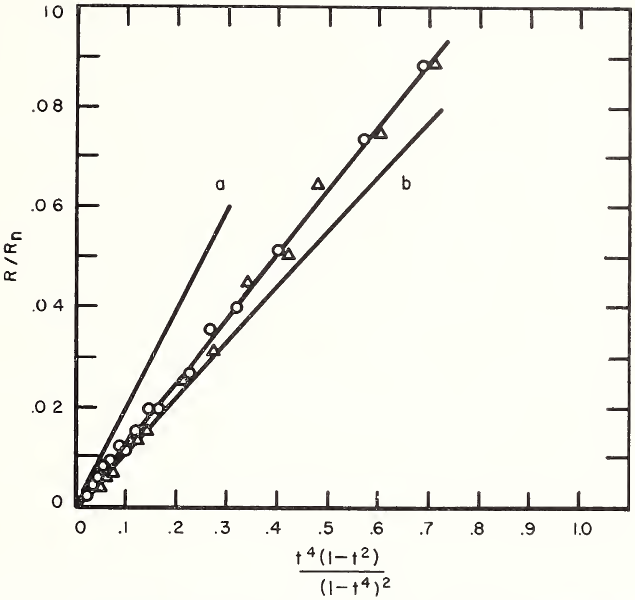

FIGURE 25.2. *Normalized surface resistance versus a function of temperature for tin.*

△, August 8, 1950; ○, August 4, 1950: Electroplated tin polished.
a, Pippard 3.2 cmθ=87°; b, Pippard 3.2 cm θ=72°.
t=T/TC; f=9,145 Mc/sec.

the expression $t^4(1-t^2)/(1-t^4)^2$, where t is the reduced temperature, T/T_c. It is apparent that the polished electrodeposited specimen does extrapolate to zero resistance at 0° K. Pippard's curves for single crystals are also shown on this curve but not in figure 25.1. The cast-tin machine-finished specimen extrapolated to about 0.75 percent residual resistance. This same specimen, after mechanical polishing, extrapolated to 0.40 percent residual resistance.

It appears, from our experiments, that both surface roughness and surface strains contribute to the resistance in the superconducting region. From the results on our pressed-tin surface and those of Fairbank, it appears that the pressing process sets up severe strains and dislocations, thus giving rise to much higher values of resistance. From the work on the machined surface and the subsequent polishing, it appears that some of the residual resistance is due to surface roughness and probably some due to slight strains set up by the machining and polishing techniques.

The experimental results obtained on lead are shown in figure 25.3. The curve shown is a plot of loaded Q versus temperature. The lead specimen used was a cast-lead machine-finished cavity. The surface conductivity of lead just above the transition temperature was 176 ohm^{-1}, somewhat above that of tin. The experiments on lead were conducted in the Collins helium cryostat; all others were conducted in external helium Dewar flasks. The temperatures above those of

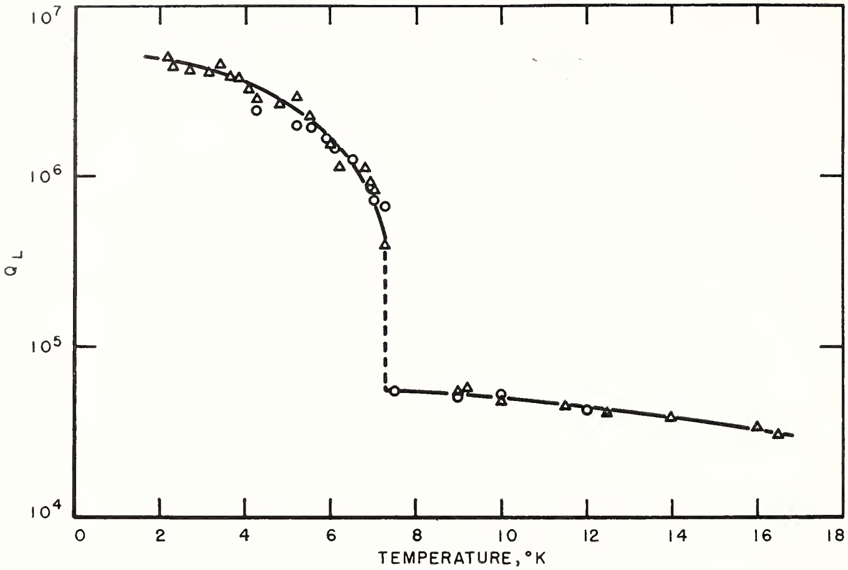

Figure 25.3. *Q_L versus temperature for lead.*

○, January 19, 1950. △, March 2, 1950. Lead cavity machine finish. f=9,165 Mc/sec.

liquid helium were measured by a constant-volume helium thermometer. The temperature measurements are not precise as no method of stabilizing the temperature was used. The scatter on lead data is somewhat worse than that of the tin data. Part of it is probably due to temperature difficulties.

If the normalized skin resistance is extrapolated to 0° K, a residual resistance of about 1 percent is obtained. This is about what one would expect from this type of surface treatment. One could conclude that lead is about as good a conductor as tin in the superconducting region.

The experimental results for an electrodeposited indium surface are shown in figure 25.4. Indium is quite similar to tin except the initial conductivity, for two specimens measured, was quite low. Whether this is the nature of indium at these frequencies or is due to an insufficient thickness of indium on the base metal will have to be resolved with future measurements. If the normalized surface resistance is extrapolated to 0° K, a residual resistance of about 0.50 percent is obtained.

Just recently we extended our work on tin to 24,000 megacycles per second, using the same techniques as before. The cavity used was a cylindrical cavity operating in the TE_{111} mode. Our results show considerably better conductivity in both the normal and superconducting regions than those of Maxwell, Marcus, and Slater.[6] The particular cavity used was made of cast tin, turned in a lathe, and then polished with gamal cloth and alumina and distilled water. Figure 25.5 shows a plot of normalized surface resistance versus temperature for two specimens, one at 24,300 megacycles, the other at 9,160 megacycles. The surfaces on both cavities were mechanically polished, and both extrapolate to nearly the same residual resistance,

---

[6] E. Maxwell, P. M. Marcus, J. C. Slater, Phys Rev. **76,** (1949).

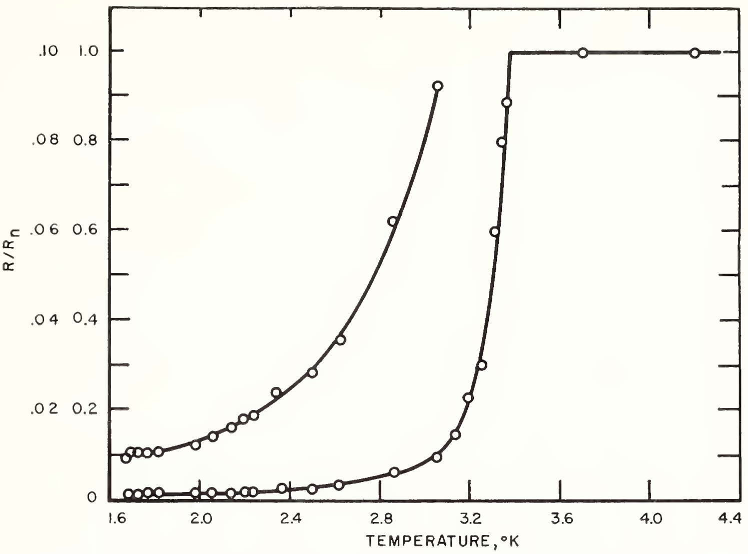

FIGURE 25.4. *Normalized surface resistance versus temperature for electroplated indium.*

$f=9{,}137$ Mc/sec. Upper curve expanded × 10.

as is shown in figure 25.6. Consequently, it was felt that the results for these two specimens could be compared at least qualitatively. However, for a rigorous comparison, both specimens should extrapolate to zero resistance at 0° K.

The normal surface resistance, R_n, varies as $\omega^{2/3}$, which experimental evidence indicates. The superconducting resistance, R, at a given

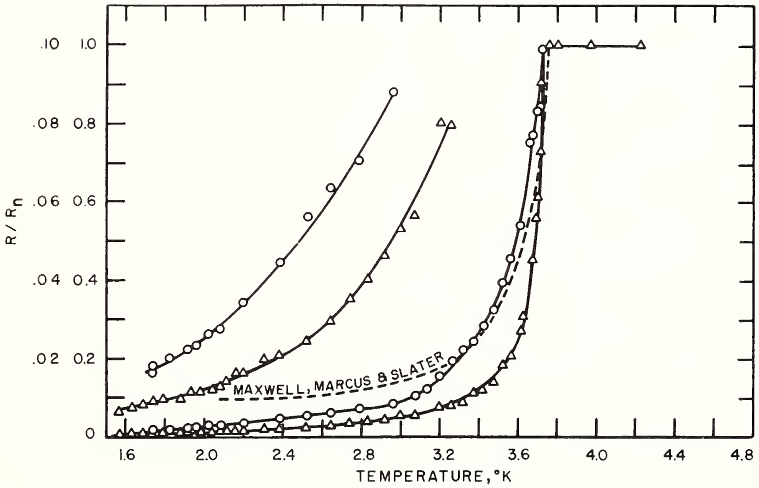

FIGURE 25.5. *Normalized surface resistance versus temperature for tin at 9,160 and 24,300 Mc/sec.*

△, September 29, 1950: Cast-tin mechanically polished, $f=9{,}160$ Mc/sec; ○, February 20, 1951: Cast-tin mechanically polished, $f=24{,}300$ Mc/sec. Upper curve expanded × 10.

temperature, sufficiently below the transition temperature, should vary as ω^2; consequently, R/R_n should vary as $\omega^{4/3}$ if $R/R_n = A(\omega)f(T)$. The $f(T)$ that fits the experimental curves is $t^4(1-t^2)/(1-t^4)^2$, where $t = T/T_c$. If $A(\omega)$ is evaluated from our curves, the value obtained for the lower frequency is 0.116, and for the higher frequency the value is 0.260. The ratios between these values is 2.24. The expected ratio from theory is 3.67. This type of disagreement has also been observed by Pippard. The experimental evidence appears to be in contradiction with the theory.

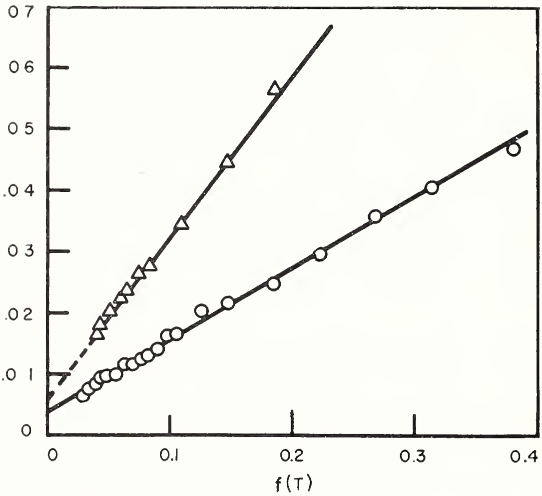

FIGURE 25.6. *Normalized surface resistance versus a function of temperature for tin at 9,160 and 24,300 Mc/sec.*

△ $f=24{,}300$ Mc/sec· ○, $f=9{,}160$ Mc/sec; $r=\frac{R}{R_N}$; $f(T)=\frac{t^4(1-t^2)}{(1-t^4)^2}$.

From the experimental evidence at the higher frequency it appears that the twilight region of superconductivity has not been reached. The small residual resistance obtained at 0° K is probably due to small surface strains and possibly some roughness. In our measurements we have only to correct for the radiation loss through the coupling holes, and by keeping this quantity small the correction is quite small. No dielectrics are used, and we do not have to correct for can-losses. The technique used lends itself readily to measuring high Q's because time can be measured precisely. For the very high Q's, timing markers generated by a crystal controlled oscillator are put on the scope. For the lower values of Q, a precision delay circuit is used to measure time. The receiver is calibrated with a precision attenuator. The measurements can be made very rapidly and, if desired, can be photographed.

26. Detection of Microwave Signals by NbN Superconductors in the Transition Region

by J. V. Lebacqz and M. G. Bodmer*

During the past several years, the cryogeny laboratory of the Johns Hopkins University has pursued investigations on radiofrequency detection by NbN bolometers. The last paper published [1] covered the results obtained up to that time in the frequency range of 1 to 10 Mc. In addition, the same phenomena were observed qualitatively in the 100-Mc frequency range. It was then decided to extend the measurements to the microwave region, between 9,000 and 10,000 Mc, where some effect of the relaxation time might be expected to appear. The present paper will review briefly the equipment used, the results obtained, and the theoretical conclusions that may be drawn from these results.

The cryostat itself is essentially the same as those used previously at this laboratory for work with infrared bolometers. The bolometer mount, however, and the "nose" of the cryostat were redesigned to permit efficient transfer of microwave energy to the NbN strip. (fig. 26.1, a and b). Several requirements have to be met. The heat losses have to be kept to a minimum; the bolometer impedance must be transformed to the impedence of the microwave transmission line; the bolometer must be mounted in good thermal contact with the 15° K sink; and adjustments of the impedance transformation have to be made without loss of vacuum.

The transmission line chosen was standard X-band wave guide. The thermal losses were minimized by the use of two choke-flange joints, permitting a slight mechanical motion of the line without unduly affecting the electrical characteristics. The vacuum seal was obtained simply by a 0.012-in. mica window glued to the output. The reactance introduced by the mica window was canceled out by an appropriate inductive diaphragm.

The bolometer was mounted in a double stub tuner, to permit obtaining the very high impedance ratio necessary (approximately 100 to 1). Unfortunately, this imposed stringent mechanical requirements on the mount and no low-loss insulating material was found on which the NbN strip could be glued, and which would maintain its mechanical properties at 15° K. Accordingly, the NbN was glued over a thin layer of Bakelite covering a copper post used as temperature sink. A typical value for the NbN strip resistance at 9,300 Mc is between 4 and 5 ohms, whereas the wave-guide impedance is between 300 and 400 ohms. It was found possible to obtain a good match (standing wave ratio less than 1.3 over a bandwidth of 10 Mc) by careful adjustment of a type 0–0 mount in combination with a parabolic-shaped moving short circuit.

The rest of the equipment included a specially built audio-amplifier (with input matched to the NbN resistance), signal generators, square-

---

*Johns Hopkins University, Baltimore, Md.

[1] J. V. Lebacqz, C. W. Clark, M. C. Williams, D. H. Andrew, Detection at radio frequencies by superconductivity, Proc. Inst. Radio Engrs. **37,** 1147 (1949).

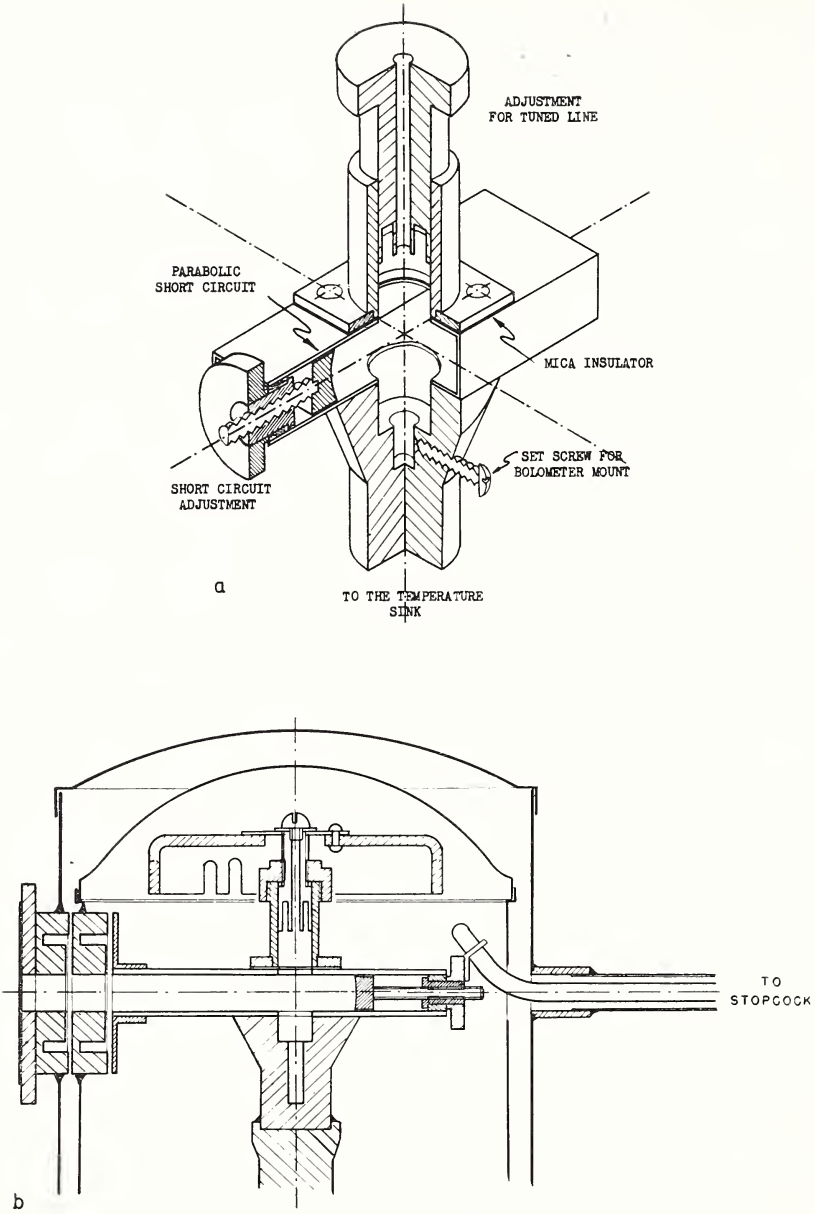

FIGURE 26.1. *Sketch of bolometer and cryostat.*

a, Double tuner; b, cross section of cryostat showing short-circuit adjustment.

wave modulator, standing-wave indicator, spectrum analyzer, d-c bias arrangement, vacuum pumps, and indicators.

The equipment described above was connected as shown in the block diagram, figure 26.2. Before its use, a series of d-c transition curves were obtained, as shown in figure 26.3. From these, it can readily be measured that the maximum rate of change of resistance as

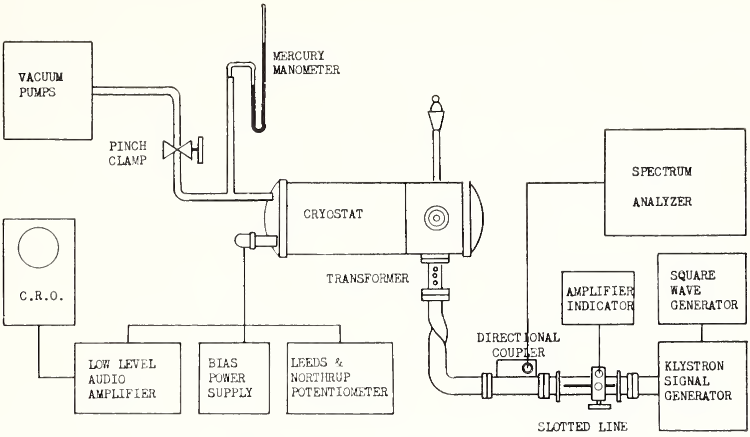

Figure 26.2. *Block diagram for microwave measurements.*

function of temperature, at constant-bias current, is about 0.8 ohm/° K. Conversely, the maximum rate of change of resistance, as a function of bias current, at constant temperature, appears to be about 100 ohms/amp at small values of bias current (<1 ma).

During the experiments on microwave detection, the line and tuner were adjusted to obtain a good match just above the transition temperature. The microwave source was then square-wave modulated and the temperature of the bolometer lowered through the transition for various values of bias current. At certain values of temperature, a pattern corresponding to the modulating signal was observed on the oscilloscope. The maximum amplitude of the demodulated output is shown as a function of temperature for various bias currents in figure 26.4, and as a function current at various temperatures in figure 26.5. In addition, typical demodulated wave shapes are shown in figure 26.6. From these, it is immediately obvious that two entirely different phenomena are taking place. At high bias currents (about 5 to 25 ma) and at a temperature of 15° K (near the middle of the transition), the original square wave modulation is not reproduced in the demodulated output; instead, the output consists of exponential curves, and

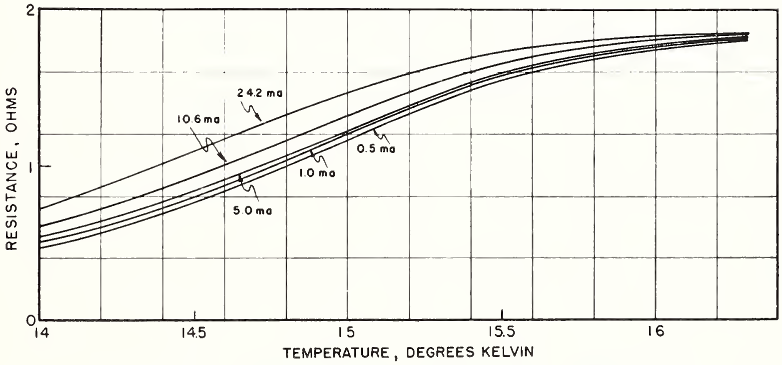

Figure 26.3. *Direct-current transition curves reduced values.*

measurements indicate that the time constant involved is approximately 600 μsec. This appears to be a bolometer heating time constant. On the other hand, at small bias currents (1 ma or less) and

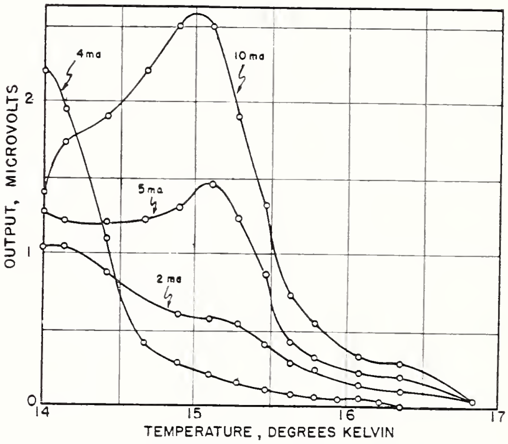

Figure 26.4. *Demodulated output as a function of temperature 9300 Mc.*

at a temperature near 14° K, the original square wave of the modulating signal is preserved, except for a slight rounding off produced by the band-pass of the audio amplifier. This indicates that little or no time lag due to heating exists under these conditions, and that the phenomenon observed is a true detection.

With these results in mind, the curves of figure 26.4 and 26.5 are easy to understand. The two peaks at 14° and 15° K in figure 26.4 are caused by the two different mechanisms of demodulation, bolometer action and detector action. Similarly, the deviation from linearity of the output-bias-current curves at low currents for tempera-

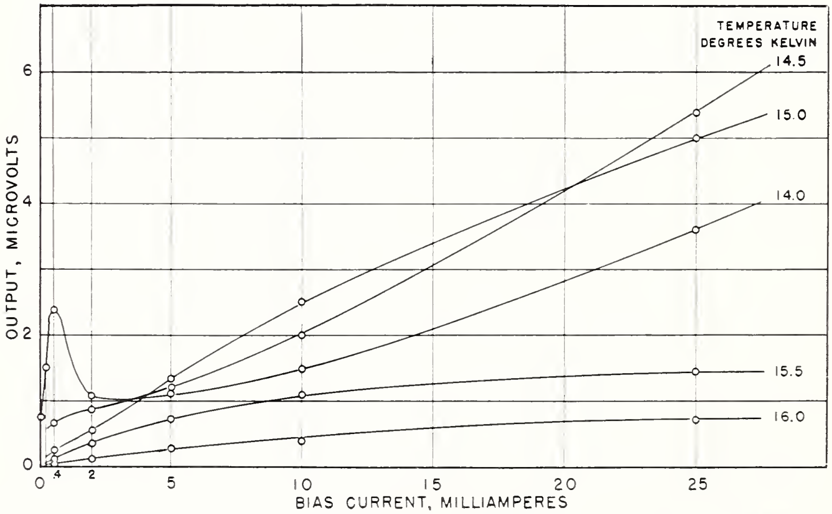

Figure 26.5. *Demodulated output as a function of bias current 9300 Mc.*

tures below 14.5° K can readily be explained in terms of the appearance of the detection phenomenon in that region.

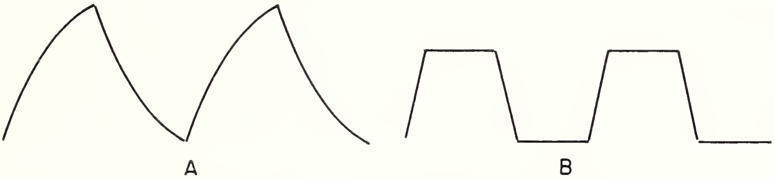

Figure 26.6. *Demodulated wave shapes.*

A, Large bias current; B, small bias current.

The mechanism of this detection effect can be understood at low radio frequencies, if the curve of resistance vs dc current (fig. 26.7) at constant temperature is considered. It might seem surprising to find the same effect for rf currents in the 10^{10}-cycle frequency range as at about 1 Mc. If, however, one considers the superconductor constant Λ(2) as being of the same order of magnitude for NbN as for other superconductors, then the explanation appears rather obvious. The resistivity of NbN, in the normal state, is probably at least 100 times that of Hg or Sn just above transition. Hence, one should expect the critical angular frequency at which skin-effect depth and supercurrent-penetration depth are equal to be approximately 10^{13} $\sec^{-1}$ for this material. This is in the lower infrared region, and it is hoped that some work in that frequency region will indicate a change in optical coefficient, coupled with the appearance of the detection phenomenon.

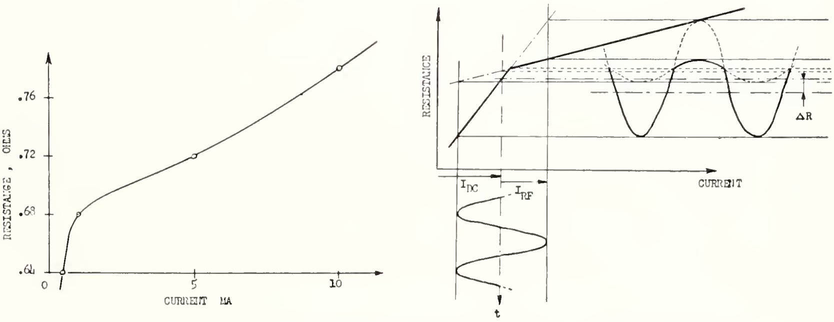

Figure 26.7. *Detection process in NbN at low radio frequencies.*

This research has been supported in part by the Office of Naval Research, for which the authors are very grateful. They extend their appreciation to the whole staff of the Cryogeny Laboratory, The Johns Hopkins University, for their constant cooperation, and especially to D. H. Andrews for the many enlightening discussions, and to Miss M. C. Williams, who painstakingly prepared the NbN bolometers.

---

[2] F. London, Superfluids, p. 29; also p. 84 (John Wiley & Sons, Inc., New York, N. Y., 1950).

27. Properties of Liquid He^3-He^4 Mixtures

by J. G. Daunt and C. V. Heer [1]

1. Introduction

Helium is unique in maintaining its liquid phase under its staurated vapor pressure to temperatures closely approaching the absolute zero. It is not surprising, therefore, that solutions of He^3 in liquid He^4 should be the subject of investigation, in order to observe the possible influence of macroscopic quantum effects on their thermodynamical behavior. The fact also that He^3 in solution in liquid He^4 does not partake in the superfluid motions, as first shown by Daunt and coworkers [1, 2],* further stresses the possibility of observation of other peculiarities of such solutions as the temperature is reduced, i. e., as the superfluid constituent of the He^4 becomes predominant. The experimental study of such solutions has been mainly concerned with measurement of the distribution coefficient, i. e., the ratio of the concentration, C_V, of He^3 in He^4 in the saturated vapor, to the concentration, C_L, of He^3 in He^4 in the solution, and this has yielded results that have been both mutually inconsistent and subject to excessive experimental scatter. It was the purpose of the experiments reported in this paper to attempt to obtain reliable data on the distribution coefficient of He^3 in the liquid He^4 over a wide temperature range and to correlate the results with such theorectical considerations as have been put forward.

In order to judge the reliability of our method of measurement of the distribution coefficient, C_V/C_L, and to assess the possibility of systematic experimental errors arising therein, a review of previous work is considered necessary and is given below. Such a review also enables the growth of the associated theoretical considerations to be followed simultaneously.

2. Survey of Previous Work

2.1 Measurements Above the Lambda Temperature

A few measurements of the distribution coefficient, C_V/C_L, of He^3 in liquid He^4 above the lambda temperature (2.18° K for pure He^4) have been previously made, using, however, only very dilute solutions. This work has been reported by Daunt, Probst, and Smith [3], for mixtures with an unrefrigerated concentration, C_3, of He^3 of 1.3×10^{-6}, and by Lane and coworkers [4], using mixtures with similar values of C_3. In both sets of experiments the concentration in the vapor phase, C_V, in equilibrium with the solution was measured by withdrawing a sample of the vapor from the low temperature and by subsequent analysis with a mass spectrograph. The value of the concentration in solution, C_L, was subsequently calculated from a knowledge of the volume occupied by the liquid and by the vapor

---

[1] The Mendenhall Laboratory, The Ohio State University, Columbus, Ohio.

*Figures in brackets indicate the literature references on p. 126.

and of the liquid and vapor densities. This method of estimation of C_V/C_L must necessarily not be a true equilibrium measurement, and hence may introduce systematic and inestimable errors. Moreover, because the total concentrations are so small ($C_3 \sim 10^{-6}$) further errors may have been introduced in the mass-spectroscopic analysis. The results of the measurements indicate values of C_V/C_L, in approximate agreement with those calculable for perfect solutions obeying Raoult's law from the equation

$$\frac{C_V}{C_L} = \frac{\overset{\circ}{p}_3}{\overset{\circ}{p}_4}, \tag{1}$$

where $\overset{\circ}{p}_3$ and $\overset{\circ}{p}_4$ are the vapor pressures of pure liquid He^3 and pure liquid He^4, respectively, at the temperature of interest. The theoretical evaluation of C_V/C_L from Raoult's law obtained from eq (1) is given by the heavy broken curve in figure 27.2.

Subsequent work above the λ-temperature on the measurement of the vapor pressures of He^3 solutions in liquid He^4 under equilibrium conditions by Lane and coworkers [5] using (concentrations $C_3 = 1.6 \times 10^{-3}$) and by Weinstock, Osborne, and Abraham [6] (using concentrations $C_3 = 20.3$ and 25%) has indicated, however, that values of C_V/C_L greater than those given by Raoult's law are to be expected. Unfortunately, the data reported are insufficient to enable exact numerical values of C_V/C_L to be calculated from these vapor-pressure measurements. On the other hand, because these measurements were taken in equilibrium and the absolute concentrations, C_3, were much higher than those in the previous work, there is reason to ascribe greater weight to the general conclusion that can be drawn from them, namely, that C_V/C_L even above the lambda temperature may be larger than that calculable from Raoult's law.

2.2 Measurements Below the Lambda Temperature

It has been in measurements of C_V/C_L below the λ-temperature that the greatest discrepancies between the various results have been evidenced, and these discrepancies have been due mainly to a lack of uniformity in the distribution of He^3 throughout the volume of the liquid phase of the solution. This lack of homogeneity in the liquid phase is primarily due to (a) the much larger heat influxes to the experimental arrangements at temperatures below the λ-temperature and (b) the fact that He^3 in solution in liquid He^4 does not partake in superfluid flow [1, 2]. The following considerations sketch briefly the various mechanisms producing concentration gradients within the body of the solution.

Figure 27.1 (a) diagramatically represents a vessel containing liquid He^4 at a temperature below the λ-temperature, connected by a tube to higher temperatures. Previous work [7] has shown that a thick, mobile flm is formed above the liquid surface, which moves toward the warmer and higher parts of the tube to some position (arbitrarily marked "a" in figure 27.1, a, where the supply of heat from the higher parts of the apparatus is sufficient to evaporate the mobile film. The vapor thus formed at "a" returns down the tube, and in condensing on the liquid surface gives up its heat of condensation. By this two-phase convective process very considerable heat influxes, $\dot{Q}$, to the liquid-helium vessel may be produced, whereas when the vessel is at a temperature above the λ-temperature, no mobile film exists, and hence no large heat influx due to the two-phase convection occurs.[2]

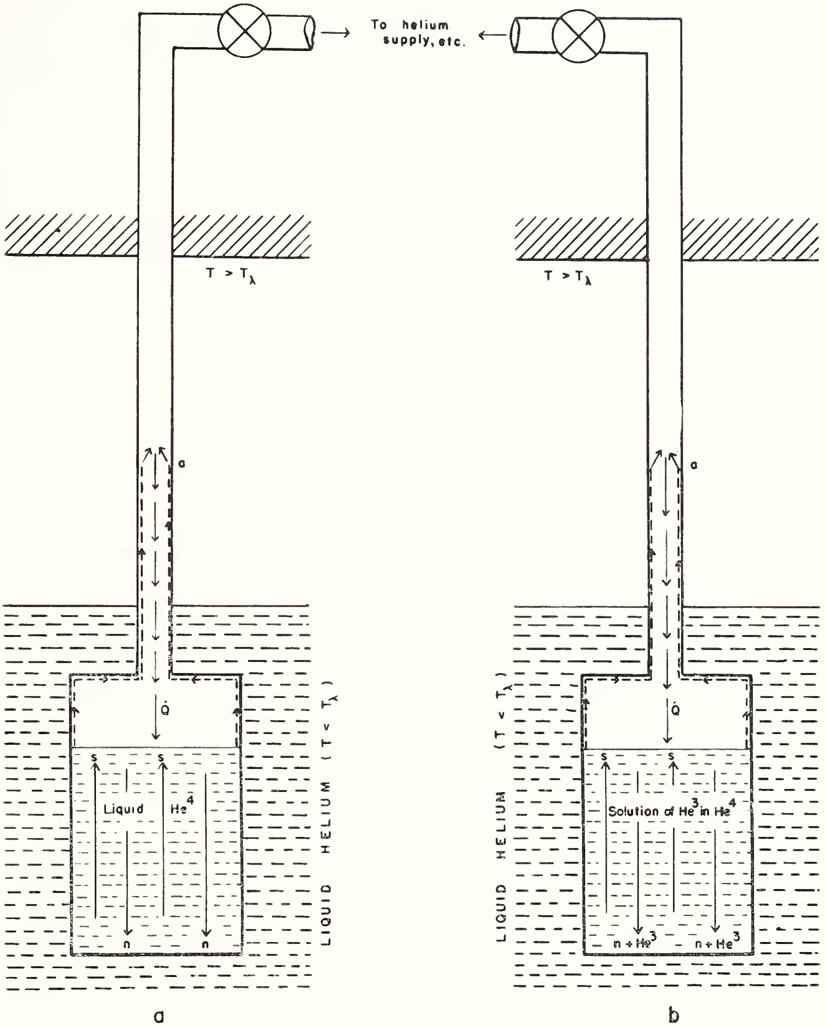

FIGURE 27.1. *Diagrammatic sketch of convection currents set up in vessels containing helium* II *or solutions of* He^3 *in helium* II.

Within the body of the liquid (see fig. 27.1, a), the large heat influx due to condensing vapor below the λ-temperature sets up an internal convection, the "superfluid" constituent moving upward toward the heat source at the surface and the "normal" constituent forming the return flow downward. When the liquid-helium vessel is above the λ-temperature no such internal convection of the superfluid and normal constituents exists.

---

[2] The marked change in the heat influx at the λ-temperature due to the occurrence of the two-phase convection has been used by Daunt and Heer, Phys. Rev. **79**, 46 (1950), to observe λ-temperatures of solutions of He^3 in He^4 below 1°K.

Figure 27.1, b, diagrammatically represents an experimental arrangement exactly similar to that of figure 1, a, the vessel containing, however, a solution of He^3 in liquid He^4, such as has been used, in principle, for some evaluations of the distribution coefficient, C_V/C_L, for these solutions [3, 4, 8]. For such an arrangement, therefore, below the λ-temperature, both the two-phase convection and the internal convection within the liquid must occur with relatively large heat influxes, $\dot{Q}$, flowing into the vessel. The distribution of the He^3 in this case must be determined as follows. As the He^3 does not partake in the superfluid flow either in the film [1] or in the bulk liquid [2], the upward flow of the mobile film contains no He^3, and hence the two-phase convection is of He^4 only, and the internal convection must be such that the superfluid flow, S, upward carries only He^4, whereas the normal flow, n, downward, being viscous, carries down the He^3 with it. The result is a marked concentration gradient of He^3 within the liquid, with the surface depleted of He^3. If, therefore, in such an arrangement the distribution coefficient, C_V/C_L, is assayed by sampling and analyzing the vapor, the result must give values of C_V that are too small, because, at best, the vapor sampled would have been in equilibrium with the solution at the surface. Moreover, this "vapor sampling" technique must introduce further error, not only because it is a nonequilibrium measurement but also because the downward vapor flow in the two-phase convection must tend to carry He^3 away from the high-temperature end of the tube and hence further reduce the observed value of C_V. On the other hand, for similar experimentation above the λ-temperature, these errors due to the two-phase convection and the internal convection would be absent.

The results obtained by Daunt, Probst, and Smith [3] and by Lane and coworkers [8] for C_V/C_L below the λ-temperature are shown in figure 27.2, and it will be seen, in agreement with the above considerations, that the values are all much smaller than would be expected even from Raoult's law (eq 1). Indeed, in one set of observations [8], C_V was found to be zero for all temperatures below 1.8° K.

The unwanted concentration gradients within the solution could in principle be removed by stirring, and this stirring could be accomplished in three ways, namely, (a) by mechanical stirring, (b) by stirring with acoustical waves, and (c) at sufficiently high average concentrations, C_3, automatically.

Method (a) has, so far, not been reported. Method (b) has been adopted by Taconis, et al. [9], using helium gas with an unrefrigerated concentration, $C_3=5\times10^{-4}$. In this arrangement, similar in general principle to that of figure 27.1, b, acoustical vibrations occurred [10] in the gas in the tube leading from room temperature to the vessel at liquid helium temperatures, the intensity of the vibrations being controlled by relative movement of another inner tube. These acoustical vibrations in the gas column are transmitted to the solution and result in stirring, the errors introduced by the internal convection thus being minimized. The experiments reported by Taconis, et al. [9], also obviated the errors outlined above that must accompany a "vapor-sampling" technique, as used elsewhere [3, 8], since the values of C_V/C_L were calculated from equilibrium measurements of the vapor pressure of the solution. These data therefore can be regarded as far more reliable than those reported previously. It is possible, however, that the values of C_V/C_L obtained from these data may be too large because the heat influx accompanying the acoustical waves may tend to raise the temperature of the vessel above that of the surrounding liquid-helium bath and hence increase the observed vapor pressure of the solution.

The results obtained (3 points) by Taconis, et al. [9] are given in figure 27. 2, together with a series of values of C_V/C_L at 1.38° K obtained with a similar technique by Taconis, Beenakker, and Dokoupil [11],[3] using solutions with concentrations of C_V, from 1.1 to 2.2 $\times 10^{-3}$. It will be seen that the values of C_V/C_L obtained all lie well above the values that would hold for a classical perfect solution (Raoult's law). Taconis, et al. consequently put forward the hypothesis that He^3 in liquid He^4 below the λ-temperature could be regarded as being in solution with the "normal" constituent of the liquid He^4 only. Assuming such a limited solubility to observe the laws for classical perfect solutions, this empirical rule leads to the following formulation for C_V/C_L:

$$\frac{C_V}{C_L}=\frac{\rho}{\rho_n}\cdot\frac{\overset{\circ}{p}_3}{\overset{\circ}{p}_4} \tag{2}$$

where ρ and ρ_n are the total density of liquid He^4 and the density of the "normal" constituent of He^4, respectively. By using the approximate result [12] (valid at least in the temperature range concerned, 1.6° to 2.18° K) that $\rho_n/\rho=S/S_\lambda$, where S and S_λ are the entropies of the liquid He^4 at the temperature of interest and at the λ-temperature, respectively, and using known values for the entropy [13], the value of C_V/C_L according to eq (2) can be calculated, and the result is shown in figure 27.2. Except for the points subsequently reported at 1.38° K [11], it will be seen that the first results of Taconis, et al. [9] are in substantial agreement with eq (2). This fact has resulted in Taconis' hypothesis, given by eq (2), being widely adopted in theoretical thermodynamical calculations regarding solutions of He^3 in He^4 below the λ-temperature [14]. It should be further emphasized that if the laws for classical perfect solutions are continued to be assumed valid, above the λ-temperature there should be no difference between eq. (2) and (1) as above the λ-temperature $\rho_n/\rho=1$. This means therefore, according to Taconis, that Raoult's law should be at least approximately valid above the λ-temperature.

In measuring C_V/C_L, the third experimental method of stirring the He^3 and He^4 solution (method c), in order to avoid unwanted concentration gradients in the liquid, has been briefly mentioned previously by us [15], and has been made use of in the experiments reported in the present paper. The general experimental arrangement set up is similar in essentials to that of figure 1, b, so that in the absence of stirring, a concentration gradient occurs within the solution such that the higher concentration is at the bottom. In such an arrangement, if the average concentration of He^3 in the solution is sufficiently high, an excess He^3 concentration at the bottom will create there an excess vapor pressure sufficient to create ebullition. The excess He^3 concentration necessary for such ebullition will be dependent on the depth of the solution. If ebullition at the bottom occurs, stirring of the solution is automatic. It is to be concluded, therefore, that in arrangements where no provision is made for mechanical or acoustical stirring, the results obtained for C_V/C_L should

---

[3] These authors consider that the stirring achieved in these experiments was not so complete as that in those previously reported [9].

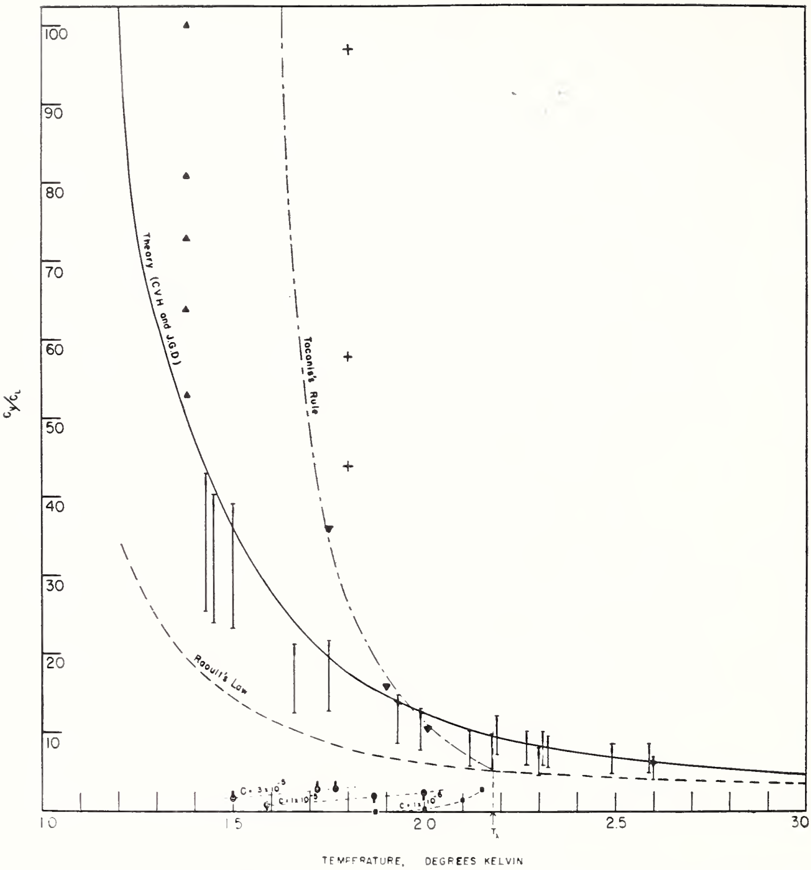

FIGURE 27.2. *Plot of C_V/C_L versus T from experiment and theory for dilute solutions of He^3 in He^4.*

————————, theory of Heer and Daunt [20]; - - - - - - - - - - - - - -, Raoult's Law for perfect classical solutions; - - - - - - - - - - - - - - -, calculated from Taconis Rule [9]; ▼, experimental results of Taconis, et al. [9]; ▲, experimental results of Taconis, et al. [11]; +, experimental results of Lane and coworkers [8]; ■, experimental results of Lane and coworkers [8]; ♁, experimental results of Daunt and coworkers [4]; ♀, experimental results of Daunt and coworkers [4]. The vertical lines give the range of values of C_V/C_L experimentally reported in this paper.

approximate more closely the correct values the higher is the initial unrefrigerated He^3 concentration of the helium. In support of this it is to be noted that the experiments of Daunt, Probst, and Smith [3] show higher values of C_V/C_L below the λ-temperature for higher values of the average concentration (see figure 27.2), and this variation is most probably due to this automatic stirring coming into partial operation rather than to the other mechanisms as have, for example, been suggested by London and Rice [16].

Finally, in this review of methods of overcoming unwanted concentration gradients in the solution, the method of Lane and coworkers [17] is of interest. The principle of their arrangement is shown in figure 27.3. By introducing the filling tube at the bottom of the vessel, the direction of heat influx is reversed and hence the He^3 tends to concentrate at the surface of the solution in the large vessel due to the two-phase and internal convection as shown in figure 27.3.

However, if the filling tube is in good thermal contact with the helium bath, this inhomogeneity of concentration in the solution may be small.[4] The vapor above the solution in the vessel was sampled in these experiments [17] by taking out gas from the large vessel through a "Breakseal." Such an arrangement, therefore, would be expected to give results for C_V/C_L higher than appropriate for the average He^3 solution concentration, owing to the tendency to

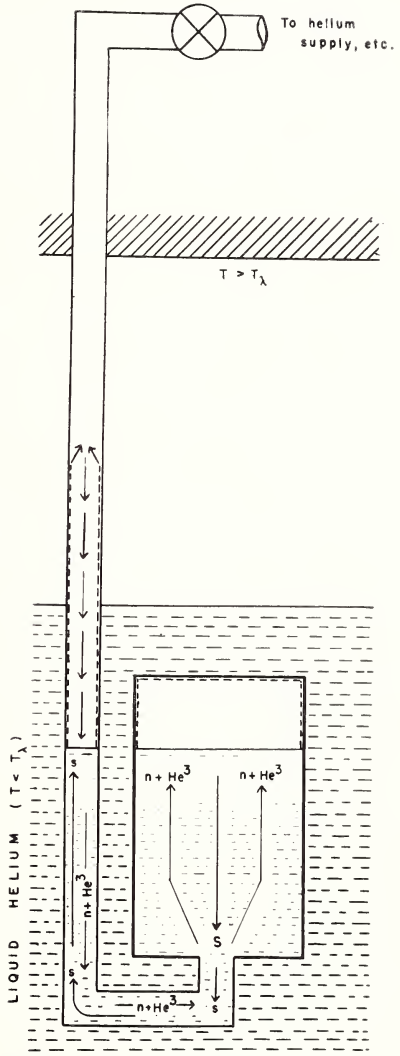

FIGURE 27.3. *Diagrammatic sketch of convection currents in experimental arrangement as used by Lane and coworkers [8] for measuring C_V/C_L below T_λ.*

---

[4] By supplying considerable heat influx to the right-hand vessel of the apparatus sketched in figure 27.3, large excess He^3 concentrations would be formed at the surface of the left-hand tube owing to the internal-convection process described above. This was employed as a method of concentrating and separating He^3 from He^4 by Lane and coworkers. See Lane, Fairbank, Aldrich, and Nier, Phys. Rev. **73,** 256 (1948) and Reynolds, Fairbank, Lane, McInteer, and Nier. Phys. Rev. **76,** 64 (1949), and by Rollin and Hatton, Phys. Rev. **74,** 508 (1948).

collect an excess He^3 concentration at the surface. That this is so is shown by the results obtained (see fig. 27.2), which are higher than would be expected either from Raoult's law (eq 1) or from Taconis' empirical expresion (eq 2).

3. Experimental Technique Employed

The experimental arrangement used by us for the evaluation of C_V/C_L is shown diagrammatically in figure 27.4. Two vessels, each having an internal diameter of 3.2 mm and a capacity of 40 mm,[3] were drilled out of a solid block of pure copper, so that they were in good thermal contact with each other. The vessels were connected to their external gas supplies by capillary tubing of 0.79-mm internal diameter, part of which was of glass so that the levels of the liquids

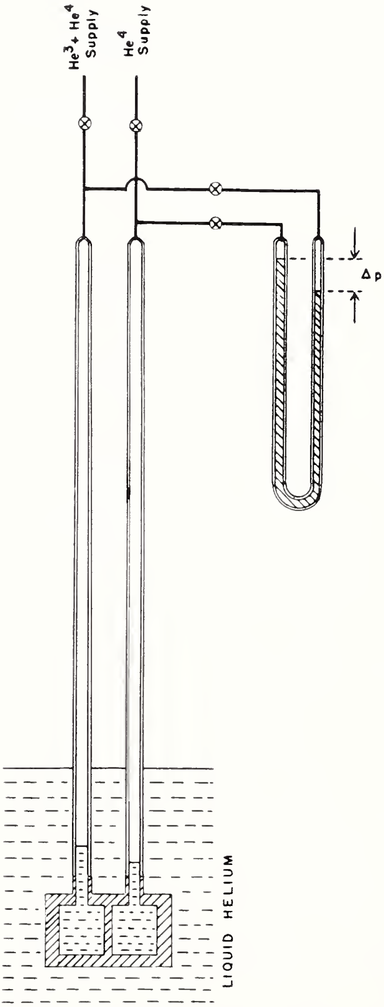

FIGURE 27.4. *Diagram of apparatus reported in this pape*r *for measurement of* C_V/C_L *for solutions of* He^3 *in* He^4.

in the two volumes could be observed directly, and the vessels immersed in a bath of liquid helium.

One vessel was filled with pure liquid He^4 and the other with a solution of He^3 in liquid He^4, having a value of C_L of about 1.5 percent, until the levels were visible in the capillaries and at any desired temperature the difference in vapor pressure between the solution and the pure liquid He^4 could be observed with an external differential oil (Octoil, S) manometer of very small dead (gas) volume (see fig. 27.4).

Significant dimensional data are given in table 27.1. Provision was made also for making a differential comparison between the vapor pressure of the pure liquid He^4 in the vessel and the vapor pressure of the helium bath. (For simplicity, this arrangement is not shown in fig. 27.4).

Table 27.1. *Dimensional data of apparatus*

Internal diameter of each copper vessel mm	3.2
Volume of each copper vessel:	
December 14, 1950, experiment mm ^{3}	50
December 21 and 22, 1950, experiments mm ^{3}	40
Diameter of glass capillaries, leading from copper vessels to room temperature mm	.79
Average volume of gas "dead" space at room temperature on He^3+He^4 line cm ^{3}	3.5

After consideration of the points enumerated in section 2 our experimental arrangement was chosen as one that would minimize systematic errors for the following reasons:

(a) The maximum height of the solution, measured from the bottom of its containing vessel, was 50 mm, which for a 1.0 percent average value of solution concentration would result in ebullition at the bottom of the vessel for a concentration excess of 15 percent at 1.5° K. At 1.8° K the error is 7.5 percent. This would therefore provide adequate automatic stirring, and would provide a surface concentration within 15 percent of the measured average value at the lowest temperature and better accuracy at higher temperatures.

(b) By having both vessels in the same copper block, the temperatures of both vessels should remain the same even above the λ-temperature.

(c) By measuring differential vapor pressure, an equilibrium measurement is made, which also is independent of the two-phase convection in the filling tubes. Moreover, for all temperatures used, the correction for thermomolecular pressure differences is negligible [18].

If Δp is the observed excess pressure of the solution over that of pure liquid He^4, then for our dilute solutions

$$\frac{C_V}{C_L}=\frac{\Delta p}{p_4^0+\Delta p}\cdot\frac{1}{C_L} \qquad (3)$$

to within the accuracy of the experiment.

(d) By observation of the height of the liquid levels, the liquid and vapor volumes could be computed at all temperatures, and hence C_L could be evaluated from a knowledge of the He^4 concentration in the unrefrigerated gas.

4. Experimental Details

He^3 supplied by the AEC was used,[5] diluted with He^4 ("well-helium") to form a mixture having an unrefrigerated He^3 concentration, C_3, of 1.0 ±0.10 percent, as estimated by volume measurements made during the dilution process. Subsequent mass-spectrographic analysis of the sample of the unrefrigerated mixture carried out at three different establishments[6] gave values of $C_3=0.99$, 1.60, and 1.65 percent. These discrepancies are disturbing and have forced us to give our results in the form of ranges of C_V/C_L within which the true values of C_V/C_L may be located.

Observations were made on three independent runs. In the last two runs, the vessels were of dimensions given above, whereas in the first run a different copper block was substituted having a vessel volume of 50 mm³, the dimensions of other parts of the apparatus being kept the same.

The temperature of the helium bath was measured by vapor-pressure measurements in the usual way, and above the λ-temperature the bath was well stirred and measurements made only on diminishing the temperature from a higher value.

At all temperatures of measurement no measurable difference of vapor pressure was observable between that of the bath and that of the vessel containing the pure He^4, indicating negligible thermomolecular pressure-difference corrections.

The observed results are given in table 27.2, in which are tabulated the observed temperatures (1949 scale [19]), the observed vapor-pressure differences, Δp, between the He^3 and He^4 solutions, and the pure liquid He^4, given both in centimeters of oil and centimeters of Hg,

TABLE 27.2.

Experiment	T	Δp		C_V/C_L[a]	
		Oil	Mercury		
	°*K*	*cm*	*cm*		
Dec. 11, 1950	2.33	7.60	0.527	5.4	8.9
	2.27	7.15	.496	5.8	9.5
	2.18	5.30	.368	5.4	8.9
	1.99	4.60	.319	7.5	12.4
	1.75	3.90	.271	12.7	21.0
	1.45	2.70	.187	23.8	39.3
	2.49	9.20	.638	4.8	7.9
Dec. 21, 1950	2.12	4.95	.344	5.6	9.3
	1.66	3.95	.274	12.4	20.4
	1.43	2.70	.187	25.4	42.0
	2.59	11.50	.798	4.9	8.0
Dec. 22, 1950	2.60	8.90	.617	3.8	6.3
	2.31	7.70	.534	5.8	9.5
	2.19	7.20	.500	7.0	11.5
	1.93	4.45	.308	8.5	14.0
	2.30	5.70	.396	4.4	7.3
	2.18	5.30	.368	5.4	8.9
	1.50	3.0	.208	23.2	38.2

[a] The two columns give the limits of the ranges of the calculated values of C_V/C_L. The lower numerical values were obtained by taking $C_L=C_3=1.65$ percent, and the higher values were obtained by taking $C_L=C_3=1.00$ percent.

---

[5] Some of the gas used in the experiments on the λ-temperatures of He^3 in He^4 solution below 1° K was employed (see [17]).

[6] We are indebted to F. L. Mohler, National Bureau of Standards, to the General Electric Co. and to the Atomic Energy Commission for the analyses.

and the calculated range of values of C_V/C_L obtained from eq (3). In this evaluation of C_VC_L, the numerical value of C_L has been set throughout equal to C_3, the He^3 concentration of the unrefrigerated gas, and the range of values of C_V/C_L has been calculated for $C_3=1.0$ to 1.65 percent. In assessing the possible deviations of C_L from the concentration of the unrefrigerated gas, estimates have been made of the quantity of He^3 present in the vapor phase at each temperature These estimates have been made in two ways: (a) by estimation of the effective (NTP) volume available to the vapor from observation of the meniscus heights of liquid in the capillary and in the main liquid-helium bath, and (b) by noting the change in the meniscus height of the solution in the capillary when the temperature was reduced from the temperature of interest to a low temperature ($T\approx 1.4$°K) where the vapor pressure is negligibly small. By both these methods it was concluded that at the highest temperature of measurement, namely, $T\approx 2.6$° K, (where the "effective" vapor volumes are largest) the amount of He^3 in the vapor phase was not larger than 12 percent of the total amount of He^3. At these temperatures, therefore, C_L may be different from C_3 by 12 percent, and at lower temperatures correspondingly smaller differences must occur. The uncertainty, however, in measurement of the unrefrigerated gas concentration, as detailed above, introduces greater possible errors and consequently it was not thought worth while to make the corrections for the differences between C_L and C_3. The results are shown in figure 27.2.

5. Comparison of the Results with Theory

A model for solutions of He^3 in liquid He^4 has been proposed by Heer and Daunt [20], based on the assumption of pure He^4 being a Bose-Einstein liquid for which the λ-temperature is identified with the degeneracy temperature of the statistics, as was originally proposed by F. London [21]. By assuming in this model that the solutions could be represented by independent perfect Bose-Einstein and Fermi-Dirac systems included in smoothed potential wells, the free energies of the systems in the pure phases and in solution could be calculated, and hence theoretical expressions obtained both for the partial vapor pressures, p_3 and p_4, of the He^3 and He^4 of such solutions, and for the distribution coefficient C_V/C_L. Marked deviations from the classical laws for perfect solutions were obtained for temperatures both above and below the λ-temperature.

In comparison with experiment, it has already been pointed out [20] that the results of vapor-pressure measurement on solutions of 20.3- and 25-percent He^3 concentration, as carried out by Weinstock, Osborne, and Abraham [22], are in close agreement with our theoretical predictions and constitute the most satisfactory experimental method of checking.[7]

However, the results reported here on the experimental evaluation of C_V/C_L, although not of high accuracy, also enable a further check with theory to be made. The experimentally observed ranges of values for C_V/C_L against temperature are plotted in figure 27.2, in which also

---

[7] It was also possible to calculate the variation of the λ-temperature, T_λ, as a function of the He^3 concentration, C_L, and, as has been described in detail by Heer and Daunt [20] the agreement between the theory and experiment is good. This agreement is somewhat surprising in view of the fact that the continuous part of the energy spectrum of the He^4 model was taken to be that of a perfect Bose-Einstein gas. The observed anomalous entropy of liquid helium II could be interpreted however by postulating an energy spectrum of a perfect Bose-Einstein gas together with an energy gap at the lowest energy levels, as has been studied in detail by Bijl, deBoer, and Michels (Physica 8, 655; 1941).

curves are shown for (a) C_V/C_L as calculated from Raoult's Law for dilute solutions (eq 1), given by the broken curve, (b) C_V/C_L as calculated from Taconis's rule (eq 2), and (c) C_V/C_L as calculated theoretically by Heer and Daunt [20], given by the full curve.

This plot of the results in figure 27.2 shows that in spite of the broad range of experimental values the evaluation of C_V/C_L by Taconis' rule gives values that are much too large at temperatures below 1.8° K. The experimentally observed results, however, are not in contradiction with the theory of Heer and Daunt. It should be noted here that although the range of values experimentally given for C_V/C_L is considerable (due to divergences in the measurement of the unrefrigerated He^3 concentration, C_3), the scatter of the results is relatively small. This is in marked contradistinction to the great scatter in the results obtained by Taconis, Beenakker, and Dokoupil [11] and by Lane and coworkers [9] (as indicated in fig. 27.2), and this gives some confidence in the general experimental method employed by us.

Moreover, it is concluded that the values of C_V/C_L for a dilute solution are higher than those calculable from Raoult's law for perfect classical solutions for T less than T_λ. For temperatures above T_λ, the accuracy of the results is insufficient to allow a definite conclusion to be drawn, but inferentially it may be supposed that Raoult's law also is insufficient and that to describe the results a quantum theory of solutions is probably necessary in which the condensation phenomenon of Bose-Einstein plays the significant role.

6. References

[1] J. G. Daunt, Probst, Johnston, Aldrich, and Nier, Phys. Rev. **72,** 502 (1947).
[2] J. G. Daunt, Probst, and Johnston, J. Chem. Phys. **15,** 759 (1947).
[3] J. G. Daunt, Probst, and Smith, Phys. Rev. **74,** 494 (1948).
[4] Fairbank, Lane, Aldrich, and Nier, Phys. Rev. **71,** 911 (1947).
[5] Fairbank, Reynolds, Lana, McInteer, Aldrich, and Nier, Phys. Rev. **74,** 345 (1948).
[6] Weinstock, Osborne, and Abraham, Phys. Rev. **77,** 400 (1950).
[7] B. V. Rollin and Simon, Physica **6,** 219 (1939); J. G. Daunt and K. Mendelssohn, Nature **141,** 911 (1938); Proc. Roy. Soc. [A] **170,** 423 and 439 (1939); Kilkoin and Lasarew, Nature **142,** 289 (1938). See W. H. Keesom, Helium, Elsevier (1942) for review of this work.
[8] Fairbank, Lane, Aldrich, and Nier, Phys. Rev. **73,** 729 (1949).
[9] Taconis, Beenakker, Nier, and Aldrich, Phys. Rev. **75,** 1966 (1949); Physica **15,** 733 (1949).
[10] See also, H. A. Kramers, Physica **15,** 971 (1949).
[11] Taconis, Beenakker, and Dokoupil, Phys. Rev. **78,** 171 (1950).
[12] L. Tisza, Phys. Rev. **72,** 838 (1947).
[13] W. H. Keesom and A. P. Keesom, Physica **2,** 557 (1935); W. H. Keesom and Westmijze, Physica **7,** 1044 (1941); see also W. Band and L. Meyer, Phys. Rev. **74,** 386 (1948).
[14] See, for example: J. W. Stout, Phys. Rev. **76,** 864 (1949). J. deBoer, Phys. Rev. **76,** 852 (1949). C. J. Gorter and J. deBoer, Phys. Rev. **77,** 569 (1950); Physica **16,** 228 and 667 (1950). O. G. Engel and O. K. Rice, Phys. Rev. **78,** 55 (1950); Phys. Rev. **78,** 183 (1950). O. K. Rice, Phys. Rev. **77,** 142 (1950); Phys. Rev. **79,** 1024 (1950).
[15] J. G. Daunt and C. V. Heer, Phys. Rev. **79,** 46 (1950).
[16] F. London and O. K. Rice, Phys. Rev. **73,** 1188 (1948).
[17] Lane, Fairbank, Aldrich, and Nier, Phys. Rev. **75,** 46 (1949).
[18] Weber, Keesom, and Schmidt, Leid. Comm. 246 (a).
[19] H. Van Dijk and D. Shoenberg, Nature **164,** 151 (1949).
[20] C. V. Heer and J. G. Daunt, Phys. Rev. **81,** 447 (1951).
[21] F. London, Nature **141,** 643 (1938); Phys. Rev. **54,** 947 (1938).
[22] Weinstock, Osborne, and Abraham, Phys. Rev. **77,** 440 (1950).

28. Phase Diagram of Dilute Solutions of He^3 in He^4 below the Lambda Point

by Henry S. Sommers, Jr.[1]

Abstract

We have studied the He^3 concentrations of both liquid and vapor phases for liquid concentrations in the vicinity of 1 percent by a method whose application requires no assumptions about the equation of state of the mixture. From a series of filling curves at various temperatures and initial concentrations, sufficient data have been obtained to give the dew point as a function of pressure, temperature, and vapor concentration. By using this data, the concentration of the vapor phase can be determined from the vapor pressure and temperature, and the liquid concentration then deduced by calculating the mass balance.

The questions of concentration equilibrium in the liquid and effect of Rollin film on the vapor phase were discussed, and the results were compared with those derived from the Pomerancheck-Taconis assumption about the solubility of He^3.

---

[1] Los Alamos Scientific Laboratory, Los Alamos, N. Mex.

29. A Bose-Einstein Model of Liquid Helium Applied to Solutions of He^3 in He^4

by W. Goad [1]

Abstract

A new model employing Bose-Einstein statistics, suggested by London, is introduced. Its thermodynamic properties closely resemble those of liquid He^4 in many respects; applied to the calculation of the ratio C_V/C_L of dilute solutions of He^3 in He^4, it gives results in agreement with Sommers' measurements.

---

[1] Los Alamos Scientific Laboratory, Los Alamos, N. Mex.

30. Solidification of He^3

by D. W. Osborne, B. M. Abraham, and B. Weinstock [1]

We have recently succeeded in solidifying He^3 and have determined a portion of the melting curve by the blocked-capillary technique.[2] The melting pressure was found to change from 40.5 atm at 1.02° K to 56.6 atm at 1.51° K.

A schematic diagram of the apparatus is shown in figure 30.1. In order to perform the experiment with the amount of gas available (190 cm^3 STP) it was necessary to keep the volume of the system small. This was accomplished by filling the Bourdon gages (B and G) with mercury and by using 0.1-mm-inside-diameter stainless-steel tubing for the U-tube (D) in the helium cryostat (E)[3] and 0.5-mm-inside diameter tubing for the connections outside the cryostat. The other U-tubes (C and F) were immersed in liquid nitrogen to prevent mercury from plugging the smaller tubing in the cryostat. The apparatus was evacuated and filled through the high-pressure valves (A and J). The gas in the reservoir (H) was compressed with mercury displaced by means of the hydraulic system (I). The Bourdon gages, which had 1-lb/in.^{2} graduations and a range of 0 to 1,000 lb/in.^{2}, were calibrated with a pressure balance while filled with mercury.

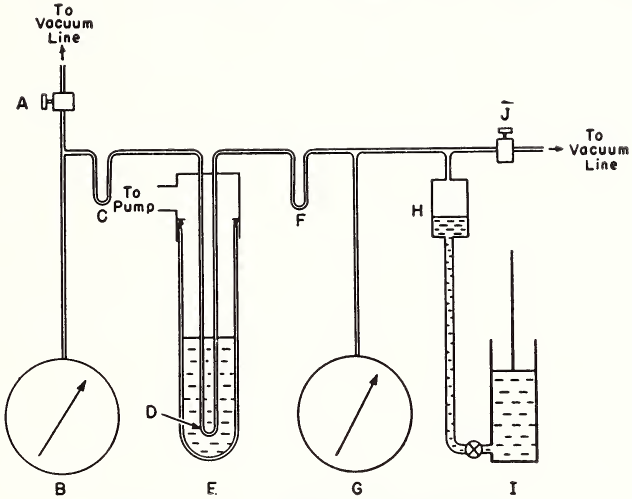

FIGURE 30.1. *Solidification apparatus.*

As the pressure in the system was slowly increased, at a constant cryostat temperature, the two gages gave the same reading until the solidification pressure was reached, and then gage (G) continued to rise while gage (B) remained constant. Upon lowering the pressure the gage readings again became equal at the solidification pressure. A single measurement was made with He^4, and the solidification pressure was found to be 25.2±0.1 atm at 1.09° K, in satisfactory

---

[1] Argonne National Laboratory, Chicago, Ill.

[2] W. H. Keesom, Communs. Physical Lab. Univ. Leiden No. 184b (1926); Helium, p. 180 (Elsevier, Amsterdam, 1942), p. 180.

[3] B. M. Abraham, B. Weinstock, and D. W. Osborne, Phys. Rev. **80**, 366 (1950).

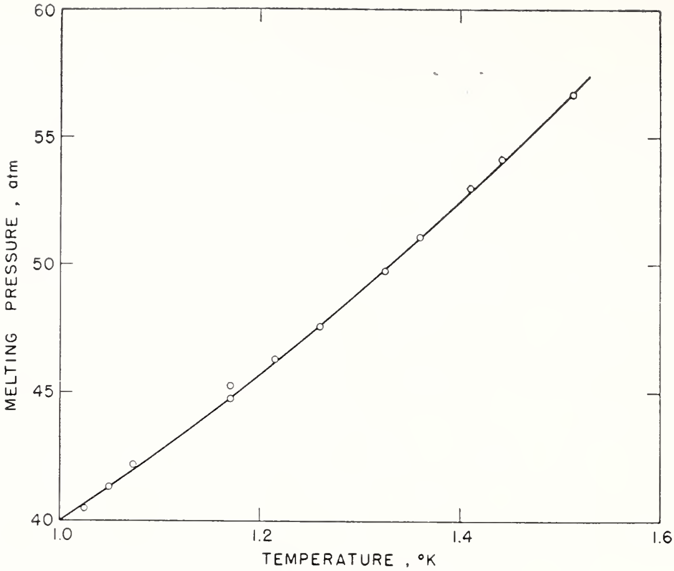

FIGURE 30.2. *Melting pressure of* He^3.

agreement with the more accurate value of 25.10 atm found by Swenson.[4] The data for He^3 are plotted in figure 30.2. The equation of the curve in this figure is

$$P=27.0+13.0T^2 \text{ atm } (1.02 \text{ to } 1.51° \text{ K}), \tag{1}$$

and it represents the He^3 melting pressure in the range of the measurements, with a mean deviation of 0.1 atm.

With the aid of eq (1) an upper limit can be calculated for the volume change on melting, ΔV, by substituting the entropy of the liquid in equilibrium with the vapor (see footnote 3) for the entropy of melting, ΔS, in the relation

$$dP/dT=\Delta S/\Delta V. \tag{2}$$

It is assumed that the thermal coefficient of expansion of liquid He^3 is positive, and hence that the entropy of the liquid decreases when the liquid is compressed from the vapor pressure to the melting pressure. The result is $\Delta V<1.2$ cm^3/mole at 1° K. This is smaller than the volume change of 2.1 cm^3/mole for He^4 at this temperature (see footnote 4) but is reasonable because of the higher melting pressure of He^3.

Also, from the relation

$$\frac{\Delta U}{\Delta V}=T\frac{dP}{dT}-P \tag{3}$$

and eq (1), it can be seen that ΔU is zero at 1.44° K and that the internal energy of the liquid is less than that of the solid below this temperature.

The melting-pressure data also point to another interesting result. As any reasonable extrapolation of the data gives a positive melting pressure at absolute zero, it appears likely that He^3, like He^4, does not have a triple point and that the liquid is the stable condensed phase at absolute zero.

---

[4] C. A. Swenson, Phys. Rev. **79**, 626 (1950).

31. Liquid-Helium Research in the Royal Society Mond Laboratory

by K. R. Atkins, C. E. Chase, and A. C. Hollis-Hallett [1]

Properties of First Sound

K. R. Atkins and C. E. Chase have studied the velocity and attenuation of first sound in liquid helium. This problem arose out of earlier work in the laboratory on the velocity of second sound below 1° K (see paper 32 in this volume). When it was known that the velocity of second sound increased rapidly as the temperature was lowered below 1° K and tended near 0° K to a value approximately equal to the velocity of first sound divided by $\sqrt{3}$, as predicted by Landau [1] [2], it became necessary to determine the velocity of first sound more accurately to enable a more reliable extrapolation to 0° K to be made in order to test the Landau relation $u_2=u_1/\sqrt{3}$ more carefully. This was done with a quartz-crystal transducer to propagate a 10-μsec long pulse of 14 Mc/s ultrasonics and to receive the same pulse after reflection from a polished brass reflector.

Figure 31.1 shows the results for the velocity as a function of temperature. The accuracy is considered to be better than 1 percent.

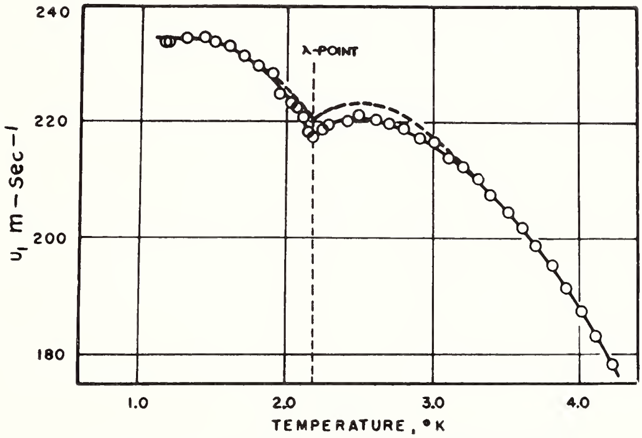

FIGURE 31.1. *Velocity of sound in liquid helium.*

- - - - - - - - -, Findlay, Pitt, Grayson-Smith, and Wilhelm. ○, present results. Path length, 4.310 cm.

Most fortunately, the velocity has leveled out to an almost constant value at 1.2° K, so that it is possible to make a plausible extrapolation to 0° K without having to extend the measurements below 1° K. The extrapolated value is 237 ± 2 m sec^{-1}. Divided by $\sqrt{3}$, this becomes 137 ± 1 m sec^{-1}, which is to be compared with a value of 152 ± 5 m sec^{-1} for the velocity of second sound at 0.1° K (Atkins and Osborne [2]. The second-sound measurements were only exploratory and not particularly accurate, and final judgment must be reserved until second sound has been more fully investigated below 1° K, but there is obviously some evidence for the existence of a

---

[1] Royal Society Mond Laboratory, Cambridge, England.
Figures in brackets indicate the literature references on p. 137.

discrepancy of the order of 10 percent. This discrepancy is not large enough to raise doubts about the fundamental principles of Landau's theory, but it does stimulate a search for reasons why Landau's relation might not be accurately obeyed.

At temperatures near 0.1° K the only important elementary excitations in the Landau theory are phonons, and it is from a discussion of their behavior that the Landau relation arises. It is important to notice, however, that at a temperature T the average frequency of the phonons is of the order of kT/h, which is still as high as $2 \text{x} 10^9$ cps at 0.1° K. The discrepancy therefore suggests that the velocity of the phonons at a frequency of $2 \text{x} 10^9$ cps is greater than the velocity measured at $1.4 \text{x} 10^7$ cps. Such a dispersion does not seem unplausible in view of what is already known about the attenuation of first sound in liquid helium II.

The broken curve in figure 31.1 refers to earlier work by Findlay, Pitt, Grayson-Smith, and Wilhelm [3] at a frequency of 1.338 Mc/s. There is some evidence for dispersion near the λ-point, but the effect is only as large as the sum of the errors in the two experiments and cannot be regarded with any confidence. The region near the λ-point is interesting for several reasons, however, and so it was studied in great detail, the results being shown in figure 31.2. The Ehrenfest relations for a second-order transition predict that there should be a discontinuity of about 2½ percent in the velocity of sound at the λ-point. It will be seen, however, that the experimental curve is falling so rapidly on either side of the λ-point, that it is impossible to verify this prediction.

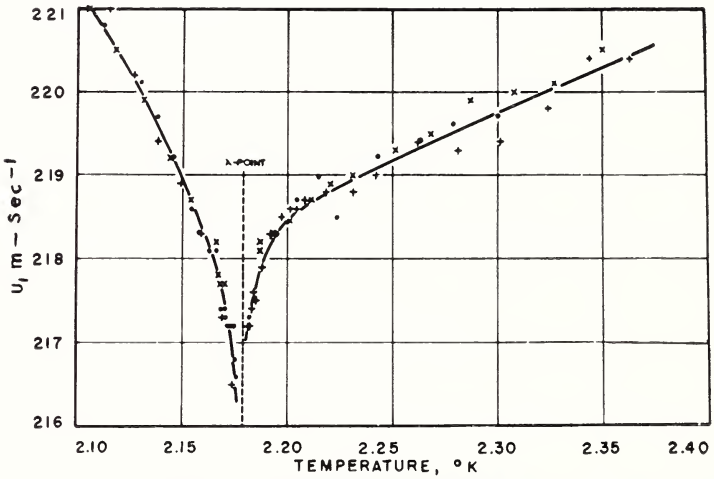

Figure 31.2. *Velocity of sound in liquid helium in the neighborhood of the λ-point.*

Path lengths: ●, 0.868 cm; +, 1.568 cm; ×, 4.310 cm.

In the course of the investigation near the λ-point, it was possible to obtain information about the effect of the hydrostatic pressure head on the temperature at a point below the surface in a bath of liquid helium (see paper 8 in this volume). In figure 31.3, the temperature is deduced from the pressure at the surface of the helium. The two separate curves above the λ-point refer to two experiments in which the surface of the liquid was 20 cm and 4 cm, respectively, above the apparatus. The separation between the two curves can be explained if we assume that the temperature of the apparatus

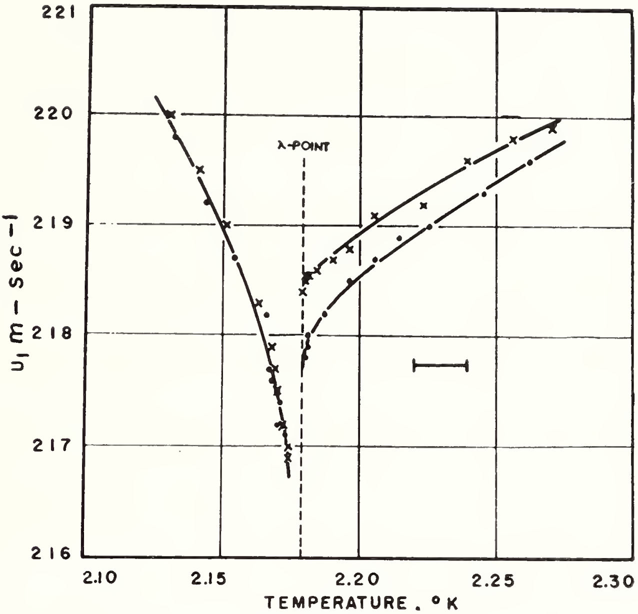

Figure 31.3. *Effect of hydrostatic-pressure head.*

×, pressure head=20 cm; ●, pressure head=4 cm; ——, expected shift due to change in hydrostatic-pressure head.

corresponded, not to the vapour pressure at the surface, but to this pressure plus the hydrostatic-pressure head.

Preliminary attenuation data confirm the earlier results of Pellam and Squire [4] and reproduce the rapid increase in attenuation near the λ-point found by them. In the temperature range below 1.5° K not investigated by Pellam and Squire there is another extremely rapid rise in attenuation. This agrees, at least qualitatively, with a theory due to Khalatnikov [5], and further experiments are in progress to make possible a more accurate comparison with this theory.

Flow Through Wide Capillaries

In the film and in very narrow channels the flow of liquid helium II is apparently frictionless until a critical velocity v_c is reached. Above v_c frictional forces come into play, but they are markedly nonlinear and have an unprecedented character. From an analysis of thermal-conduction experiments in wider capillaries and slits Gorter and Mellink [6] have concluded that the new frictional force is, in fact, a force of mutual friction between the normal and superfluid components, varying approximately as the cube of their relative velocity. To extend the relevant evidence, experiments have been performed on isothermal, pressure-induced flow through wide capillaries (K. R. Atkins) and on the damping of the torsional oscillations of a single disk and piles of disks immersed in the liquid (A. C. Hollis-Hallett).

The capillaries used by Atkins varied in bore from $2.6\text{x}10^{-3}$ to $4\text{x}10^{-2}$ cm. Care was taken to eliminate corrections arising from film flow and thermomechanical effects. End corrections due to the change in kinetic energy of the liquid upon entering and leaving the capillary were measured and allowed for. Figure 31.4 shows a typical set of curves, giving the mean velocity of flow as a function of the pressure gradient.

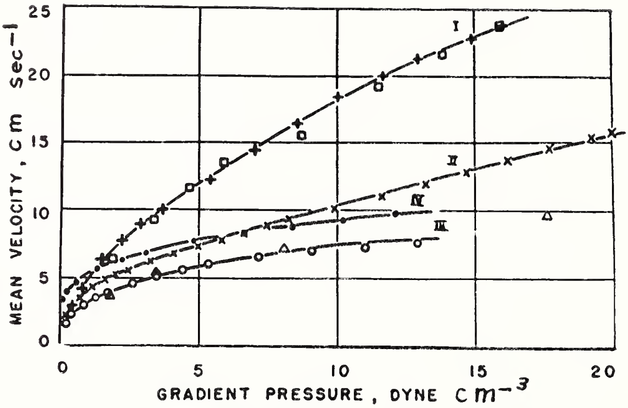

FIGURE 31.4. *Mean velocity as a function of the pressure gradient at 1.22° K.*

Capillary:	*Symbol*	*l (in cm)*
I	+	8.04
I	□	1.75
II	×	7.90
III	○	8.03
III	△	0.83
IV	●	7.76

In curves of this type the critical velocity appears as an intercept on the velocity axis. It is clear that when the internal diameter is greater than $8\text{x}10^{-3}$ cm, the critical velocity is less than 1 cm sec^{-1} It will be seen, however, that the curve for the finest capillary of bore $2.6\text{x}10^{-3}$ cm runs parallel to that for the capillary of bore $8.15\text{x}10^{-3}$ cm but 2 cm sec^{-1} above it. This suggests the existence of a critical velocity of at least 2 cm sec^{-1} in this very fine capillary, but it should be emphasized that such fine capillaries are very difficult to work with, and it is not possible, as yet, to have complete confidence in this result.

For isothermal flow in wide capillaries the mutual-friction theory of Gorter and Mellink predicts a mean velocity of flow

$$\bar{v}=\frac{\rho_s}{\rho}\left(\frac{\text{grad p}}{A\rho\rho_n}\right)^{1/3}+\frac{r^2\,\text{grad}\,p}{8\eta_n},$$

in which r is the radius of the capillary, A is a constant appearing in their theory and determining the magnitude of the mutual friction, and the other symbols have their usual meaning. The experimental results can be fitted approximately to an expression of this type by choosing values of A and η_n, which have the right order of magnitude. No more is to be expected in the case of A, which, as deduced from thermal-conduction experiments, is an ill-defined quantity varying with both the radius of the capillary and the velocities of flow. The situation with respect to the term $r^2\,\text{grad}\,p/8\eta_n$ is more unsatisfactory.

This part of the flow can be investigated by subtracting curves for capillaries of different radii. It is found to be linearly proportional to grad p within the experimental error, but does not vary as r^2. Moreover, it is independent of temperature in the range 1.2° to 1.5° K, whereas η_n is a rapidly varying function of temperature in this region.

It therefore appears that, although the Gorter-Mellink theory explains the order of magnitude of the flow in wide capillaries, it is inadequate to explain the results in detail and must be supplemented by the postulate of some other type of frictional force. This conclusion is considerably strengthened by the oscillating-disk experiments now to be described.

TABLE 31.1. *Details of the capillaries*

Capillary	Internal diameter	Cross-sectional area of reservoir
	cm	*cm*^{2}
I	4.40×10^{-2}	3.50
II	2.03	0.892
III	0.815	.201
IV	.262	5.71×10^{-3}

Oscillating Disk Experiments

Hollis-Hallett has repeated an experiment originally due to Andronikashvili [7, 1946]. A pile of mica disks performed torsional oscillations in liquid helium. From the period of the oscillations it was possible to deduce the effective moment of inertia, and hence the effective density of the liquid carried round with the disks. From the damping of the motion it was possible to obtain information about the frictional forces. At small amplitudes the results were in satisfactory agreement with those of Andronikashvili. The effective density corresponded to ρ_n, indicating that only the normal component was moving with the disks and the superfluid component was stationary. Within the experimental error the logarithmic decrement was consistent with the values for the viscosity, η_n, of the normal component given by Andronikashvili [7, 1948]. (The experiments with a single disk have given more accurate values for η_n in good agreement with Andronikashvili.)

As the amplitude of oscillation was increased the above simple situation began to break down, and the new frictional forces came into play. The period began to increase as the superfluid component was dragged into motion by the disks, and, in some of the experiments with short periods, the effective density eventually increased to its bulk value, ρ, so that all the liquid was then carried round with the disks. At the same time, the new frictional forces began to manifest themselves as an increase in decrement (fig. 31.5). This figure clearly shows how the effect was small near the λ-point and then increased steadily as the temperature was lowered. A similar variation of decrement with amplitude was observed in the case of a single disk, but no variation in period was detected, the mass of liquid carried round by the disk being too small to make any appreciable addition to its moment of inertia.

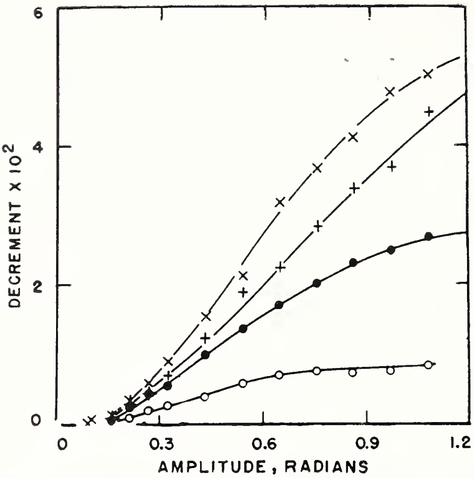

Figure 31.5. *Excess decrement above the small amplitude value as a function of amplitude.*

Pile of 18 disks spaced 1.22×10⁻² cm apart. Period=12.0 sec. ×, 1.56°K; +, 1.79°K; ●, 1.99°K; ○, 2.145°K.

In figure 31.6 the increase in decrement between small amplitudes and an amplitude of 0.2 radian is plotted as a function of temperature for the single disk. The lower curve is derived from the theory of Zwanniken [8], which is based on the Gorter-Mellink assumption of a force of mutual friction. The magnitude of this mutual friction

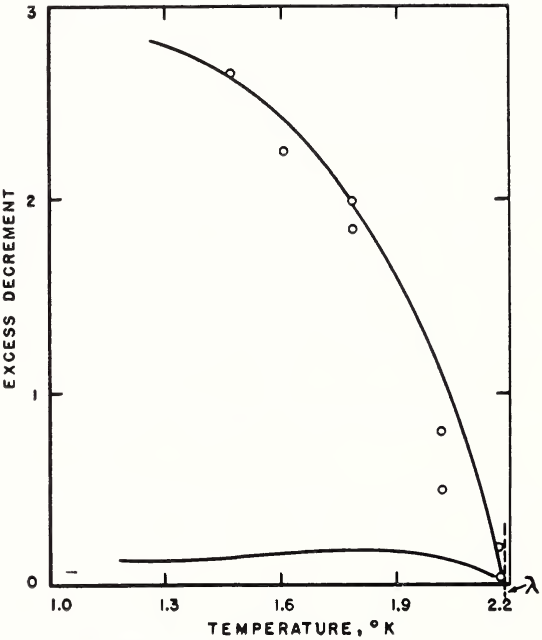

Figure 31.6. *Excess decrement (arbitrary units) at 0.2 radian as a function of temperature.*

○, experimental results for a single disk at a period of 3.78 sec. Lower curve: predicted by Zwanniken on the basis of the Gorter-Mellink theory.

is deduced from thermal conduction experiments. It will be seen from figure 31.6 that the Gorter-Mellink theory fails to explain even the order of magnitude of the extra damping. The theory has also been worked out for the pile of disks, and there is again a disagreement with experiment.

The failure of the Gorter-Mellink theory to explain the damping of the oscillating disk and flow through capillaries suggests the existence of some extra frictional force. This does not exclude the possibility that the mutual friction is also present and is the most important factor in thermal-conduction experiments. Another possibility is that the two-fluid theory in its simple form begins to break down above the critical velocity, and it is then no longer permissible to formulate two separate hydrodynamical equations for the normal and superfluid components.

References

[1] L. Landau, J. Phys. (USSR) **5,** 71 (1941).
[2] K. R. Atkins, and D. V. Osborne, Phil. Mag. **41,** 1078 (1950).
[3] J. C. Findlay, A. Pitt, H. Grayson-Smith, J. O. Wilhelm, Phys. Rev. **54,** 506 (1938).
[4] J. R. Pellam and C. F. Squire, Phys. Rev. **72,** 1245 (1947).
[5] I. Khalatnikov, J. Exptl. Theoret. Phys. (USSR) **20,** 243 (1950).
[6] C. J. Gorter and J. H. Mellink, Physica **15,** 285 (1949).
[7] E. L. Andronikashvili, J. Phys. (USSR) **10,** 201 (1946); J. Exptl. Theoret. Phys. (USSR) **18,** 429 (1948).
[8] G. C. J. Zwanikken, Physica **16,** 805 (1950).

32. Propagation of Second Sound Below 1° K

by D. V. Osborne [1]

Peshkov [1],[2] Maurer and Herlin [2], and Pellam and Scott [3] have shown that the velocity of second sound in liquid helium II increases as the temperature is decreased below 1° K. Atkins and Osborne [4], have confirmed this result and have found that the velocity reaches 152 ± 5 m/sec at 0.1° K. This interpretation of their experiments, however, is not entirely free from complications, and the present paper is designed to fulfill the undertaking given in the original letter that a full analysis (due to the present author) would be published shortly. It is intended to describe the observations in more detail, to explain how the velocity of second sound is deduced from them, and to mention what other information may be obtained by suitable analysis.

To revise the technique briefly, a direct-current pulse of duration 100 μsec was fed into a constantan heater at one end of a glass tube (0.5 cm in diameter and 3.40 cm long) closed at both ends, except for small holes for the admission of liquid helium. The resulting second-sound pulse was received at the other end of the tube by a phosphor-bronze resistance thermometer, and the signals from this thermometer were amplified and displayed on a cathode-ray tube in the usual way.

Figures 32.1 shows actual oscillograms of the received temperature pulses at temperatures of 0.44°, 0.48°, 0.54°, and 0.60° K, respectively, on a time base of about 3½-msec total duration. The trace goes from left to right, and the faint, sharp negative spike near the left-hand end shows when the input pulse started. The larger sharp, positive spike immediately following it is also related to the input pulse and is to be ignored when studying the received pulse. Two essential features stand out clearly from these oscillograms. The first is the increase of velocity with falling temperature, shown by the decrease in the time interval between the input pulse and the rise of the received pulse. The second is the great lengthening of the received pulse at the lower temperatures.

It might be thought from figure 32.1, a, that the delay becomes effectively zero at the lowest temperature, i. e., that the velocity approaches infinity, but this is not so, as shown by figures 32.2, a and b. In these oscillograms the time-base speed has been increased so that the whole trace now occupies about 0.8 msec. The rise of the received pulse up to about the maximum is visible on the upper trace, but the long tail is off the right-hand end of the time base. The gap in the upper trace indicates the time occupied by the input pulse; the rise of the received pulse can be seen to start at a time that is distinctly later than the end of this interval. The lower trace is an attempt to display time-calibration markings on the same oscillogram, but, because of inferior design in the (commercial) oscilloscope, cross-talk has produced some confusion. For the actual measurement of velocities, the point of occurence of the input pulse with respect to

---

[1] Royal Society Mond Laboratory, Cambridge, England.

[2] Figures in brackets indicate the literature references on p. 144.

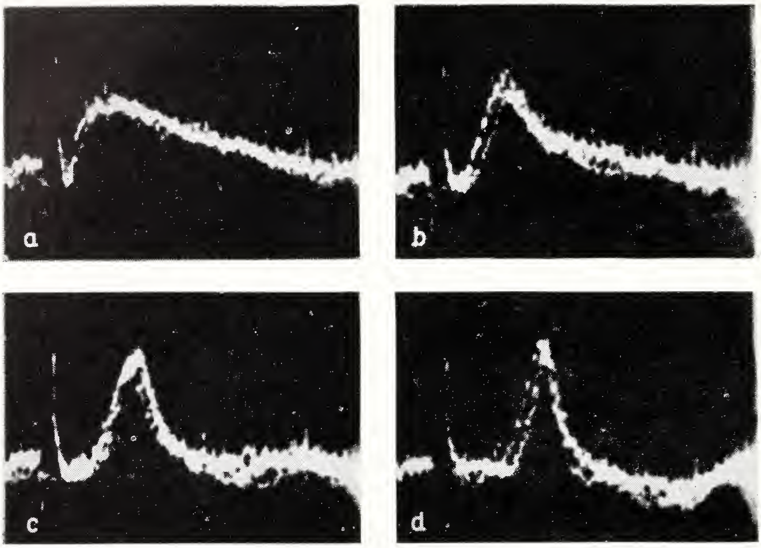

Figure 32.1. *Oscillograms of received temperature pulses; time base approximately 3½ msec.*

the calibration marks was accurately preset, and the calibrator trace was used only for timing the received pulse. As cross-talk was not serious after the end of the input pulse, no error was introduced by this procedure. The velocities shown on the graph in reference [6] were all obtained from oscillograms like those of figure 32.2, never

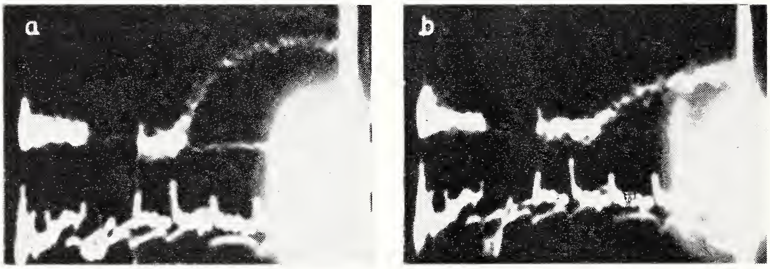

Figure 32.2. *Oscillograms of received temperature pulses; time base approximately 0.8 msec.*

from those like figure 32.1. The procedure was simply to divide the known length of the path of propagation by the time interval between the start of the input pulse and the start of the received pulse. The analysis that follows will justify this procedure.

An oscillogram like figure 32.1, a, is far more reminiscent of the propagation of a short heat pulse in an ordinary thermal conductor than of wave propagation. The finite delay revealed by the more detailed oscillograms figures 32, a and b, however, indicates that the conduction equation alone would not be a good description of the observations. We consider, therefore, the following pair of well-known equations, applicable to the propagation of electric waves along a transmission line:

$$\left.\begin{aligned} L\frac{\partial I}{\partial t}+RI&=-\frac{\partial V}{\partial x} \\ C\frac{\partial V}{\partial t}+GV&=-\frac{\partial I}{\partial x} \end{aligned}\right\} \tag{1}$$

Here V and I are voltage and current, or, in the thermal problem, temperature and heat flow; L and C are the inductance and capacity per unit length, and R and G are the resistance and leakage conductance per unit length; we consider propagation in one dimension only, along the x-axis. Deferring for a moment the actual translation of L, C, R, and G into thermal terms, we note that, if $R=G=0$, then

$$\frac{\partial^2 V}{\partial t^2}=\frac{1}{LC}\frac{\partial^2 V}{\partial x^2}. \tag{2}$$

This is the ordinary wave equation obeyed by electric waves on a lossless line and, to a good approximation, by second sound above 1° K. If, on the other hand, we set $L=G=0$, we have

$$\frac{\partial V}{\partial t}=\frac{1}{RC}\frac{\partial^2 V}{\partial x^2}, \tag{3}$$

the equation of heat conduction. By setting $G=0$ we obtain

$$\frac{\partial^2 V}{\partial t^2}+\frac{R}{L}\frac{\partial V}{\partial t}=\frac{1}{LC}\frac{\partial^2 V}{\partial x^2}, \tag{4}$$

and a similar equation holds if $R=0$. The latter equation is evidently worth investigation as a possible source of solutions combining the properties of solutions of (2) and of (3).

Equations (1) can be solved explicitly for a delta function input, using laplace transforms, as described, for example, by Carslaw and Jaeger [5]. The boundary conditions are

$I=0$ at $t=0$, except at $x=0$,

$I=0$ at $x=l$ for all t,

$I=Q\delta\ (t)$ at $x=0$,

where $\delta\ (t)$ is the Dirac delta function, which is zero if $t\neq 0$, infinite if $t=0$, and which has the property

$$\int_{-\infty}^{+\infty}\delta(t)dt=1.$$

The solution for V is then

$$\frac{V(x,t)}{\gamma Q}=\sum_{j=1}^{\infty}\left\{e^{-\rho b_j}\delta(t-b_j)+H(t-b_j)\sigma e^{-\rho t}\left(\frac{tI_1(\sigma\sqrt{t^2-b_j^2})}{\sqrt{t^2-b_j^2}}+I_0(\sigma\sqrt{t^2-b_j^2})\right)\right\}, \quad (5)$$

where

$\gamma^2=L/C$

$\rho=R/2L+G/2C$

$\sigma=R/2L-G/2C$

$b_1, b_2, b_3, b_3, \ . \ . \ . \ =x/v,(2l-x)/v,(2l+x)/v,(4l-x)/v,(4l+x)/v, \ . \ . \ .$

$v^2=1/LC$

l=length of tube (between closed ends)

$H(u)$=Heaviside's step function

$=0$ for $u\leqq 0$

$=1$ for $u>0$

$I_0(u)=-iJ_1(iu)$

$I^1(u)=J_0(iu)$.

where $J_n(u)$ are Bessel functions of the first kind.

This solution, although formidable in appearance is most perspicuous when dissected. The summation represents nothing but expansion in a series of echoes, which, for practical use, may be terminated at the second term, the first two terms being equal for $x=1$. ($b_1=b_2=l/v$). The first term within the summation bracket is the original delta function propagated at velocity v without distortion, but attenuated by a factor $e^{-\rho b_j}$. The second term within the bracket is a generalization of the solution of the heat-conduction equation with this distinction, that it is not allowed to come into operation until $t=x/v$, i. e., until the arrival of the delta function, being suppressed at earlier times by the function H.

If we put $L=G=0$, the standard solution for a heat conduction pulse is obtained. If we put $R=G=0$, we have

$$\frac{V(x,t)}{\gamma Q}=\sum\delta(t-b_j),$$

which is, as we should expect, simply the original pulse being reflected back and forth without distortion or attenuation. Further trial shows that if either $G=0$ or $R=0$ ($\sigma=\rho$ or $\sigma=-\rho$), the solution, suitably modified to include the finite length of the input pulse, gives a good representation of the observed second-sound signals. In other words, the propagation is governed by eq (4), which may be written

$$\frac{\partial^2 V}{\partial t^2}+\frac{1}{\tau}\frac{\partial V}{\partial t}=v^2\frac{\partial^2 V}{\partial x^2},$$

where

$v^2=1/LC$

$\tau=L/R$ or C/G.

The time interval between the transmitted pulse and the beginning of the received pulse is x/v, and the time of rise of the received pulse is related to τ. The values of v calculated from the observed time intervals on this basis are those appearing in [6]. The value of τ is found to be about 27 ± 5 μsec for temperatures between 0.13° and 0.35°K.

The simplest explanation of eq (6) is that the two second-differential coefficients are the terms usually appearing in the equation of second-sound propagation, and that the $\partial V/\partial t$ term is due to some viscous or other dissipative effect that becomes important at very low temperatures. In this case we shall have

$$v^2=u_2^2=\frac{\rho_s}{\rho_n}\frac{TS^2}{c}$$

and predictions about the behavior of ρ_n, S, and c as T approaches zero may be related to the observed values of v. In the original paper, it was claimed that u_2 approached $1/\sqrt{3}$ of the velocity of first sound as T approached zero, in agreement with the prediction of Landau (1941). But new measurements by Atkins and Chase [6] of the velocity of first sound down to 1.1° K have now established that this quantity tends to 235 m/sec at the absolute zero, rather than the 272 m/sec estimated by extrapolation from earlier data, which extended only down to 1.5° K. The new value divided by $\sqrt{3}$, would predict a value of 135 m/sec for u_2 at the absolute zero, whereas the observed value at 0.1° K is 152 ± 5 m/sec and is still rising appreciably with falling temperature. It is very doubtful whether any systematic error in the measurements could account for so wide a discrepancy.

The experimental fact that u_2 appears to remain finite near the absolute zero can be used to draw some conclusions about the behavior of ρ_n in this region. If it is assumed that $S\propto T^n$ then it follows that $\rho_n\propto ST$; if $S\propto T^n e^{-\epsilon/kT}$, then $\rho_n\propto ST^2$. It can also be shown, without any assumptions for S, that ρ_n cannot be proportional to S near the absolute zero.

A word may be said about possible interpretations for the value of τ. It might be a manifestation of relaxation between normal and superfluid components, like that proposed by Band and Meyer [7]. If this be so, then the relaxation time must be of the order of 30 μsec. We note that since ρ_n is not proportional to S, conservation of entropy is inconsistent with conservation of normal fluid and some such relaxation phenomenon is therefore likely to occur.

A second possibility is that of viscosity damping. No data whatever are available for the calculation of this effect, but the calculation by Landau and Khalatnikov [8] based on various forms of collision between elementary excitations gives a viscosity which increases rapidly as the temperature falls. The chief contribution comes from phonon-phonon scattering and the mean free path for this process is of the order of 40 m at 0.2° K, so that further theoretical work is needed before such a theory can be applied to the present results.

[1] V. P. Peshkov, J. Exptl. Theoret. Phys. (USSR) **18**, 951 (1948).
[2] R. D. Maurer and M. A. Herlin, Phys. Rev. **76**, 948 (1949).
[3] J. R. Pellam and R. B. Scott, Phys. Rev. **76,** 869 (1949).
[4] K. Atkins and D. V. Osborne, Phil. Mag. [7] **41,** 1078 (1950).
[5] H. S. Carslaw and J. C. Jaeger, Operational methods in applied mathematics, 2d ed. (Oxford University Press, New York, N. Y., 1948).
[6] K. R. Atkins and C. E. Chase, see paper 31, page 131.
[7] W. Band and L. Meyer, Phys. Rev. **73,** 226; **74,** 386 (1948).
[8] L. Landau and I. M. Khalatnikov, J. Exptl. Theoret. Phys. (USSR) **19,** 637 and 709 (1949).

33. Pressure Dependence of Second-Sound Velocity in Liquid Helium II*

by R. D. Maurer and Melvin A. Herlin [1]

Introduction

The properties of liquid He II have been explained most satisfactorily by the "two fluid" concept advanced in the theories of Tisza [1] [2] and Landau [2]. Each theory regarded liquid helium as composed of a "normal fluid" fraction and a "superfluid" fraction, although the origin of these two fluids was assigned to different molecular mechanisms. In the temperature range just below the lambda-point, Tisza, following the suggestion of London, considered the transverse excitations to be similar to those of a Bose-Einstein gas, appropriately modified by the liquid state. Experiments showing no superfluidity in He^3 have borne out this view, as opposed to the roton model of Landau. On the other hand, Landau considered the longitudinal excitations, the Debye phonons, as a component of the normal fluid flow only, rather than as associated with the fluid as a whole, which was Tisza's view. The phonons are masked by the Bose-Einstein excitations at higher temperatures, but below about 1.1° K their effect is evident. The rise in second-sound velocity [3 to 5] at low temperature and the sustained existence of the waves without undue attenuation tends to bear out the hypothesis that the new type of excitation predominant below 1° K is associated with the normal fluid flow only, and not with the superfluid. The present experiment takes advantage of the large pressure dependence of first-sound velocity in liquid helium to investigate whether this low-temperature excitation is indeed a phonon effect.

Experiment

Second sound is of a type of wave motion most easily excited by the heating of liquid helium. Pellam has developed a pulse method [4, 6] which was used by the authors to measure the velocity to below 1° K at vapor pressure [3]. Peshkov has created standing waves to determine the velocity at vapor pressure [5] down to 1° and at higher pressures [7] down to 1.3°.

A pulse method of exciting second sound similar to that formerly used in this work [3, 6] was employed again. The chief innovation was the installation of a delay line in the timing mechanism. This permitted a view of the pulse on a faster, continuous sweep and hence a more accurate determination of its leading edge. A DuMont 246 oscillograph was used to trigger the pulse generator and to actuate the delay line. The pulse generator excited the carbon resistor of the second sound chamber. Another carbon resistor, acting as a resistance thermometer, received the second sound pulse, which was amplified and fed into the vertical deflection plates of a second 246D oscillograph. This last oscillograph was triggered by the delay line. The

---

*This article appears also in Phys. Rev. **81**, 444 (1951).

[1] Research Laboratory of Electronics, Massachusetts Institute of Technology, Cambridge, Mass.

[2] Figures in brackets indicate the literature references on p. 150.

movable marker of the receiver oscillograph could be adjusted on the sweep so that it coincided with the edge of the pulse. By reading the marker dial and by knowing the delay, one could obtain the transit time for the pulse. The capacitative pick-up within the Dewar from the transmitting pulse could be amplified easily to give a sharp leading edge when viewed on the final oscillograph. In doing this, we could not detect any instrumental delay caused by the timing system.

The second-sound chamber itself was sealed with solder for immersion in a liquid helium bath. Inside the chamber a thin sleeve separated the carbon resistors and determined the fixed path of 4.23 cm. Four capillaries with an inner diameter of 0.020 in. led to the chamber. Two of these acted as electric shields for the wires while the other two were pressure lines, one to condense in helium gas from a tank and the other to observe pressure equilibrium with a check gage. Liquid helium exists under a temperature gradient in the capillaries so that the heat leak from the lambda-temperature to the chamber is limited only by the inner diameter. The size of these pressure capillaries was a compromise between this heat leak and the persistent clogging of the line by frozen materials. The pressure values of the experiment were determined on the input side by an Ashcroft Laboratory test gage. A Distillation Products MB200 diffusion pump with three Kinney VSD forepumps was used to remove vapor from the liquid-helium bath.

Temperature measurements were made with a McLeod gage through a tube in the pumping line above the Dewar arrangement, as described formerly [3]. The equivalence of temperatures obtained from the McLeod gage and those inside the chamber was established by constructing a dummy chamber of the same dimensions as the real one but filled with iron ammonium alum. Liquid helium under pressure was supplied to this chamber. A mutual inductance bridge was used to measure the relative paramagnetic susceptibility of the salt at different McLeod gage values and at two different chamber pressures. The susceptibility of the salt, and hence the mutual inductance, varies as $1/T$. Figure 33.1 shows that the mutual inductance

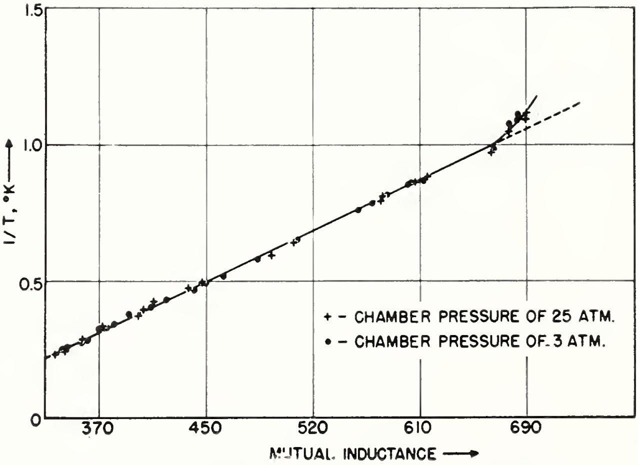

FIGURE 33.1. *Plot of the mutual inductance of the salt in the dummy chamber versus the reciprocal of the temperature as obtained from McLeod gage readings.*

Values were taken with the liquid helium in the chamber at two different pressures. The extrapolated broken line gives the true temperature in terms of that obtained from McLeod gage readings.

gives a straight line, except at low temperatures, when plotted against this variable obtained from the McLeod values. The deviation below 1° is attributed to the pumping-pressure drop from the bath as observed previously [3] and is not due to any radical change in heat conductivity of the helium in the capillaries. The data below 1° were corrected from this curve.

Results and Conclusions

The data for the second sound velocity as a function of temperature and pressure are shown in figure 33.2. They agree, to within experimental error, with the measurements down to 1.3° K by Peshkov [7].

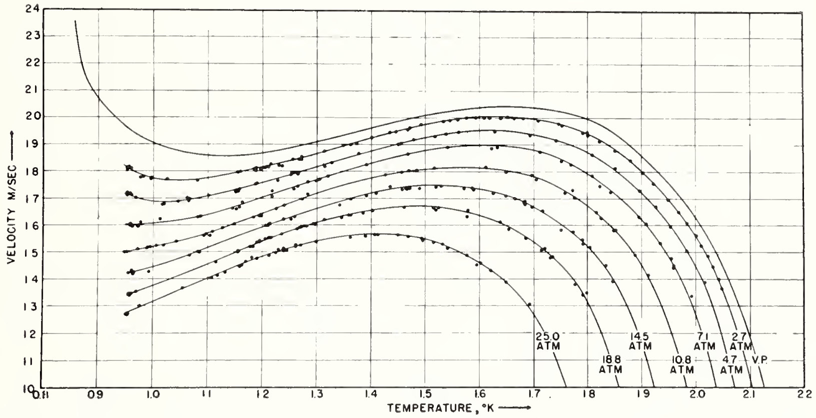

FIGURE 33.2. *Velocity of second sound as a function of temperature and pressure.* Experimental points for the vapor pressure curve are not shown.

The velocity of second sound along the vapor-pressure line as previously reported [3] was remeasured with the present apparatus and is also shown. The maximum deviation of the points is ±1 percent from the curves drawn through them.

Landau's proposal that the phonons contribute to the normal fluid flow implies that at the absolute zero of temperature the second-sound velocity must approach the value $c_1/\sqrt{3}$, where c_1 is the velocity of ordinary (first) sound [2]. The value of c_1 at the vapor pressure is about 250 m/sec, which is an order of magnitude larger than the velocity of second sound. The second-sound velocity must therefore rise rapidly as the temperature is lowered. The first-sound velocity increases with pressure, so that the second-sound curves at various pressures must cross somewhere in the temperature region below 0.95° K. if they are to arrive at Landau's value of velocity.

It has been found, however, that a computation based on a linear superposition of the terms giving the entropy and normal fluid fraction for the Bose-Einstein and phonon contributions to the excitations does not agree quantitatively with the observed velocity. The experimental curve shows no indication of the phonon term down to 1.2° K, but is rising rapidly at 1.0°. A phonon term simply added to the Bose-Einstein term extrapolated from higher temperature does not show an appreciable rise until about 0.6°. Landau gets the rise at 1° by using a roton expression which decreases more rapidly (exponentially instead of algebracially), but the phonon term is then too large in comparison to be absent at 1.2° as observed. The suddenness of the onset of the phonon contribution below 1.2° suggests the possibility that an interaction between the Bose-Einstein excitations and the phonons is removing the former rapidly as the latter becomes sufficiently large in comparison.

Nevertheless, the temperature at which this rise must begin corresponds to the point at which the entropy of the phonons begins to be of the same order of magnitude as the entropy of the Bose-Einstein excitations as the temperature is lowered. The pressure dependence of this temperature can be computed from the known pressure dependence of the first-sound velocity, and compared with the observed pressure dependence. The phonon nature of the low-temperature contribution to the second-sound curve can be checked by this comparison. To remove the possibility of phonon Bose-Einstein interaction from affecting the result, this pressure dependence will be obtained in the limit of small phonon contribution.

An empirical value of the Bose-Einstein entropy can be obtained by extrapolation from measurements between 1.2° and the lambda-point, and is given to sufficient accuracy for the present purpose by,

$$S_{BE}=S_{\lambda}(T/T_{\lambda})^{5.4},$$

where S_{λ} is the entropy at the lambda point, and T_{λ} is the lambda temperature. The entropy of the phonons is given by Debye's expression,

$$S_{ph}=16\pi^5k^4T^3/45h^3c_1^3\rho,$$

where k is Boltzmann's constant, h is Planck's constant, and ρ is the density. The temperature at which deviation from the extrapolated second-sound velocity curve occurs may then be given approximately by,

$$S_{ph}=\text{const}\times S_{BE},$$

where the value of the constant determines the amount of deviation. This expression can be expected to hold only for small deviations. Solving for temperature,

$$T_d^{2.5}=\text{const}\times \mathrm{T}_{\lambda}^{5.5}/c_1^3\rho S_{\lambda},$$

where the new constant is a combination of the previous constant and of Boltzmann's and Planck's constants, and T_d is the temperature at which the observed second-sound velocity deviates a certain amount from the value extrapolated from high temperature. Rather than to pass to the small phonon contribution limit, the constant may be eliminated by use of the logarithmic derivative,

$$\frac{1dT_d}{T_d dP}=2.2\frac{1dT_{\lambda}}{T_{\lambda}dP}-0.4\frac{1dS_{\lambda}}{S_{\lambda}dP}-1.2\frac{1dc_1}{c_0 dP}-0.4\frac{1d\rho}{\rho dP}.$$

The first two terms arise from the Bose-Einstein contribution to the entropy, and their sum has the numerical value of −0.008. The second two terms arise from the phonon entropy, and their sum has the numerical value of -0.029. The total pressure dependence of T_d is therefore,

$$(1/T_d)dT_d/dP = -0.037 \text{ deg/atm-deg},$$

of which about 80 percent comes from the phonon term in the entropy. This large fraction is due to the large pressure dependence of first-sound velocity in liquid helium.

The observed pressure dependence of T_d can be obtained from the curves of figure 33.3. If the phonon term were not present in the expression for second-sound velocity, the velocity would go to zero with the square root of the temperature [1, 2]. The ratio $c_2/T^{1/2}$ therefore exhibits a horizontal straight line at higher temperature but somewhat below the lambda-point, which may be easily extrapolated to low temperature. The deviation from the extrapolated line is then taken from the rising part of the curve at low temperature. Lines of constant deviation are shown for various values of the deviation. The corresponding values of dT_d/dP are plotted against the amount of deviation in figure 33.4. The values of dT_d/dP and $(1/T_d)\ dT_d/dP$ are nearly the same because T_d is near 1° K. The extrapolated value at zero deviation is in good agreement with the value computed above.

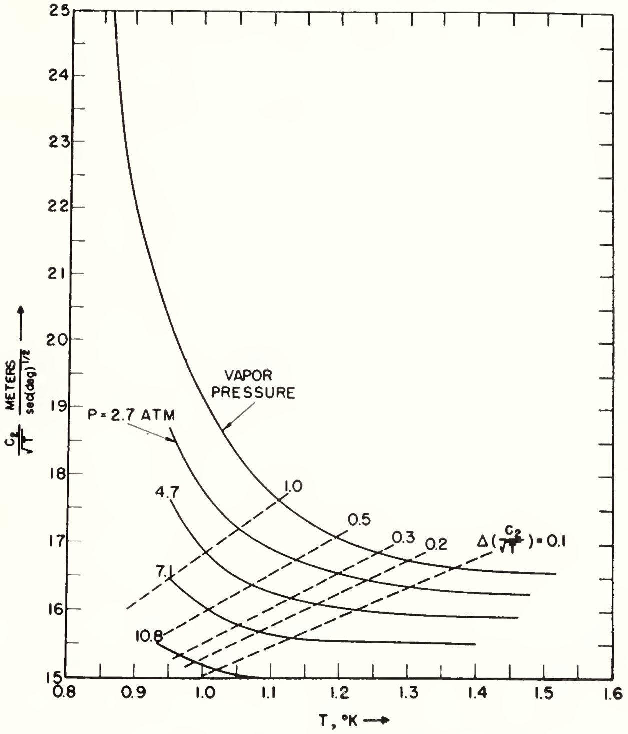

FIGURE 33.3. *Plot of $c_2/T^{1/2}$ versus T for various pressures.*

The high-temperature portions of the curves extrapolate to low temperatures as horizontal lines. Lines of constant deviation from the extrapolated horizontal line, $(c_2/T^{1/2})$, are shown for various values of the deviation. The temperatures of constant deviation, T_d, are given by the intersections of the P=constant and $(c_2/T^{1/2})$=constant curves.

This agreement supports the hypothesis that the phonons contribute to the normal fraction of fluid only and are responsible for the rise of second-sound velocity at low temperature. The phonons do not, however, combine linearly with the Bose-Einstein excitations, unless the Bose-Einstein spectrum is greatly different from what has been assumed heretofore.

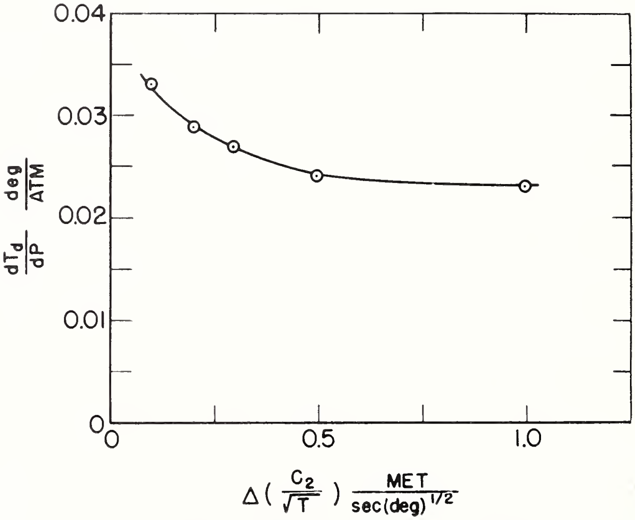

FIGURE 33.4. *Pressure derivative of the temperature of constant deviation, (dT_d/dP), as a function of the amount of deviation, $(c_2/T^{1/2})$, taken from figure 33.3.*

As T_d is near 1° K, dT_d/dP is nearly the same as $(1/T_d)dT_d/dP$. The value expected from the phonon contribution to the normal fluid flow at small deviations is about 0.037.

The authors are indebted to R. P. Cavileer and W. B. Wilbur for the manufacture of liquid helium and to A. R. Sears for assistance with the electronics. H. H. Kolm and E. H. Jacobson contributed notably to the early phases of the experiment.

References

[1] L. Tisza, Phys. Rev. **72,** 838 (1947).
[2] L. Landau, J. Phys. (USSR) **5,** 71 (1941).
[3] R. D. Maurer and M. A. Herlin, Phys. Rev. **76,** 948 (1949).
[4] J. R. Pellam and R. B. Scott, Phys. Rev. **76,** 869 (1949).
[5] V. Peshkov, J. Phys. (USSR) **10,** 389 (1946); J. Exptl. Theoret. Phys. (USSR) **18,** 1951 (1948).
[6] J. R. Pellam, Phys. Rev. **75,** 1183 (1949).
[7] V. Peshkov and K. N. Zinovyeva, J. Exptl. Theoret. Phys. (USSR) **18,** 438 (1948).

34. The Thermal Rayleigh Disk in Liquid Helium II

by J. R. Pellam and W. B. Hanson [1]

Introduction

The tendency of a flat obstacle suspended in a fluid velocity-field to turn perpendicular to the direction of particle velocity is exemplified by the Rayleigh disk. The hydrodynamics of this situation are shown in figure 34.1. A fluid flow of initial undisturbed velocity, v, encounters a thin circular disk at an angle Θ. Resultant distortion of this flow results in a highly variable velocity distribution over the surface of the disk. For example, the splitting of adjacent stream lines on the front side of the disk, at point 1, results in stagnation, whereas at point 2 behind the disk, a tangential flow velocity persists; similarly, stagnation and tangential flow exist at points 4 and 3, respectively.

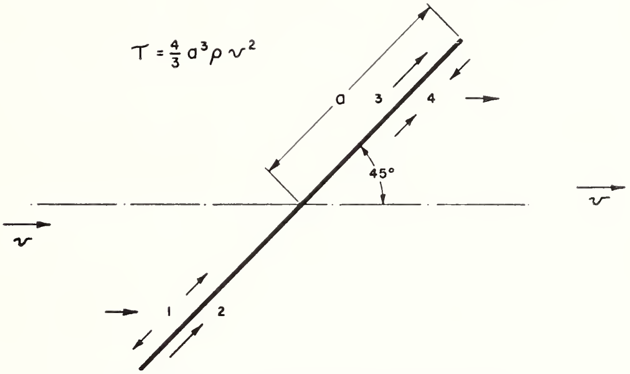

FIGURE 34.1. *Fluid flow around a disk.*

Undisturbed fluid flowing at velocity v.

As a result of these velocity differences between points on the opposite faces of the disk, unbalanced Bernoulli pressures exert a net couple tending to aline the disk crosswise to the flow. By way of example, the Bernoulli pressure at point 1 (stagnation) exceeds that at point 2, and the pressure at 4 exceeds that at 3. Hence a net couple exists for these sets of points. An exact mathematical expression due to Konig for the torque τ, on a disk of radius a, including an integration of such torque over the entire disk, gives

$$\tau = \frac{4}{3} \rho v^2 a^3 \sin 2\theta \qquad (1)$$

in terms of fluid density, ρ, and particle velocity, v. In the experimental arrangement used, θ was 45 degrees, and hence the factor $\sin 2\theta$ reduced to unity.

National Bureau of Standards, Washington, D. C.

It can easily be seen by reversing the direction of the stream lines in figure 34.1 or examining the Konig expression, that the torque is independent of the direction of particle flow. Accordingly, for application to cases involving periodic flow the instantaneous direction of particle excursion is irrelevant, so that the device functions as a rectifier and thus as a detector.

The Thermal Rayleigh Disk

We have just seen that the Rayleigh disk tends to swing crosswise to the propagation axis of an ordinary sound wave, regardless of the instantaneous direction of particle flow, so that both halves of the cycle contribute constructively. This same property enables the Rayleigh disk to detect the internal counterflow associated with heat flow in liquid helium II.

Even though net particle flow and net momentum remain zero for this internal flow, so that to first order neither vibration microphones nor pressure microphones respond, the disk recognizes variations of Bernoulli-type pressure over its surface. In the same manner that a pressure decrease is associated with regions of increased flow velocity for classical fluids, so does a pressure decrease accompany increased heat current in helium II.

The condition of zero net-particle velocity (to first order) for heat flow or thermal vibration in liquid helium II is customarily written

$$\rho_n v_n + \rho_s v_s = 0. \tag{2}$$

Here ρ_n and ρ_s are the densities of the normal- and superfluid components, respectively, and v_n and v_s are the corresponding particle velocities. However, although the individual fluid momenta balance out, the net energy density is the simple sum of the separate contributions. Otherwise stated, the Rayleigh disk responds to kinetic-energy density, thus detection occurs.

Even when the internal counterflow accompanying thermal current in helium II is periodic, as for second sound, the disk still responds indiscriminately to both halves of the cycle. Hence, as for classical sound, this rectifying action results in detection of second sound and in measurement of its time-average intensity. We now proceed to compute separately the expected torques exerted on the disk by the normal and by the superfluid components, and then to compute the joint effect of the two fluids.

Assuming that normal fluid interaction with the disk conforms to the classical formula (1), we have for the normal-fluid contribution to the torque τ_n (for $\Theta = \pi/4$)

$$\tau_n = \frac{4}{3} a^3 \rho_n \langle v^2{}_n \rangle. \tag{3}$$

As the mean square value of particle velocity $\langle v_n{}^2 \rangle$ is introduced, eq (3) gives the average value of torque. It will prove useful to express v_n directly in terms of the heat-flow density, $\dot{H}$, which may be done by employing the entropy-flow relationship

$$\frac{\dot{H}}{T} = \rho S v_n \tag{4}$$

in terms of absolute temperature, T, net fluid density, ρ, and entropy S, of liquid helium. Combining (3) and (4) we have

$$\tau_n = \frac{4}{3} a^3 \rho_n \frac{\langle \dot{H}^2 \rangle}{(\rho S T)^2} \tag{5}$$

in terms of the time-average value of heat current squared $\langle \dot{H}^2 \rangle$.

Similarly, using (2) and (4) we get for the torque due to superfluid

$$\tau_s = \frac{4}{3} a^3 \rho_n \left(\frac{\rho_n}{\rho_s}\right) \frac{\langle \dot{H}^2 \rangle}{(\rho S T)^2}, \tag{6}$$

where $\langle \dot{H}^2 \rangle$ again enters to give the time-average value of the torque.

Finally, the combined torque exerted by the composite action of the two fluid components on the disk should be the direct sum of these individual contributions.

$$\tau = \tau_n + \tau_s = \frac{4}{3} a^3 \frac{\rho_n}{\rho_s} \frac{\langle \dot{H}^2 \rangle}{(\rho S T)^2}. \tag{7}$$

The theoretical curves for $\tau_n/\langle \dot{H}^2 \rangle$, $\tau_s/\langle \dot{H}^2 \rangle$, and $\tau/\langle \dot{H}^2 \rangle$ given by (5), (6), and (7) are plotted as functions of the temperature in a later section, where comparisons with experimental results are made.

Apparatus

A composite view of the assembled equipment is presented in figure 34.2. The Rayleigh disk assembly itself rests within a Dewar containing liquid helium II. Horizontal slots are used in the Dewar system in addition to the conventional vertical slots, in order to provide apertures for entry and exit of the optical beam employed to observe disk deflections.

The disk, D, employed for detecting the second-sound field consists of a galvanometer mirror ½ in. in diameter. As indicated in figure 34.2, this disk is suspended at the midpoint of a horizontally oriented cylindrical glass cavity, E. Resonance of second sound within this cavity is achieved by introducing (electrically) periodic heating at the proper frequency, through the thermal driving element, F, of carbon resistor strip comprising one endwall of the cavity. The distribution of heat-flow density, $\dot{H}$, along the axis of the cylinder is indicated for the condition of resonance in the corresponding drawing of figure 34.2.

A system similar to that employed for galvanometer suspensions is used for protecting the copper torsion ribbon, H, from strain or shock when not in use. By turning screw I with a rod, J, extending through a vacuum gland, the mirror and mica damping vane assembly may be lowered to a position where the end of rod G settles into the glass nacelle N. When the whole apparatus is immersed in liquid helium II the screw, I, serves to raise the disk to the center of the cavity and to adjust its angular orientation. The central adjustment of rod G within the circular orifice, L, is accomplished by an over-all adjustment of the entire Dewar assembly.

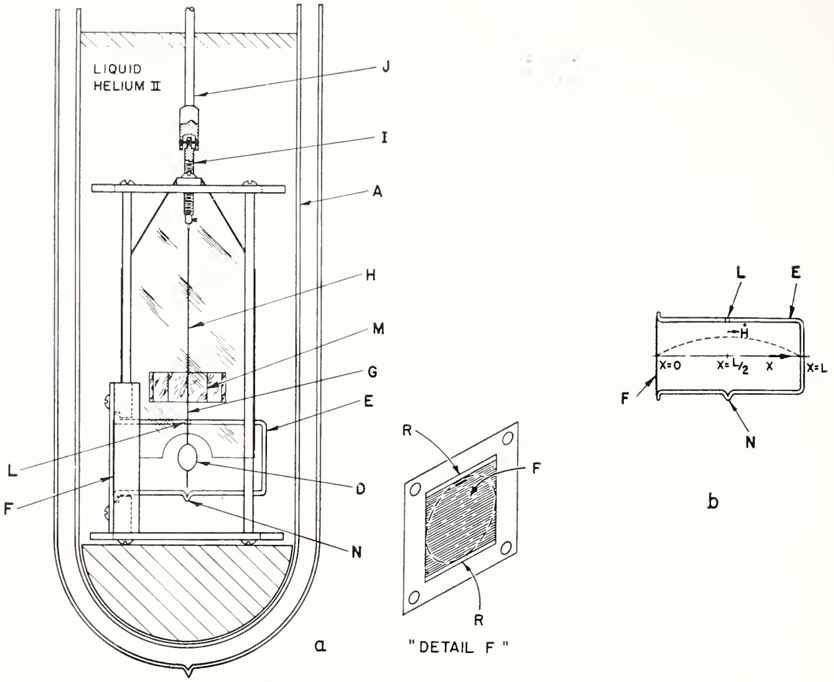

Figure 34.2. *Details of experimental apparatus.*

a, Rayleigh-disk assembly. Detail F shows structure of heater element. b, Thermal half-wave resonator. Heat-flow distribution within resonant cavity (dotted line H).

The small deviations of the disk from its equilibrium orientation caused by the second-sound field are observed and measured by the resultant deflection of a light beam. A light source projects light down the axis of the resonant cavity onto the Rayleigh disk, which serves as its own deflection mirror. Upon reflection from the disk, the beam emerges at right angles to fall in focus upon a scale.

The introduction of a known uniform heat-flow density to the cavity is accomplished by means of the electric heating element, F. The thin carbon layer surface of F in contact with helium II supports a uniform electric-current density between two parallel electrode strips, R, along the opposite edges of the square element (see fig. 34.2) Heat generated in the "triangular corners", where no direct contact with helium is made, is further suppressed by laquer applied to these areas.

The driving voltage across F is provided by a signal generator that has been calibrated by a standard signal to read directly to better than 1 part in a thousand over the frequency range used.

Measurement Procedures

The virtually complete inherent quiescence of liquid helium II gives the disk-vane system such a degree of stability that the total zero-point shift of the indicator spot on a scale 50 cm distant is less than 1/2 mm over a period of several hours. This property of the system, beside adding to the reproducibility of the data, allows one to work at very low power levels. Only within the resonance chamber, E, in the presence of second-sound waves sustained by an externally maintained driving stimulus, does the suspended system experience a torque.

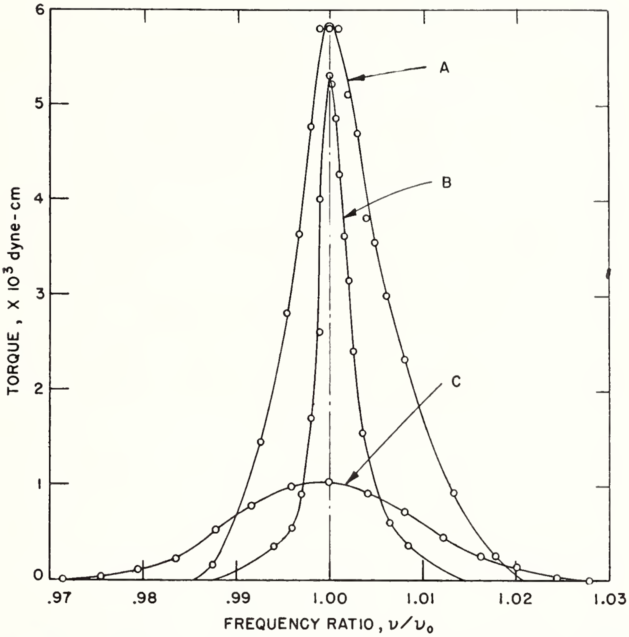

Figure 34.3. *Typical resonance curves for three characteristic temperatures.*

Torque τ versus relative frequency, ν/ν_0.
A, τ=1.28° K; ν_0=196.4 cps.
B, τ=1.75° K; ν_0=211.2 cps.
C, τ=2.18° K; ν_0=48.8 cps.

Samples of typical resonance curves are shown in figure 34.3. Here torque, τ, (of the order of millidyne-centimeter) is plotted versus relative frequency, ν/ν_0, for three characteristic temperatures at constant heat input, $\dot{H}_0$. In this regard, data on wave-velocity versus temperature obtained from the resonant frequency, ν_0, displays the usual characteristics, i. e., a maximum of about 20.3 m/sec at 1.65° K, falling off somewhat at lower temperatures and dropping abruptly toward zero as the lambda-temperature is approached.

As is evident from these curves, both the shape and magnitude of the resonance response (for the same heat input, $\dot{H}_0$) vary with temperature. The maximum torque, $\tau_{\max}$ may be observed directly from the height of the resonance peak and the resonance reinforcement factor, f, is revealed by the band width (sharpness) of the curve.

In analogy to the treatment for classical resonating systems, a reinforcement factor, f, for the present experiment may be represented by

$$f=\dot{H}/\dot{H}_0=2/\pi\ \frac{\nu_0}{\Delta\nu}=\frac{2}{\pi}\ Q,$$

where $\Delta\nu$ is a band width. More specifically, $\Delta\nu$ denotes the frequency spread between the two points on the curve (on either side of resonance) for which torque, τ, drops to one-half maximum value. The quantity f is the factor by which heat-current input, $\dot{H}_0$, at the generator wall is "amplified" by resonance to the effective value $\dot{H}$ for the midportion of the cavity. The quantity $\nu_0/\Delta\nu$ is, of course, just the usual Q for a resonant system.

Observations and Results

From eq (7) we see that the torque should vary with the fourth power of the applied voltage (as $\dot{H}\sim V^2$). In order to establish this, and also the fact that Q should be independent of the voltage, the series of curves in figure 34.4 were taken at a constant temperature.

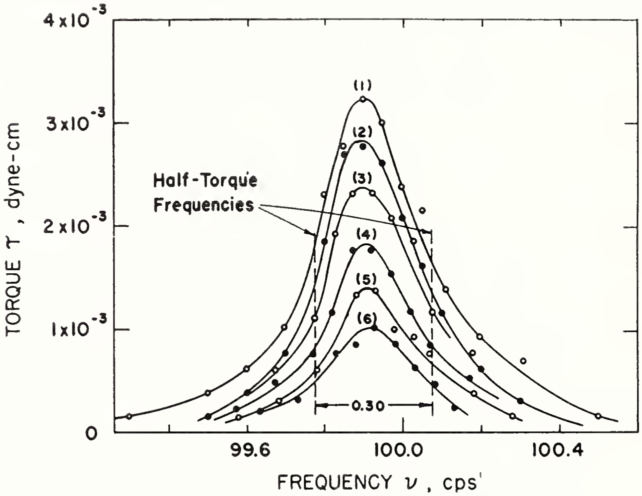

FIGURE 34.4. *Band width independent of power level.*

Series of resonance curves (τ versus ν) at constant ambient temperature, T (1.88° K), for various voltages, V_{rms}; half-torque frequencies are indicated by parallel broken vertical lines (constant band width, $\Delta\nu_s$=0.30 cps).

Driving voltages, V_{rms}: (1), 1.65 volts; (2), 1.55 volts; (3), 1.45 volts; (4), 1.35 volts; (5), 1.25 volts; (6), 1.15 volts.

It is evident from these curves that Q is indeed quite insensitive to the applied voltage. Figure 34.5 shows a plot of log $\tau_{\max}/Q^2$ versus log V_{rms} for the same set of curves. The line of slope 4 is seen to be a good approximation to the actual data, hence we may be confident that we are working at power levels where (7) applies.

We are now in a position to compare the observed torques with the predicted values. In view of the experimentally verified $\langle\dot{H}^2\rangle$ dependence, the theoretical curves may legitimately be plotted in terms of $\tau_n/\langle\dot{H}^2\rangle$, $\tau_s/\langle\dot{H}^2\rangle$, and $\tau/\langle\dot{H}^2\rangle$, respectively, as functions of the temperature. These curves are shown in figure 34.6, where the dotted line represents the contribution by normal fluid alone, the dashed line represents the contribution by superfluid alone, and the solid line represents that due to the two fluid components jointly. In the numerical evaluation of expressions (5), (6), and (7) for these plots, Andronikashvilli's measurements of fluid densities, ρ_n and ρ_s, and Kapitza's measurements of the temperature-entropy product

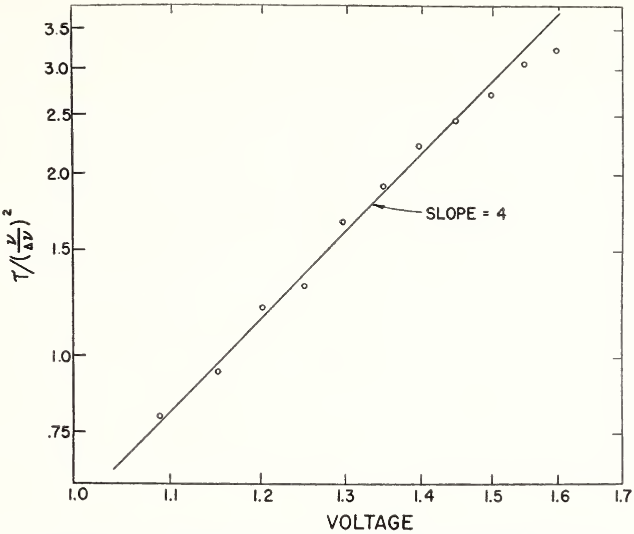

Figure 34.5. *Fourth-power dependence of torque on voltage.*

Measured $(\tau_{max}(/(\nu_0/\Delta\nu)^2$ versus driving voltage, V_{rms}; slope equal to four on log-log scale ($T=1.88°$ K).

TS were employed. These curves terminate at the lower limit of Andronikashvilli's ρ_n/ρ_s measurements.

It will be noted from these curves that the torque due to superfluid, $\tau_s/\langle \dot{H}^2\rangle$, rises sharply in the immediate vicinity of the λ-point.

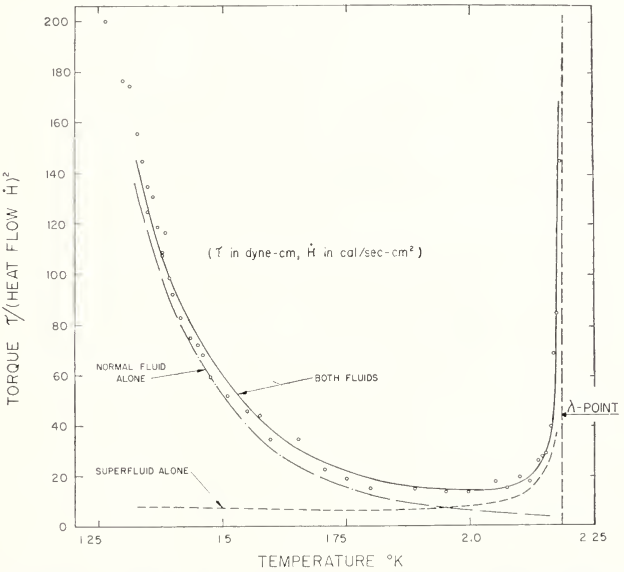

Figure 34.6. *Torque ratios, $\tau\langle \dot{H}^2\rangle$, as functions of temperature, T.*

Experimental and theoretical values.

Theoretical predictions indicated by curves: —·—·—·—· represents $\tau_n/\langle \dot{H}^2\rangle$, the expected torque for normal fluid; ---------- represents $\tau_s/\langle \dot{H}^2\rangle$, the expected torque for superfluid; and ________ represents $\tau/\langle \dot{H}^2\rangle$, that predicted for both. The circles ○ are the observed values.

Thus the superfluid contribution appears to be enhanced most in the temperature range for which the superfluid concentration is least. This takes place because as superfluid becomes sparse its particle velocity, v_s, increases to maintain zero net momentum transfer (according to eq 2); and the simultaneous dependence of torque on particle velocity squared more than offsets the effects of decreased superfluid density. It may likewise be observed that a similar trend also occurs in the torque curve for normal fluid at low temperatures, where ρ_n becomes small.

The actual measured values of the torque $\tau/\langle \dot{H}^2 \rangle$, are indicated by the circles plotted in figure 34.6. It is apparent that the observed torques are not only of the same order of magnitude as the predicted values, but also the same general trends are observed. In particular, $\tau/\langle \dot{H}^2 \rangle$ is observed to increase by a factor of eight over its value at 2.1° K as one approaches the λ-point. This is what would be expected if the superfluid were contributing its share to the torque exerted on the disk. Similarly, at temperatures below 1.75° K the torque increases again, as would be expected if the normal fluid were contributing its share to the torque. In the intermediate region, where neither fluid component is expected to predominate, the observed results conform closely to the expected combined effects of the two fluids. Thus it would appear that each fluid component contributes its share to the torque on the Rayleigh disk, and that the total observed torque is the sum of these individual torques. This is interpreted as fully verifying eq (7).

35. Apparatus for Measuring the Pressure Dependence of the Viscosity of Liquid Helium[1]

by H. H. Kolm and Melvin A. Herlin[2]

The viscosity of liquid helium as a function of temperature has only been measured at the vapor pressure. These measurements were first made by Keesom and MacWood,[3] who observed the damping of a 5-cm-diameter copper disk oscillating in liquid helium about its axis against the restoring torque provided by a phosphor-bronze suspension wire. The disk oscillated with a period of about 30 sec and was observed during about 15 periods. Measurement of the damping and changes in the frequency of oscillation were then used in conjunction with an approximate theory to derive $\eta\rho$ (viscosity $\times$ density) for liquid helium and the slip at the helium-metal interface. The latter proved negligible.

In order to provide information concerning the phonon contribution to the viscosity of liquid helium, we developed apparatus capable of measuring viscosity inside a metal pressure chamber. The chamber, which is immersed in the helium bath, contains a 1-cm-diameter disk made of Alnico 5 magnetized along a diameter and suspended by

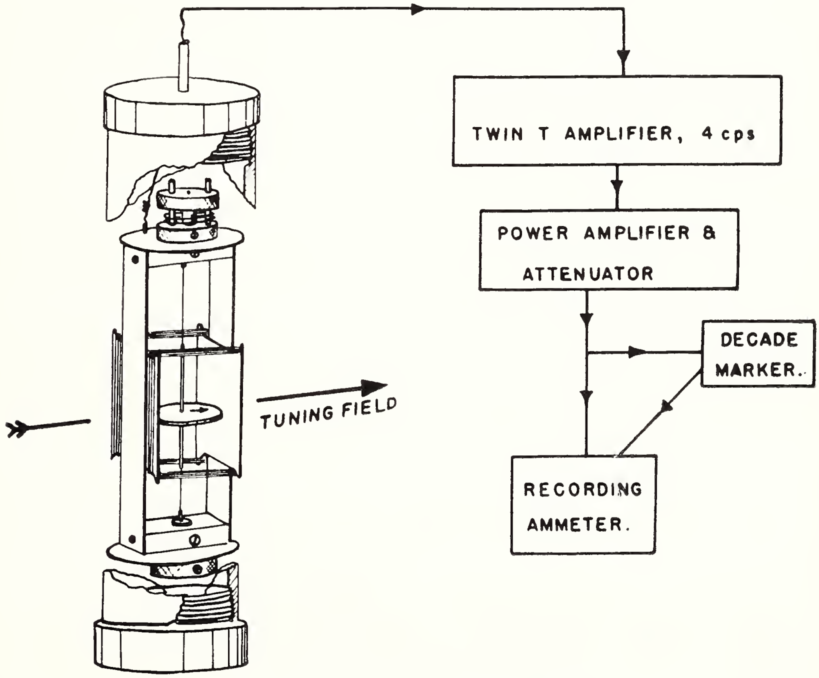

Figure 35.1. *Sketch of viscosimeter.*

---

[1] This work has been supported in part by the Signal Corps, the Air Matériel command, and Office of Naval Research.

[2] Research Laboratory of Electronics, Massachusetts Institute of Technology, Cambridge 39, Mass.

[3] W. H. Keesom and G. E. MacWood; Physica **5**, 737 (1938).

means of two phosphor-bronze wires attached to the extremities of a thin, rigid shaft passing through its center and has a natural period of about 1 sec (shown in fig. 35.1). A second set of Helmholtz coils located outside the Dewar system provides a d-c magnetic field along the direction of magnetization of the disk, and this field is adjusted to increase the frequency of the disk to about 4 cps. Most of the restoring torque is thus provided magnetically, a measure that reduces to a minimum the inevitable residual damping due to the suspension.

Motion of the disk is observed by amplifying and recording the voltage induced in the inner set of coils, and in this manner the damping can conveniently be measured during several hundred periods.

Preliminary measurements made thus far show approximate agreement with the results of other authors, although they indicate the need for additional measures to reduce the noise level.

36. Remarks on Scattering of Slow Neutrons by Liquid Helium

by Louis Goldstein [1]

The experimental investigation of the slow neutron scattering properties of liquid helium is of multiple interest. It should confirm, among others, the results on the coherent scattering of X-rays and go far beyond this in yielding, possibly, information on the properties of the liquid not available in the X-ray diagrams.

The coherent scattering of slow neutrons leads, indeed, to the spatial distribution of the helium atoms around one chosen arbitrarily in the liquid. This result is based on the classical Ornstein-Zernike static liquid model.[2] According to the latter, the interatomic forces establish in the liquid an orderly arrangement of the atoms around one situated at the origin of the coordinate system. The concentration of the liquid atoms $n(r,T)$ at some distance, r, from the origin, at temperature T, may be written as

$$n(r,T)=n_0(T)+g(r,T), \tag{1}$$

where $n_0(T)$ is the average over-all liquid concentration, and $g(r,T)$ is a local correction to the mean concentration arising from the intermolecular forces that are responsible for the spatial ordering or correlation of the liquid atoms. The quantity $g(r,T)$ is the correlation concentration. This has the following limiting properties. At large distances, r, that is, r large in comparison with the range of the interatomic forces, the correlation has to vanish, and the mean concentration $n_0(T)$ should prevail. Explicitly,

$$\lim_{r\text{ large}} n(r,T)=n_0(T); \qquad \lim_{r\text{ large}} g(r,T)\rightarrow 0. \tag{2}$$

At small separations, the repulsive character of the interatomic forces creates a vacuum around a liquid atom, and here

$$\lim_{r\text{ small}} n(r,T)\rightarrow 0; \qquad \lim_{r\text{ small}} g(r,T)\rightarrow -n_0(T). \tag{3}$$

These limiting values of the concentrations are valid, provided the temperature of the liquid is small in comparison with its critical temperature, T_c. The present discussion will be limited throughout to temperatures $T<T_c$.

Assuming the spatial distribution function (1), the coherent scattering cross section, per unit solid angle and per liquid atom, can be shown to be given by

$$\sigma_L(\Delta k,\, T)=\sigma_\infty F_L^2(\Delta k,\, T), \tag{4}$$

where σ_∞ is the infinitely heavy or bound-atom slow-neutron coherent cross section per unit solid angle, and F_L^2 is the coherent intensity

---

[1] University of California, Los Alamos Scientific Laboratory, Los Alamos, N. M.

[2] L. S. Ornstein and F. Zernike, Amsterdam Proceedings **17**, 793 (1914).

structure factor per liquid atom. The cross section, σ_∞, is further defined by

$$\sigma_\infty = (\sigma_s/4\pi)\ (1+A^{-1})^2, \tag{5}$$

where σ_s is the total slow-neutron scattering cross section of the atom under consideration, and A is its mass in units of the neutron mass. The quantities σ_s or σ_∞ are specific nuclear constants, independent of the neutron energy. The structure factor, F_L^2, depends both on the liquid temperature and the quantity

$$\Delta k = 2k \sin\theta = (4\pi \sin\theta)/\lambda; \qquad \lambda = h/p, \tag{6}$$

which measures, in units of $(h/2\pi)$, the linear momentum loss of the neutrons or X-ray photons in the coherent-scattering process, whereby they have been deflected through an angle (2θ) from their direction of incidence. The length of the neutron or photon propagation vector is k, p is their linear momentum, and λ the de Broglie wavelength of the neutrons or the X-ray wavelength. The structure factor is found to be given by

$$F_L^2(\Delta k, T) = 1 + 4\pi \int_V g(r, T)\, \frac{\sin\,(r\Delta k)}{r\Delta k}\, r^2 dr, \tag{7}$$

for atoms such as He^4 with vanishing nuclear spin. The integral on the right-hand side extends over the whole volume, V, of the liquid, or, essentially, over the whole space as $g(r,T)$ is a rather short range function at temperatures $T < T_c$. In the preceding formulation of the neutron scattering, all interactions between the neutrons and atomic electrons, both of magnetic or, possibly, nonmagnetic origin, have been neglected.

A glance at the general formula (7) shows that for small Δk values, or small-angle slow-neutron or X-ray scattering,

$$\lim_{\Delta k \to 0} F_L^2(\Delta k, T) = 1 + 4\pi \int g(r, T) r^2 dr = 1 + G(T). \tag{8}$$

In this limit the structure factor becomes independent of the details of the scattering process, such as the neutron wavelength and scattering angle. It depends only on the space integral of the correlation concentration, a quantity that is associated with a specific macroscopic property of the liquid. Indeed, one proves in the present static liquid model that

$$1 + G(T) = \overline{\Delta N^2}/N, \tag{9}$$

where the right-hand side is the mean-square fluctuation per liquid atom $\overline{\Delta N^2}$, of the total number of liquid atoms, N. On the other hand, according to statistical thermodynamics,[3]

$$\overline{\Delta N^2}/N = n_0 k T \chi_T, \tag{10}$$

χ_T being the isothermal compressibility of the liquid; k is Boltzmann's constant. Hence, the knowledge of the mean concentration, $n_0(T)$, or the density, together with that of the compressibility, determines the small-angle-intensity structure factor. It is worth noticing

---

[3] A. Einstein, Ann. Phys. **33**, 1275 (1910).

here that the limiting structure factor (8) or (9) was first obtained explicitly by Einstein[3] in his statistical thermodynamic theory of coherent scattering of long-wave visible radiation by liquids elaborated after the original suggestions of Smoluchowski.[4] The latter author was first to recognize that the existence of coherent-scattering processes of visible radiation in liquids owes its origin to concentration fluctuations. In this phenomenon, the quantity Δk is small at all scattering angles, since λ, the wavelength of the radiation, is very large in comparison with the range of the correlation density $g(r,T)$. It is interesting that the rigorous molecular structure factor formula (7) reduces in this limit of large λ to the thermodynamic formula (9) or (10). This, of course, was to be expected on general physical grounds. Indeed, when the wavelength of the incident radiation is large in comparison with the range of the correlation function, over which the interatomic forces govern the orderly arrangement of the liquid atoms, then the existence of this local ordering remains entirely unnoticed by the radiation whose scattering should be independent of the local distribution and depend only on the over-all statistical thermodynamic properties of the liquid, as expressed by eq (10).

Using the density and compressibility of liquid helium,[5] it was found that the small-angle structure factor (9) or (10) is independent of the temperature, for all practical purposes, between 1° and about 3° K. This means that the forward or small angle coherent scattering cross section of slow neutrons or X-rays remains constant in the He II and He I regions, in the latter up to about 3° K.

The question that arises now concerns the temperature variation of the large-angle scattering structure factor (7). It can, however, be proved that the preceding conclusion concerning the small-angle structure factor remains approximately justified at all angles. In other words, the liquid-helium slow-neutron or X-ray coherent structure factor should only vary rather slowly with temperature up to about 3° K. In particular, according to the present model, no important variation of the coherent structure factor should be observed in passing from the He II into the He I region. Apparently, this result is in agreement with some experimental data on X-ray scattering.[6] The X-ray diagrams obtained with the two liquid modifications did not disclose any definitely observable changes. It should be remembered here that the asymptotic ideal Bose-Einstein He model predicts a rather important qualitative modification of both the coherent[7] and incoherent[8] scattering cross sections in crossing the transition line. If the X-ray data on liquid helium, obtained in rather difficult experiments, are accepted to be fully representative, then one might say that the interatomic forces seem to mask completely the Bose-Einstein statistical features of the coherent scattering, assuming that B. E. statistical effects are present in this liquid. A repetition of the X-ray work and the experimental investigation of slow-neutron scattering might provide a clearer interpretation of the coherent scattering processes in He. The preceding small temperature dependence of the coherent structure factor is a consequence of the fact that the static liquid model operates with purely spatial distributions of the liquid atoms whereby the tacit averaging over the different states of motion of the liquid as a whole does

---

[4] M. v. Smoluchowski, Ann. Phys. **25**, 205 (1908).

[5] W. H. Keesom, Helium (Elsevier, Amsterdam, 1942).

[6] W. H. Keesom and K. W. Taconis, Physica **5**, 270 (1938); J. Reekie, Proc. Cambridge Phil. Soc. **36**, 236 (1940).

[7] L. Goldstein, Phys. Rev. **83**, 289 (1951).

[8] L. Goldstein, D. W. Sweeney, and M. Goldstein, Phys. Rev. **77**, 319 (1950).

not seem to affect the scattering properties of the fluid in its two modifications. This small temperature dependence ceases already below the boiling point and the whole coherent scattering process becomes more and more anomalous as the critical region is approached. Here, as pointed out previously[7] [9] slow neutrons might be used to obtain additional information on the critical opalescence properties of the liquid.

So far we have considered only coherent scattering processes. The situation appears to be different with the incoherent scattering of slow neutrons in liquid helium. In this phenomenon, both energy and momentum are exchanged by the neutrons and the liquid as a whole. Let us assume then, that in He II the liquid atoms are distributed essentially over two types of states of motion, as suggested by a number of properties of this liquid. In He I this division does not seem to exist. It may then be reasonable to expect that the mechanism of energy and momentum exchange between the neutrons and He II be different from that realized between the neutrons and He I. One might thus expect a change in the incoherent slow-neutron cross section per liquid atom as the temperature of the liquid increases from below to above the lambda point.

It is, of course, clear that experimentally both the coherent and incoherent processes are observed simultaneously, the two phenomena being of practically equal importance because of the comparable masses of the neutron and He^4 nucleus.[10] The two processes have to be separated in order to recognize clearly their respective trends of variation with liquid temperature. The disentangling of these two types of scattering processes is possible to a fair degree of approximation. The experimental investigation of the slow neutron incoherent scattering in liquid helium may yield new information on the energy spectrum of the liquid in its two modifications.

We should like to add finally that the preceding considerations are quite general and valid for any liquid. They appear to indicate that the experimental investigation of the slow-neutron incoherent scattering may become a possible tool for obtaining some insight into the energy spectra of liquids.

---

[9] L. Goldstein, Bul. Am. Phys. Soc. **25**, 38 (1950).

[10] See, in this connection, L. Goldstein and D. W. Sweeney, Phys. Rev. **80**, 141 (1950).

37. Flow Properties of Helium II

by K. Mendelssohn [1]

All experiments on liquid helium II have shown that the flow properties are of an unusual and complex nature. The ordinary concept of viscosity is not applicable as the rate of flow cannot be expressed by the usual type of equation. However, as the diameter of the flow channel is decreased, the character of the liquid transport becomes less complex, but the flow properties are now quite non-classical. In particular, the rate of flow is largely independent of the pressure gradient and the length of the channel.

Up to the present time all observations have been made by measuring the transported mass per unit time and the pressure difference at the ends of the flow tube. The question therefore arises as to the pressure gradient inside the channel itself. Using as the flow channel the gap between two circular flat disks, the liquid was made to flow radially in or out of this arrangement. A groove was cut at an arbitrary place between the ends of the channel, and a "static tube" for measuring the intermediate pressure in the channel was attached to this groove (see fig. 37.1). In flow under gravity it was then observed that the whole of the pressure gradient was taken up by the narrower part of the channel, the static tube registering the same pressure as one end of the channel. In this case the ratio of the classical flow resistances between the two sections of the channel was 4:1. The experiments were repeated, using two porous membranes instead of a gap between parallel plates. With this arrangement the classical resistance of the two sections of the flow channel could be made more equal. However, even with a ratio of resistances as close as 4:3 the entire pressure drop was still concentrated on the slightly higher resistance (see fig. 37.2).

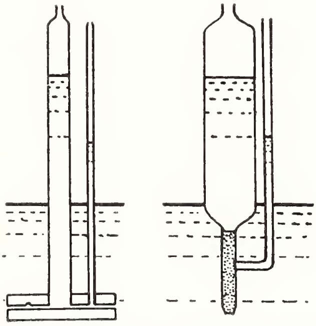

FIGURE 37.1. *Arrangements for the flow of liquid helium II through a slit between parallel plates and through rouge powder.*

The intermediate pressure is measured by a "static tube."

---

[1] Clarendon Laboratory, Oxford, England.

The above result shows that at least in one section of the channel the flow of helium II takes place under zero pressure gradient. This is analogous to an earlier observation on the helium film, in which it could be shown that at speeds smaller than the critical, film transfer would occur from one volume of liquid to another of equal level height. As in the present experiment the static tube was attached at an arbitrary position in the flow channel, and as it is also apparent that the ratio in the flow resistances of the sections is immaterial, one is tempted to conclude that the limitation of the flow rate will in fact occur at the end of the channel. In other words, it seems as if there exists some place in the flow arrangement at which the whole pressure drop takes place. What exactly would be the physical significance of such a pressure discontinuity is difficult to understand as we have as yet no detailed theory of the flow phenomena in liquid helium.

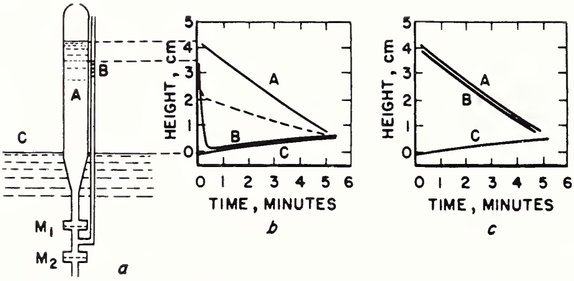

FIGURE 37.2. *Flow of liquid helium* II *through two porous membranes, M_1 and M_2, whose normal flow resistances are in the ratio 4:3.*

Reversal of the position of M_1 and M_2 shows that in superflow the total pressure drop is concentrated on M_1. (a) Sketch of Apparatus; (b) M_1 and M_2, arranged as in (a), and (c) M_1 and M_2 interchanged

Flow of liquid helium II cannot only be produced under a gradient of pressure but also under a gradient of temperature. Using again the same arrangement of flow between plane glass plates, one of the volumes of liquid connected by the flow channel was heated. This caused a transport of liquid in the direction toward the higher temperature, as was expected from earlier work. For small flow rates the pressure in the static tube was again identical with that in one of the volumes of liquid, showing zero pressure gradient. However, in liquid helium II, pressure and temperature are connected in a unique way by H. London's equation. The observed fact of zero pressure gradient along one section of the flow channel therefore shows that the temperature gradient in the same section must also be zero. On the other hand, this section of the channel now carries also a heat current. According to the well-known thermal effects in helium II, the heat supplied to one volume connected with the channel will appear in the other volume by withdrawal of liquid of low entropy from the latter. This process constitutes a heat transport through the channel, and since it takes place, as our experiment shows, under zero temperature gradient it must be isothermal. Thus we find in liquid helium II mass flow under zero pressure gradient and heat flow under zero temperature gradient.

These phenomena are, however only maintained for small flow velocities. It had been expected that, as the heat input into the arrangement is increased, the isothermal heat transport would break down and a temperature gradient would be set up in the channel itself. This will be indicated by a rise in the pressure recorded by the static tube. Such an effect did actually occur for very high heat currents, but in all cases it was preceded by a decrease in the intermediate pressure. This depression effect is no transient phenomenon as a definite value of pressure, smaller than the pressure in either volume, is recorded for each heat current. The effect is quite large. Our arrangement did not permit observation of a greater depression of the helium level in the static tube than 2 cm, and we were in no case able to determine the minimum intermediate pressure because it always exceeded this depression. Although it is impossible to give at this stage a definite explanation of the phenomenon, we are inclined to regard it as evidence for the first appearance of dissipation of kinetic energy.

The depression effect sets in at a well-defined heat input that only depends on temperature, and it thus appears that it marks a sudden change in the flow character as a certain rate of flow is exceeded. The concept of such a critical flow rate is fairly well established for the helium film, but is not generally accepted for the bulk liquid. Gorter and Mellink believe that friction in liquid helium II should make its appearance with the cube of the flow velocity, and according to such an assumption a critical flow rate should not exist in the liquid. However, besides the depression effect there appear a number of other features in our observations, which all indicate a sudden change in the character of the flow beyond a given velocity. In particular, it was found that whereas at low velocities the flow rate was almost directly proportional to the heat input, this relation changed rather abruptly at the critical velocity.

Experiments with wider slits show that the comparative simplicity of the flow character was lost when changing from slits of about 10^{-4} cm width to bigger ones of 10 to 50 times this diameter.

A different type of complication arose when, instead of slits, tubes were used that had been closely packed with jewelers rouge. All the phenomena observed with the narrow with the narrow slit in a temperature gradient were also present in the powder-filled tubes under similar conditions. There was again the same depression of the level in the static tube, occurring when a certain velocity was exceeded, and below this velocity this level was coincident with the level in one of the volumes of bulk liquid. However, the conditions under gravitational flow were quite different from those with the narrow slit. It was found that the level in the static tube always took up an intermediate position between the levels in the two volumes of bulk liquid. Thus while flow under a thermal gradient behaves in the same manner in the slit and the powder tube, these two arrangements yield different results for flow under a gravitational gradient. Unfortunately our measuring arrangement with the powder tube allowed only a certain range of velocities on which observations could be made, and we cannot as yet decide whether the difference in behavior shown in this tube for the two different kinds of flow may be due to our exceeding a critical velocity. In particular, it will be necessary to investigate more closely the flow properties corresponding to small pressure heads, for which our results so far are, of course, least accurate. It can, however, be said that for the greater pressure heads, where the relation between pressure and velocity can be well established, the liquid in the powder tube seems to obey the laws of turbulent flow.

Finally, some experiments on the film might be mentioned. Except for one earlier experiment in which we used a double beaker, the observations made on the transfer film always refer to flow under the critical rate. A number of experiments have now been made with film flow at less than the critical rate. First of all, the experiments with double beakers have been repeated under conditions that prevented the establishment of temperature differences between the three volumes of liquid helium connected by the two films. This was a point on which we had not been quite sure in the earlier work, but the present experiments have completely confirmed our earlier results. This double-beaker experiment, which was designed in close analogy to an electric circuit containing a superconductor, is probably the most direct and the most sensitive test for the absence of dissipation in the flow of liquid helium.

Subcritical flow was also observed in experiments in which the film was drawn through a narrow slit above the liquid level into a vessel

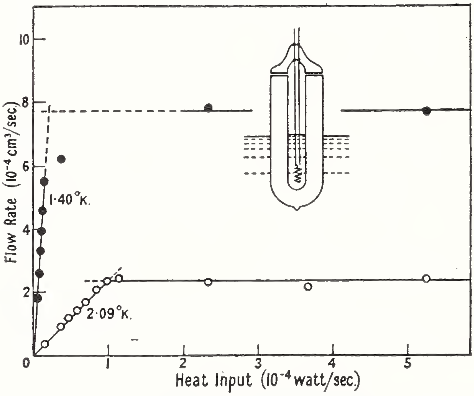

FIGURE 37.3. *Film flow under thermal potential.*

to which heat was supplied. In this way flow rates of any velocity up to the critical velocity could be produced. The results of this work show that it is quite impossible to produce film flow at rates beyond a critical flow rate that depends on temperature. Above this limit the flow rate remains at the critical value and is independent of the heat input. At low heat inputs, on the other hand, the flow rate was found to be exactly proportional to the rate of heat supply, thereby showing the complete absence of a velocity-dependent friction, such as is postulated by Gorter and Mellink for the bulk liquid.

A third set of experiments was concerned with the manner in which bulk liquid is changed into the film and back into bulk liquid. These observations showed that when bulk liquid is allowed to run down onto a surface that is larger than the circumference of the container from which this liquid originally issued, it will form a true film again. Thus it is shown that even below the highest liquid level in the system a film can be formed that obeys the same rules as the film above the liquid level.

38. Transport Rates of the Helium II Film Over Various Surfaces[1]

by Jay Gregory Dash[2] and Henry A. Boorse[3]

Liquid helium II film transport over various surfaces has been studied by a new method in which a cylindrical capacitor, using liquid helium as the dielectric, is employed as a depth gage. Changes of liquid level in the capacitor resulting from film transport produce changes in capacitance, which in turn cause frequency changes in a high-frequency circuit. The details of this method of measuring changes in liquid level are described. The film transport rates, measured to 1.25° K, were found to depend on the surface over which the transport takes place; at 1.25° K the highest rate observed was 51×10^{-5} cm^3/sec cm for etched copper and the lowest, 7.5×10^{-5} cm^3/sec cm for glass. The rates were also measured at various temperatures over iron in the magnetized and unmagnetized state and over a superconductor in the superconducting and in the normal state. No differences were noted. In the latter case, the thermal conductivity of the container is abruptly changed by the application of a greater than critical magnetic field; the absence of an effect supports the view that heat transfer plays no significant role in determining the transport rate.

Introduction

The pioneer investigations of Daunt and Mendelssohn [1] [4] on the properties of the He II film indicated that the transport rate was not affected by the underlying material. This conclusion was reached as the result of an exploratory investigation, in which a copper beaker was used instead of the glass containers employed for the most part in the study, and as a result of the transfer over copper wires. Further investigation of this aspect of the transfer appears to have been neglected until recently, when the present authors [2, 3] and Mendelssohn and White [4, 5] described experiments which show that the original conclusion is not substantiated. The purpose of the present paper is to set forth in greater detail the experiments which led to this altered viewpoint.

Before proceeding with this description, it may be worth while to point out that theories of the He II film have been advanced by Frenkel [6], Schiff [7], Temperley [8], and Bijl, de Boer, and Michels [9]. The first two authors have considered helium atoms to be under the influence of gravity and of the van der Waal attractive forces of the walls. This treatment indicates that film thicknesses on conducting surfaces are greater, by about a factor of two, than films on dielectrics. Film flow, according to Frenkel, should be limited by viscosity. For He II the theoretical result becomes ambiguous because of the presence of a zero viscosity, or superfluid, component. Temperley has treated the film as an adsorbed phase in which He atoms occupy bound sites on the surface of the solid wall. The adsorbed layers farthest from the wall are assumed to occupy only a fraction of the available sites, and film flow is considered to arise from a transition of atoms from their existing sites to empty neighbors. The influence of the wall is con-

---

[1] Sponsored in part by the Office of Naval Research.

[2] Columbia University. Research completed under an AEC Predoctoral Fellowship. Present address, Los Alamos Scientific Laboratory, Los Alamos, N. Mex.

[3] Barnard College, Columbia University, New York, N. Y.

[4] Figures in brackets indicate the literature references on p. 181.

siderably smaller for these layers than the influence of the underlying He layers, and film flow rates should be essentially the same for all wall materials. Bijl, de Boer, and Michels limit the film thickness by means of the De Broglie wave length of the superfluid particles, thus implying that film thickness and transport rate are independent of surface material. Finally, it may be mentioned that no attempt has been made to account for the fact that the film flow is directed toward a region of lower gravitational potential.

The general disagreement between these proposed explanations of the He II film and the fact that no data for transport over surfaces other than glass, except that of Daunt and Mendelssohn's, existed at the time our studies were initiated, led us to undertake a more thorough examination of this part of the phenomenon.

Experimental Method

The method which has been used by most investigators to measure film transport rates consists in observing, by means of a cathetometer, the change in height with time of the free surface of a small volume of liquid He II contained in a transparent vessel. The free surface must, of course be either above or below the level of the main bath in order for film transport to occur. In determining the rate, allowance must be made for the loss due to the evaporation of liquid helium in the transport vessel during the period of observation. If significant evaporation takes place, then the measured rate for film flow from the container will be higher than the true value, and the measured rate into the container smaller than the true value. It has been customary to average these rates to correct for evaporation and to thus obtain the "true" value of the transport rate at any temperature; this procedure is certainly a step in the direction of accuracy, but it should be noted that not enough is known about the transport to be sure that other factors are not present, which, in the absence of evaporation, might produce a difference between the outward and inward transport.

Although the optical method has the virtue of simplicity and directness, it also suffers from the defect that it requires an external source of radiation to illuminate the film and the helium container. This source of radiation must be filtered to exclude infrared; otherwise the measurements are seriously disturbed. The optical method also loses some of its directness if the transfer over opaque materials is to be studied; in this case an auxiliary transparent vessel must be used and the change of the liquid level in the transparent vessel used as a measure of the change of liquid level inside the container. Finally, the optical method appears to be entirely unsuited to measurements in the region below 1° K as in this region radiation from external sources seriously interferes with temperature stability. For these reasons it was decided to abandon the method of direct observation and to attempt the development of a more favorable technique.

In this connection the dielectric properties of liquid He II appeared to offer several very desirable features, namely, a very low dielectric loss [10] and an electric polarization practically independent of temperature [10, 11] in the He II range. Experiment showed that if the liquid were introduced as the dielectric in a closely spaced cylindrical capacitor, connected in a high-frequency circuit, the resulting change in frequency could easily be determined.

To apply this method to the determination of the transport rates of liquid He II, the arrangement shown in figure 38.1 was adopted. Here the cylindrical capacitor having a core, C_1, and a shell, C_2, is centered, by means of a threaded post, in the container or "bucket", B, constructed from the material over whose surface the transport rate is to be determined. C_1 and C_2 are insulated from each other by four longitudinal strips of Teflon spaced at 90° intervals, the mean annular separation between the capacitor walls being 0.005 in. A small hole, *b*, drilled through the bottom of shell C_2 allows free passage of the He II between the bucket and the capacitor annulus. Thus the capacitor is used as a depth gage for the liquid in *B*, and any change in the liquid level in *B* due to transport or evaporation, or both, causes a corresponding change in the liquid level in the capacitor. This in turn is reflected as a frequency change in the oscillating circuit, of which the capacitor is a part. The time taken to determine a transport rate (the number of milliliters of liquid transported per centimeter of periphery per second) at any given temperature is determined by the periphery of the bucket and the volume of liquid contained within it. Typical dimensions for *B* were 0.625 in. inside diameter and 1.7-in. over-all length.

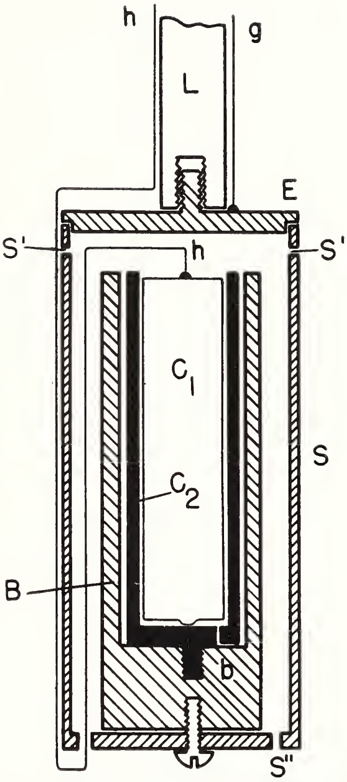

FIGURE 38.1. *Detail of transport-vessel assembly showing capacitor depth gage and radiation shield.*

The bucket and depth gage assembly were enclosed by a copper radiation shield, S, pierced by holes S' and S''. These holes allow free passage of the liquid in filling B. During a rate measurement the bottom of the shield is immersed in the bath in order to minimize any temperature gradients between the bath and the bucket. As a result of the holes, S', the pressure above the bath and bucket B are maintained equal. The whole assembly is fastened to a Lucite rod, L, which in turn is suspended by a string attached to a winch at the top of the cryostat. The general arrangement is shown in figure 38. 3.

The inner cylinder, C_1, of the capacitor was electrically connected to the external measuring apparatus by the fine copper wire, h; the outer cylinder, C_2, was grounded outside the apparatus by means of the copper wire, g.

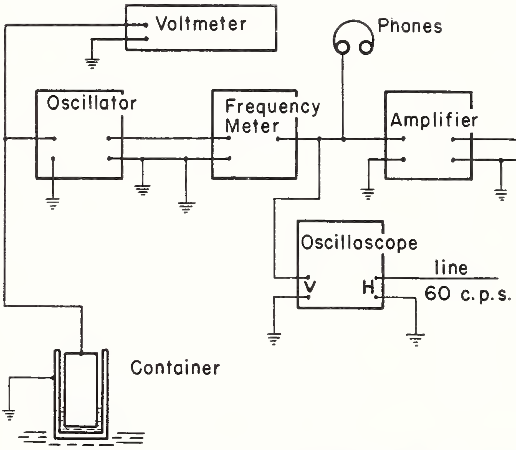

Figure 38.2. *Block diagram of the measuring circuits.*

The circuit for measuring the frequency changes is given by the block diagram in figure 38.2. The cylindrical capacitor is connected in parallel with the tuned circuit of radio-frequency oscillator of high stability [12] and a voltmeter to provide a continuous reading of the circuit excitation. An amplifying and buffering stage feeds the oscillator signal to a heterodyne frequency meter, oscillating at nearly the same frequency. The beat note is observed on an oscilloscope and fed to an audio amplifier. This amplified signal is connected to a simple frequency discriminator consisting of a large resistance in series with an air-core inductance. The voltage across the inductance, proportional to frequency, is rectified, filtered, and supplied to a recording potentiometer. It is thus possible to obtain an instantaneous and continuous record of the liquid level in the capacitor. The frequency dependence of the potentiometer circuits is obtained by calibrating the recording potentiometer response by means of the harmonics of line frequency, as seen on the oscilloscope. Alternatively, depth measurements can be made by reading the vernier scale of the frequency meter, with the beat frequency set to zero on the oscilloscope.

The fractional frequency change of the oscillator from the completely full to the completely empty condition of the capacitor was approximately 1 percent of the mean frequency. The frequency instability of the oscillator and heterodyne frequency meter was approximately 60 cps/hr at 100 kc. Under the experimental conditions the emptying times for the various buckets ranged between extremes of about 2 and 30 minutes. The over-all reproducibility of the observations, including the small frequency drift, is estimated at about 5 percent.

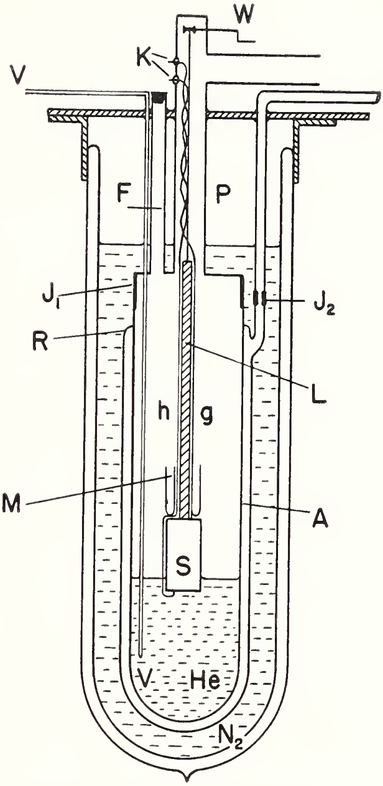

FIGURE 38.3. *Arrangement of helium cryostat and transport-vessel assembly.*

Cryostat Design

The mechanical mounting of the depth gage and container assembly within the cryostat is shown in figure 38.3. The inner He Dewar is of Pyrex glass completely silvered except for a half-inch clear vertical stripe. Copper-glass seals J_1 and J_2 provide vacuum-tight joints between the Dewar and its top cap and a pump line, respectively.

Liquid helium was introduced through filling tube *F*, and was subsequently cooled by pumping through tube *P*. Helium-bath temperatures were determined by a vapor-pressure thermometer, consisting of mercury manometers attached to the low-conductivity tube, *V*, which terminated at the bottom of the Dewar.

The vacuum-tight winch, *W*, previously noted, was used to raise and lower the container assembly, *S*. Wires *h* and *g* are brought out of the cryostat through the seals, *K*. Several Pyrex glass containers, *M*, attached to the supporting rod, *L*, were used to check transport rates over glass by the visual method. If solid air contamination were present, abnormal rates were observed and measurements were discontinued.

Experimental Details

Bowers and Mendelssohn [13, 14] have demonstrated that films of solid air deposited on transfer surfaces lead to He transport rates considerably higher than those obtained with clean surfaces. Accordingly, precautions were taken to avoid this contamination. Before filling the inner Dewar with liquid helium, the liquid space and pumping lines were successively evacuated and filled with pure He gas.

Precooling to liquid-nitrogen temperatures was achieved by filling the outer Dewar with liquid nitrogen. He transfer gas was then introduced to the annulus, *A*. After the establishment of temperature equilibrium within the He space, *A* was pumped to a high vacuum. Liquid helium was then transferred into the cryostat.

Vapor pressures of the liquid helium were determined by a 12-mm bore absolute mercury manometer and a calibrated Dubrovin scale-of-nine vacuum gage. Vapor pressures were maintained constant to 0.1-mm by a manostat-controlled [15] solenoid valve located in the pumping line. Heat influx to the He bath, measured by the rate of descent of the liquid level, was approximately 50 cal/hr, and a single filling of liquid sufficed for 7 hours of experimentation.

Calibration of the depth gage with changes in depth of the liquid He in the container was carried out as follows: The container was lowered into the bath until fully immersed, and the bath maintained at a convenient constant temperature below the lambda point. Oscillator frequency readings and cathetometer observations of the bath

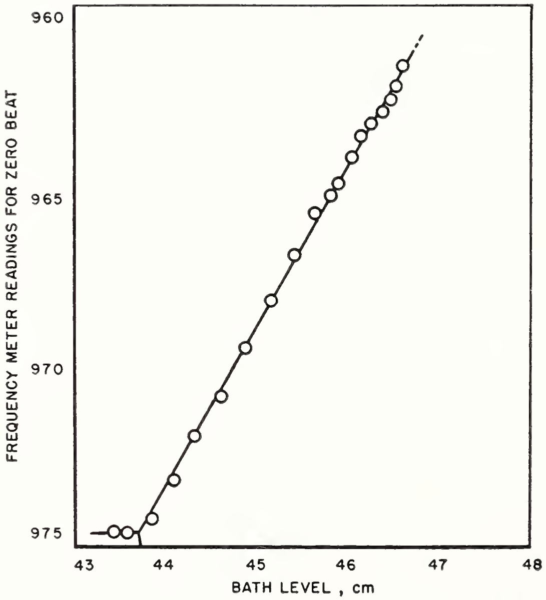

FIGURE 38.4. *Depth-gage calibration curve (4.1 divisions/cm).*

level were taken simultaneously as normal evaporation caused the liquid level in the He Dewar to fall. The rate of decline of the bath level at the calibrating temperature was considerably smaller than the rate of fall of liquid level in the bucket arising from film transport. This condition assured that the levels of the liquid in the bath and in the container dropped at the same rate. The calibration procedure therefore gave an over-all measure of depth gage "sensitivity" in frequency-meter scale divisions per centimeter change in liquid level. The most frequently used depth gage had a sensitivity of 4.10 ±.06 div/cm. A sample calibration, obtained by adjusting the frequency meter so that the oscilloscope showed a zero beat, is given in figure 38.4.

To verify that the radio-frequency field within the capacitor had no effect on the transport rate, the bucket was next filled by immersion in the bath and then raised so that emptying transport took place. For this check, the output of the frequency meter was connected to the recording potentiometer and the deflection of the recording pen observed versus time elapsed in minutes after lifting the bucket. The result is shown in figure 38.5. It will be noted that the oscillator

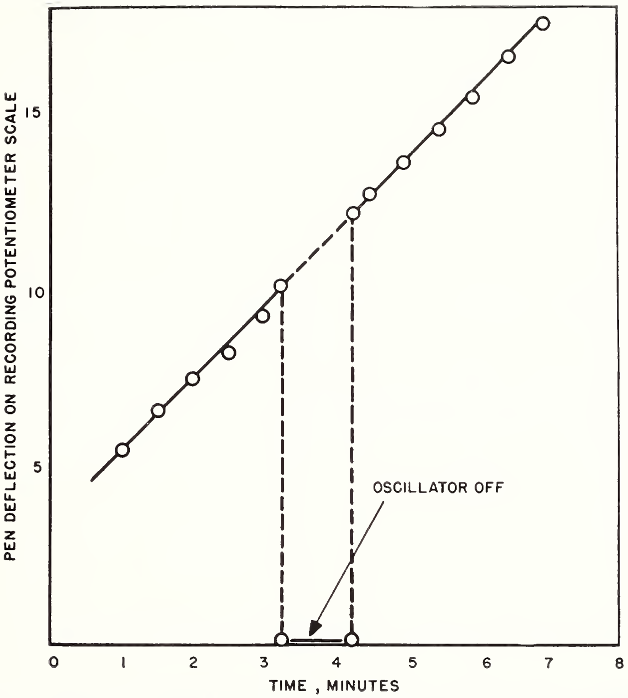

Figure 38.5. *Effect of radio-frequency field on the transport rate; (emptying transport) $T=1.3°$ K.*

was switched off for 1 minute during the course of the transport. If the radio-frequency field had produced any appreciable heating, either as a result of dielectric loss in the helium or the Teflon spacers, this effect would have been apparent as a parallel shift of the upper linear segment of the emptying trace to the right of the extension of the lower segment of the trace. (Removing heat would make the emptying time longer.) No such displacement is apparent nor was any found in the numerous checks that were taken during the course of the measurements.

Optical determinations of transport rate over the auxiliary containers of Pyrex glass were made at the beginning of each experiment to determine whether the surfaces had been contaminated with solid air. If contamination had occurred, as evidenced by a different rate than that previously determined for glass [1], measurements were abandoned for the day and the apparatus warmed to room temperature and flushed thoroughly with pure He gas. In order to detect the possible progressive contamination of surfaces during the course of a run, measurements were taken at successively lower, and then at successively higher temperatures. Transport rates taken at the beginning and at the end of the run were then compared.

Rates were obtained both for filling and emptying the various containers. No significant differences were observed for these two conditions. This result indicated the effectiveness of the radiation shield and the absence of any significant heat leak to the bucket assembly.

Results

The dependence of transport rate on the position of the liquid level below the container rim was found to correspond qualitatively with the results of other investigators [1, 5, 16]. A typical emptying curve, given in figure 38.6, shows the initially varying rate while the liquid level is near the lip of the container, and the constant rate thereafter. (As noted in the figure, frequency changes were determined in this instance by noting the beat frequency in multiples of 60 cycles as presented on the oscilloscope.) All transport rates given in the various final results correspond to the constant rates determined from the straight portions of the curves.

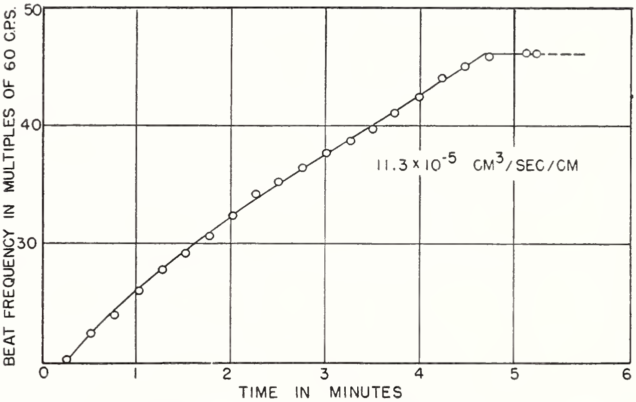

Figure 38.6. *Typical liquid level versus time-empting curve for determination of transport rate.*

Copper

Initial measurements with a carefully machined copper vessel yielded a maximum film transport rate approximately twice that previously published for glass. To verify this result, a number of measurements was made with containers of varying dimensions, the annular liquid spaces ranging from 0.005 to 0.090 in. Within the experimental error, the results were identical, a typical determination being shown in figure 38.7. As a check on these measurements, the

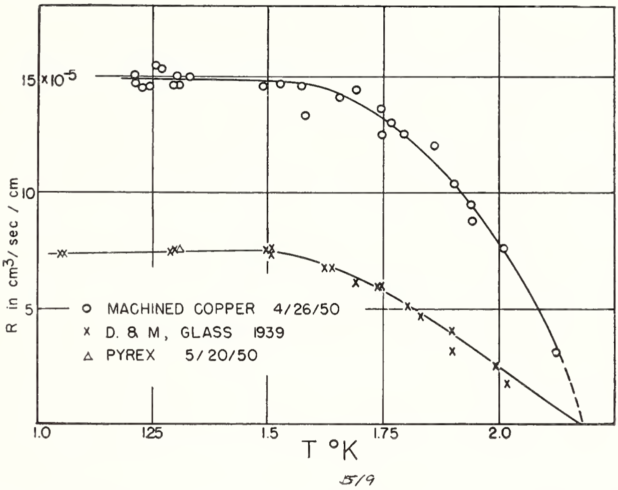

FIGURE 38.7. *Film-transport rate for machined copper and check point for Pyrex glass.*

transport at 1.3° from a Pyrex glass container was studied by the depth-gage technique. The result was identical with that of Daunt and Mendelssohn [1].

A machined-copper container that had yielded transport rates as shown in figure 38.7 was etched for 2 minutes in 0.1 *N* nitric acid and then reinstalled in the cryostat. This container gave the high rates shown in figure 38.8. Owing to an insufficient amount of liquid helium in the bath during this experiment, only three rate determinations could be made at temperatures below 1.89° K. The shape of the curve therefore cannot be determined with the same cer-

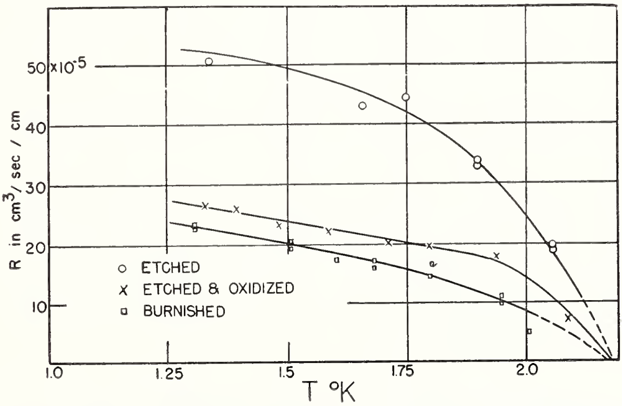

FIGURE 38.8. *Film-transport rate for various copper surfaces.*

tainty as the other two in this figure. Nevertheless, it appears that all three are similar in showing an increasing rate at the lowest temperatures reached.

Microscopic examination of this etched surface indicated considerable surface roughness, and this may contribute to the high transport rate. Attempts were made to determine the increase in perimeter by photographing the container edges under high magnification, but the results were not considered reliable for comparison purposes.

The etched container was then allowed to oxidize in air for 2 days at room temperature. The result of this treatment, also given in figure 38.8, shows a large decrease in rate, together with some change in temperature dependence.

In order to observe additional effects of surface preparation, measurements were made on a burnished-copper container. The effect of burnishing, i. e., the production of an amorphous surface layer by high local temperature and pressure during polishing, is seen from figure 38.8 to reduce the rate still further but to produce a temperature dependence similar to the etched-and-oxidized material.

Stainless Steel

The results of a single run on machined 18–8 stainless steel are presented in figure 38.9 The curve appears similar to that for burnished copper, there being a continued increase in rate with decline in temperature.

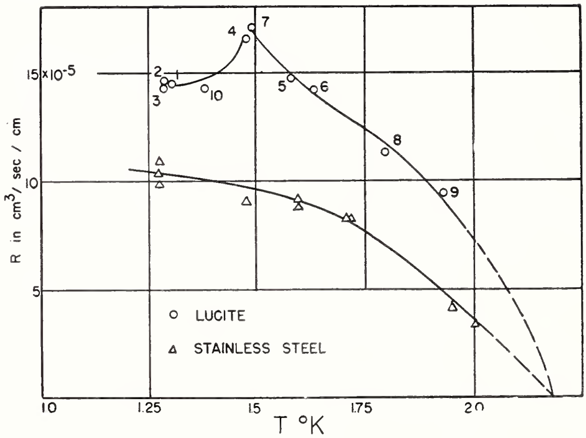

Figure 38.9. *Film-transport rate for stainless steel and Lucite.*

Lucite

It was considered desirable to determine the transport rate over the surface of a dielectric other than glass and owing to its machinability, Lucite was chosen. The container surfaces were polished with rouge after machining. This vessel showed the unusual temperature dependence exhibited in figure 38.9. Numbers alongside the experimental points refer to the chronological order in which the data were taken; it thus appears that the peak at 1.5° was reproduced. The singular nature of the curve is noteworthy. The results, however, are submitted as tentative, pending further investigation.

Lead and Iron

An exploratory investigation was made of the possible effects of ferromagnetic and superconducting substratum on the transport rate, using, respectively, cold-rolled steel and lead vessels. The data for these two materials are given in figure 38.10.

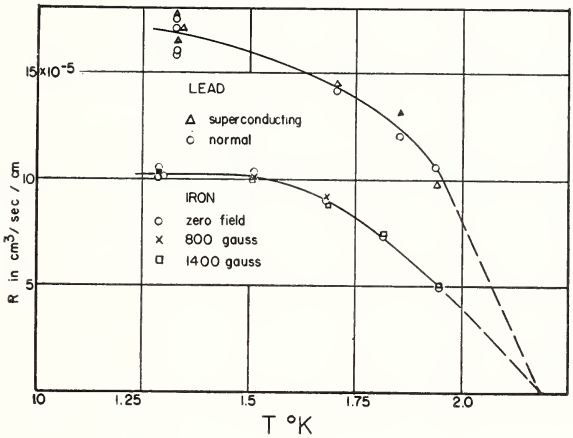

FIGURE 38.10. *Film-transport rate over lead in the normal and superconducting states, and over iron with and without an externally applied magnetic field.*

If a transfer of heat plays a part in determining the transport rate, it might be expected that an abrupt change in the thermal conductivity of the container material would disclose this effect. It is rather striking to realize that such an abrupt change can be brought about by applying a magnetic field of sufficient strength to a superconductor, the thermal conductivity in the superconducting state being usually much smaller than in the normal state at the same temperature. Lead, for instance, at 2° K shows conductivities [17] differing by about 900 percent.

A lead container was therefore constructed and measurements of the transport rate were made with the metal in the superconducting and in the normal state; as figure 38.10 shows, no appreciable difference in the rate was observed. It should be remarked, however, that the experiment was carried out after a dark oxide layer had formed on the surface of the material. Although it seems unlikely that this circumstance should have completely masked an effect if it were present, further investigation is planned.

Measurements of the transport rate over a magnetized and unmagnetized ferromagnetic surface were made, using cold-rolled steel. Although the fields applied in this case (up to 1,400 oersteds) were not sufficient to produce saturation, here again the absence of any perceptible effect makes it seem unlikely that any effect exists (fig. 38.10).

Discussion of Results

All experiments on the transport of the helium film have lead to the conclusion that other conditions being the same, the transfer of liquid from a container to a bath is limited by the narrowest part of the containing surface located above the upper liquid level. Under the conditions prevailing in these experiments, this narrowest part is the inner perimeter of the transfer vessel *B* of figure 38.1. As the film is of the order of 10^{-6} cm thick, it might be expected that the geometric perimeter would have little meaning as far as the transport is concerned, and that instead, the film would "see" the microscopic perimeter and its flow would be adjusted accordingly.

If this were true, it would appear reasonable to expect that a given glass vessel would not maintain its rate with age or with extreme temperature cycling over a period of months; microscopic surface cracks could increase in depth or in number or both, or alternatively it might be argued that a microscopic deposit from whatever source would in time tend to reduce the surface roughness. In any event such changes would be apparent as an altered transport rate. Apparently no effect of this kind has been observed. This suggests that the microscopic perimeter is not the effective perimeter for transport, a view that is supported by the agreement of the transport rates obtained from the various machined-copper containers, all of which gave rates as shown in figure 38.7

An extension of this argument against the effectiveness of the microscopic perimeter may be made by noting that if the transport were a function of the temperature and the microscopic perimeter and nothing else, then all substances should show rates, which, while differing from each other, should exhibit the common characteristic of rising like glass to a maximum value at approximately 1.5° K and remaining sensibly constant thereafter. A glance at figure 38.11, in which the rates for the various substances are plotted on the same scale, shows that this is not the fact. Although glass, machined copper, and iron show similar curves, the others (omitting lucite) display the distinctly different characteristic of a rising rate down to the lowest temperatures reached. It thus appears to be a legitimate conclusion that the substratum plays a significant role in the transport phenomenon.

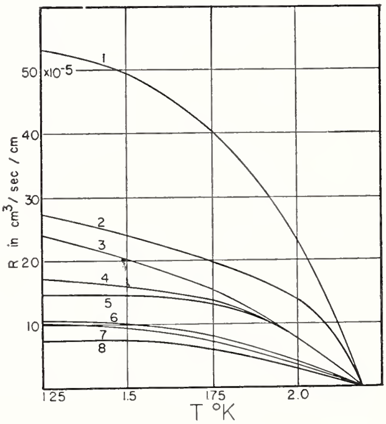

FIGURE 38.11. *Comparison of the transport rate over various surfaces.*

(1) etched copper; (2) etched and oxidized copper;
(3) burnished copper; (4) lead; (5) machined copper;
(6) iron; (7) 18-8 stainless steel; (8) glass.

It is rather interesting to observe that support for this view can also be drawn from the experiments of Bowers and Mendelssohn [14] on the effect of thin layers of solid gases deposited on the walls of a glass transport vessel. They found that as additional amounts of solid air, neon, or hydrogen were added to the glass surface, the rate increased to a saturation value and further addition produced no effect. This may be explained by assuming that as the first layers or partial layers are laid down, both the glass and the solid gas are effective as a substratum in determining the rate, but as more gas is added, the solid formed finally covers the glass surface to such a thickness that the transport is characteristic of a solid air, neon, or hydrogen surface. These layers do not need to be very thick to significantly alter the transport as their effect on the transport can be readily detected, even though the solid gas is not visible. The He II film is thus presumably thicker than the first solid-gas film, and on this basis could not affect the perimeter for transport. It would appear, therefore, that it is the substratum and not an altered perimeter that is the effective agent in changing the transport rate.

The authors express their thanks for the support given to this research by the Linde Air Products Co. and by the Research Corporation. They are indebted to Albert Brown, Sheldon Datz, Leonard Lesensky, and Bernard Smith for assistance during the course of the measurements and to Joseph Leon of T. I. Taylor's laboratory in the Department of Chemistry, Columbia University, for assistance with the microscopic examination of the copper surfaces. Finally, it is a pleasure to acknowledge the active interest and fruitful suggestions of Donald B. Cook and Mark W. Zemansky.

References

[1] J. G. Daunt and K. Mendelssohn, Proc. Roy. Soc [A] **170,** 423 (1939).
[2] H. A. Boorse and J. G. Dash, Phys. Rev. **79,** 734 (1950).
[3] H. A. Boorse and J. G. Dash, Phys. Rev. **79,** 1008 (1950).
[4] K. Mendelssohn and G. K. White, Nature **166,** 27 (1950).
[5] K. Mendelssohn and G. K. White, Proc. Phys. Soc. [A] **63,** 1328 (1950).
[6] J. Frenkel, J. Phys. USSR **II,** No. 5, 365 (1940).
[7] L. I. Schiff, Phys. Rev. **59,** 839 (1941).
[8] H. N. V. Temperley, Proc. Roy. Soc. [A] **198,** 438 (1948).
[9] A. Bijl, J. de Boer, and A. Michels, Physica **8,** 655 (1941).
[10] C. J. Grebenkemper and J. P. Hagen, Phys. Rev. **80,** 89 (1950).
[11] M. Wolfke and W. H. Keesom, Physica **3,** 823 (1936).
[12] J. K. Clapp, Proc. Inst. Radio Engrs. **36,** 356 (1948).
[13] R. Bowers and K. Mendelssohn, Nature **163,** 870 (1949).
[14] R. Bowers and K. Mendelssohn, Proc. Phys. Soc. [A] **63,** 1318 (1950).
[15] J. J. Beaver and D. J. Beaver, J. Ind. Eng. Chem. **15,** 359 (1923).
[16] R. T. Webber, H. A. Fairbank, and C. T. Lane, Phys. Rev. **76,** 609 (1949).
[17] W. J. de Haas and A. Rademakers, Physica **7,** 992 (1940).

39. Adiabatic Oscillations in Liquid Helium

by John E. Robinson[1]

Abstract

Adiabatic oscillations of liquid helium II in communicating vessels were discussed, with a view to a new way of measuring the entropy of helium II by mechanical means.

---

[1] Duke University, Durham, N. C.

40. Helium II Films

by D. G. Henshaw [1] and L. C. Jackson [2]

In a previous paper [2]* an optical method has been described for measuring the thickness of the helium film. The method is based on the fact that plane polarized light is reflected from a metallic mirror as elliptically polarized light. A thin film of transparent material covering the mirror changes the ellipticity of the light, and if the optical constants of the system are known, this change in ellipticity can be correlated with the thickness of the film. Using this method, measurements were made of the thickness of the helium film formed on a stainless-steel mirror (to increase the accuracy of setting the mirror was coated with monolayers of barium stearate [6]) at heights above the liquid surface of 2 to 12 mm and for temperatures from 1.1° K to the λ-point. The measurements have now been extended to greater heights above the liquid-helium surface.

In order to do this, a stainless-steel mirror 7 cm long, 1 cm wide, 0.2 cm thick, and optically polished on one face was prepared. A layer of barium stearate one molecule thick was deposited on the upper 5 mm of the mirror and a layer three molecules thick on the rest of the mirror, giving a sharp horizontal "1–3 boundary" near the top of the mirror. The latter was supported from its base by a nickel wire and was mounted inside a radiation shield of copper. Two slits were cut in the upper part of this shield for the incident and reflected beams. The nickel rod supporting the mirror and shield was spot-welded to a tungsten rod, which was in turn sealed into a long glass rod supported from the upper part of the helium cryostat. Two cotton wicks, bound on to the radiation sheild, formed a path for the transfer of liquid from the main bath to the top of the shield and the support where it evaporated. This served the dual purpose of ensuring temperature uniformity of the enclosure surrounding the mirror and of causing the liquid-helium level to fall at such a rate that it traversed the whole mirror in some 2 hours, a convenient rate for the observations. The measurements were made in a small Linde-type liquefier of the pattern used in this laboratory [3].

To verify that the results obtained with the "long mirror" agreed with those previously obtained with the "short mirror", thickness versus height curves were plotted for $T=1.49°$ K over the range 0.25 to 1.2 cm (fig. 40.1). In this figure, film thickness has been assumed to be proportional to the change in nicol reading (a procedure that is correct for the readings with the long mirror but not quite correct for the short one), and as different optical systems were used for the two curves, the thicknesses have been arbitrarily equated at the 1-cm height level. The agreement of the two sets of readings is reasonable, the maximum deviation being of the order of 10 percent. It was thought that this agreement was sufficient to warrant the extension of the thickness measurements to a height of 7 cm above the liquid-

---

[1] H. H. Wills Physical Laboratory, University of Bristol, Bristol, England. On leave from the National Research Council of Canada.

[2] H. H. Wills Physical Laboratory, University of Bristol, Bristol, England.

*Figures in brackets indicate the literature references on p. 190.

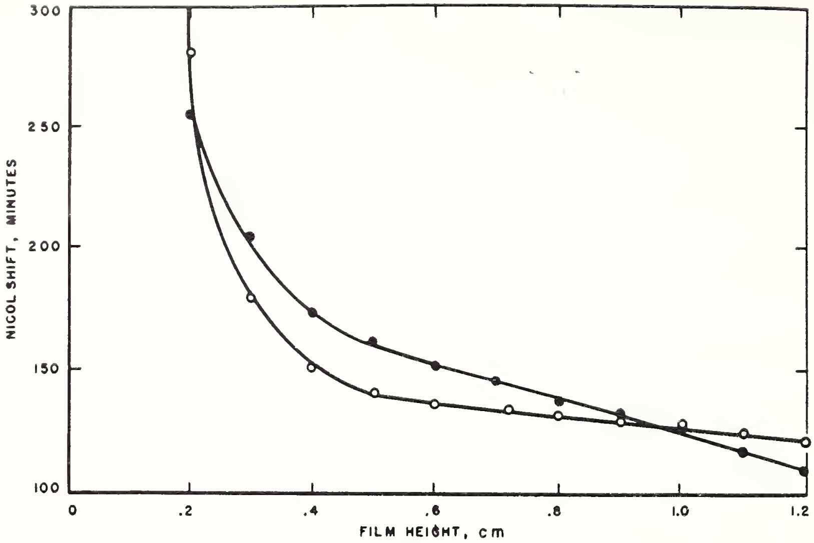

FIGURE 40.1. *Film thickness versus height at T 1.45° K for "short mirror" and for "long mirror."*

●, Short Mirror; ○, long mirror.

helium level. A series of measurements were then made at 1.26°, 1.49°, 1.70°, 1.80°, and 1.92° K. Table 40.1 gives film thicknesses as a function of height at a given temperature. The values in the table are the average of at least two distinct determinations.

The thickness at a height of 1 cm at a temperature of 1.49° K measured with the long mirror and the beaker mirror (to be described later), together with Atkins' observations of film thickness on glass, are shown in figure 40.2.

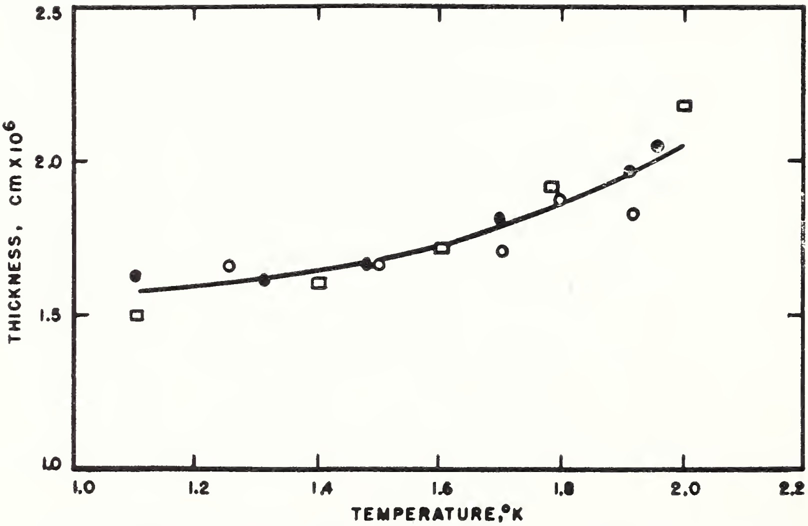

FIGURE 40.2. *Film thickness versus temperature at height of 1 cm.*

○, long mirror; ●, beaker mirror; □, Atkins.

When log-log plots are made of the thickness at any temperature as a function of the height of the film, approximately straight lines are obtained, so that to a first approximation the thickness can be represented by an expression of the type $t=K_0/h^{1/n}$, where n has the values to be found in table 40.2.

Table 40.1. *Film thickness as a function of height, h, and temperature, T*

h	Thickness at —				
	1.26° K	1.49° K	1.70° K	1.80° K	1.92° K
	cm	*cm*	*cm*	*cm*	*cm*
1	1.66×10^{-6}	1.66×10^{-6}	1.70×10^{-6}	1.82×10^{-6}	1.88×10^{-6}
2	1.38	1.47	1.46	1.50	1.57
3	1.19	1.23	1.26	1.28	1.36
4	1.00	1.01	1.03	1.08	1.17
5	0.88	0.91	0.90	0.97	1.02
6	.82	.84	.87	.88	0.90
7	.75	.75	.83	.84	.82

Table 40.2.

Temperature	*K*	*n*
°*K*		
1.26	1.70×10^{-6}	2.59
1.49	1.76	2.52
1.70	1.78	2.59
1.80	1.90	2.47
1.92	2.00	2.38

When finally analyzed the measurements on the thickness of the stationary helium II film will give some information about the forces of attraction between the helium atoms and those of the substrate. The phenomena of "creep" of helium II—the transfer of liquid with or without a difference of gravitational potential by means of the film—are of considerable importance because the laws governing the rate of transfer are not those of ordinary hydrodynamics. Measurements have now been made on the thickness of the moving film with a view to obtaining information on the mechanism by which the liquid is transferred. By combining the thickness measurements with others of the volume rate of transfer, the average velocity of the liquid helium in the creeping film has been deduced.

The optical method used in the determination of the thickness of the stationary helium film can also be applied to the moving film. A cylindrical stainless-steel beaker with an external diameter of 6 mm and an internal diameter of 4 mm has a strip 2 mm wide ground on the outside parallel to the axis and polished to form a plane mirror. Barium stearate layers deposited as before on the outside of the beaker give a "1–3 boundary" about 4 mm below the rim of the beaker and so permit the measurement of the thickness of the moving film on the outside of the beaker at the position of the boundary. A glass capillary tube, B, (fig. 40.3) is attached to the bottom of the beaker by means of a Kovar-glass seal and a copper-nickel tube, the latter supporting the beaker inside the radiation shield, C. The variation of the level of the liquid helium in the beaker can then be followed by observing the meniscus in the glass capillary by means of a traveling microscope. The disk, D, serves to maintain the beaker central in the unsilvered tail of the liquid-helium Dewar, and the complete assembly is supported by a glass rod that can be moved up or down and rotated about a vertical axis. The glass beaker, E, containing liquid helium serves to provide additional thermal protection for the stainless-steel beaker during the observations. Figure 40.4 is a general view of the experimental arrangement.

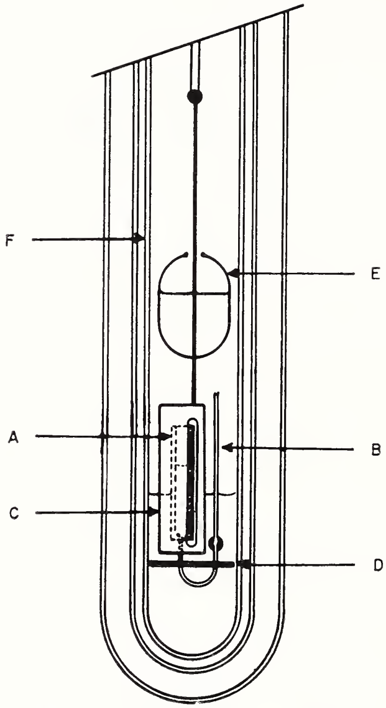

Figure 40.3. *Mirror beaker with radiation shield and support.*

The procedure in any set of observations was as follows. With the steel beaker completely immersed in the liquid helium the temperature was set to some desired value below the λ-point and the beaker then raised until the 1–3 boundary was at some known height above the outer liquid-helium level. Simultaneous observations were then made of the film thickness and of the liquid-helium level inside the beaker as a function of time. The position of the outer level did not change appreciably during the time required for the beaker to empty by creep. The temperature was then raised to a few tenths of a degree above the λ-point and the zero setting of the nicol determined. The whole procedure was then repeated for other values of the height of the measuring point above the liquid-helium level and for different temperatures covering the range 1.1° to 2.0° K. A further series of observations was made by partially immersing the empty steel beaker in liquid helium II and by observing the film thickness and creep rate as the beaker filled.

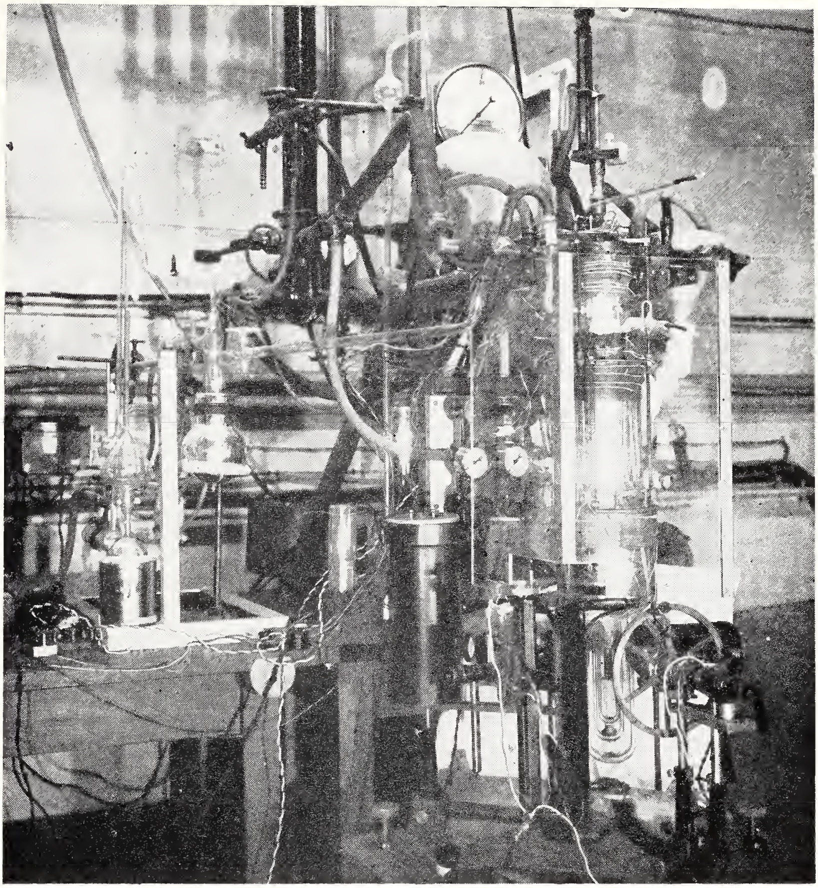

Figure 40.4. *General view of apparatus.*

A typical curve for emptying the beaker is shown in figure 40.5, where the level of the liquid inside the beaker is plotted as a function of the time ($T=1.89°$ K). It exhibits the usual features of such a curve, a high and variable rate of transfer of helium for the first 3 mm from the rim of the beaker, followed by an almost constant rate until the inner and outer levels are almost coincident. In the case of filling, the observed rate of transfer is constant except for the last millimeter or so of difference between the levels. The observed film thickness is independent of the position of the inner level over the range in which the transfer rate is constant. Within the accuracy of the observations, the thickness of the moving film at a given height and temperature is the same as that of the stationary film as determined on the "long mirror".

Table 40.3 shows some typical results for a height of 1 cm above the outer liquid level, showing the measured volume rate of transfer and the measured film thickness. The value of the thickness at 2.0° K is an extrapolation of the curve beyond the last measured point at 1.94° K. The fourth column gives the average velocity of flow of the helium, assuming that the whole of the liquid is moving with

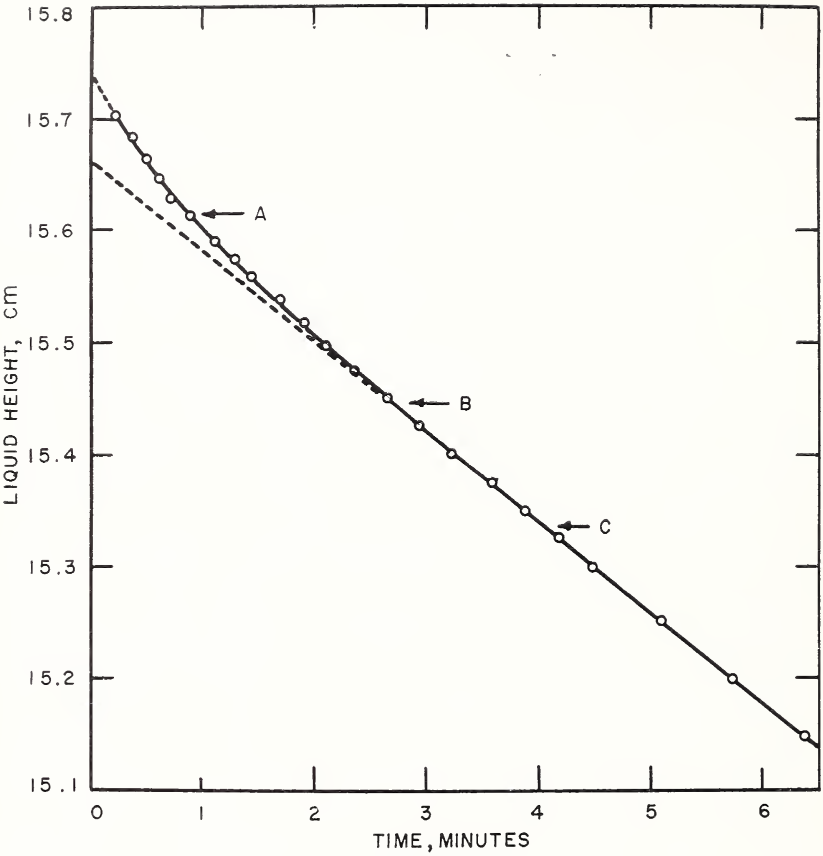

Figure 40.5. *Creep curve for mirror beaker at T 1.89° K.*

the same velocity throughout any cross section of the film. If, on the other hand, one makes the usual assumption that only the superfluid component of the helium II moves in the film transfer and that the film has the same normal fluid-superfluid composition as the bulk liquid, one obtains the velocities, $\bar{v}_s$, given in the fifth column.

Table 40.3.

T	V	t	$\bar{v}$	$\bar{v}_s$
°*K*	*(cm/sec)/cm*	*cm*	*cm/sec*	*cm/sec*
1.1	16.9×10^{-5}	1.63×10^{-6}	69	70
1.3	16.9	1.63	69	73
1.5	16.8	1.66	68	77
1.7	16.1	1.82	59	79
1.9	12.8	1.94	44	79
2.0	8.5	(2.06)	($27._5$)	(65)

As the point of observation (the 1–3 boundary) was 3.8 mm below the rim of the beaker, the velocities given in table 40.3 have to be increased by approximately 11 percent to give the actual values of $\bar{v}$ or $\bar{v}_s$ at the rim on the outside of the beaker. If it is assumed that the thickness of the film on the inside of the beaker varies with height above the liquid level in the same way as that of the film on the outside, then when the inside level is nearly the same as that of the liquid outside, the maximum velocity of the liquid on the film will be that at the rim on the inside of the beaker. Thus for the conditions of table 40.3 (1–3 boundary 1 cm above outside liquid level) this maximum velocity will be obtained by multiplying the figures of column 5 of the table by $1.1 \times r_2/r_1 = 1.65$ (r_1, the inner radius of beaker=2 mm; r_2, the outer radius=3 mm). Thus the maximum velocity of the superfluid at 1.1° K becomes 116 cm/sec and at 1.9° K, 130 cm/sec.

Insofar as the volume rate of creep is independent of the difference in height of the inner and outer surfaces of the liquid helium at any temperature, the relation $\bar{v}_s t = \text{constant}$, is satisfied for the data given above. The average velocities, $\bar{v}_s$ are, however, considerably greater than those given by the relation

$$\bar{v}_s = h/4 r_1 m t,$$

where h is Planck's constant, and m is the mass of the helium atom, which has been suggested as applicable to the helium film [1, 4, 5]. Using the above expression, one obtains from the data given in table 40.3 $\bar{v}_s = 48.4$ cm/sec at 1.1° K and $\bar{v}_s = 40.7$ cm/sec at 1.9° K.

The values for the thickness of the film and the volume rate of creep all refer to those conditions for which a constant rate of creep was observed, i. e., from point B of figure 40.5 onward and similarly for other temperatures. In the earlier part of the curve from time zero up to the point B a very striking phenomenon is observed. When the full beaker is lifted partly out of the liquid, the part of the mirror not immersed is seen to be covered with a large number of bright specks of light moving downward and eventually disappearing into the liquid helium below. Fifty or more may be simultaneously visible immediately after the beaker has been raised. corresponding, on the assumption of a uniform distribution, to some 500 specks on the outside of the whole beaker. As the level of the liquid in the beaker falls, the number of specks decreases steadily, and the phenomenon ceases when the inner level is a few millimeters below the rim of the beaker.[3] Thus in figure 40.5 the observer reported that at point A the number of specks visible had decreased considerably, at point B only two or three specks could be seen, and at point C no specks were present. It will be seen that the region in which the specks are present coincides closely with that in which an anomalously high creep rate is observed.

The bright specks, which are obviously "drops" of liquid helium, are somewhat elongated in the direction of motion, are ⅒ to ⅓ mm long and move downward with a velocity of about 1 cm/sec. It is not yet possible to say anything quantitative about the dimensions of the drops in the direction perpendicular to the mirror. They are certainly much thicker than the normal creeping film observed when the drops have ceased, as it is not possible to measure their thickness with the existing mica compensating plate. The drops are too small for it to be possible to determine visually whether they show interference contours. It is thus not yet possible to state whether the drops account quantitatively for the extra rate of transfer in the ini-

---

[3] It was proved by separate experiments that the specks are not liquid helium II, which clings initially to the beaker as the latter is lifted and then drains back into the liquid below. The beaker cannot be lifted rapidly enough for this effect to be observed in helium II.

tial part of the creep curve. However, it seems reasonable to suppose that the straight part of the creep curve represents a flow of helium II characteristic of the continuous film, and that in the initial curved part the excess helium is transported in the form of discrete drops. It will be noted that these drops move much more slowly than the film itself and presumably slide over the surface of the latter.

The length of time during which the drops are visible has been studied as a function of the temperature and of the height of the rim of the beaker above the outer level of the liquid helium. With the temperature held constant at 1.5° K the length of time during which drops were visible rose from 10 sec when the rim of the beaker was 2.5 mm above the outer liquid-helium level to 100 sec when the rim was 7.5 mm above the liquid and then remained constant as the distance was increased to 30 mm. The same kind of variation was observed at other temperatures, the maximum duration of the drops rising from 88 sec at 1.1° K to 250 sec at 1.9° K.

The drop phenomenon has also been observed with a clean stainless-steel surface not covered with barium stearate, and with a glass beaker, the plane mirror of which was coated with aluminium.

---

[1] A. Bijl, J. de Boer, and A. Michels, Physica **9**, 655 (1941).
[2] E. J. Burge and L. C. Jackson, Proc. Roy. Soc. (London)[A] **205**, 270 (1951).
[3] L. C. Jackson and H. Preston-Thomas, J. Sci. Instr. **28**, 99 (1951).
[4] F. London, Report Intl. Conf. Low Temp., Cambridge, p. 1 (1946).
[5] K. Mendelssohn, Report Intl. Conf. Low Temp., Cambridge, p. 35 (1946).
[6] A. Rothen, Rev. Sci. Instr. **16**, 26 (1945).

41. Some Preliminary Thermodynamic Studies on Helium Adsorbed on Titanium Dioxide

by J. G. Aston and S. V. R. Mastrangelo[1]

The isotherm of helium on TiO_2 (rutile, 10.2 m^2/g) has been accurately measured at 2.41° K and shown to be stepwise, with discontinuities at the end of the "anomalous first layer" and of the succeeding layer.

The anomalous first layer has exactly twice the density of the solid under its equilibrium pressure at this temperature.

Heat-capacity measurements in the adsorbed phase at certain coverages have been made between 1.6° and 2.7° K, paralleling those

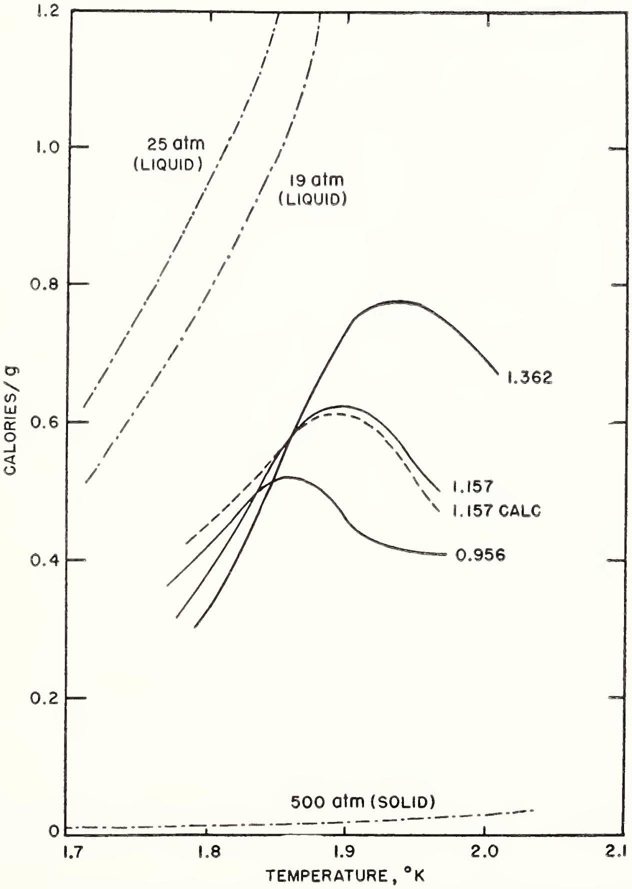

Figure 41.1. *Specific heat of adsorbed helium compared to the liquid and solid in bulk.*

---

[1] School of Chemistry and Physics, Pennsylvania State College, State College, Pa.

of Frederikse,[2] and with essentially the same results. They can be shown to agree quantitatively with those calculated by assuming that each layer makes a contribution to the heat capacity equal to that of bulk helium under pressure. The effective pressure on each layer is determined from the shift in the lambda point of successive layers, which varies from above 30 atm for the first solid layer to the saturation pressure for the extreme outer liquid layers.

In figure 41.1 are shown graphs of the measured heat capacities corrected to constant coverage at coverages of 0.956, 1.157, and 1.362 cm^3 STP of helium per gram, respectively The dotted curve is the calculated one for 1.157 cm^3 STP of helium per gram, based on the curves for bulk helium shown in part by the dot-dashed curves. Although the precision is of the order of a few percent, the experimental curve may be in error by as much as 40 percent at the high temperatures where the correction for evaporation into the dead space is large.

An isotherm has been derived analogous to that of Brunauer, Emmett, and Teller, based on the assumption that the absolute values of the energies of the molecules in the layers are related as follows: $E_1=E_2=E_n>E_{n-1}=E_{n-2}=E_L$. This predicts that the so-called "anomalous first layer" actually consists of $n(n=1,2,3,4$ or more) solid layers, the value of n, depending on the temperature. The value of n can be predicted from the pressure on the layers and the temperature by finding the equilibrium pressure of solid helium with liquid helium and hence the number of layers with pressures equal to or higher than this value. The predictions are in agreement with experimental values of n obtained from B.E.T. type plots along with solid densities for all observed cases.

---

[2] H. P. R. Frederikse, Physica **15**, 860 (1949).

42. Thermal Conductivity of Liquid Helium I

by Claude Grenier [1]

The thermal conductivity of liquid helium between 2.2° K and its normal boiling point at 4.2° K was first reported by W. H. Keesom and A. P. Keesom.[2] These authors only reported one quantitative result, viz: 6×10^{-5} cal/deg cm sec at the temperature 3.3° K. The experiments by Pellam and Squire [3] on the ultrasonic absorption in liquid helium make it possible to calculate the dependence on temperature of the heat conductivity if the classical theory of sound attenuation is assumed valid over the entire temperature range of liquid helium I. Such a calculation predicts an enormous increase of the thermal conductivity starting at 3° K as the temperature is lowered to the transition point of liquid helium II. Thus, it was of interest to make a direct investigation of the thermal conductivity. The results clearly indicate that the heat conductivity remains nearly constant with temperature, even quite close to the transition point. A complete account of the measurements and results has been submitted by the author to Physical Review for publication.

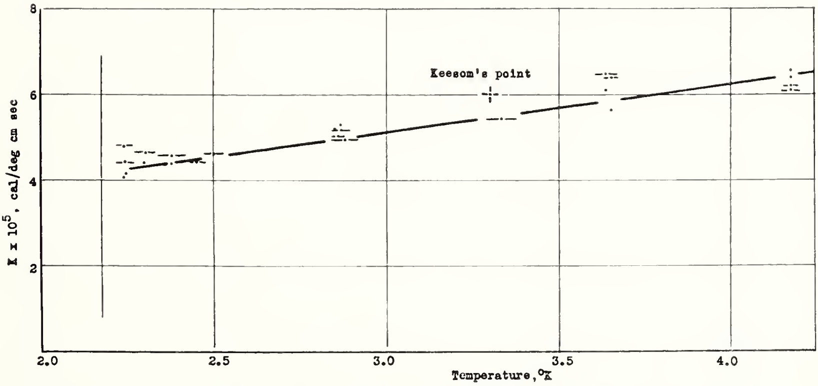

FIGURE 42.1. *Thermal conductivity of He I as a function of temperature.*

Figure 42.1 shows our experimental results of the heat conductivity as a function of temperature. At 3.3° K we have very good agreement with the value given by Keesom and Keesom (see footnote 2). Recently some preliminary results on the heat conductivity of liquid helium were reported by Bowers and Mendelssohn,[4] and our results are in agreement with their work. Considering the liquid as though it were a gas, and using the measured specific heat at constant volume

---

[1] The Rice Institute, Houston, Tex.
[2] W. H. Keesom and A. P. Keesom, Physica **3**, 359 (1936).
[3] J. R. Pellam and C. F. Squire, Phys. Rev. **72**, 1245 (1947).
[4] R. Bowers and K. Mendelssohn, Nature **167**, 111 (1951).

and the measured viscosity, we find that the gas theory for heat conductivity, $K=2.5\eta c_v$, is rather close to our results. Table 42.1 gives the comparison.

TABLE 42.1. *Heat conductivity of liquid helium* I

Temperature .... °K....	2.24	2.50	3.08	4.2
K, experimental ... cal/deg cm sec....	4.4	4.6	5.1	6.3×10^{-5}
K, gas theory	3.7	3.2	3.3	4.5×10^{-5}

Viscosity measured by Bowers and Mendelssohn, Proc. Phys. Soc. [A] **62** 894 (1949).
Specific heat taken from W. H. Keesom, Helium, p. 218 (Elsevier Press, 1942).

43. Evaporation Rate of Liquid Helium I

by Aaron Wexler [1]

In connection with a study of the emissivity of metals at low temperatures, a quantitative analysis has been made of the factors involved in the design of storage containers for liquid helium. Experiments confirm the analysis, which has resulted in an exceedingly simple liquid nitrogen protected liquid-helium, container having a helium evaportation rate of 1 percent per day.

The hemispherical emissivity of commercially polished copper at 4.23° K was determined for black-body radiation. For radiation corresponding to that emitted by a black body at 77.1° and 297.1° K, the measured emissivities are 6.9×10^{-3} and 1.29×10^{-2}, respectively. These data are discussed in relation to the recent theoretical work of Reuter and Sondheimer.

The heat of vaporization of helium at 4.228° K was determined to be 4.93 cal g^{-1}, in substantial agreement with the data of Dana and Kamerlingh Onnes. Kistemaker's thermodynamic considerations questioning the accuracy of these data are evaluated in terms of the new determination.

1. Introduction

The present study of the factors governing the rate of evaporation of liquid helium is the first phase of an investigation of the emissivity of metals at low temperatures. There are both fundamental and practical aspects of this problem. In the wavelength region of practical interest, the recent theory [1] [2] of the anomalous skin effect in metals of Reuter and Sondheimer predicts for the low-temperature emissivity of pure metals a wavelength dependence that is radically different from that implied by the classical theory. The Reuter and Sondheimer theory awaits experimental confirmation in this spectral range.

As will be demonstrated, the experimental check of the quantitative analysis of the factors involved in the flow of heat into liquid-helium containers can yield data on the low-temperature emissivity of metals in the interesting range mentioned above. In addition, the heat of vaporization of liquid helium may be determined concomitantly; this seemed particularly worth while in view of the doubts raised by Kistemaker [2] on thermodynamic grounds concerning the accuracy of the experimental determinations of Dana and Kamerlingh Onnes [3] above 4° K.

A survey of the literature indicates but a single reference [4] to a storage container for liquid helium. It is a Pyrex glass vessel of 8-liters capacity, surrounded by liquid air; it was estimated to be able to hold helium for at least 4 days. Conservative estimates by us indicated that it should be possible to design an all-metal container of at least 15 times greater efficiency; this major discrepancy, together with the facts already cited, militated for the initial approach to the problem, namely, the emphasis on container design. As is now well known [5], in the case of liquid hydrogen a detailed study of its evaporation rate could have led to the discovery of the ortho-para equilibrium many years before it was predicted and actually found experimentally. This fact made the study of the reasons for the large

---

[1] Westinghouse Research Laboratories, East Pittsburgh, Pa.

[2] Figures in brackets indicate the literature references on p. 209

difference between the theoretically possible efficiency and the reported efficiency of helium containers all the more interesting.

The practical interests in efficient storage containers need no elaboration. The availability of such containers for liquid helium and for parahydrogen would be of value both to the research work in a field of increasing activity and to possible applications of low-temperature phenomena. In addition, such containers might make make economical the shipping of these elements in the liquid phase and could eliminate the need for a liquefaction plant on the part of users of the refrigerants.

2. Analysis of the Problem

Our studies were based on a container of very simple design, as shown in figure 43.1. The liquid-helium container itself consists of two concentric spherical shells, A and B, with a high vacuum between the shells, and C is an Inconel neck tube of low thermal conductance. The entire container is immersed in another conventional metal Dewar vessel containing liquid nitrogen.

The physics of a vacuum vessel for the storage of liquefied gases, with special reference to the storage of liquid oxgyen, has been discussed thoroughly in the *Report of the Oxygen Research Committee of Great Britain* [6]. The Report lists seven causes of heat flow to the inner vessel of a vacuum container: 1. Conduction through the residual gas in the vacuum space; 2. convection through the residual gas in the vacuum space; 3. radiation across the vacuum space; 4. conduction along the neck of the flask; 5. radiation through the neck aperture; 6. conduction through supporting materials, if any, crossing the vacuum space; and 7. convection in the interior space of the flask and neck.

For liquid-oxygen containers, whose ambient conditions are those of the atmosphere, practically the only factor of importance is radiation across the vacuum space. At the time the Report was written, conduction through the residual vacuum had to be considered; improved vacuum technique has made this factor negligible. The only other factor of any consequence is conduction along the neck of the flask, although its contribution is minor.

It is necessary to reconsider the analysis presented in the Report, for it will be seen that for a helium container the important factors are different from those governing the efficiency of an oxygen container.

The vapor pressures of all substances, with the exception of hydrogen and helium, are so low at liquid-helium temperatures that the first two factors become entirely negligible. The last two factors may also be eliminated. Radiation through the neck aperture, however, can be of real significance. If the walls of the neck tube were perfectly reflecting, the heat-leak effect would be the same as that resulting from the piping into the liquid of all of the radiation from a room-temperature black body of surface area equal to that of the neck-tube opening. For a neck tube of the size we used (about 1.5 cm in diameter), this would result in an evaporation rate of about 3 liters/day. As our work dealt with evaporation rates of the order of 100 ml/day, the contribution by this effect had to be considered, even if only a few percent of the radiation funneling down the tube reached the liquid. Our observations in this connection and the steps taken to minimize the losses due to this cause will be outlined later.

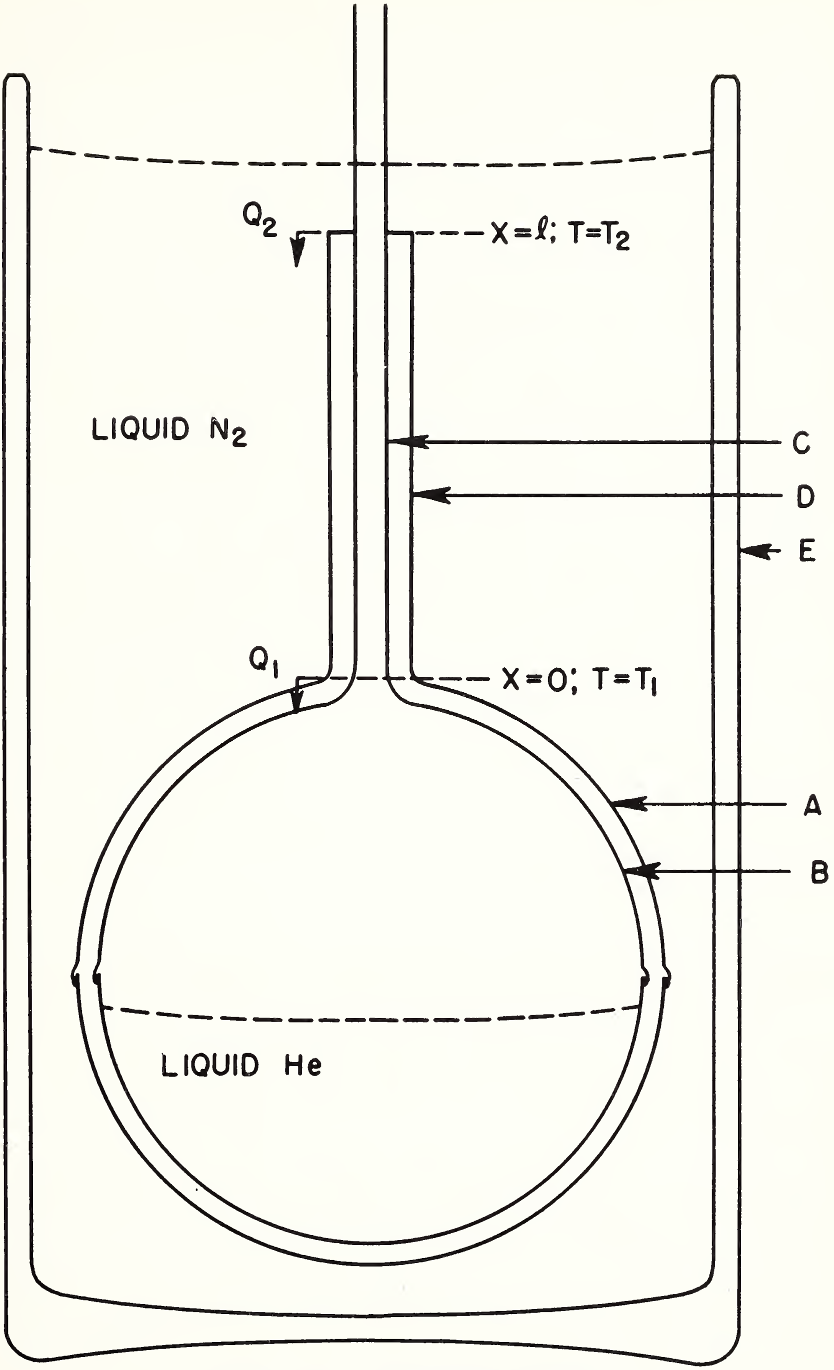

FIGURE 43.1. *Liquid-helium container.*

The other factors, radiation across the vacuum space and conduction along the neck of the flask are all important and must be considered together. The problem to be considered is the following: The copper vessel, B, may be regarded as an isothermal body at temperature T_1, the temperature at which the helium boils at the given pressure above it. At a distance, l, along the neck tube, the temperature is fixed at T_2, the temperature of the shielding bath. Heat is conducted down the tube at the rate, Q_2, at $x=l$, Q decreasing as $x \rightarrow 0$ because of heat exchange with the effluent gas (see fig. 43.1). The rate of liquid-helium evaporation is thus determined by Q_1+Q_R, i. e., the sum of the rate of heat entering by conduction along the tube and that due to radiation heat transfer between surfaces A and B. The calculation of the evaporation rate may be made in a straightforward manner on the assumption that heat exchange between the effluent gas and the neck tube is perfect. Across any section of the tube

$$Q=kA(dT/dx), \tag{1}$$

where k is the thermal conductivity of the tube, and A is the cross-sectional area of the metal wall. If the specific heat of the gas is denoted by C_p, and if n is the number of moles per second of gas flowing out of the system, the assumption of perfect heat exchange implies

$$dQ=nC_p\, dT. \tag{2}$$

In practice, the termal conductivity of the neck tube is found to be a linear function of temperature

$$k=a+bT. \tag{3}$$

The integration of (2) yields

$$n=\frac{A}{lC_p}\left[\{a+b(T_1-g)\}\ln\left(1+\frac{T_2-T_1}{g}\right)+b(T_2-T_1)\right], \tag{4}$$

where $g=Q_1/nC_p$.

As n is linearly related to Q_1+Q_R,

$$n=\beta(Q_1+Q_R), \tag{5}$$

so that

$$Q_R=n\left(\frac{1}{\beta}-C_pg\right). \tag{6}$$

C_p is assumed to be temperature independent and equal to the specific heat at constant pressure of an ideal monatomic gas. The value of β is related to the reciprocal of the heat of vaporization, L. If all of the liquid evaporated were to contribute to n, then $\beta=L^{-1}$. Actually, because the space occupied by the evaporating liquid is taken up by the vapor, not all of the evaporating liquid contributes to the gas current. In fact, it may be shown [7] that

$$\beta=(1-\rho_v/\rho_l)/L, \tag{7}$$

where ρ_v and ρ_l are the respective densities of the vapor and liquid.

Calculations based on the foregoing may be made as follows. The most interesting calculations are those for the evaporation rate as a function of the radiation heat transfer, Q_R. Equation (4) permits the calculation of n as a function of g. For given combinations of n and g thus determined, the corresponding values of Q_R are calculable from (6). The highest value of g appearing in the calculations is $g=1/\beta\, C_p$.

The application of these considerations indicated the possibility of making a highly efficient container for liquid helium. The design indicated in figure 43.1 was chosen for its simplicity and for the possibility it offered of permitting the determination of the radiation heat transfer to a polished copper surface at the helium boiling point. The approximately spherical shells were made of spun hemispheres, which were soldered together. Two containers were studied. Both had inner spheres that were made of copper whose outer surface was made highly reflecting by buffing and hand polishing with a commercial polish. The outer sphere of one of the containers, hereinafter called container A, was made of monel having a sandblasted inner surface. The other container, B, had a copper outer sphere whose inner surface was highly polished by the same method used for the outer surface of the inner spheres. At the joining diameter of the inner spheres there was a band of solder; its width was kept less than 0.5 cm. Its surface, which was highly polished, represented less than 6 percent of the surface area of the inner sphere. The inner spheres had a volume of 9,250 ml and the outer ones a volume of 12,500 ml. The corresponding surfaces facing the vacuum, therefore, were 2,140 cm^2 and 2,610 cm^2, respectively. The neck tube was a 20-cm length of hard-drawn Inconel tubing, ⅝-inch outside diameter and 0.0105-inch wall. In the range of temperatures involved, the thermal conductivity of the metal is well represented by $k=1.21T-2.28$ mw cm^{-1} deg^{-1}.[3]

It is assumed that the bath temperature is at 77.1° K and that that of the helium is 4.23° K. The other values used are 20.8 w-sec/mole deg for C_p; 0.0107 mole/joule for β; and 4.87 cal/g for the heat of vaporization of the liquid.

One extreme case is that for zero heat exchange between the effluent gas and the wall of the neck tube. Under these circumstances, the evaporation rate is

$$Q_1+Q_R=\frac{A}{l}\left[a(T_2-T_1)+\frac{b}{2}(T_2^2-T_1^2)\right]+Q_R. \tag{8}$$

If $Q_R=0$, the upper limit of the evaporation rate for our container would be 770 ml/day, corresponding to $Q_1=0.0227$ w.

The other extreme case is the one for perfect heat exchange, which is a condition very likely to be approached at low rates of flow of a gas whose thermal conductivity is high. Figure 43.2 shows the results of the application of eq (4) and (6) to our container. The predicted evaporation rate for $Q_R=0$ is 82 ml/day, corresponding to $Q_1=2.41\times10^{-3}$ w. Thus the importance of good heat exchange is emphasized by a comparison of this number with that deduced for zero heat exchange.

---

[3] This relation was deduced from data kindly supplied in advance of publication by J. E. Zimmerman, of Carnegie Institute of Technology. His measurements were made on a sample of metal from the same lot as that from which our tubing originated. Although the data are good to better than 5 percent, Mr. Zimmerman has found large differences in the thermal conductivity, depending upon the temper of the alloy. Due care must therefore be taken in the application of this relation to other samples of Inconel.

The implications of the analysis as indicated in figure 43.2 are very interesting. It will be seen that as Q_R increases from zero, the evaporation rate (Q_1+Q_R) changes rather slowly. This results, of course, from the fact that the increased flow of effluent gas is effective in substantially reducing Q_1. The calculations show that when the radiation heat transfer rises to a value that is equal to the rate of heat entering the helium container when $Q_R=0$, the evaporation rate increases by only 20 percent over that for $Q_R=0$. Hence, if for a given container Q_R happens to be of the order of or less than Q_1 when $Q_R=0$, attempts to decrease Q_R by using better reflecting materials or incorporating radiation shields would not appreciably decrease the evaporation rate.

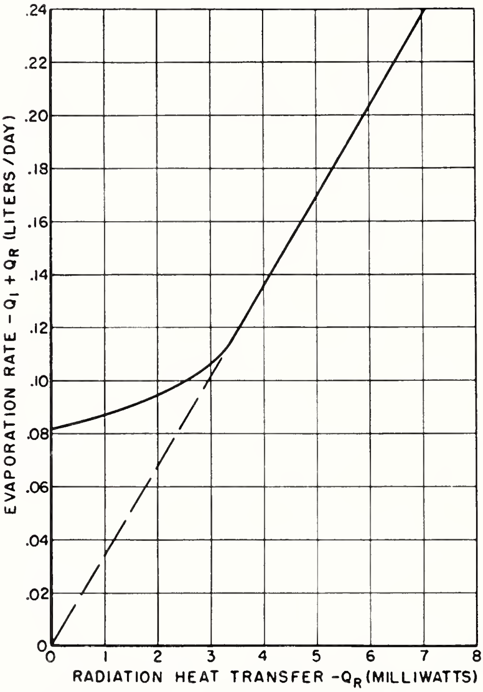

FIGURE 43.2. *Calculated evaporation rate.*

The method for the determination of the heat of vaporization and of the radiation heat transfer follows directly from eq (6). If the evaporation rate is plotted as a function of the power Q_h dissipated in a heater immersed in the liquid helium, then when $Q_1 \rightarrow 0$, the evaporation rate will be proportional to Q_h. The slope of the straight line is β, from which the heat of vaporization may be calculated by means of eq (7). Moreover, the radiation heat transfer is just the separation between the experimental straight line and that parallel to it and passing through the origin. Thus the intercept of the experimental straight line on the evaporation rate axis is indeed Q_R.

These remarks may be made more concrete by referring to figure 43.3, which was obtained from the same calculations on which figure 43.2 is based. The curve was drawn for the initial condition $Q_1=Q_R$.

This method of determining Q_R makes the assumption that the heat dissipated in the heater results in isothermal boiling away of liquid helium. If the heat not only evaporates helium but also raises its temperature, the effect of Q_h upon the evaporation rate would be less than that shown in figure 43.3, and, in fact, for large values of Q_h the curve of figure 43.3 would curve toward the Q_h axis. On the other hand, the possibility of the removal of liquid in an amount greater than that corresponding to isothermal boiling by mist and spray that is carried along with the evaporated vapor was discussed by Dana and Kamerlingh Onnes [3], from whose paper we have taken the heat-of-vaporization data for liquid helium. These workers found no evidence for either of these effects, and in the application of the method outlined above it would appear that if for large values of Q_h, the evaporation rate is accurately linearly dependent on Q_h, and if the slope is derivable from the heat of vaporization, this would constitute a confirmation of the absence of these undesired effects.

The existence of the initial interval of small slope in figure 43.2 is a consequence of the large value of β for helium. For other liquefied gases, this interval will be smaller. It is important to note, nevertheless, that the method, indicated in figure 43.3, of separating heat transfer across the vacuum space from other sources of heat influx is usable even for small values of β or if the heat exchange is not perfect. For maximum accuracy in deducing Q_R by this method, however, it is manifestly desirable to reduce to a minimum the initial value of Q_1.

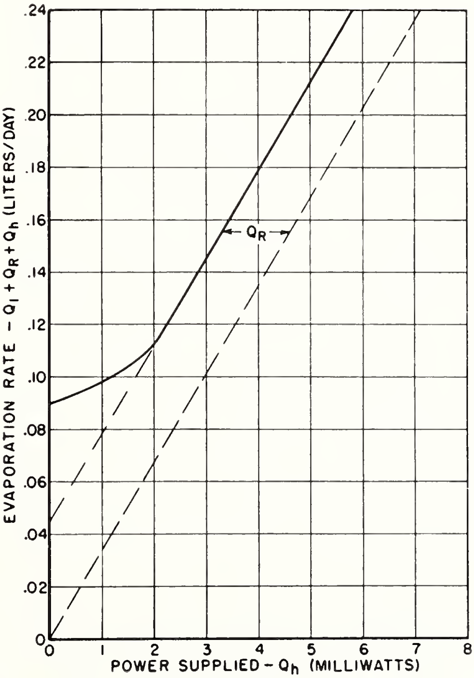

FIGURE 43.3. *Determination of radiation heat transfer.*

3. Radiation Heat Transfer

Radiation heat transfer to a metallic surface, whose resistivity lies in the residual resistivity range, involves fundamental problems with respect to the emissivity of the surface. The radiation heat transfer, H, between two concentric spheres is readily calculable [8] if the emissivities of the surfaces are known:

$$H=\frac{A_i \sigma e_i e_o}{e_o+e_i(1-e_o)\rho}(T_o^4-T_1^4). \tag{9}$$

In this relation, the subscripts i and o refer to the inner and outer surfaces, respectively. A_i is the surface area of the inner spherical shell, $\sigma=5.72\times10^{-12}$ w/cm² deg ^{4} is the Stefan-Boltzmann constant, e_i and e_o are the emissivities, T_i and T_o the absolute temperatures of the surfaces, and $\rho=A_i/A_o$ is the fraction of the radiation reflected from the outer surfaces that strikes the inner surface directly. In our work $T_o^4 \gg T_1^4$, so that $T_o^4 \simeq T_o^4-T_1^4$ to a good approximation. If the internal surface of the outer sphere is regularly reflecting, $\rho=1$. If $e_i \ll e_o$, then

$$H=A_i \sigma e_i T_o^4, \tag{10}$$

which means, of course, that the radiation flux in the interspace between the two surfaces is essentially black-body radiation corresponding to the temperature T_o. If H is measured under these conditions, then a knowledge of e_o is not necessary for an evaluation of e_i.

The classical work of Drude and of Hagen and Rubens [9] established the relation

$$(1-R)=e=36.5(\rho/\lambda)^{1/2}, \tag{11}$$

where R is the reflectivity at normal incidence on the surface of a metal, e its emissivity, ρ its resistivity in ohm-centimeters, and λ the wavelength in microns of the radiation used. Considered as a function of wavelength, the emissivity of a metal at constant temperature will thus vary as $\lambda^{-1/2}$. When the wavelength decreases, however, and the period of the radiation becomes comparable with or less than the time of relaxation of the conduction electrons, the emissivity is independent of the wavelength. At low temperatures new phenomena are possible, for the mean free path of the electrons may become comparable to or greater than the skin depth for penetration of the electric field. Under these circumstances, the assumption implicit in the classical theory that the electric field may be considered as spatially constant, as far as the motion of electrons is concerned, is not valid except at sufficiently long wavelengths for which the skin depth is large compared with the free path and at sufficiently short wavelengths at which the penetration depth is large compared with the distance traveled by an electron during one cycle of the electric field. At intermediate wavelengths, the recent theory of the anomalous skin effect of Reuter and Sondheimer [1] is applicable. The predictions of this theory may be indicated by referring to the authors' calculations of $(1-R)$ at normal incidence as a function of λ for pure silver at liquid-helium temperatures. At the long wavelength end of the spectrum, $(1-R)$ varies classically as $\lambda^{-1/2}$. In the microwave region between 4 and 0.1 cm, the variation is as $\lambda^{-2/3}$. The curve rises to a maximum of 1.5×10^{-3} at 69 μ, and beyond this point $(1-R)$ drops to the classical value in the visible range, beyond which it goes to zero. The classical theory for wavelengths in the region of maximum yields a wavelength independent value of $(1-R) < 10^{-5}$. A wavelength range of special interest is that between about 40 and 3μ. For the case of perfectly specular surface reflection of electrons, the Reuter and Sondheimer computation gives $(1-R)$ in this range as varying as λ^n, where $n > 1$.[4] This is the spectral range that is encountered in the design of liquid-helium containing apparatus. In the microwave region, the theory of Reuter and Sondheimer finds experimental support [10, 11, 12]. The only datum that we have been able to find in the micron range is that given by Scott, et al. [13] for chemically deposited silver at 20° K encompassed by a similar surface at room temperature. The value given for the hemispherical emissivity is 0.03, being a factor of 20 greater than the maximum emissivity expected theoretically. It is possible that this number is appreciably higher than the actual value of e for such a surface; for at the time that this work was done, the effect of the ortho-para conversion of the liquid hydrogen, possibly catalyzed by frozen oxygen, was not recognized. Further, these workers assumed that the emissivities of the warm and cold surfaces were equal. This could lead to an estimate of the emissivity of the cold surface which is too large by a factor of two.[5] In view of the state of the experimental data in the micron range, there is clearly a need for experimental work.

For a calculation of the evaporation rate of our container B on the basis of figure 43.2, the emissivities of the surfaces were required. Conservative estimates could be made on the basis of experimental data available at elevated temperatures.

The Hagen-Rubens eq (11) pertains to normally emitted monochromatic radiation, and has received experimental confirmation in the micron range at temperatures above room temperature [9, 14]. The extension to polychromatic hemispherical emissivity in the micron range at elevated temperatures also finds reasonably good experimental verification [15]. At lower temperatures, on the other hand, the observed hemispherical emissivities are several-fold larger than the calculated values [16]. Thus the lowest observed emissivity for a copper surface at 90° K, exposed to room-temperature black-body radiation, is given by Blackman, et al, as 0.019, a value 2.5 times greater than the theoretical one. These authors attributed the discrepancy to the presence of surface films, particularly oxide films, and possibly to the difference in resistivity of the surface layers as compared with that of the bulk of the material. It was in view of the foregoing that for the estimate of the evaporation rate of our container, we took 0.02 for the emissivity of both surfaces. Actually, on the basis of the theory of Reuter and Sondheimer, this estimate for the copper surface at liquid-helium temperature could be too high by a factor of 10. From eq (9), the maximum radiation heat transfer expected is thus 4.3×10^{-3} w for container B. From figure 43.2 it is seen that this corresponds to an evaporation rate of 146 ml/day.

---

[4] T. Holstein has treated the problem in this wavelength region, and finds that the wavelength dependence is critically dependent upon p, the fraction of electrons that are reflected specularly. If $p=0$, his result is that $(1-R)$ is independent of λ at a level corresponding to $(1-R)_{\max}$. The details of this work are to be published.

[5] In a communication to the author, R. B. Scott has pointed out that one has to consider also the fact that the surfaces facing the vacuum were not polished; they had a slightly dull appearance, probably because of microscopic roughness and also the possible adherence of some of the so-called "bloom" that appears in the silvering process.

Hence, we expected an evaporation rate between 82 ml/day and 146 ml/day, which implies the possibility of more than an order of magnitude improvement in the efficiency of liquid-helium storage containers as compared with the one that has been described in the literature.

4. Experimental Details

The experiments consisted of measuring the evaporation rates of liquid helium in containers A and B, whose construction was indicated in section 2. The liquid helium in the containers was maintained at 772.0 ± 0.1 mm Hg with the aid of a thermostatted manostat.[6] Thus our experiments all refer to helium boiling at 4.228° K. Gas-flow measurements were made with a wet-test meter; one revolution of the meter pointer corresponds to 0.1 ft.^{3} The calibration of the meter made before and after the experiments was constant to ±0.2 percent; the calibrations were made with a 0.1 ft^3 meter prover that was calibrated by the National Bureau of Standards. In order to maintain constant the water level in the wet-test meter, the gas issuing from the container was passed through a water saturator before it entered the meter.

In the measurement of rates of evaporation of low-boiling liquids, pressure control is of paramount importance. Changes in the pressure have marked effects on the flow rate [17], and it is important to note that these effects are proportional to the mass of the liquid. It is necessary to meter an amount of gas that is sufficiently high to give the desired precision. In view of the pressure control and the fact that for each flow-rate determination we metered at least 1.0 ft^3, possible errors due to this factor were made entirely negligible.

The temperature of the nitrogen bath was determined by fluctuations of the atmospheric pressure, which led to a temperauture fluctuation of ±0.02 deg. Actually, at any given pressure, measurements with a platinum resistance thermometer probe showed that the bath temperature was constant to ±0.005 deg.

The initial experiments gave erratic results; the fluctuations in the evaporation rate were traced to the funneling of radiation down the neck tube. This could be completely eliminated by the simple expedient of blackening the inside of the neck tube with Aquadag down to the liquid-nitrogen temperature level. The introduction into the neck tube of a metal test tube, which provided a radiation shield at the liquid-nitrogen level, also resulted in consistently reproducible data. In practice, both of these precautions were taken, and, under these circumstances, the evaporation rates for containers A and B were 112 ml/day and 96 ml/day, respectively. These values are entirely in accord with the analysis presented in section 2; it was thus very desirable to check for quantitative agreement with the analysis by experiments that yield data of the type indicated by figure 43.3.

In order to facilitate the installation of a heater whose leads did not contribute to the heat leak and in order to improve heat exchange [18] between the gas and the wall of the neck tube, a ½-inch outside diameter, by 0.010-inch-wall Inconel tube (from the same lot and of the same temper as the neck tube) was inserted into the neck tube. The leads, each a 10-foot length of number 40 constantan

---

[6] For this purpose, we have found the model number 5 Cartesian Manostat manufactured by The Emil Greiner Co., very useful. The manostat was thermostatted at about 300° K to a constancy of ±0.02 deg.

wire, were spiraled about the inserted tube, and the evaporating gas was made to pass up the annulus between the two tubes. The heater was a 50,000-ohm wire-wound constantan resistor. With a regulated d-c power supply,[7] the power dissipated in the heater could be kept constant for many hours to ±0.01 percent. A Leeds & Northrup type K–2 potentiometer was used to measure the current through the heater and the potential drop across it; it is estimated that the power measurements are accurate to ±0.02 percent. The data obtained are tabulated in table 43.1 and are plotted in figure 43.4.

The last four points on the straight-line portions of the curves of figure 43.4 can be fitted by a linear equation that reproduces all of the points to ±0.1 percent. The slopes of the two straight lines agree within these limits and have the value 30.03 $(\mathrm{ft}^3/\mathrm{hr})/\mathrm{w}$ at NTP. As a check on the method, curve A was redetermined with a 500,000-ohm heater; the experimental points coincided with those obtained with the 50,000-ohm heater to ±0.1 percent. With the aid of eq (7) and the densities of the liquid [19] and vapor [20] phases, we calculate that the heat of vaporization of helium at 4.228° K is 4.93 cal/g. A discussion of this determination will be given in the next section.

TABLE 43.1. *Evaporation rate of liquid helium at 4.228° K*

	Container A	Container B
Inner surface	Polished copper	Polished copper.
Outer surface	Sandblasted monel.	Do.
Ambient temperature °K	77.08±0.02	75.05±0.02.
ΔH_v cal/g	4.93	4.93.
Q_R mw	3.00	1.67.

Heater power	Evaporation rate (ft³/hr at NTP)	Heater power	Evaporation rate (ft³/hr at NTP)
mw		*mw*	
0.000	0.1462	0.000	0.1417
1.839	.1597	1.785	.1530
2.265	.1638	2.374	.1570
4.223	.2152	3.299	.1649
8.876	.3568	4.216	.1783
12.613	.4706	8.862	.3161
17.786	.6256	12.590	.4285
23.272	.7894	17.896	.5877
		23.556	.7571

The intercepts of the straight lines on the evaporation-rate axis give the radiation heat transfer for containers A and B to be 3.00×10^{-3} w and 1.67×10^{-3} w, respectively. These values of Q_R may be inserted in the equations developed in section 2, and, if one adjusts suitably the parameter A/l, which may be in error by as much as 5 percent, one can reproduce curves A and B identically. The values of Q_R thus determined may also be used for a calculation of the evaporation rates of the containers themselves, i. e., without the added heat-exchange tube. The evaporation rates may in fact be obtained from figure 43.3; the calculated values for containers A and B are 106 ml/day and 92 ml/day, which are in fair agreement with observed values of 112 ml/day and 96 ml/day. Although the discrepancies correspond to the maximum differences attributable to the uncer-

---

[7] We are indebted to D. J. Grove, of our Laboratories, for making available to us this power supply of his own design.

tainty in A/l_1, there is the suggestion that at least part of the differences is due to imperfect heat exchange in the neck tube.

The hemispherical emissivity of polished copper at 4.228° K for radiation corresponding to that emitted by a black body at 77.1° K may be calculated from the determined value of $Q_R=3.00\times10^{-3}$ w for container A. This calculation may be made with the aid of eq (9) on the assumption that $e_o \gg e_i$. It may be estimated that such an assumption will lead to an uncertainty in e_i of less than 5 percent. The calculated value of the emissivity under these conditions is 6.9×10^{-3} and corresponds to a black-body radiation spectrum having a maximum intensity at 37.4 μ. As, in addition to the absolute value of the emissivity, the wavelength dependence is of crucial interest, the evaporation rate was determined for a 297.1° K black-body radiation spectrum having a maximum intensity at 9.71 μ. The flow rate had to be measured with a different flow-meter arrangement whose accuracy was estimated as ±4 percent. With this arrangement the observed flow rate was 36.9 ft³/hr at NTP and corresponds to $e_i=1.29\times10^{-2}$.

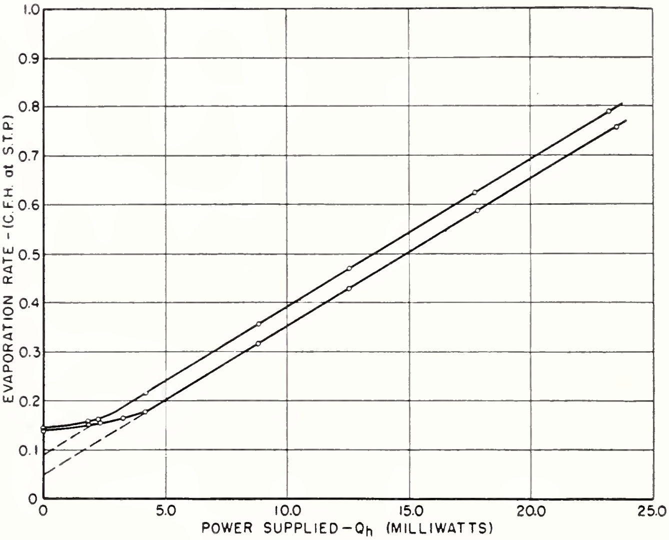

FIGURE 43.4. *Liquid helium evaporation rates at 4.228° K.*

Upper curve for container A; lower curve for container B

It may be worth noting here our observations of the effects of spontaneous vibrations of the helium-gas column between the liquid level and the vent tube of a given container. Such oscillations have been observed many times [21], and an attempt has been made to treat the problem theoretically [22]. If the vent tube of the container is closed or restricted with a rubber tube, for example, oscillations within the container may be felt by holding the rubber tube. It was found that the intensity of such oscillations, which are accompanied by an influx of heat at a rate that may be a thousand times that due to normal heat leak, is a function of the liquid-helium level. We were careful to work under such conditions that the effects of this phenomenon could be neglected.

For completeness is included figure 43.5, which is based on data obtained early in the work in order to check the principle of the method used in determining Q_R and ΔH_v. In figure 43.5 is presented the evaporation rate of liquid nitrogen at 77.12° K in a container that differed from container B in that incorporated in it was a copper-shielded activated charcoal pump in contact with the liquid-nitrogen-cooled surface. The outer surface of this container was at room temperature, 297.1° K. The accuracy of the evaporation-rate measurements was ±1 percent. From the data it was estimated that 97 percent of the initial losses is due to heat transfer across the vacuum space, which is consistent with known facts. The heat of evaporation calculated from these data is 1,345±13 cal/mole, which includes a correction of 0.5 percent made in accordance with eq (7). This determination is in satisfactory agreement with the value deduced from the data of Giauque and Clayton [23] for the same temperature, namely, 1,344.2±1 cal/mole.

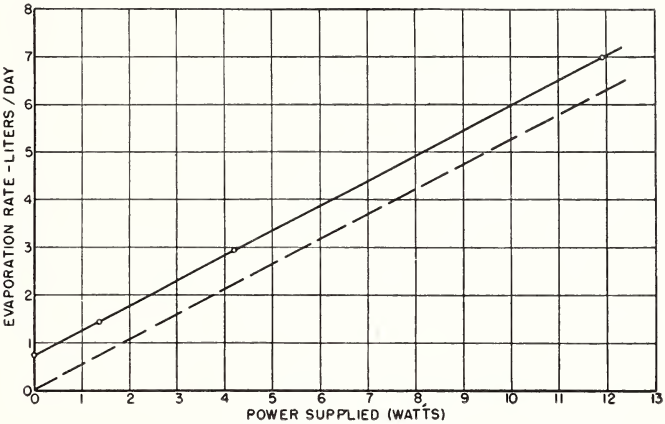

FIGURE 43.5. *Liquid-nitrogen evaporation rate at 77.12° K.*

5. Discussion

The emissivities determined for polished copper at 4.228° K are 6.9×10^{-3} for black-body radiation at 77.1° K and 1.29×10^{-2} for black-body radiation at 297.1° K. The theoretical expectations should not be appreciably different from those computed for silver at liquid-helium temperatures at the wavelengths corresponding to the maximum intensities in the black-body spectrum, namely, 37.4 and 9.71 μ, on the basis of the Reuter and Sondheimer theory. The calculated values are 1.0×10^{-3} and 20×10^{-4}, respectively. Not only is absolute agreement lacking, but the experimentally determined emissivities increase as $\lambda^{-1/2}$ and do not decrease. It is of course possible that the surface is not representative of the bulk metal and that surface roughness is responsible for the large values of the absorption. Such considerations have in fact been offered to explain anomalously high resistive losses in the microwave region [9, 10, 11]. The difficulty here is that in order to obtain a $\lambda^{-1/2}$ wavelength dependence, the absolute values of e must be much higher than those that are observed. These questions require further experimental study, and more precise determinations of the emissivities of metals as a function of their temperature and of the frequency of the radiation, with special emphasis on the treatment of the surface, are in progress.

Recently Kistemaker [2], on the basis of an equation that results from the equating of the Gibbs free energies of the liquid and the saturated vapor, concluded that above 3.5° K the values of the heat of vaporization of helium measured by Dana and Kamerlingh Onnes [3] are 6 percent too low. The thermodynamic relation used by Kistemaker involves the virial coefficients of helium, as well as the specific heat of the liquid. The experimental determinations of Dana and Onnes may be assumed to be accurate to 1 percent; the only data they required was the densities of the liquid under its saturated pressure [19].

The heat of vaporization of helium at 4.228° K as extrapolated from the data of Dana and Kamerlingh Onnes is 4.87 cal/g. The accuracy of our value of 4.93 cal/g depends on that of the determinations of both the liquid density [19], $\rho_l = 0.1253$ and the vapor density [20], $\rho_v = 0.01637$ g/cm^3. Except for errors due to inaccuracies in ρ_l or ρ_v, our determination is considered to be accurate to better than 0.5 percent. The Clausius-Clapeyron equation

$$\Delta H_v = T\left(\frac{1}{\rho_v} - \frac{1}{\rho_l}\right)\frac{dp}{dT}$$

yields the value 5.31 cal/g. This strongly suggests that the vapor density is in error, and if ρ_v is taken as 0.01755, all three values become identical.

With respect to container design, the experimental results confirm the analysis and demonstrate the possibility of making extremely efficient storage containers for liquid helium. It would be quite feasable to build storage containers of moderate size that would hold liquid helium for a year or more after the initial filling.

6. References

[1] G. E. H. Reuter and E. H. Sondheimer, Proc. Roy. Soc. (London) [A] **195,** 336 (1949).
[2] J. Kistemaker, Physica **12,** 281 (1946); also Leiden Comm. Supplement 95a.
[3] L. I. Dana and H. Kamerlingh Onnes, Leiden Comm. 179c.
[4] W. F. Giauque, Rev. Sci. Instr. **18,** 852 (1947).
[5] A. H. Larsen, F. E. Simon, and C. A. Swenson, Rev. Sci. Instr. **19,** 266 (1948).
[6] The Report of the Oxygen Research Committee, London, H. M. S. O. (1923).
[7] R. B. Scott, W. J. Ferguson, and F. G. Brickwedde, J. Research NBS **33,** 1 (1944) RP1592.
[8] O. A. Saunders, Proc. Phys. Soc. **41,** 569 (1929).
[9] E. Hagen and H. Rubens, Ann. Physik **11,** 873 (1903).
[10] A. B. Pippard, Proc. Roy. Soc. (London) [A] **191,** 370 (1947).
[11] E. Maxwell, P. M. Marcus, and J. C. Slater, Phys. Rev. **76,** 1332 (1949).
[12] W. B. Nowak and J. C. Slater, Phys. Rev. **76,** 469 (1949).
[13] R. B. Scott, J. W. Cook, and F. G. Brickwedde, BS J. Research **7,** 935 (1931) RP385.
[14] C. Hurst, Proc. Roy. Soc. (London) [A] **142,** 466 (1933).
[15] C. Davisson and J. R. Weeks, Jr., J. Opt. Soc. Am. Rev. Sci. Instr. **8,** 581 (1924).

[16] M. Blackman, A. Egerton, and E. V. Truter, Proc. Roy. Soc. (London) [A] **194,** 1947 (1948).
[17] A. Wexler and W. S. Corak, Rev. Sci. Instr. **21,** 583 (1950).
[18] R. B. Jacobs and S. C. Collins, J. Applied Phys. **11,** 491 (1940).
[19] H. Kamerlingh Onnes and J. D. A. Boks, Leiden Comm. 170b.
[20] E. Mathias, C. A. Crommelin, H. Kamerlingh Onnes, and J. C. Swallow, Leiden Comm. 172b.
[21] K. W. Taconis, et al., Physica **15,** 733 (1949), also Leiden Comm. 279a.
[22] H. A. Kramers, Physica **15,** 971 (1949); also Leiden Comm. Supplement 100a.
[23] W. F. Giauque and J. O. Clayton, J. Am. Chem. Soc. **55,** 4875 (1933).

We thank T. Holstein for very helpful discussions concerning the theoretical aspects of this work. Our thanks are also due to Hofman Laboratories, Incorporated, Newark, N. J., for providing the containers designed on the basis of the analysis contained in this paper and, in particular, to H. Jacket, of Hofman Laboratories, Incorporated, who supervised their construction and assisted in taking the initial data. We are also grateful for valuable discussions with K. Mendelssohn, R. B. Scott, and D. Shoenberg at the Low Temperature Symposium held at the National Bureau of Standards. Finally, we acknowledge the assistance of our colleagues, particularly W. S. Corak and G. T. Cunningham.

44. Methods of Determining Very Low Thermodynamic Temperatures. Measurements With Potassium-Chromium-Alum

by D. de Klerk [1]

Introduction

A problem of high importance in the region of adiabatic demagnetization is the exact determination of absolute temperatures. At ordinary temperatures problems arise only when a higher accuracy than 1 part in 10^5 is needed. At the lowest temperatures, now obtainable with the magnetic method, the best accuracy is about 10 to 20 percent.

At present, several methods are available for the determination of thermodynamic temperatures.

1. *Thermodynamic-caloric method* [1].[2] This is based on Kelvin's relation

$$\text{đ}Q = TdS. \tag{1}$$

When a well-known quantity of heat, $\text{đ}Q$, is supplied to a demagnetized sample, and when the corresponding variation of its entropy is dS, the thermodynamic temperature can be calculated from (1).

As entropies cannot be measured directly, for the practical performance of this method use is made of a "thermometric parameter." This is a property of the salt that is strongly dependent on its temperature, so that it can be used as a secondary thermometer.

For absolute-temperature determinations two independent measurements must be made. First, an experimental relation must be found between the parameter and the entropy; then the variation of the parameter must be determined when a well-known quantity of heat is supplied to the salt. From these data the thermodynamic temperature can be derived as a function of the parameter.

As a thermometric parameter, different properties are needed in different parts of the demagnetization region. At the higher temperatures the magnetic susceptibility is often used, or the equivalent "magnetic temperature" $T^* = (C/\chi)$. At the lower temperatures this magnetic temperature is not very strongly dependent on the absolute temperature. Here it is replaced by the imaginary part of the a-c susceptibility, χ'', or by the remanence, Σ.

The relation between the thermometric parameter and the entropy of the salt is determined in the following way: The decrease of entropy during the isothermal magnetization at the initial temperature can be derived from the magnetization curve. During the adiabatic demagnetization the entropy is constant, so the entropy at the final temperature is known. Immediately after the demagnetization the thermometric parameter can be determined, and from this the relation between the entropy and the parameter is found.

---

[1] Kamerlingh Onnes Laboratory, Leiden, Holland.

[2] Figures in brackets indicate the literature references on p. 222.

In caloric measurements the difficulty is encountered that at the lower temperatures the heat conductivity of the paramagnetic salts becomes very poor, making it difficult to distribute an amount of heat homogeneously over a sample. The three methods used are:

(a) Using a heating coil. In this case the heat supply is very inhomogeneous. Good results can be expected only above 0.2° K.

(b) Using gamma rays. As the absorption coefficient is small, the heat absorption is sufficiently homogeneous. This method can be used over the whole region of temperatures.

(c) Using the a-c losses when the salt is placed in an a-c magnetic field. This method can be used only when relaxation or hysteresis effects occur in the salt, i. e., below the curie point and in some cases just above it.

2. *Theroretical method.* This is based on the calculations of Van Vleck and his cooperators [2, 3]. This method is closely related to the foregoing one. The caloric measurements are replaced by theoretical considerations. Theroretical relations are proposed for M and U as functions of H and T, and from these relations, expressions can be derived for T^* and S in zero magnetic field as functions of T. So a relation between S and T^* is found, and this can be verified by experiment. Unfortunately, the temperature itself is eliminated in this way, but when agreement is obtained between the theoretical and the experimental curves in a wide region of tempeartures, it seems plausible that the theoretical relations are correct. Good results are found from this method only in the upper part of the temperature range, because at the lower temperatures systematic deviations occur between the theoretical and experimental curves.

3. *Magnetic method* (proposed by Garrett [4]). The necessary data are derived from the measurement of adiabatic magnetization curves. The differential susceptibility $(\partial M/\partial H)_S$ is measured along as adiabate as a function of an external field, H. In low fields we have the relation

$$\left(\frac{\partial M}{\partial H}\right)_S=\left(\frac{\partial M}{\partial H}\right)_{H=0}\left(1-\frac{3}{2}\Xi H^2\right), \tag{2}$$

where

$$\Xi=\frac{1}{\chi}\left(\frac{\partial \chi}{\partial S}\right)_{H=0}\left(\frac{\partial \chi}{\partial T}\right)_{H=0}$$

$$\chi=\left(\frac{\partial M}{\partial H}\right)_{H=0}.$$

The quantity Ξ can be derived experimentally for a number of adiabats, and as $(\partial\chi/\partial S)_{H=0}$ can be derived from the entropy curve, $(\partial\chi/\partial T)_{H=0}$ can be calculated, and from its course with $\chi_{H=0}$ the absolute temperature can be integrated.

4. *Temperatures in External Magnetic Fields.* These can be determined [5] from the thermodynamic relation

$$\left.\begin{aligned}\left(\frac{\partial T}{\partial H}\right)_S&=-\left(\frac{\partial M}{\partial S}\right)_H\\ \text{or}\qquad T-T_0&=-\int_{H_0}^{H}\left(\frac{\partial M}{\partial S}\right)_H dH.\end{aligned}\right\} \tag{3}$$

When adiabatic magnetization curves are measured, the quantity $(\partial M/\partial S)_H$ can be determined as a function of H and S, and temperature differences on adiabats can be found by integration. When the temperatures in zero field are determined with one of the foregoing methods, the temperatures in external fields can be calculated.

Experimental Results

At present only in the case of potassium-chromium-alum, $CrK(SO_4)_2.12H_2O$, have all these methods of absolute-temperature determination been realized. Although the different methods are realized with different samples, the agreement in most cases is not bad. I shall discuss these investigations in some detail. For reasons of convenience, the sequence is changed in such a way that the theoretical method is considered first and then the caloric.

Theoretical Method. Because entropy measurements are needed for most of the methods for temperature measurement given above, the necessary data can be deduced from the measurements of several authors. As an example, we mention the measurements of Casimir, de Haas, and de Klerk [6]. The results were given in an $S(T)$ diagram (see fig. 44.1). So their measured T^* values were reduced to values of T with the help of the theoretical formula, and the results were compared with the theoretical $S(T)$ curve. Only one parameter could be chosen to obtain the best agreement, e. g., the Stark splitting of the fourfold degenerate ground level of the Cr^{+++} ion in the crystalline electric field. When this splitting was chosen so that good agreement was obtained near 0.5° K, the experimental points agreed with the theoretical $S(T)$ curve down to $T=0.07°$ K.

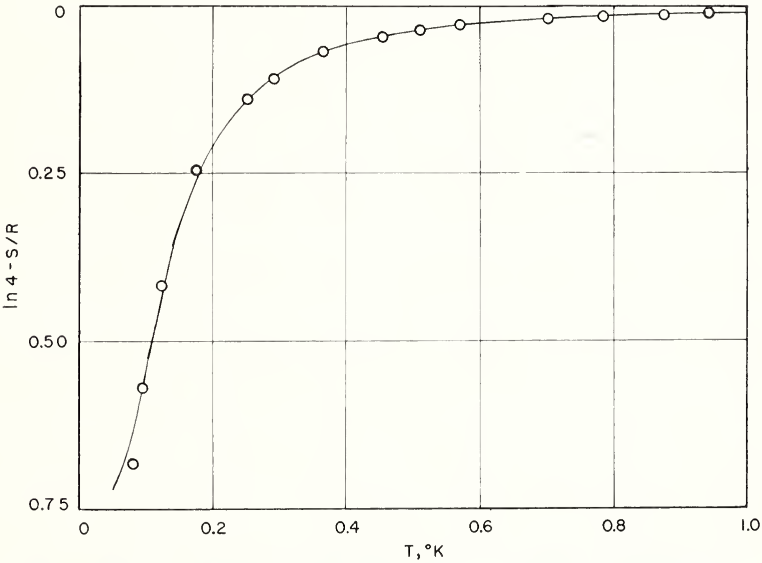

FIGURE 44.1. *Entropy of chromium-potassium-alum as a function of temperature.*

○, experimental points of Casimir, de Haas, and de Klerk; the curve is calculated from theory, using a splitting parameter $\delta=0.270°$K.

A small systematical difference occurred in such a way that between 0.2° and 0.08° K the temperatures of the experimental points were slightly too low, and below 0.08° K they were slightly too high. Below $T=0.07°$ K, big differences suddenly occur between the experimental and the theoretical points, so here the method breaks down.

Thermodynamic-Caloric Method. (a) Measurements with a heating coil were performed only by P. H. Keesom [7]. Down to 0.3° K the results were in agreement with other measurements. Below this temperature large differences occurred. Probably below 0.3° K the thermal equilibrium in the sample was poor. This supposition was corroborated by direct measurements of the heat conductivity of chrome alum by Garrett [8].

(b) Measurements with help of gamma radiation were made by Bleaney [9]. The investigations were extended down to $T^*=0.075°$, $T=0.045°$ K. From the relation between T and T^* found in the experiment and from the amounts of heat supplied to the salt, the absolute specific-heat data could be derived (see fig. 44.2). Down to 0.2° K good agreement was obtained with the theoretical specific-heat curve. Between 0.2° and 0.08° K the experimental specific heat was slightly lower; below 0.08° K it was higher than the theoretical curve. This result is in remarkably good agreement with the measurements of Casimir, de Haas, and de Klerk mentioned above. Although the parameter of the Stark splitting was slightly different, the deviations from the theoretical curves were quantitatively the same in both cases.

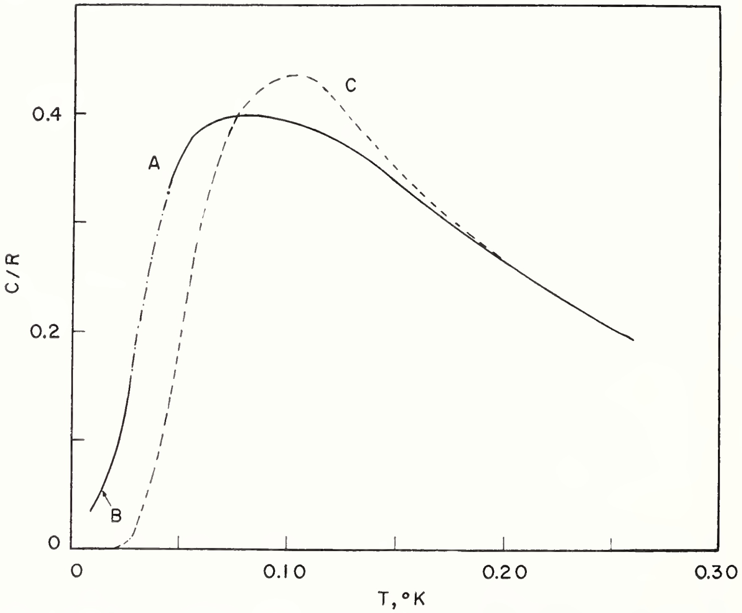

FIGURE 44.2. *Specific heat of chromium-potassium-alum as a function of temperature.*

A, Experimental curve of Bleaney; B, experimental curve of de Klerk, Steenland, and Gorter; C, theoretical curve for splitting parameter $\delta=0.245°$ K.

(c) Measurements with the help of a-c heating were carried out by de Klerk, Steenland, and Gorter [10]. As heat absorption from a magnetic field occurs only at the lowest temperatures (below $T=0.03°$ K), no agreement could be obtained with theoretical formulas. It followed that the absolute temperatures were much lower than the corresponding magnetic ones (see table 44.1), the difference being even a factor 10 at the lower temperatures.

At $T^*=0.033°$, $T=0.0040°$ K, the magnetic temperature showed a minimum (so χ showed a maximum, see fig. 44.3), and this point can be considered as some kind of a curie point as below this temperature remanence occurs, and hysteresis loops can be measured.

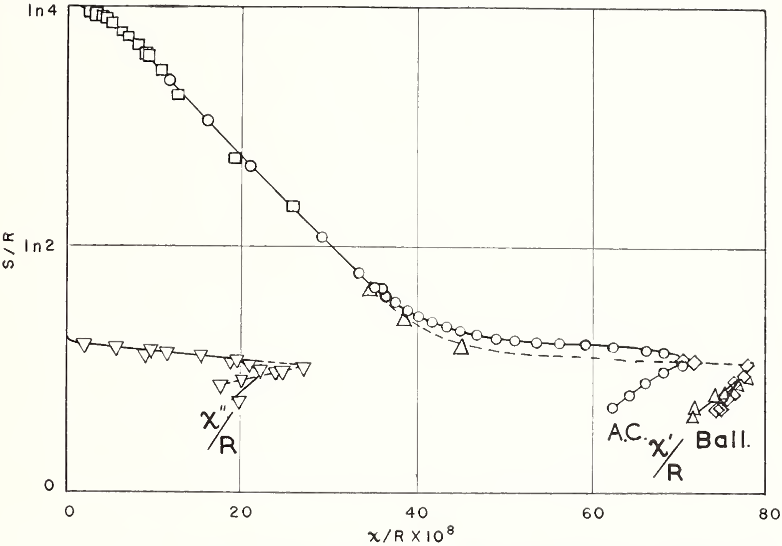

FIGURE 44.3. *Susceptibility of chromium-potassium-alum as a function of entropy.*

◇, Susceptibility measured ballistically; vibration time of galvanometer: 7 sec; △, susceptibility measured ballistically, vibration time of galvanometer: 0.2 sec; ○, real part of a-c susceptibility, 225 cycles; ▽, imaginary part of a-c susceptibility, 225 cycles, plotted on a tenfold magnified scale. The difference between ◇, △, and ○ is caused by relaxation effects in the salt.

Although the phenomena below the curie point are rather complicated, they show similarity with the antiferromagnetism found in some substances at higher temperatures [11]. An experimental result, which so far lacks theoretical interpretation, is that a very pronounced minimum occurs in the slope of the $S(T)$ curve at $S/R=0.4$, whereas such a minimum should be expected at $S/R=\ln 2$ (see fig. 44.4). This, however, is in qualitative agreement with the specific-heat curve of Bleaney of figure 44.2, since it can be seen at once that the entropy content of this specific heat is higher than $R \ln 2$.

The thermometric parameters used below the curie point were the imaginary part of the a-c susceptibility, χ'', and the remanence, Σ, in a field of 1.08 oersteds.

Magnetic Method. Garrett [12] published some Ξ values (see formula 2) without calculating absolute temperatures from them. Using the Leiden entropy data, we made some calculations. It followed that the parameter for the crystalline Stark splitting was in good agreement with other determinations, but the course of dT^*/dT with temperature deviated from the values of Casimir, de Haas, and de Klerk and from those of Bleaney. Garrett's Ξ values proved to be too high.

Also some Ξ values were derived from the measurements of adiabatic magnetization curves made at Leiden. The external magnetic fields used in these experiments, however, proved to be too high, so only the slope of the $\chi(H^2)$ curves could be determined in zero field. This was insufficiently accurate, and wrong values were found for the splitting parameter and for dT^*/dT. This is unfortunate, as this method might be useful in the region between $T=0.05°$ and 0.03° K, where, until now, no good temperature determinations were available. We are planning to repeat these measurements with a higher accuracy.

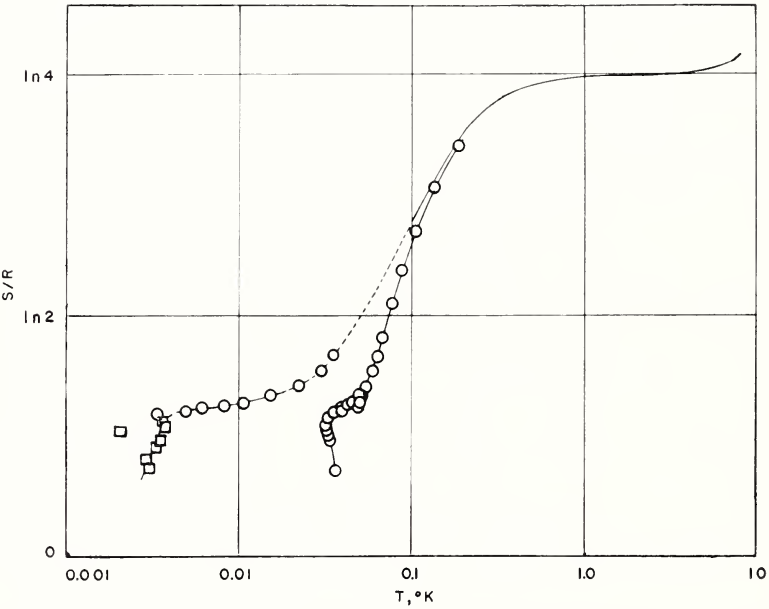

FIGURE 44.4. *Entropy of chromium-potassium-alum as a function of T (left-hand curve) and as a function of T* (right-hand curve).*

○, T* as a thermometric parameter; □, remanence as a thermometric parameter.

TABLE 44.1

S/R	T^*	T	S/R	T^*	T
0.585	0.064	0.035	0.427	0.040	0.0065
.539	.060	.031	.423	.038	.0056
.485	.054	.022	.416	.036	.0047
.472	.052	.018	.406	.034	.0041
.460	.050	.015	.399	.033	.0039
.450	.048	.012	.326	.034	.0035
.442	.046	.010	.306	.0345	.0033
.436	.044	.0088	.256	.036	.0029
.431	.042	.0075			

Temperatures in External Magnetic Fields. I shall report the results of some recent investigations made in Leiden. The measurements were made with the help of the ballistic mutual-inductance bridge shown in figure 44.5. The effect of the salt on the secondary coil surrounding it was compensated for the greater part with a variable mutual inductance adjusted to a suitable value. Susceptibility measurements are made by reversing a small field (of the order of 1 oersted) in the primary coils. When the field is not reversed but switched on and off in both directions, remanences are determined at the same time.

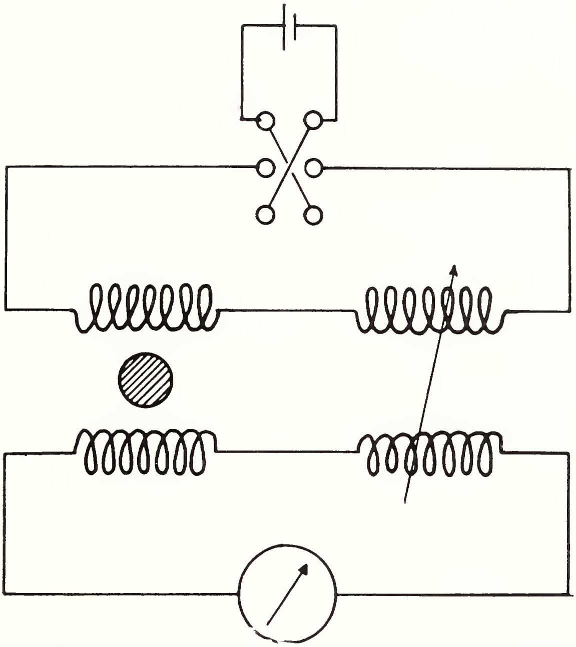

FIGURE 44.5. *Ballistic mutual inductance bridge for susceptibility and remanence measurements.*

Two methods are available to measure a magnetization curve: (1) An external field can be applied parallel to the small measuring field (x-direction). In this case the quantity $(\partial M/\partial H)_S$ is measured, and the magnetization curve can be integrated from the experimental results. (2) The external field can be applied perpendicularly to the small measuring field (y-direction). Now, when a spherical sample is used, we have

$$\frac{M_x}{H_x}=\frac{M_y}{H_y}. \tag{4}$$

The quantity determined in the experiment is M_x/H_x, and from the value of the external field, H_y, the moment, M_y, can be derived. (When an ellipsoidal sample is used, the relation (4) is replaced by a more complicated one [13] containing the demagnetization corrections both in the x- and the y-directions.) The latter method was applied in our measurements, the external field being produced by a Helmholtz coil, giving fields up to 500 oersteds.

As the heat insulation of a demagnetized sample is never perfect, we always have a heat leak of about 30 ergs per minute. At the lower temperatures, where the heat conductivity is very poor, the thermal equilibrium in the salt is disturbed in a short time. For this reason the magnetization curve should be measured in as short a time as possible. Therefore, we used a galvanometer with a vibration time of 0.2 second. A deflection could be recorded photographically every second. With this method a magnetization curve, using 12 different fields, could be passed through three times within 5 minutes.

A difficulty occurred at the temperatures below the curie point, as here relaxation effects were found with relaxation times comparable with the vibration time of the galvanometer. These effects caused double deflections of the galvanometer, whose interpretation proved to be complicated. It follows from an estimate that when the relaxation time of the salt is only one-tenth of the $(1/e)$-time of the galvanometer when aperiodically damped ($0.1/2\pi$ times the vibration time of the galvanometer when undamped) serious errors are introduced when the susceptibility is derived from the maximum deflections, in particular when the bridge is approximately balanced. This is illustrated in figure 44.6. Perhaps both the relaxation time and the correct susceptibility might be derived from a close analysis of the galvanometer deflection, but until now we did not succeed in this. Some characteristic deflections are shown in figures 44.7, A and B.

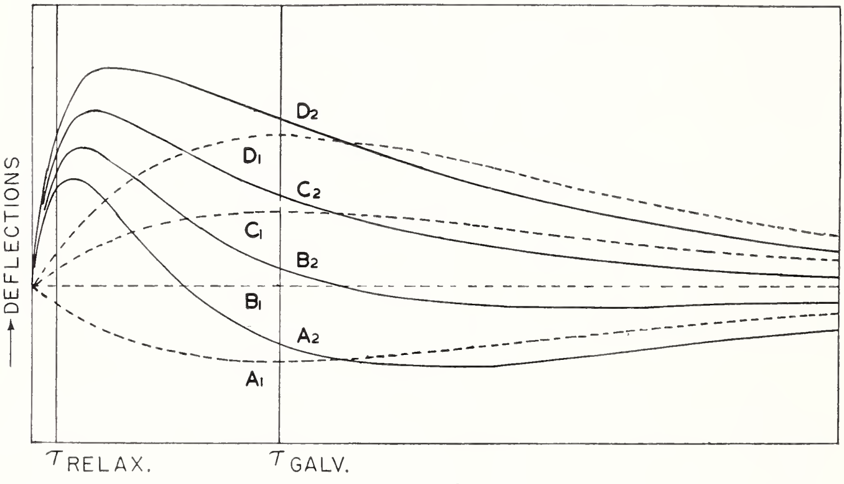

Figure 44.6. *Calculated galvanometer deflections as functions of time.*

- - - - - - - - -, Deflections when no relaxation effects occur in the salt; in case B_1 the bridge is exactly balanced; in case A_1 the effect of the salt is undercompensated with the variable mutual inductance of figure 44.5; in cases C_1 and D_1 it is overcompensated. ————, deflections when the relaxation time of the salt is one-tenth of the $1/e$-time of the galvanometer.

As the adiabats were measured with different values of the compensating mutual inductance, we succeeded in constructing a number of magnetization curves which probably give the correct susceptibility values, but systematical mistakes are not completely excluded. Therefore, the values given here have a preliminary character, but some interesting qualitative conclusions can still be derived from them.

The magnetization curves are shown in figure 44.8. Above $S/R=$

0.45 they do not show remarkable effects, the decrease of χ with the field being more or less proportional to H^2. Just above the curie point the susceptibility in zero magnetic field suddenly increases enormously (see also fig. 44.3). From figure 44.8 it follows that this is the case only in small magnetic fields; at about 25 oersted quite normal susceptibilities are already found. Because of the maximum in the susceptibility in zero field, the lowest adiabats start at a somewhat smaller χ than those at higher entropies. In quite small fields, however, the curves intersect, and then the sequence is normal again.

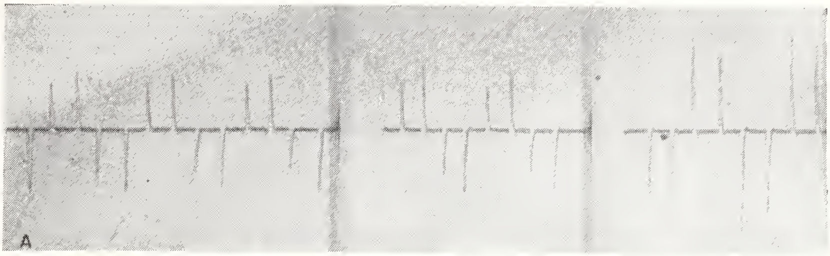

Figure 44.7, A. *Galvanometer deflections recorded photographically.*

The measuring field was switched on and off alternately in opposite directions. The difference in subsequent deflections is caused by the remanence of the salt.

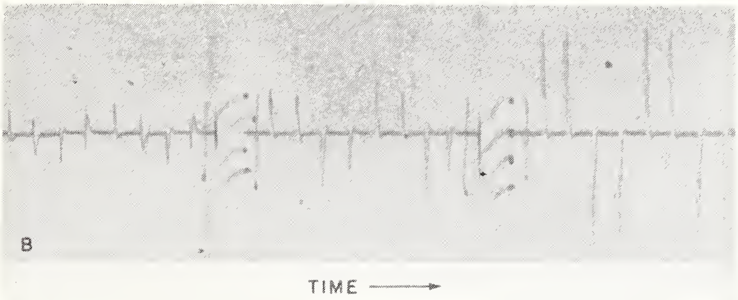

Figure 44.7, B. *Galvanometer deflections analogous to those of figure 44.7, A, but showing double deflections.*

From the curves in figure 44.8, an $S(\chi)$ diagram with lines of constant H can be derived. It is shown in figure 44.9. From this graph values of $(\partial M/\partial S)_H$ can be derived, and by integrating them over adiabats (horizontal lines in fig. 44.9) the variation of temperatures on the adiabats can be found according to formula (3). Maxima in χ in the curves of figure 44.9 are found only in the lower fields. Below these maxima $(\partial M/\partial S)_H$ is positive; so here an increase in H gives a decrease in T. Above 25 oersteds, however, all the $S(\chi)$ curves have a negative slope. Hence an increase in H gives a rise in T. The slopes of the $S(\chi)$ curves in the neighborhood of the maxima prove to be very uncertain; thus the course of T with H on an adiabat is uncertain, but we could calculate some orders of magnitude.

The ΔT versus H curves for different values of S are represented in figure 44.10. For low external fields we can write approximately

$$\Delta T = -\frac{1}{2} (\partial\chi/\partial S)_{H=0} H^2. \qquad (5)$$

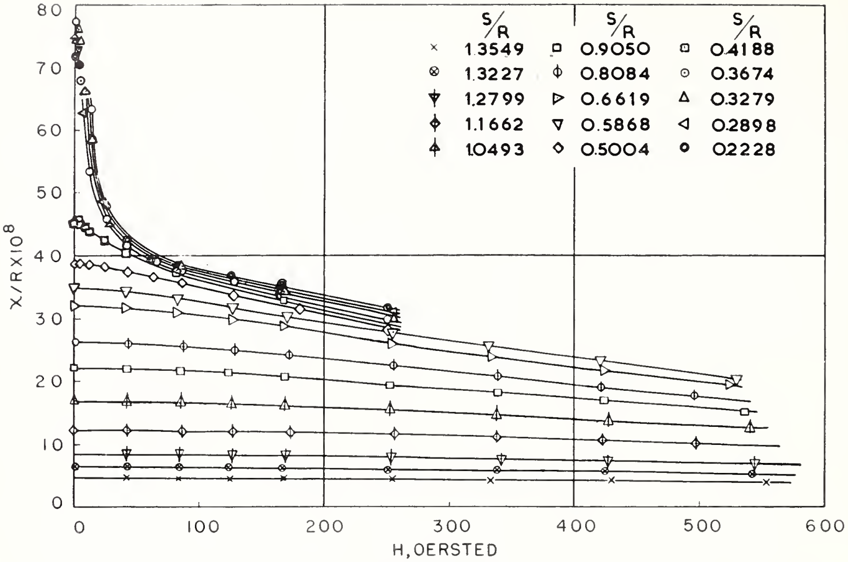

FIGURE 44.8. *Adiabatic magnetization curves for chromium potassium alum.*

Susceptibility as a function of field strength.

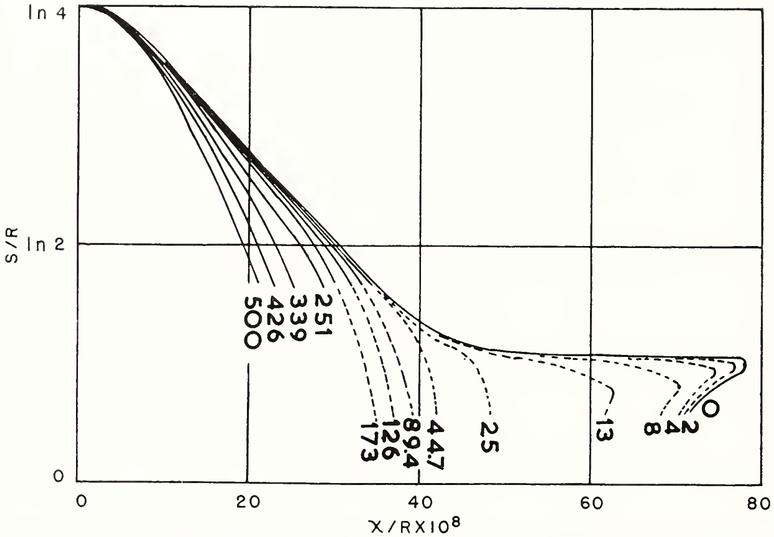

FIGURE 44.9. *Susceptibility of chromium potassium alum as a function of the entropy.*

Lines of constant magnetic field. Values are given in oersteds for curves.

From the slope of the $S(\chi)$ curve in zero field it follows that in the higher region ($S/R>1.3$) the increase of T with H in low fields must be relatively steep, but in a large region somewhat lower ($0.7<S/R<1.3$) the slope is practically constant, so here the increase of T in a given field must be practically independant of the entropy. In higher external fields, however, we must expect that H/T becomes nearly a

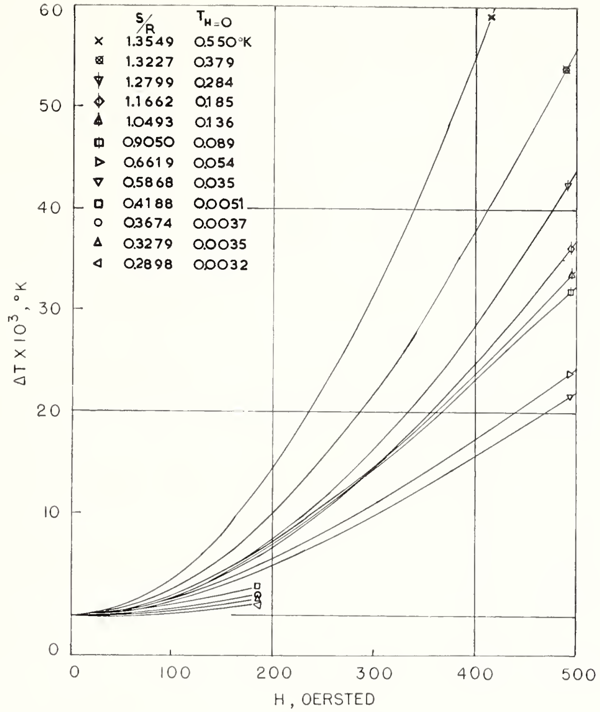

FIGURE 44.10. *Variation of temperature with field on adiabatic magnetization curves for chromium-potassium-alum.*

constant. Therefore the slope of the $T(H)$ curves must decrease with falling entropy. At the higher temperatures this is in agreement with the experimental results, within the limits of accuracy. In the neighborhood of the curie point, however, where the $S(\chi)$ curve in zero field has a flat part again, the $T(H)$ curves in low fields should again become steeper. As this is not true, (5) is no more fulfilled, which is not surprising.

Below the curie point the temperature on an adiabat passes through a minimum, as was mentioned before, although the decrease is very small, smaller than that found by Kürti [14] in the case of iron-ammonium-alum (in fig. 44.10 it is hardly visible). Kürti remarked that when the temperature on an adiabat passes through a minimum, the entropy on an isotherm shows a maximum. This can hardly be explained with normal ferromagnetism (parallel spins), but it follows quite naturally in the case of antiferromagnetism (antiparallel spins).

Finally, I must mention that the measurements of Bleaney [9, 15] with microwaves show that chromium-potassium-alum, the substance on which until now most measurements were made, is not the most suitable substance. The Stark splitting of about 0.25° K found in most experiments proved to be a combination of two splittings, viz, of 0.388° and 0.22° K. This is probably the cause of the small deviations from the theoretical $S(T)$ curve below 0.2° K, although no numerical interpretation of the deviations could be given. There are, however, some chromium-alums showing only one Stark splitting, chromium-cesium-alum, chromium-rubidium-alum, and chromium-methylamine-alum. We expect better agreement with theory for these salts than for the potassium-alum. At present the methylamine-alum is being prepared at Leiden, and we hope to give the results of the investigations with this substance in due time.

The measurements in external magnetic fields were performed in cooperation with C. J. Gorter and M. J. Steenland. Assistance during the measurements and the calculations was rendered by F. F. Bos, J. A. Beun, G. de Vries, and J. Vlieger.

---

[1] W. H. Keesom, Physica, **2,** 805 (1935); Commun. Kamerlingh Onnes Lab. Univ. Leiden, Suppl. 77c.
[2] J. H. van Vleck, J. Chem. Phys. **5,** 320 (1937).
[3] M. H. Hebb and E. M. Purcell, J. Chem. Phys. **5**, 338 (1937).
[4] C. G. B. Garrett, Proc. Roy. Soc. (London) [A] **203,** 375 (1950).
[5] W. F. Giauque and D. P. MacDougall, J. Am. Chem. Soc. **57,**, 1175 (1935); **58,** 1032 (1936); **60,** 376 (1938).
[6] H. B. G. Casimir, W. J. de Haas, and D. de Klerk, Physica, **6,** 365 (1939) Commun. Kamerlingh Onnes Lab. Univ. Leiden, Suppl. 256c.
[7] P. H. Keesom, Thesis, Leiden (1948).
[8] C. G. B. Garrett, Phil. Mag. **41,** 621 (1950).
[9] B. Bleaney, Proc. Roy. Soc. (London) [A] **204,** 216 (1950).
[10] D. de Klerk, M. J. Steenland, and C. J. Gorter, Physica, **15,** 649 (1949); Commun. Kamerlingh Onnes Lab. Univ. Leiden, Suppl. 278c.
[11] J. W. Stout and M. Griffel, Phys. Rev. **76,**, 144 (1949); N. J. Poulis, J. van den Handel, J. Ubbink, J. A. Poulis and C. J. Gorter, Phys. Rev. **82,** 552 (1951).
[12] C. G. B. Garrett, Cérémonies Langevin-Perrin, p. 43 (Paris, 1948).
[13] H. B. G. Casimir, Magnetism and very low temperatures, Cambridge Physical Tracts, p. 21 (1940).
[14] N. Kürti, Conference on ferromagnetism and antiferromagnetism (Grenoble, 1950, in press).
[15] B. Bleaney, Proc. Roy. Soc. (London) [A] **204,** 203 (1950).

45. Behavior of Single Crystals of Cobalt-Ammonium-Sulfate Below 1° K

by Stephen Malaker [1]

Cobalt-ammonium-sulfate is one of the Tutton salts and a monoclinic crystal, having arrangements developed from the space group C_{2h}^{5}. It is known from microwave measurements [1] [2] that there is a large hyperfine-structure coupling for the Co^{++} ion, and from the microwave data Bleaney [2] calculated a nuclear specific-heat constant, $A_n = 16 \times 10^{-4} R$, where R is the gas constant, for the tail of the Schottky specific heat, i. e., where $C_v = A_n / T^2$.

The tetragonal electric field from the six waters of hydration surrounding the Co^{++} ion removes all orbital degeneracy, so that the electronic ground state is simply a Kramers doublet. Interaction between neighboring magnetic dipoles should spread the sharp spectral lines into a band, and this is indicated by the small lines above and below the sharp lines in the spectrum shown in figure 45.1. Both the nuclear and dipole-dipole specific heat (and also exchange, if present) should go as A/T^2 in the appropriate temperature region.

Measurements have been made on single crystals, using the random dilution technique [3] to reduce dipole-dipole coupling. The method of measurement was that of Garrett [4], which consists in superposing a constant parallel magnetic field on the salt already in the a-c field of a Hartshorn bridge circuit.

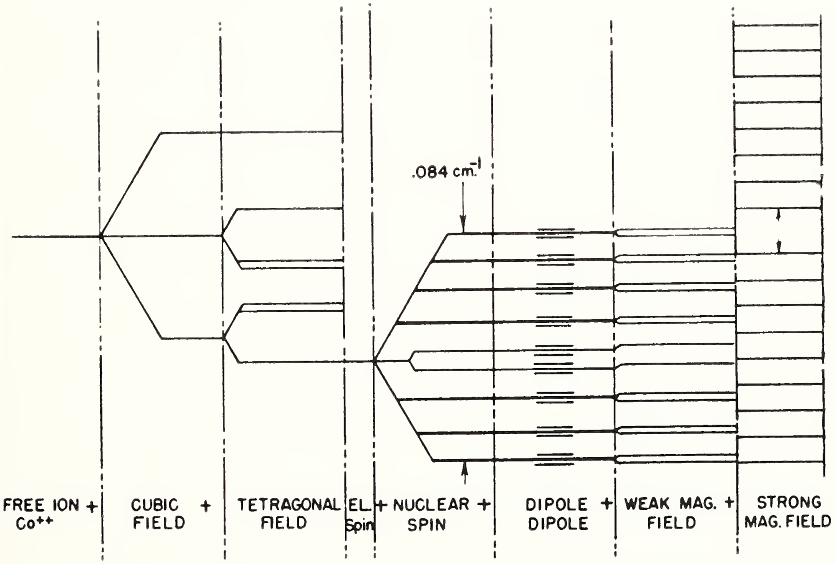

FIGURE 45.1. *Energy level scheme for* Co^{++} *in cobalt-ammonium-sulfate.*

---

[1] Oak Ridge National Laboratory and Catholic University, Washington, D. C. Now at Ohio State University, Columbus, Ohio.

[2] Figures in brackets indicate the literature references on p. 228.

Assuming a Curie law for susceptibility and an A/T^2 law for specific heat, one can easily deduce that

$$\Xi = \frac{2}{3H^2}\frac{\delta\chi}{\chi_0} = \frac{C}{A} \text{ constant}, \tag{1}$$

where Ξ is the Garrett [4] parameter, H is the superposed constant parallel field, $\delta\chi$ is the change in susceptibility due to H, χ_0 is the isothermal susceptibility in zero field, and C is the Curie constant.

The results of such measurements are shown in table 45.1 and are plotted in figure 45.2. In figure 45.3 the intercept at infinite dilution

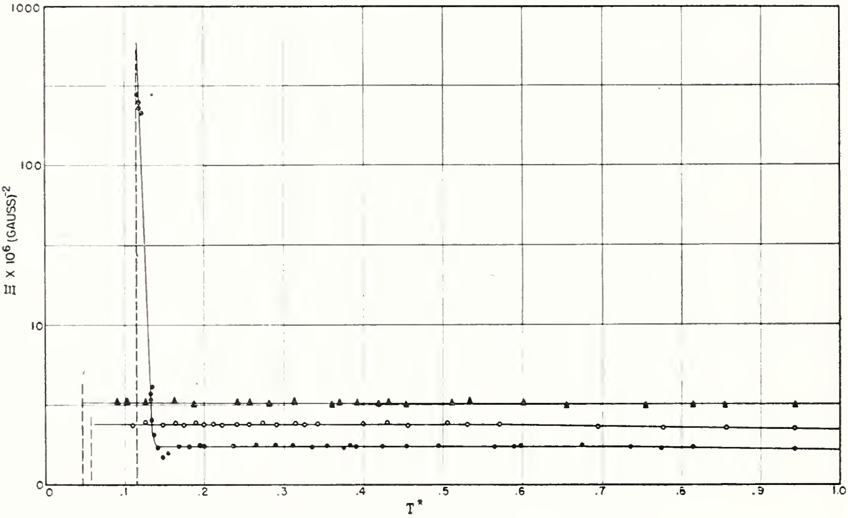

FIGURE 45.2. *Ξ parameter as a function of T^*.*

Dashed vertical lines show T^* final after demagnetizing from same H/T (13.50 kilogauss/degree). ●, Pure cobalt-ammonium-sulfate; ○, Zn diluted; ▲, Mg diluted.

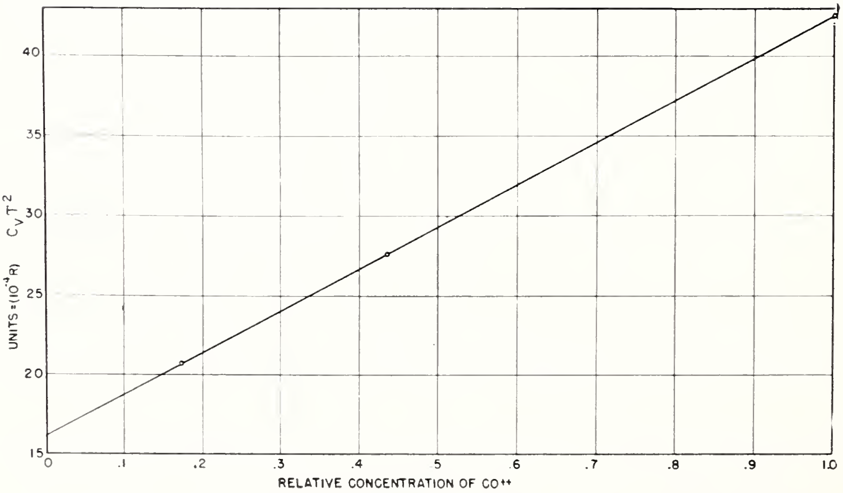

FIGURE 45.3. *Specific heat constant A, as a function of* Co^{++} *concentration.*

is 16×10^{-4}. Because the concentrations of the diluted salts were measured colorimetrically and polarimetrically they are known only to about ±2 percent, thus the intercept may be $A_n=15.9-16.1\times10^{-4}\,R$, in good agreement with the specific heat calculated from microwave data [1].

Table 45.1.

Crystal	Weight	Relative concentration of cobalt	Ξ	Weight of cobalt	A
	g		*Gauss*$^{-2}$	*Percent*	
Pure cobalt-ammonium-sulfate	2. 461	1. 000	2.43×10^{-6}	14. 91	42.55×10^{-4}
Colbalt-ammonium-sulfate diluted with zinc-ammonium-sulfate	2. 729	0. 436	3. 76	6. 5 0. 2	27. 45
Cobalt-ammonium-sulfate diluted with magnesium-sulfate	2. 351	. 174	5. 01	2. 6 0. 1	20. 61

Measurements were made along the K_2 magnetic axis of the single crystals, which were grown from saturated solutions. The Curie constant was measured by using a single crystal of chromium-potassium-alum and measuring its susceptibility in the liquid-helium range. From a knowledge of the chrome-alum Curie constant, and the ratio of the slopes of the calibrating curves for chrome-alum and cobalt-ammonium-sulfate, one could determine the Curie constant for cobalt-ammonium-sulfate. This was determined experimentally to be 0.858 as compared with a calculated value of 0.854, using $S=\frac{1}{2}$, and a g-factor [1] of 3.0.

Demagnetizations were made along the K_1 magnetic axis, using the transverse field of an electromagnet. From demagnetization data one can calculate entropy removals, and the experimental points are found to lie along a curve (see fig. 45.4) fitted by using a g-factor of 6.5

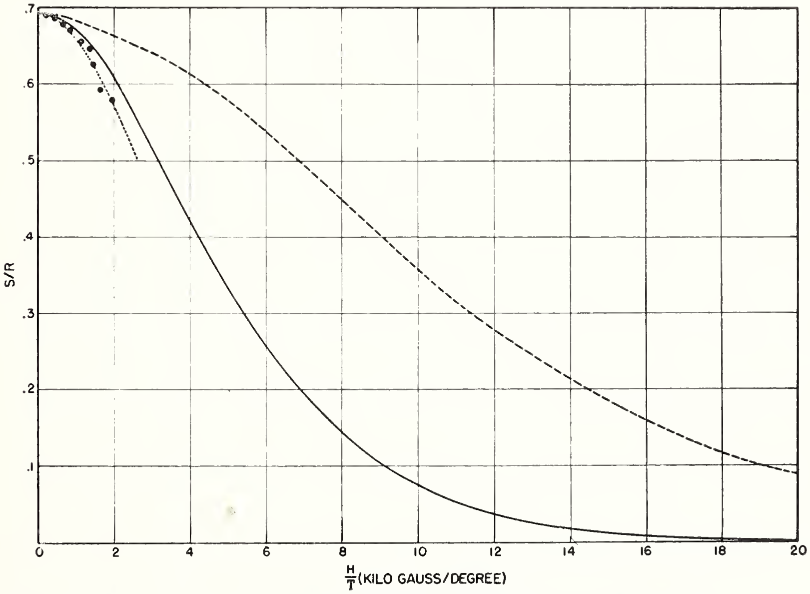

Figure 45.4. *Entropy of electronic system in cobalt-ammonium sulfate,* $Co(NH_4)_2(SO_4)_2\cdot6H_2O$.

———— K_1 axis ($g=6.2$); - - - - - - - K_2 and K_3 axes ($g=3.0$); . . . . experimental ($g=6.55$).

rather than the 6.2 calculated from microwave data [1]. The entropy curves are calculated from the formula

$$\frac{S}{R}=\ln 2 \cosh \frac{\beta}{2kT} \sqrt{(g_{ik}H_k)^2}=\frac{\beta}{1kT} \sqrt{(g_{ik}H_k)^2} \tanh \frac{\beta}{2kT} \sqrt{(g_{ik}H_k)^2}, \qquad (2)$$

where S=entropy, β=Bohr magneton, k=Boltzmann constant, R=gas constant, g_{ik}=tensorial g-factor.

If one assumes a Curie-Weiss law for the susceptibility ($\chi=C/T-\Delta$), then the Garrett parameter has the form

$$\Xi=\frac{C}{A}\left(1+\frac{\chi\Delta}{C}\right)^3 \qquad (3)$$

so that a plot of $(\Xi)^{1/3}$ against susceptibility should be a straight line whose slope gives Δ. From figure 45.2, it is seen that such a plot gives a $\Delta \leq 0.002°$ K along the K^2 axis.

In figure 45.5 is shown a plot of the warm-up curve for pure cobalt-ammonium-sulfate. It can be seen that the salt becomes antiferromagnetic. The temperature at which χ'' appears, i. e., at which hysteresis absorption commences is ~0.125° K, which is precisely the the same temperature at which the Garrett parameter increases suddenly (due to saturation effects, see fig. 45.2.) The maximum in the real part of the susceptibility occurs at ~0.092° K. It will be observed in figure 45.5 that a slight change in slope of both χ' and χ'' occurs at about 10 minutes, which would seem to indicate that one is over the Curie-point specific-heat hump. The results were quite reproducible as the heating in this region was due only to the hysteresis absorption, the "natural heat leak being ~0.06 erg/sec.

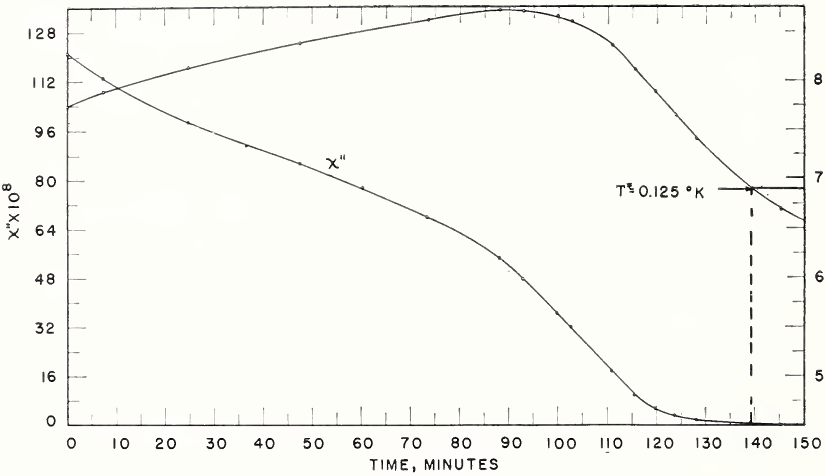

FIGURE 45.5. *Reproducible warm-up curve for pure cobalt-ammonium-sulfate.*

Observing now that the Δ is too small to make itself felt at 0.09° K, one can assume that exchange forces are negligibly small. In this case the remainder of the measured specific heat $[(42.55-16)\times 10^{-4}R]=26.5\times 10^{-4}R$ can be ascribed to dipole-dipole coupling. As exchange appears to be too small to account for the antiferro magnetism, one is forced to look for another mechanism. That mechanism presumably is dipole-dipole coupling.

As is well known, dipole-dipole interaction is usually not amenable to nearest neighbor calculations, but the results of such a calculation in the present case bring such remarkable agreement with experimental results that they are reported herewith.

The difference between the present calculation and previous ones is that the magnetic ion is not placed in a spherical cavity but rather in an ellipsoidal cavity, that is to say, there is a preferred direction in the lattice, the ellipsoidal cavity having the same eccentricity as the g-factor ellipsoid. Considering the extreme anisotropy of the crystal and the strong LS coupling in this salt [5], such a model is not as naive as appears at first glance.

It is useful to define a local field, H_{loc}, the magnitude of which can be derived from $(H_{\mathrm{loc}})^2$, the average of the square of the internal field acting on an ion. This internal field arises from magnetic neighbors and is given by:

$$H_{\mathrm{loc}}{}^2 = 2g^2\beta^2 S(S+1)\sum_{i>j} r_{ij}{}^{-6}, \tag{4}$$

where β is the Bohr magneton, $S=\frac{1}{2}$ for cobalt-ammonium-sulfate [5], and r_{ij} is the distance between the ith and jth atoms.

Utilizing the preferred direction notion, a field is acting on the ion i, and it is necessary to consider only the contribution of the large g-factor along the K^1 axis, i. e., $g=6.5$. The locations of nearest neighbors are shown in table 45.2.

TABLE 45.2.

$a=9.25$ A, $b=12.5$ A, $c=6.2$ A are unit cell dimensions and $d^2=(a^2+b^2)/4$; $\delta=84°$; all taken from crystallographic data of Hofmann [6]

Number of ions	Location	Distance		H_{loc}
				Gauss
4	$1/2\sqrt{a^2+b^2}$	7.78	nearest neighbors	522
2	c	6.2		
2	b	12.5	next nearest neighbors	310
4	$\sqrt{d^2+c^2+2c^2d^2\cos\delta}$	9.95		
4	$\sqrt{d^2+c^2-2c^2d^2\cos\delta}$	9.95		

As seen in figure 45.6, the assumption of dipole-dipole induced antiferromagnetism provides exactly the proper conditions for alinement of adjacent spins, in opposite directions. Figure 45.6 (a) is a view of the *ac* plane in which K_1 lies (K_1 was determined experimentally to be the short diagonal of the parallelogram represent the *ac* face), and figure 45.6 (b) is a view of the *ab* plane perpendicular to the K_1 axis.

Considering only six nearest neighbors, H_{loc} is found to be 522 gauss.

Inclusion of the 10 next-nearest neighbors and assumption of antiferromagnetic alinement of spins gives a $H_{\mathrm{loc}}=310$ gauss, which corresponds to $aT_c=0.087°$ K, very close to the susceptibility maximum. Inclusion of further neighbors comes in a rapidly converging series, and the T_c would be slightly higher than 0.09° K.

Whether such calculations will prove fruitful for other types of cobalt salts is not yet clear. Measurements on $CoSO_4{}'7H_2O$ have been made by Fritz and Giauque [8], but their experiments go down

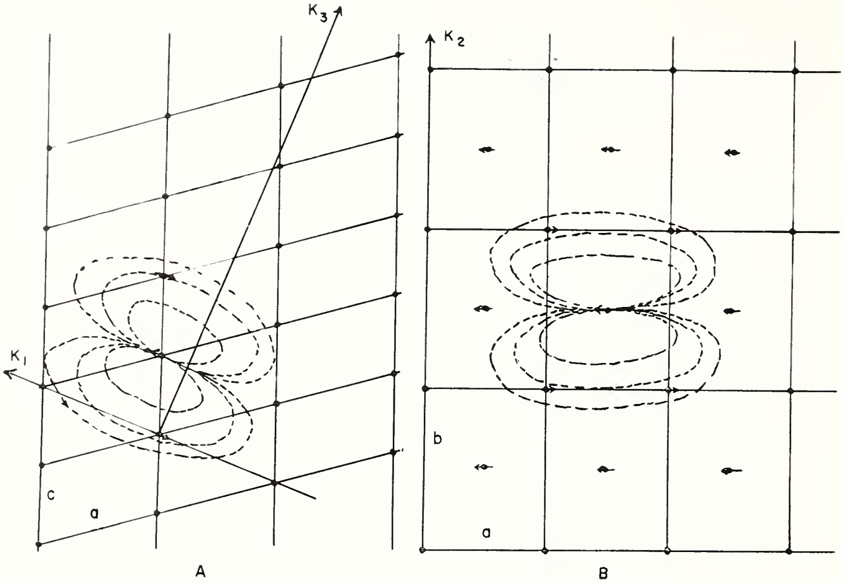

FIGURE 45.6. *Crystallographic diagram for cobalt-ammonium-sulfate.*

only to temperatures of 0.16° K, above the temperature at which dipole-dipole antiferromagnetism should appear. Preliminary calculations show that such an effect should occur in $CoSO_4'7H_2O$ at temperatures of the order of 0.05° K. Such a calculation is necessarily rough because of the lack of specific crystallographic data [9] on $CoSO_4'7H_2O$.

A similar calculation for $CcCl_2$ where the strong electric fields due to the halogens surrounding the Co^{++} might give an orbital quenching effect similar to that found in hydrated salts gives Curie temperatures an order of magnitude too low. It is possible that the effect is due to an accident of crystal structure, being peculiar to crystals of magnetic tetragonal symmetry.

The experimental work described herein was done on a fellowship from the Oak Ridge Institute of Nuclear Studies, for whose assistance the author is deeply grateful.

[1] B. Bleaney and J. Ingram, Nature **164,** 116 (1949).
[2] B. Bleaney, Phys. Rev. **78,** 214 (1950).
[3] R. J. Benzie and A. H. Cooke, Nature **164,** 837 (1949).
[4] C. G. B. Garrett, Thesis, Trinity College (1949).
[5] M. H. L. Pryce, Proc. Phys. Soc. **63** [A], 25 (1950); Nature **164,** 116 (1949).
[6] W. Z. Hofman, Kristalogr. **78,** 279–333 (1931).
[7] J. H. Van Vleck, Theory of electric and magnetic susceptibilities, p. 285 (Oxford University Press).
[8] J. J. Fritz and W. F. Giauque, Jr., Am. Chem. Soc. **71,** 2168–75 (1949).
[9] Wyckoff, Structure of crystals, p. 318 (Chemical Catalog Co., Ind. Ed.).

46. A New Effect Found in Paramagnetic Crystals Below 100 Millidegrees Absolute: The Critical-Field Curve Bounding the Antiferromagnetic State

by C. G. B. Garrett [1]

Introduction

The purpose of this paper is to summarize the evidence for the existence of "critical-field" phenomena in antiferromagnetic crystals, considering in particular the results of some magnetic measurements made at temperatures below 1° K on a single crystal of cobalt-ammonium sulfate [1].[2] This material is of interest because the spins, due to large spin-orbit coupling and a tetragonal electric crystalline field, are extremely anisotropic. There are two sets of ions in the crystal, but one of the macroscopic magnetic axes (the K_1 axis) is only 33° away from the directions of "easy magnetization" of the spins in either set. There is thus one direction in the crystal along which alinement is most likely to occur, and hence this material is a particularly favorable case if one is interested in studying the way in which alinement occurs and how such alinement behaves under the influence of parallel or perpendicular magnetic field.

First, it will be necessary to summarize the experimental results for this particular material. Then an attempt will be made to interpret these results along the lines of existing theories of the antiferromagnetic state, and, finally, tentative conclusions may be drawn as to the possibility of similar phenomena being found in other materials showing antiferromagnetic properties.

Experimental Results for Cobalt Ammonium Sulfate

A spherical crystal of cobalt-ammonium sulfate was cooled to temperatures below 1° K by means of the technique of magnetic cooling. Absolute temperatures were estimated by standard methods, and measurements were made of the a-c magnetic susceptibility and its dependence upon steady parallel field. The results of interest in connection with the critical-field phenomena are those along the K_1 axis (details are given in [1]). It was found that along this axis the a-c susceptibility for very small fields decreased sharply with temperature below the Curie point, but that the superposition of a steady parallel field produced an increase in susceptibility up to quite a sharp maximum in a field of the order of a few hundred gauss. The true nonlinearity in susceptibility has to be disentangled from effects due to magneto-caloric warming or cooling, but these are comparatively small at temperatures below the Curie point, and may be allowed for. From these measurements an H-T "phase diagram" may be constructed (fig. 46.1) showing lines of constant magnetization (isochores)

---

[1] Lyman Laboratory of Physics, Harvard University, Cambridge, Mass.

[2] Figures in brackets indicate the literature references on p. 233.

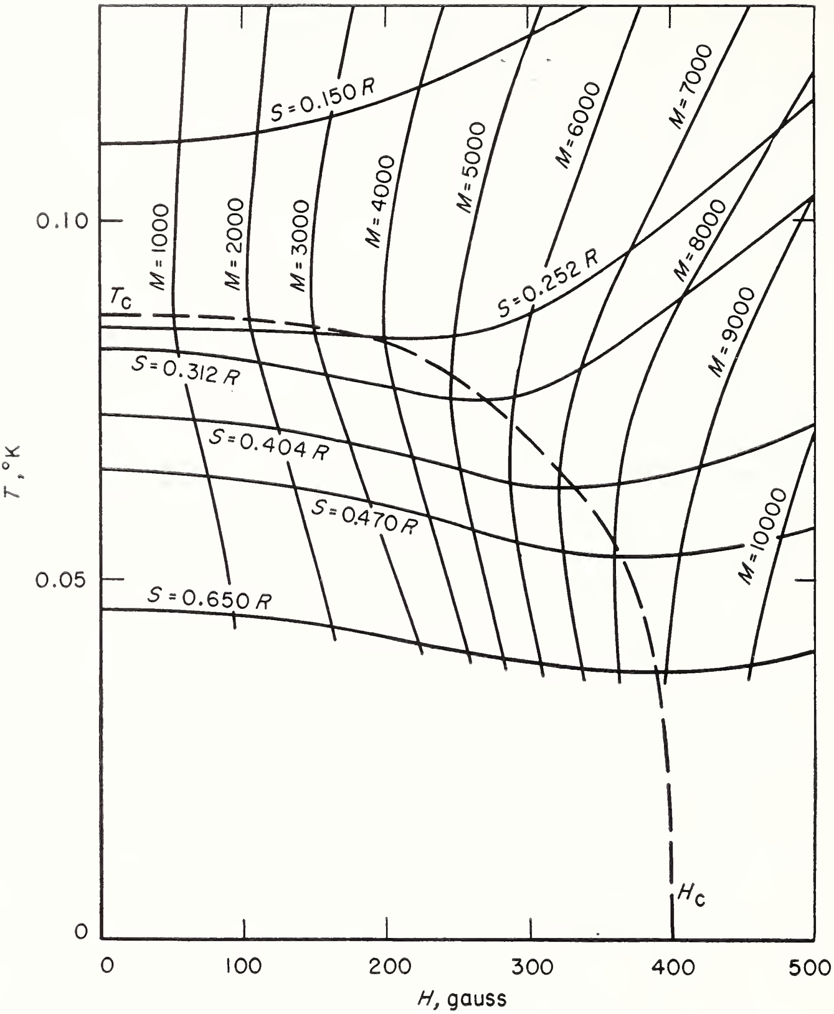

Figure 46.1. *"Phase-diagram" for cobalt-ammonium sulfate.*

and lines of constant entropy (isentropics). The minima in the isochores coincide with the minima in the isentropics—as must necessarily be so from general thermodynamical arguments—and correspond roughly with the above-mentioned peaks in the a-c susceptibility.

Qualitatively the interpretation of the experimentally determined phase diagram is that outside a certain critical curve (the locus of the minima in the isochores and in the isentropics) the material is behaving very much as any simple paramagnetic material should behave; the susceptibility is increasing with decreasing temperature, as the ordering effect of a magnetic field is competing more and more successfully against the disordering effect of thermal agitation, while at any one temperature the entropy (disorder) of the system decreases progressively with the application of a stronger and stronger field. But inside the critical curve the behavior is anomalous, in that neither of these statements is correct.

Theoretical Models

Usually the appearance of antiferromagnetism in a material is associated with exchange interaction between the magnetic ions. What is not clear is whether in a crystal in which exchange effects are small or altogether absent ferromagnetism or antiferromagnetism might be produced by dipole-dipole (magnetic) interaction alone. That the anomalous properties of cobalt-ammonium sulfate are antiferromagnetic in origin follows both from the general similarity between the behavior of this material and that of materials like manganese oxide and manganese selenide with transition points at much higher temperatures [2], and from the observed fact that within the critical curve the entropy increases during isothermal magnetization, indicating a competition between a tendency to antiparallel alinement in zero field and the necessity for parallel alinement in a large field. Also it appears from a quantitative study of the specific heat of cobalt-ammonium sulfate (see [1] for details) that exchange is considerably smaller than dipole-dipole interaction in this crystal. But at the present time it is not possible to assert that the antiferromagnetic transition point in cobalt-ammonium sulfate is really due to dipole-dipole interaction rather than exchange. It is therefore necessary to consider from the theoretical point of view both possible mechanisms.

Dipole-Dipole Interaction

Sauer [3] and Luttinger and Tisza [4] have made calculations on the lowest energy state of a paramagnetic crystal at absolute zero and in zero field, on the assumptions of cubic symmetry and taking account only of dipole-dipole interaction between the ions. The answer is shape-dependent; for a long ellipsoid the lowest state appears to be the parallel one (ferromagnetism), whereas for a sphere the lowest state is antiparallel. Sauer and Temperley [5] have developed, on the basis of Sauer's calculations, a simple Bragg-Williams model to take account of nonzero fields and temperatures. They find that the appearance of the ordered state is confined to the region of low fields and temperatures by a critical curve very much of the form found experimentally for cobalt-ammonium sulfate; they also predict a maximum in the differential susceptibility qualitatively the same as that found, and their numerical values for the critical temperature (for zero field) and critical field (at absolute zero) are in agreement within a factor of 2 with those found, respectively by direct measurement and by extrapolation. Unfortunately, there are serious points of disagreement between experiment and Sauer and Temperley's theory, quite apart from any distrust one might have for the sweeping assumptions made in the theoretical treatment. The most serious trouble is that Sauer and Temperley expect that the transition should change from second to first order at temperatures below two-thirds the critical temperature. In practice, the transition is found to be smooth (second order at least) down to 0.4 T_C, the lowest temperature accessible experimentally. However, in default of any more elaborate theory of dipole-dipole antiferromagnetism, we may say that Sauer and Temperley's model gives a reasonable qualitative account of the properties of cobalt-ammonium sulfate, and in particular would lead one to interpret the critical curve as the limit of the ordered (antiparallel) state of the material.

Exchange Interaction

Van Vleck [6] has proposed a simple model of antiferromagnetism for a material in which exchange is the dominant ordering factor. On his theory in its simplest form the lattice is divided into two sublattices, and the spins in either sublattice sit in an "effective field", the vector sum of the externally applied field and an interaction field proportional to the average spin of the ions in the other sublattice. van Vleck himself considered only the application of external fields small in comparison with the internal fields due to "spontaneous antiferromagnetism," but his theory may easily be extended to the case of strong fields (Garrett, to be published). Again, one finds the appearance of a critical-field curve. Inside the curve the most stable state is that in which the average spins of the ions in the two sublattices are unequal (in zero field, numerically equal but of opposite sign), whereas outside the critical curve the average spins in the two sets are equal, a Curie-Weiss law being followed for small fields.

Applying this theory to cobalt-ammonium sulfate, supposing for the moment that here, too, exchange is dominant so far as the cooperative phenomena are concerned, it may be noted that agreement with experiment is rather better than Sauer and Temperley's theory in two respects: (1) the numerical value of $\mu H_C/kT_C$ is closer, and (2) the general form of the transition is better represented, in that on van Vleck's theory the transition should be second order at all temperatures.

The general conclusion of this section is that one would expect some sort of critical curve on the assumption either of dipole-dipole interaction or of exchange. In either case, we are concerned with the appearance of what is effectively a "condensed phase," so that in some ways the problem is formally similar to the problems of superfluidity and superconductivity. At the present time we have to be content with what are really no more than semidescriptive models for the way in which dipole-dipole interaction and exchange can set up ordering in the crystal, so that perhaps one must not be disappointed if at the present stage quantitative agreement between theory and experiment is impossible to attain.

Critical Curve in Other Materials

If the theoretical arguments outlined on p. 231 are correct, we should also expect to find critical-field phenomena in any other antiferromagnetic—remembering that it is essentially a directional property, associated with the direction of easy magnetization in a single crystal. On any theory, or indeed on quite general arguments, one expects that the ratio $\mu H_c/kT_c$ should be of the order of unity. This enables us to predict the order of magnitude of the critical fields for typical materials. For salts used in magnetic cooling experiments the fields are of the order of a few hundred gauss. For materials like manganese oxide or selenide, with transition points of about 100° K and spins with moments again of the order of a Bohr magneton, the critical field would be of the order of 5.10^5 gauss, that is to say, well outside the range of fields experimentally obtainable. One should, however, be able to detect a small lowering of the transition point for these materials on applying a field of the order of 10^4 gauss, and such a lowering has actually been reported by Squire. Finally, it is of interest to speculate on the possible behavior of a nuclear paramagnetic material, such as lithium fluoride at temperatures of the order of the microwave line width (10^{-6} °K). If these materials turn out to be antiferromagnetic at a temperature of this order, we should expect critical-field phenomena, the critical field at the absolute zero being about 1 gauss. This, incidentally, emphasizes the importance of using only a minute magnetic field for measurement of susceptibility in a nuclear demagnetization experiment.

Conclusion

The properties of cobalt-ammonium sulfate, found from experiments below 1° K, strongly suggest that some sort of critical-field phenomenon may play an important part in all antiferromagnetic materials. Further information is now required on this and on other similar salts. Particularly informative would be a systematic survey of the influence of magnetic dilution and of sample shape on the antiferromagnetic properties, and in particular on the critical-field curve as such measurements would be very helpful in deciding whether dipole-dipole interaction or exchange is responsible for the observed ordering effects found in typical paramagnetic salts used in magnetic cooling experiments.

References

[1] C. G. B. Garrett, Proc. Roy. Soc. [A] **206,** 242 (1951).
[2] C. F. Squire, Phys. Rev. **56,** 922 (1939).
[3] J. A. Sauer, Phys. Rev. **57,** 142 (1940).
[4] J. M. Luttinger and L. Tisza, Phys. Rev. **70,** 954 (1946).
[5] J. A. Sauer and H. N. V. Temperley, Proc. Roy. Soc. [A] **176,** 203 (1940).
[6] J. H. van Vleck, J. Chem. Phys. **9,** 85 (1941).

47. A New Experimental Method for the Measurement of Temperature and Entropy at and Below 1° K

by L. D. Roberts and J. W. T. Dabbs [1]

In connection with the nuclear alinement program at Oak Ridge National Laboratory, in which the hyperfine structure coupling [2] [3] is used, it became necessary to determine the behavior of the paramagnetic salts used, especially as to temperature variation with magnetic field during adiabatic demagnetization. Thus, determinations of absolute temperatures in the presence of magnetic fields are required. It appears that the method described here is particularly well adapted to this type of measurement and shows promise of reasonable accuracy.

The well-known expressions given by Casimir [4] and others

$$\Delta T = \int_{H_1}^{H_2} \left(\frac{\partial M}{\partial S}\right)_H dH \text{ and } \Delta S = \int_{H_1}^{H_2} \left(\frac{\partial M}{\partial T}\right)_H dH,$$

where the first integral is taken along an isentropic path, and the second along an isotherm, form the basis for the method. We shall hereafter refer to these as case I and case II, respectively.

In case I the method is as follows: Two identical secondary coils connected in opposition are placed in the highly uniform field of a large solenoid magnet that surrounds the experimental Dewar flasks. In each of these coils a sphere of paramagnetic salt is placed, the two samples being nearly identical, and the relative positions of the samples and coils are so adjusted that the net quantity of charge generated in the secondary circuit, upon switching off a field, H, from the large solenoid, is proportional to the difference in magnetization of the two spheres. With the aid of an auxiliary coil, one isothermally magnetizes the two spheres in slightly different fields, and thus to slightly different entropies at ~ 1° K. This known entropy difference (calculated from the Brillouin function, or measured, as in case II) now remains constant after the system is made adiabatic and after the incremental field, ΔH, is switched off.

One then measures the difference in magnetization of the two samples by switching off various magnetic fields, H, and obtains this difference, $\Delta M(H)$, as a ballistic galvanometer deflection. In switching off a field, H, one obtains directly a deflection proportional to the difference in magnetization at field H, and because ΔS is constant the deflection is also proportional to the required partial derivative, $(\partial M/\partial S)_H$, for sufficiently small differences. Now one needs only to perform a numerical integration over the values thus obtained to know the temperature change in going through a given range of magnetic field.

---

[1] Oak Ridge National Laboratory, Oak Ridge, Tenn.

[2] C. J. Gorter, Physica **14**, 504 (1948).

[3] M. E. Rose, Phys. Rev. **75**, 213 (1949).

[4] H. B. G. Casimir, Magnetism and very low temperatures (Cambridge University Press, 1940).

Case II measurements may be carried out in a similar manner, with the only change that the two samples are now held at constant, and slightly different, temperatures, instead of using the auxiliary magnetizing coil. This may be done by means of two liquid He baths. The same type of measurement as in case I now yields the required partial derivative, $(\partial M/\partial T)_H$, and a similar integration gives the entropy removed by the application of a given field in the isothermal magnetization process.

Equipment has been built for the case I measurements and preliminary results are promising.

48. Some Laboratory Aids to Cryomagnetic Research

by Warren E. Henry[1]

Some of the design principles and characteristics of three laboratory devices will be briefly discussed, namely, (1) a metal cryostat for liquid helium, (2) a control chamber, and (3) a tension limiting lift.

Our interest in metal cryostats arose from the need, in cryomagnetic research, of maximum experimental working space for limited total space in a high magnetic field, as in the Bitter magnets.[2] The plausibility of a contemplated Dewar design requires a consideration of the following heat sources: (1) Radiation (a) from the top of the Dewar, (b) from the radiation shield. (2) Gaseous conduction and convection. (3) Conduction down the walls of the Dewar.

For experimental Dewars of reasonable size (say 1 to 2 liters) to be used for a few hours of operating time, one can reduce the heat leak due to the first two sources to an unobjectionable minimum. The effect of (3) can be calculated by a finite difference technique, using the rough thermomechanical model shown in figure 48.1. The vertical axis is temperature, which is single-valued in X; the horizontal arrows represent heat flow, $\dot{Q}$, and the vertical arrows represent mass flow, $\dot{M}$. The cells, R_i, are all cylinders of equal volume in the mixed space. The quantity of heat, $\dot{Q}_i$, coming from the walls pushes the mass, $\dot{M}$, up into the next cell. Now, if we take an arbitrary temperature interval, ΔT_0, as the temperature difference between adjacent cells, the corresponding coordinate space interval is X_0 for the top cell, X_1 for the next, and so on. The X's are in general not equal. The length of the heart (thin-walled part) of the Dewar is given by

$$l=\sum_0^N X_n \tag{1}$$

The problem is simplified by choosing

$$\Delta T_0=T_n-T_{n+1}=\text{constant}. \tag{2}$$

The heat flow rate into cell R_i is given by

$$\dot{Q}_i=\dot{M}C_p\Delta T_0 \tag{3}$$

the index being left off of the C_p, the heat capacity of the gas, because of the reasonable constancy of it throughout the temperature range. Knowledge of this quantity makes it possible to write down a recursion formula relating the heat flow down the walls of adjacent cells,

$$\dot{H}_n=\dot{H}_{n+1}+\dot{M}C_p\Delta T_0, \tag{4}$$

---

[1] Naval Research Laboratory, Washington, D. C.

[2] F. M. Bitter, Rev. Sci. Instr. **10**, 373 (1939).

the total heat flowing into the Dewar being given by

$$\dot{H}_0=\sum_{n=0}^{N}\dot{M}C_p(T_n)\Delta T_0+\dot{M}L=\dot{M}[C_p(T_0-T_n)+L]=\frac{K_0A\Delta T_0}{X_0}, \tag{5}$$

where $N+1$ is the number of cells, K_0 is the thermal conductivity of the walls of the top cell, A is the cross-sectional area of the wall, and L is the heat of vaporization of the liquid at the boiling point. From eq (5) one may calculate X_0, the depth of the first cell. This done, the calculation of the entire depth of the Dewar is carried out from

$$l=\sum_0^N X_n=X_0\left[1+\sum_0^{N-1}\frac{N+1+\alpha}{N-n+\alpha}f_n(T)\right], \tag{6}$$

use having been made of a recursion formula relating adjacent X's derived from (4). K_n is the thermal conductivity in the nth cell,

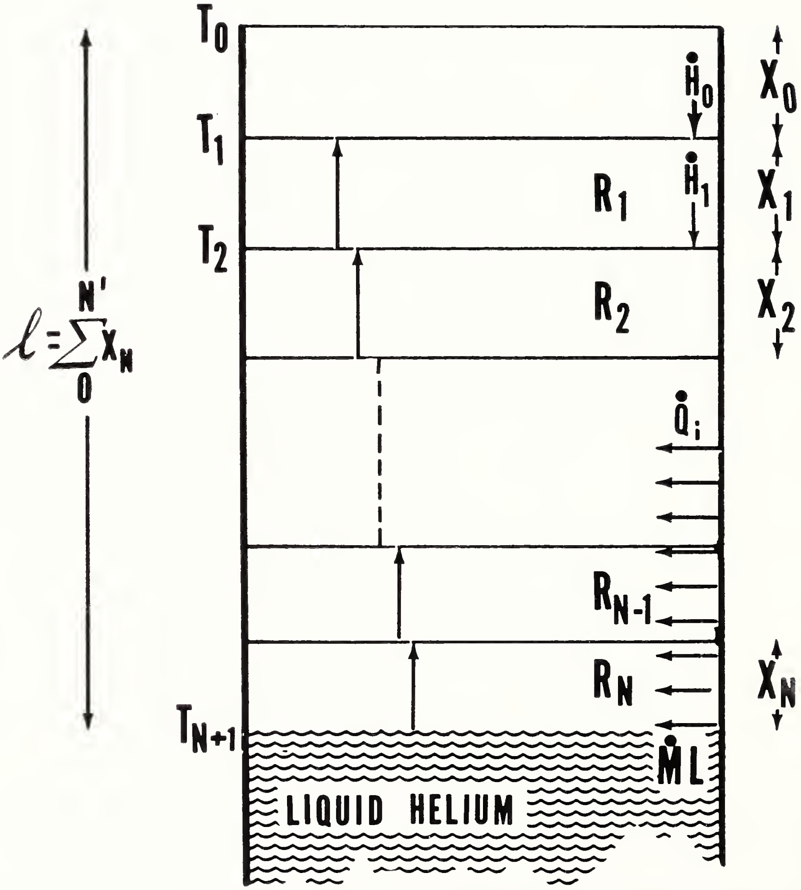

FIGURE 48.1. *Thermomechanical model of a liquid-helium container for analyzing a heat-flow problem with good exchange.*

The independent variable is T. Direction of heat flow from walls to gas is nearly horizontal and the mass flow is vertical.

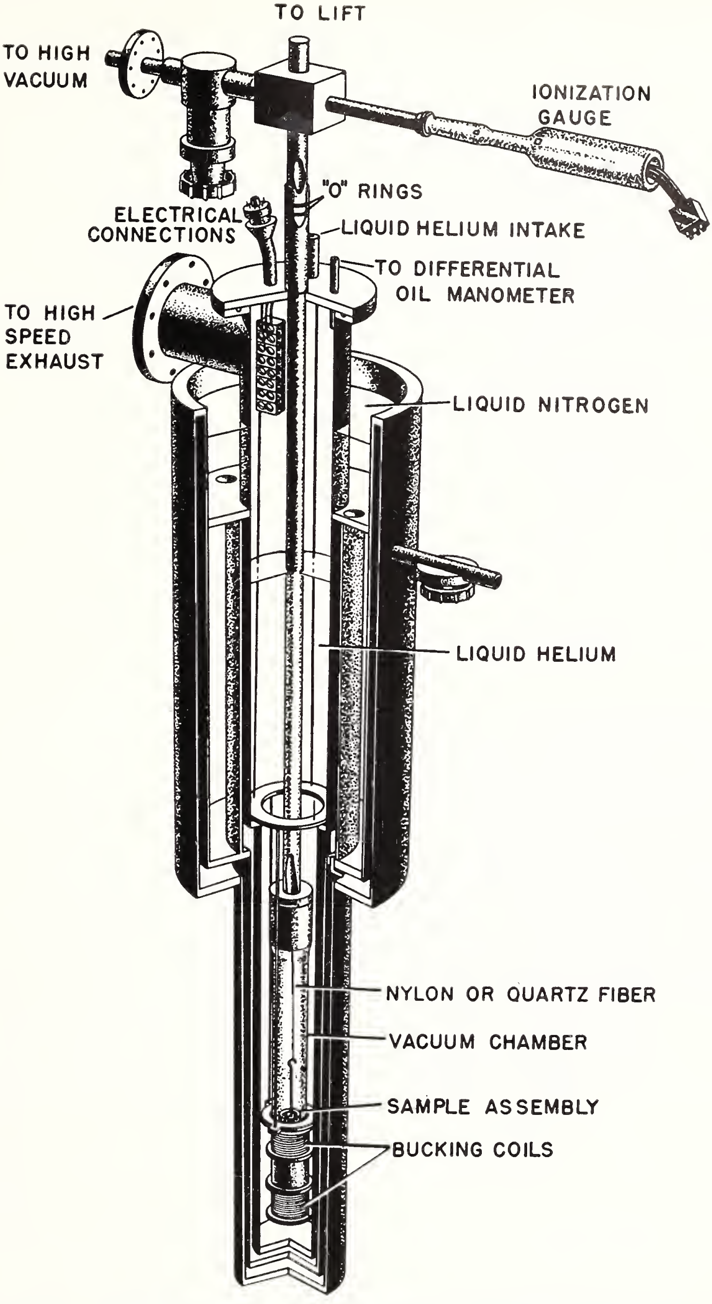

FIGURE 48.2. *Metal cryostat for liquid helium with movable high-vacuum sample assembly.*

Initial low temperatures are produced by rapid pumping on liquid helium. "○" rings prevent loss of vacuum over helium during vertical motion of lift.

and α is determined by the ratio between the heat of vaporization and the heat capacity of the helium over the range. $f_n(T)$ corrects for the change in thermal conductivity with temperature and is the ratio between the thermal conductivity at T_n and K_0. If this ratio is assumed $=1$, an upper value of l is calculated.

Computations are simplified and at the same time made more exact by the assumption of linear variation of thermal conduction with temperature. This assumption is justified both theoretically [3] and experimentally [4] for certain types of low-conductivity alloys.

A Dewar was designed on this basis, and a leak rate of about 35 cm^3/hr was observed. This 4-inch Dewar, through open pumping, reached a temperature of 1.1° K, and is shown in figure 48.2. A description of a $1\frac{1}{16}$-inch Dewar designed to fit into the $1\frac{1}{8}$-inch Bitter magnet is to be found elsewhere.[5]

The second device is a control chamber (similar in general design principle to a chamber developed independently by Ketchen [6]) for protecting experimental samples of reactive materials during preparation and assembly in a controlled atmosphere. The sample container is placed in a special antechamber, which is flooded with inert gas, evacuated, and then filled with the gas. (This precaution is to reduce the hazard and loss due to explosion of the sample container.) This antechamber is then placed in the main control chamber with gloves installed, as shown in figure 48.3. Now with the transparent 1-inch Lucite plate in place (sealed off by a rubber gasket and grease) and the gloves covered, the chamber and the gloves are simultaneously

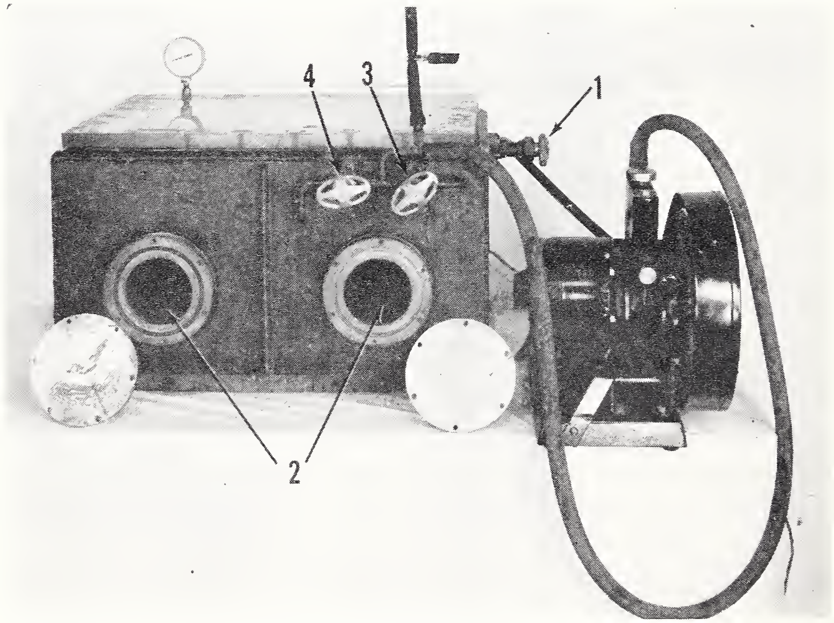

FIGURE 48.3. *Controlled atmosphere chamber.*

(1) Gas-inlet valve for flushing; (2) portholes to gloves; (3) control valve for chamber; (4) control valve for gloves.

---

[3] A. H. Wilson, Proc. Camb. Phil. Soc. **33**, 371 (1937).
[4] J. E. Zimmermann, Bul. Am. Phys. Soc. **26**, 13 (1951).
[5] W. E. Henry and R. L. Dolecek, Rev. Sic. Instr. **21**, 496 (1950).
[6] E. E. Ketchen, F. A. Trumbore, W. E. Wallace, and R. S. Craig, Rev. Sic. Instr. **20**, 524 (1949).

evacuated and simultaneously filled to 1 atmosphere of an inert gas. The glove covers are removed, and sample manipulation can begin. The design problem here consists in providing convenience for manipulation and strength to withstand the outside pressure since the chamber is 24 by 18 by 12 inches.

We come now to the third device. In making magnetic measurements, such as differential moment measurements, it is sometimes advantageous to effect a precise displacement of a sample with respect to a coil or coil system. Figure 48.2 shows such a situation, where the sample shown must be subjected to a precise vertical motion. If the motion must take place within a short time by means of a suspension that can only withstand a limited tension, a special lift is desirable.

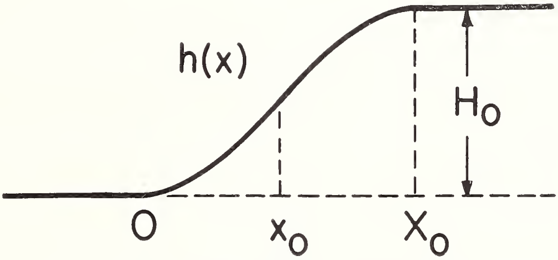

FIGURE 48.4. *Curve for path of a point in the vertical shaft of the lift assembly in the coordinate system of the horizontally propelled carriage.*

Let us consider a desired displacement, H_0, shown in figure 48.4, to be achieved though a horizontal displacement, X_0. Make $\dot{x}$ constant. Then, for a bounded acceleration, and therefore a limited tension, the vertical motion may take place in two steps: (1) acceleration from 0 to x_0 and (2) deceleration from x_0 to X_0 to prevent a jerk at the end of the excursion. The analytical form of the function $h(x) \leq H_0$, is

$$h(x) = \begin{cases} 0 & ; \quad x \leq 0 \\ \dfrac{A_{\max} x^2}{2} & ; \quad 0 \leq x \leq x_0 \\ H_0 - \dfrac{g}{2}(X_0 - x)^2; & \quad x_0 \leq x \leq X_0 \\ H_0 & ; \quad X_0 \leq x \end{cases}$$

where $A_{\max}$ is the maximum acceleration, and g is the acceleration of gravity.

The horizontal motion is produced manually, but a motor could be used. A schematic diagram of the lift assembly is shown in figure 48.5. This lift is connected to the sample container, which is moved with respect to the coils in the liquid helium shown in figure 48.2.

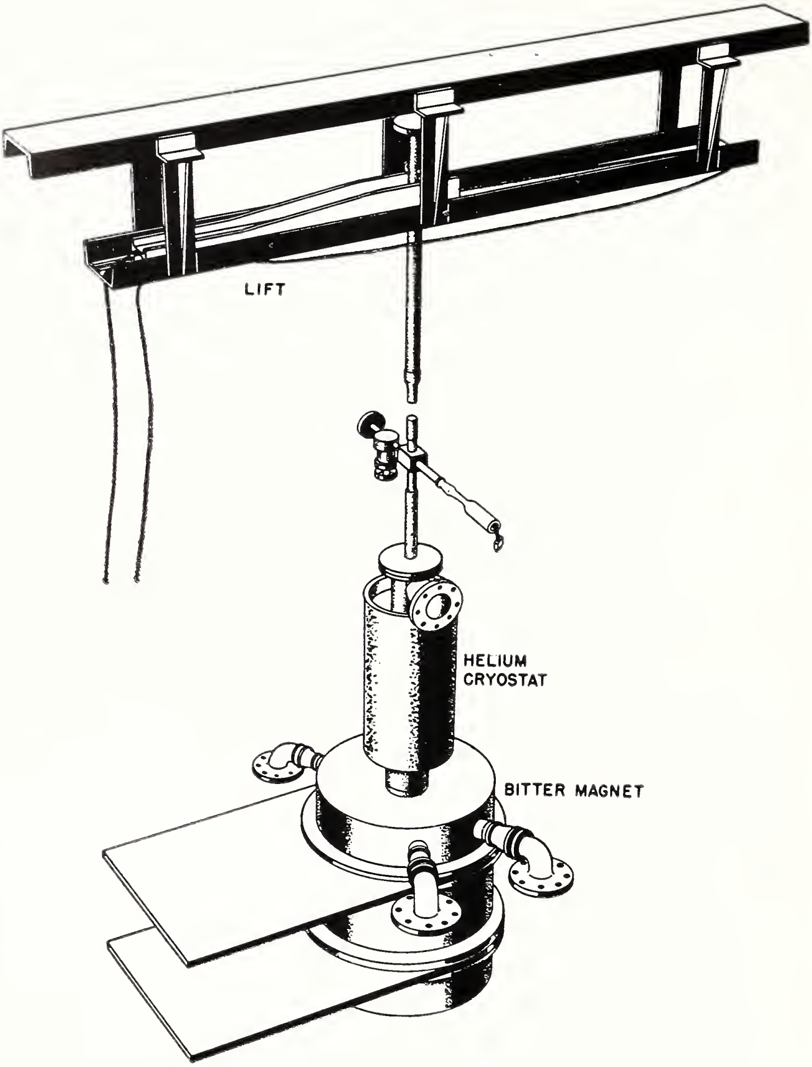

Figure 48.5. *Complete lift assembly.*

49. Current Sensitivity and Other Characteristics of Metal Films at Low Temperatures

by A. van Itterbeek [1]

A few years ago in cooperation with L. de Greve [2] I found that nickel films possess a negative temperature coefficient. In figure 49.1 is shown the resistance of a nickel film as a function of temperature. The position of the minimum on this curve depends strongly on the thickness of the film and the condition of formation of the film (condensed in vacuum or sputtered in different kinds of gases). Further, we observed that at low temperatures the resistance is a function of the current (see fig. 49.2), whereby the resistance decreases as the current is increased.

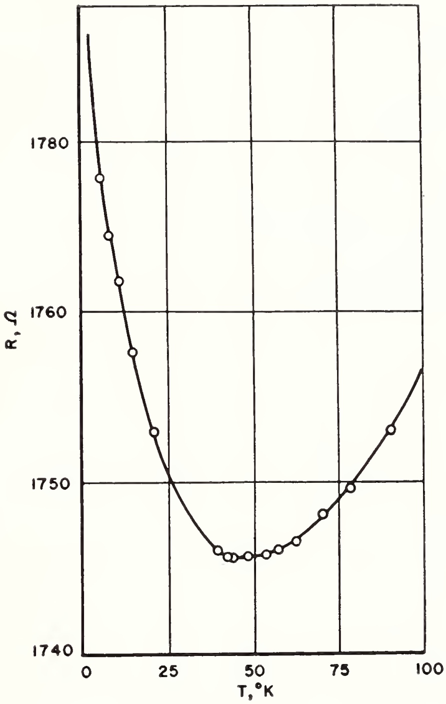

FIGURE 49.1. *Resistance of thin nickel films as a function of temperature.*

In 1950 we measured, together with Dr. de Greve and M. Lambeir,[3] the electric resistance of thin iron films as a function of temperature, and we also found that the behavior of the iron films is the same as that of nickel films (see fig. 49.3).

---

[1] Laboratory of Low Temperatures and Technical Physics, Louvain, Belgium; Kamerlingh Onnes Laboratory, Leiden, The Netherlands.

[2] A. van Itterbeek and L. de Greve, Experimentia **3**, No. 7 (1947).

[3] A. van Itterbeek, L. de Greve, and R. Lambeir, Med. Kon. VI Acad **12**, No. 1 (1950).

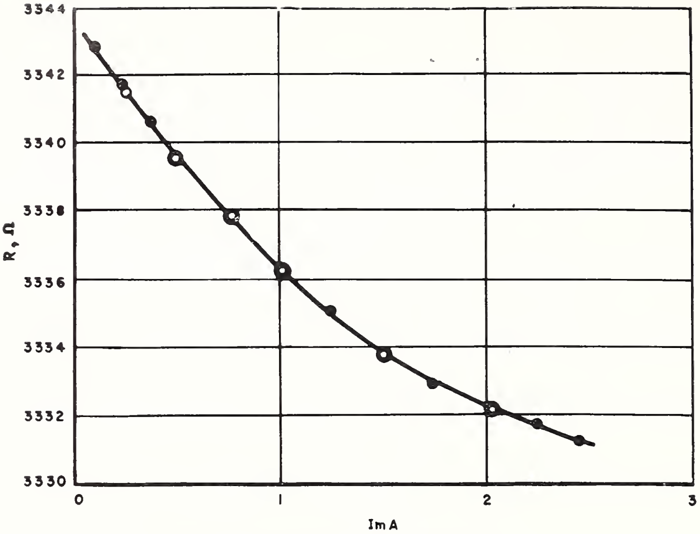

FIGURE 49.2. *Current dependence of the resistance of a thin nickel film.*
Thickness: 47 mμ; T=54.3° K; ●, increasing intensity of current; ○, decreasing intensity of current.

The appearance of a negative temperature coefficient for thin metal films has also been observed by Vodar and collaborators [4] for other metals, such as platinum and tungsten. For those metals, however, the phenomenon appears only for very thin films (a few angstroms), whereas for the ferromagnetic films the temperature coefficient becomes negative for films with a thickness of about a 1000 A.

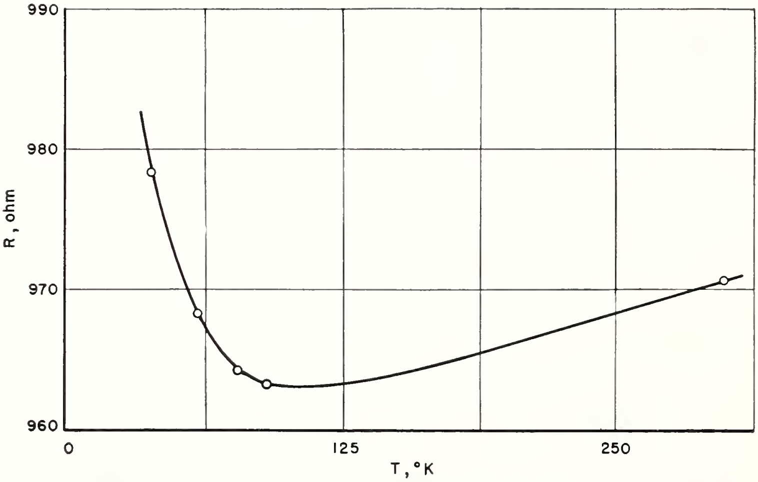

FIGURE 49.3. *Resistance of thin iron film as a function of temperature.*

In 1950 we especially investigated in Leiden, with R. Lambeir and G. J. van den Berg,[5] how at liquid-helium temperatures the electric resistance depends upon the current intensity. Thus we observed a

---

[4] N. Moscovitch and B. Vodar, Compt. rend. **230,** 934 (1950).
[5] Publication in Physica pending.

very steep decrease of the resistance by increasing the current or the electric field (see figs. 49.4 and 49.5). For these experiments the metal films were dipped into liquid helium. This decrease depends strongly on the temperature and the thickness of the film. From figure 49.5 we see that this decrease is about 60 percent at 2.1° K for a film of about 300 A, whereas it is only 6 percent at 1.4° K for a film of about 3000 A.

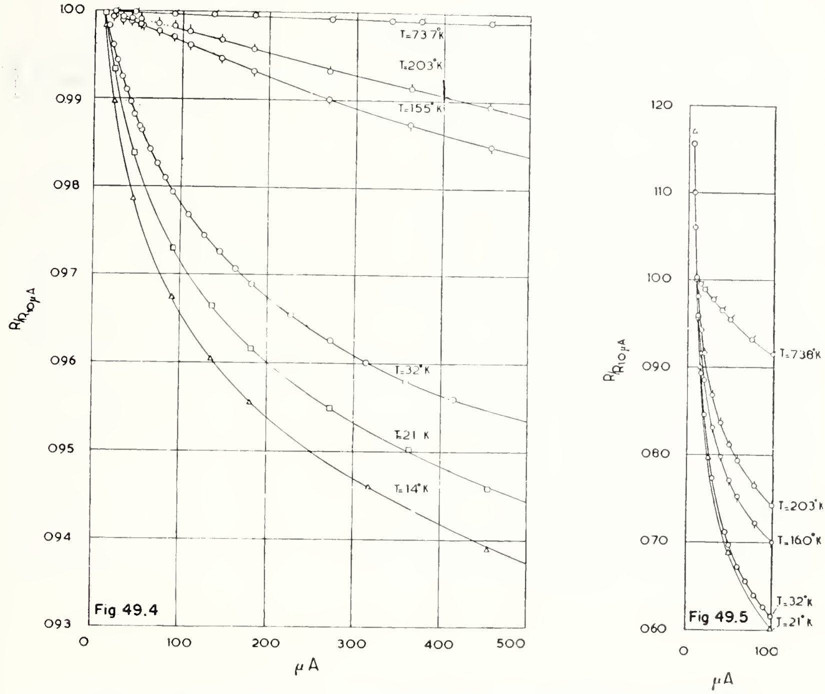

Figures 49.4 and 49.5. *Current dependence of thin film resistance.*

New measurements that we made recently revealed that for still thinner films the decrease of the resistance can reach about 300 percent for currents smaller than 1μa, so that it is practically impossible to determine the value of the electric resistance for a current zero. These last films are obtained by condensation in vacuum. In order to explain this steep decrease, C. J. Gorter suggested that the electric resistance would depend, just as for a semiconductor, upon an activation energy that is comparable with kT at very low temperature. This activation energy would determine the condition for the electrons to jump between the small grains of which the thin films are built up. This agrees with the picture given by Cabrera and Terrien [6] concerning the structure of the films.

We observed pictures and also electron diffraction diagrams of our nickel and iron films by means of the electron microscope at the laboratory of Louvain. Thus we could observe that our films of iron (fig. 49.6) are very amorphous. Pictures taken from silver (fig. 49.7), tin, or gold films, however, differ completely from the structure of the films of metals with a high melting point. The grains are

---

[6] N. Cabrera and J. Terrien, Rev. optique 28, 635 (1949).

larger and probably separated by a layer a few molecules thick. The electron diffraction rings of these films are very sharp compared with those of the iron films.

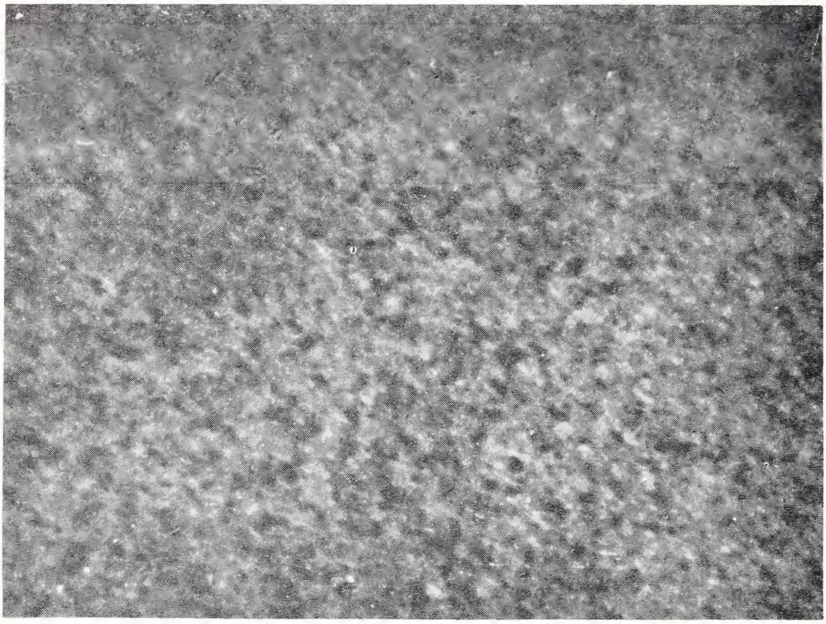

FIGURE 49.6. *Iron film (thickness 100 mμ). Magnification 72,000.*

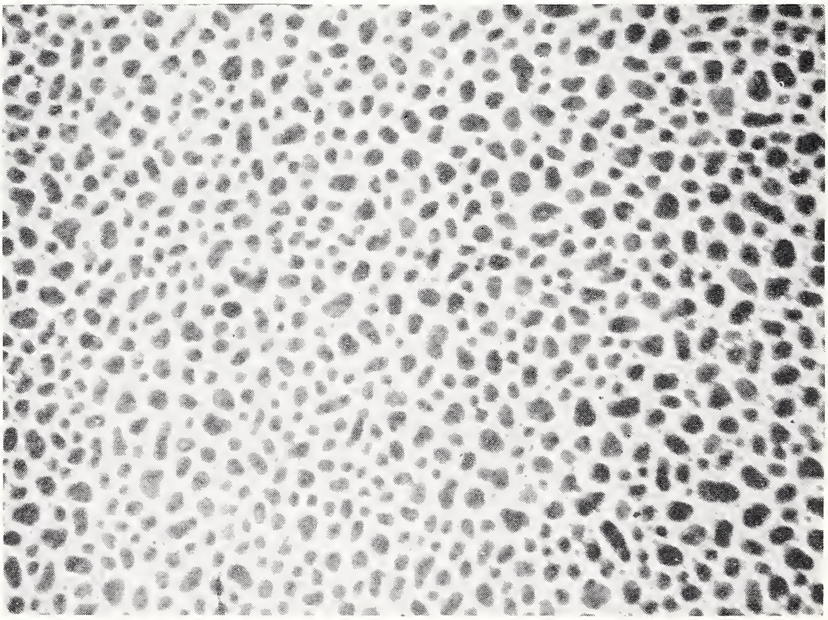

FIGURE 49.7. *Silver film (thickness 30 mμ). Magnification 72,000.*

In our measurements on the superconductivity of thin films, we started with measurements on Nb films. Just as for the nickel and iron films, we found for the thinnest films a negative temperature coefficient. For the thicker films, however, the temperature coefficient becomes more and more positive. We found also that the thinner the film, the lower the transition temperature. (This investigation, which is not finished at present, will be reported in a later paper).

Pictures of these films taken with the electron microscope revealed a structure similar to that shown by the nickel and iron films. Our Nb films are obtained by sputtering in a neon gas from a circular electrode of spectrographically pure Nb supplied by Johnson, Matthey, and Co. of London.

50. Electric Conductivity of Graphite at Liquid-Helium Temperatures[1]

by Lothar Meyer, G. S. Picus, and W. G. Johnston[2]

The electric conductivity of synthetic graphite has been investigated. The graphite filaments were produced by thermal decomposition of pure methane.[3] The filaments showed strong orientation of the graphite planes parallel to the filament axis (fiber structure). Figure 50.1 shows a graph of the recorder trace of reflected X-ray intensities for the 002 and 100 planes as the function of the angle between the filament axis and the normal to the plane formed by incident and reflected radiation. From the width of the X-ray diffraction lines the grain size of the graphite in these filaments was estimated to be 200 to 300 *A*.[4]

Figure 50.2 shows the mounting of the specimens, and figures 50.3 and 50.4 some representative results. Filaments 2 and 6 were made

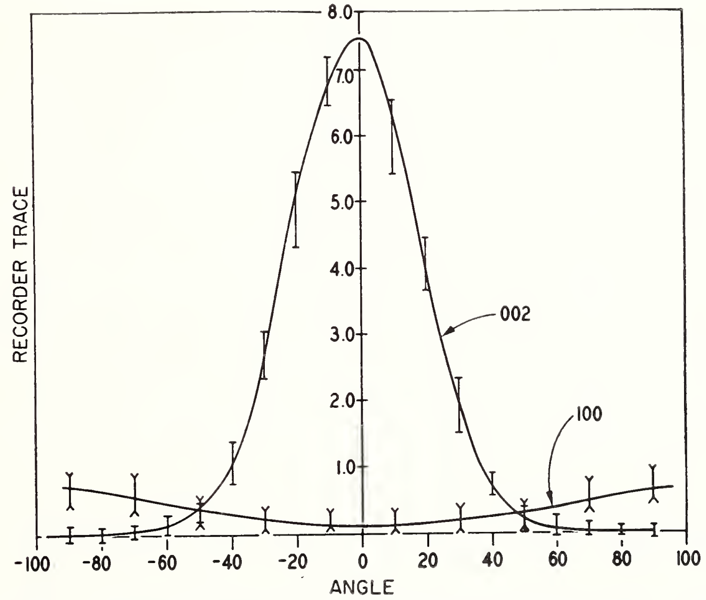

Figure 50.1. *Relative orientation of crystallites in graphite filaments. Graph of recorder trace.*

---

[1] Supported by U. S. Atomic Energy Commission.

[2] Institute for the Study of Metals, University of Chicago, Chicago, Ill.

[3] L. Meyer, Trans. Faraday Soc. **34**, 208 (1938).

[4] Assuming that the line broadening is only due to the grain size, and neglecting other influences on the line width in this approximation. This seemed justified as strain and similar mechanical deformation have qualitatively the same influence on the electric conductivity.

at 2,100° C and cooled slowly, filament 3 at 2,100° C and cooled rapidly The absolute values of the conductivities at room temperatures were:

Filament 2: 2.9×10^3 ohm^{-1} cm^{-1}.
Filament 3: 2.2×10^3 ohm^{-1} cm^{-1}.
Filament 6: 2.6×10^3 ohm^{-1} cm^{-1}.

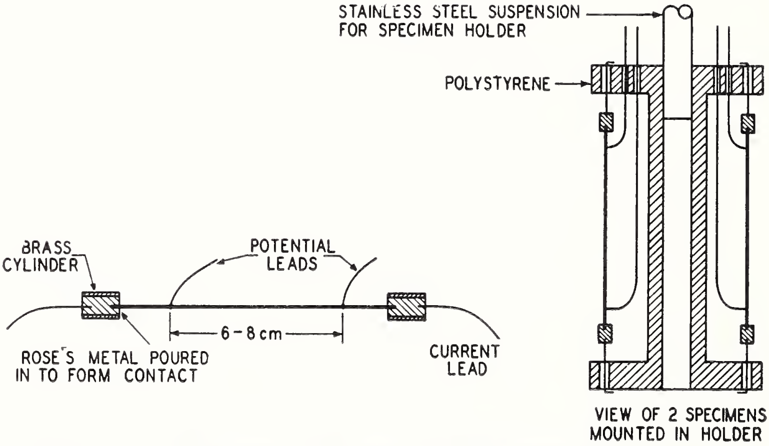

Figure 50.2. *Mounting of filaments for low-temperature measurements.*

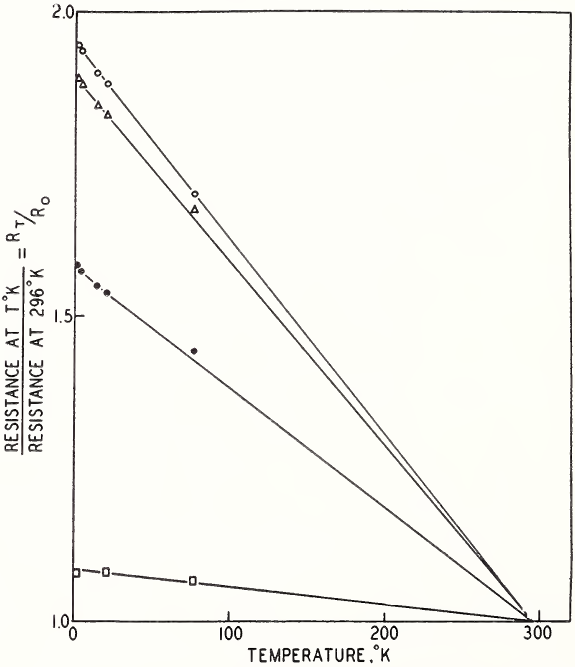

Figure 50.3. *Filament resistance from 1° K to room temperature.*

Specimen
○ C-2 }
● C-3 } Graphite filaments
△ C-6 }
□ C-4 Untreated carbon core

Measurements of natural graphites from different sources confirmed qualitatively the earlier Leiden results.[5]

The results obtained with the fine-grained material are not consistent with existing theories. According to the extension by Bowen,[6] of Wallace's [7] original theory for small grain size, one should expect that the electric resistivity shows a minimum as a function of temperature, and follows a $1/T$ dependency at temperatures below the minimum. Wallace states that in graphite the lower band is completely filled, and just touches the next higher band. The more or less metallic behavior of graphite at room temperature is due to the fact that electrons are thermally lifted from the lower band into the conduction band. If, as in fine-grained material, the mean free path of the electrons is determined by the temperature-independent grain size, the conductivity becomes proportional to the number of electrons in the conduction band, i. e., proportional to T, or the resistivity proportional to $1/T$. We did not find this type of temperature dependency in the range between room temperature and helium temperatures. The behavior is more like that of a poor metal, i. e., where even at the lowest temperatures some electrons still remain in the conduction band.[8]

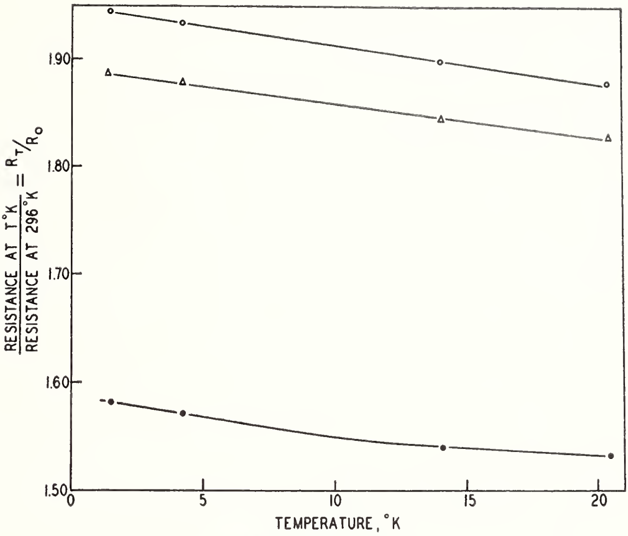

Figure 50.4. *Filament resistance from 1° to 20° K.*

---

[5] H. Kamerlingh Onnes and K. Hof, Leiden Comm. 142b. W. J. de Haas and P. M. van Alphen, Leiden Comm. 212e.

[6] D. Bowen, Phys. Rev. **76**, 1878 (1949).

[7] P. R. Wallace, Phys. Rev. **71**, 622 (1947).

[8] As chemical impurities that might act as donors of electrons are probably not present, there still remains the possibility that strain, mechanical deformations, or the grain boundaries represent mechanical impurities that act as donors. We are investigating this question.

The suggestion by Mrozowski [9] that there exists an energy gap between the filled-up band and the conduction band that would make graphite a real semiconductor is not supported by these results. Also, the fact that natural graphite crystals show at liquid-helium temperatures a conductivity that exceeds that at room temperature by more than the factor 30 makes it more probable that the two bands overlap slightly instead of being separated by an appreciable energy gap.

---

[9] S. Mrozowski, Phys. Rev. **77**, 838 (1950)

51. Normal Resistivities at Low Temperatures

by K. Mendelssohn [1]

The measurement of electric resistances of the pure metals at low temperatures was one of the earliest researches after the liquefaction of hydrogen and helium. However, the technique usually applied only permitted the determination of resistance values at temperatures in the liquid range of the cryogenic working substances. In particular, a large gap remained between hydrogen and helium temperatures. It is, however, in this region that the temperature dependence of the resistance is usually most interesting. For most metals the temperature region below 4° K which is accessible with liquid helium can contribute little to our knowledge because the resistance is independent of temperature. On the other hand, the region between 4° K and the boiling point of hydrogen at 20° K represents a factor 4 in the absolute temperature, and it is here that the most accurate information on the power law of the electric resistivity can be obtained. It was only with the advent of the desorption method that this gap was first bridged, and we have now also adapted the expansion method for observations in this interval of temperatures.

According to Grüneisen's formula, the temperature variation of the resistivity, r, is given as

$$r=\left(\frac{T}{\theta}\right)^5\int_0^{\theta/T}\frac{x^5dx}{(e^x-1)(1-e^{-x})},$$

where T is the absolute temperature, and θ is the Debye characteristic temperature of the metal. Since for high temperatures the integral approximates to $1/4\ (\theta/T)^4$, the resistivity will become proportional to the absolute temperature. For very low temperatures, the integral will be constant, and the resistivity should therefore be proportional to the fifth power of the absolute temperature. This is also the power law that Bloch has postulated from his one-electron theory.

As only a few metals have been investigated in the temperature region intermediate between helium and hydrogen temperatures, it was decided to make a systematic study of the temperature dependence of the resistivity of all metals. So far, results have now been obtained on the alkali metals and on the alkaline-earth metals (see fig. 51.1). The only metal of these two groups that shows complete agreement with the Bloch theory is sodium, which has a resistance tending indeed to T^5 at low temperatures. The power index actually observed for the different specimens was ≈ 4.85, but it has to be remembered that the T^5 law represents a limiting case for the absolute zero of temperature and that at finite temperatures the influence of the lattice vibrations must decrease the index. This influence is stronger the lower the characteristic temperature of a metal is. Accurate comparison with the theory therefore requires, in the case of sodium, evaluation of the Grüneisen formula, which yields the correct power index of 4.85 for this region. The agreement is not so good for

---

[1] Clarendon Laboratory, Oxford, England.

lithium, in which a power index of ≈4.55 was observed. As lithium has a higher value of θ than sodium, we should expect the T^5 to be followed below 20° K. The disagreement with the theory is small but significant. It is known that in other electronic properties, too, lithium is inferior to sodium, a behavior that may be due to insufficient shielding of the valency electron by the helium shell from the attraction of the nucleus.

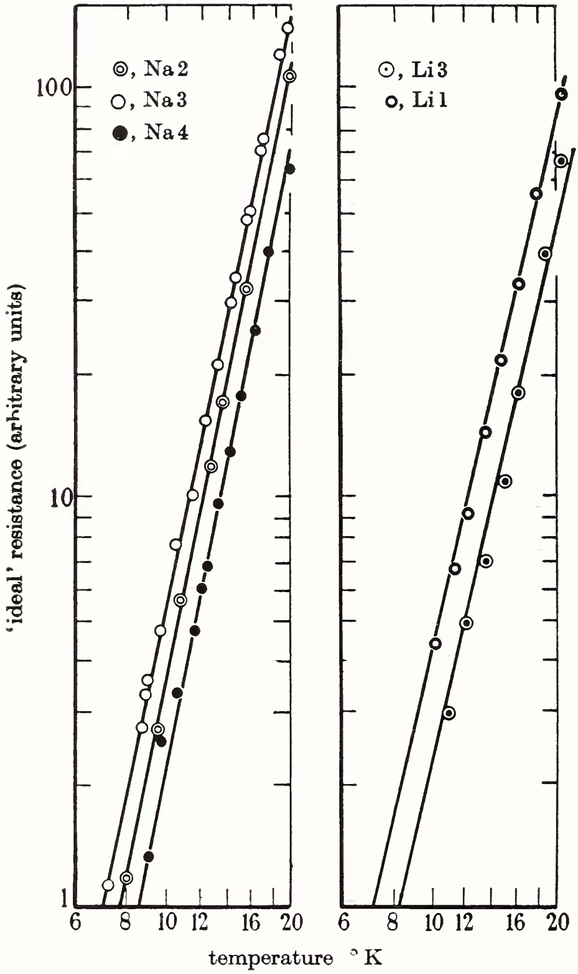

FIGURE 51.1. *Logarithmic plots of the results for sodium and lithium.*

Potassium was found at the lowest temperatures and for the purest specimen also to yield a T^5 law, but comparison with theory at higher temperatures is difficult. This whole research has again drawn attention to the insufficiency of our knowledge of the vibrational energy spectrum of the lattice. There is wide disagreement between the values of the Debye characteristic temperature obtained by different methods for the same metal, which is accentuated by the fact that in most cases it is impossible to fix the same θ value for one property of the substance over the whole temperature range.

Rubidium and cesium do not show agreement with the theory, and the same is true for the alkaline-earth metals (see fig. 51.2). In all these cases, the concept of quasi-free electrons does not seem to be applicable in the same way as in sodium. It is at present impossible to obtain some of the alkaline-earth metals sufficiently pure to draw definite conclusions as to their electronic behavior. In the case of beryllium, there are doubts whether the fairly high resistances observed were due to impurities or whether the metal is essentially a rather poor conductor.

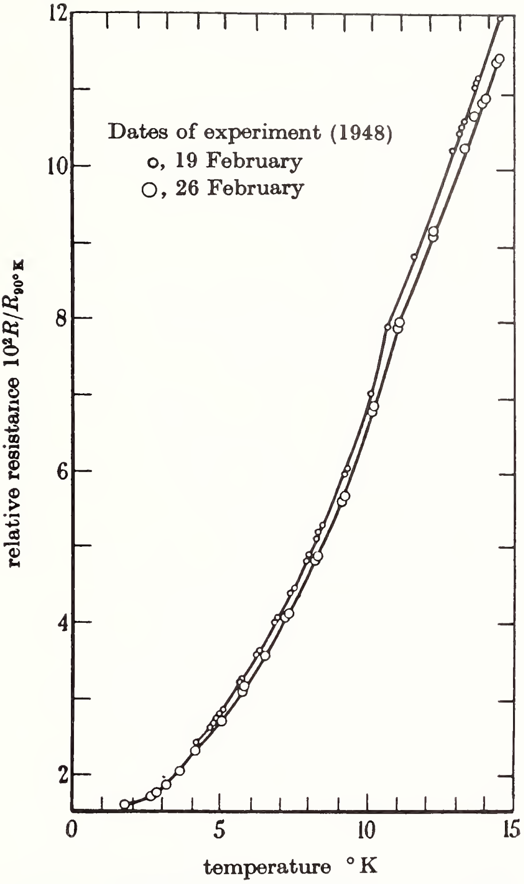

FIGURE 51.2. *Resistance variation at low temperatures of cesium (specimen Cs2).*

The power index of the temperature variation of the resistivity was derived from the "ideal" values, i. e., those resistances that were left after subtraction of the temperature independent "residual" resistance. In most cases, and in particular in the alkali metals, the residual resistances of the samples were small enough to make the evaluation of the ideal resistivity sufficiently accurate. However, there were two phenomena that made the application of Matthiesen's rule difficult. One was the observation of a minimum in the resistivity of magnesium that is similar to that found in some of the measurements on gold. All four samples of magnesium used by us exhibited this phenomenon, and as the material used to make them was obtained from three different sources, it is tempting to think that the minimum may be a basic property of the metal (see fig. 51.3). However, it has to be remembered that the refining processes

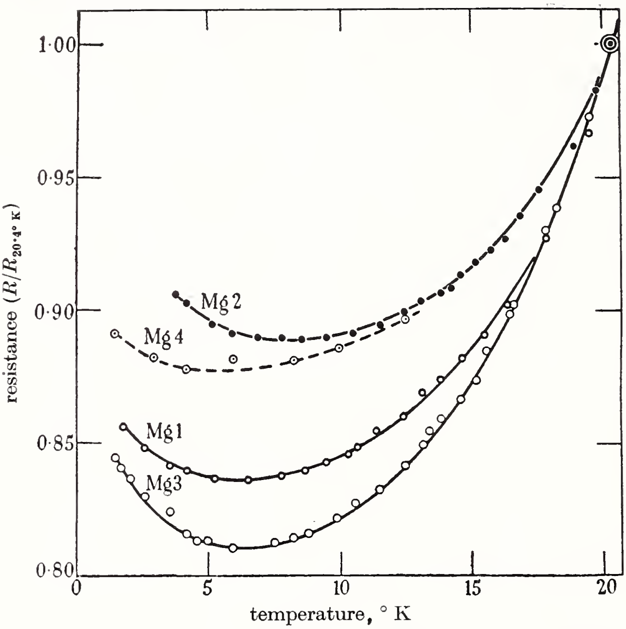

Figure 51.3. *Temperature variation of electric resistance of magnesium.*

used may have been rather similar and left similar impurities. There is indeed a fairly significant amount of aluminium and particularly manganese in the three samples for which analyses were available, and one might suspect that the presence of either or both of these impurities is responsible for the occurrence of the minimum. It is probably quite incorrect, as has sometimes been done in the case of gold, to correlate the minimum with the total amount of impurity of any kind in the specimen under investigation. In fact, it is postulated by the theory of scattering and also borne out by the experimental evidence that general impurity simply results in an increase in the temperature-independent residual resistance. Theory gives no indication how a minimum in the resistivity can be caused, and it therefore seems more reasonable, when attributing the minimum to impurity, to make a specific impurity responsible.

The other anomaly observed was rather inconspicuous but could nevertheless be recognized clearly with the accuracy of our resistance determinations. It was found that in some specimens of potassium, cesium, and barium the resistance curve showed small kinks. Detailed experiments in the case of potassium made it fairly certain that these kinks were caused by a very small impurity of sodium. Although repeated distillation of the available pure potassium did not remove the anomaly, the latter did not occur when potassium glass was used for the distillation vessel. There is reason to believe that similar impurities are responsible for the similar anomalies in cesium and barium, but no theoretical reason for the particular type of anomaly in the resistance curve can be given.

52. Infrared Absorption by Metals at Low Temperatures

by K. G. Ramanathan [1]

The classical formula for absorption, A, and reflectivity, $\boldsymbol{R}$.

$$A=(1-\boldsymbol{R})=2\left(\frac{\nu}{\sigma}\right)^{1/2},$$

where ν is the frequency of radiation, and σ is the d-c conductivity ot the metal, suggests the possibility that superconductors might be perfect reflectors of infrared waves. To test this idea, Daunt, Keeley, and Mendelssohn [1] [2] made experiments with lead and tin which indicated no observable differences in A between the normal and superconducting states. However, Daunt, Keeley, and Mendelssohn did not claim high accuracy for their measurements, nor did they make any quantitative absolute estimates of A. Recent work by H. London [2] and Pippard [3] on the surface resistance of superconductors in the microwave region suggested the possibility of a small change in infrared absorption occurring below their transition temperatures. It was therefore decided to make new measurements on the infrared absorption of an electropolished surface of tin in its normal and superconducting states with an apparatus designed to give results accurate to about 1 percent. It was also the aim in this work to measure quantitatively the absorption by some pure metals and alloys and to compare the results with those predicted by various theories.

In the apparatus used for the investigation, continuous infrared radiation from a black-body source at room temperature passes down the cryostat through a German-silver tube of about 1 cm diameter polished on the inside to increase the effective intensity by multiple reflections at the wall. The radiation emerging at the bottom falls on the flat-polished surface of a metal specimen soldered on top of one of two identical gas thermometers enclosed in an evacuated metal chamber, immersed in liquid helium. The rise in temperature of the gas thermometer, due to absorption of radiation by the specimen, is measured by the difference in level produced in an oil manometer which connects the two thermometers differentially. The rate at which radiation is absorbed by the surface is obtained by comparing the change in level it causes with that produced by the dissipation of electrical energy at a known rate through a coil wound round the specimen thermometer. With this arrangement absorptions are measured at various temperatures of the helium bath. In order to observe as accurately as possible whether there was any change in absorption when the specimen became superconducting, the measurements were carried out at 2°K alternately in the normal and superconducting states, the normal state being produced with the aid of a magnetic field. The intensity of the source, which it is necessary to know in order to make quantitative estimates of absorption, was

---

[1] Royal Society Mond Laboratory, Cambridge, England. Presented by D .Shoenberg.

[2] Figures in brackets indicate literature references on page 259.

deduced from measurements on the alloy eureka on the assumption that its absorption is given by the classical formula.

The measurements on tin indicate that down to 2°K, the absorption remains the same in the normal and superconducting states to within 1 percent, the uncertainty being probably less than ½ percent. Quantitative estimates of absorption by the various metals and alloys investigated are shown in column 2 of table 52.1. All the measurements, except the last two, were made on specimens with electropolished surfaces. The mean wavelength to which the absorption measurements refer is deduced by using Planck's formula for the frequency distribution of black-body radiation. If the incident intensity is given by $\int_0^\infty E_\nu d\nu$, the total energy absorbed can be represented by $\int_0^\infty C\nu^\alpha E_\nu d\nu$, where C and α are independent of the frequency, ν. The measured absorption is the ratio of $\int_0^\infty C\nu^\alpha E_\nu d\nu$ to $\int_0^\infty E_\nu d\nu$, which can be equated to $C\nu_1^\alpha$, where ν_1 is the mean frequency. It is found that the mean wavelength, λ_1, is 14.0 μ when $\alpha=\frac{1}{2}$, as in the classical theory, and changes little when α is varied from ½ to 1.

TABLE 52.1. *Infrared absorption by metals at $\lambda=14$ μ*

Metal	Experimental	Theoretical			
		Classical	Classical+ relaxation	Anomalous skin effect	Anomalous skin effect+ relaxation
	%	%	%	%	%
Copper	0.62	0.10	0.003	0.94	0.1
Aluminium	1.11	.13	.004	1.03	.08
Lead	1.15	[1] .14	[1] .003	[1] 1.18	[1] .07
Tin	1.24	.04	.0004	1.14	.01
Tin+1% indium	1.25	.65	.084	1.26	.1
Tin+5.4% indium	1.74	[1] 1.64	[1] .18	[1] 1.64	[1] .19
Brass	1.78	1.84	.96	1.84	.96
Eureka	6.33		5.62	6.33	5.62
Staybrite	8.23	6.53	5.66	6.53	5.66
Bismuth-tin, eutectic	7.63	2.57	1.20	2.57	1.20
Copper [2]	1.47	0.10	0.003	0.94	0.1

[1] These calculations were made by using the resistance value above the transition temperature of the metals.

[2] Mechanically polished surface.

The values of absorption for the different metals calculated from various theories are given in columns 3 to 6 of the table. The formula of classical theory has been used in column 3, while in column 4 the absorption is assumed to be given by

$$2(\nu/\sigma)^{\frac{1}{2}}(-\omega\tau+\sqrt{1+\omega^2\tau^2})^{\frac{1}{2}}$$

where $\omega=2\pi\nu$, and τ the "relaxation" time is equal to $\sigma m/Ne^2$, N being the number of electrons per cubic centimeter, e the electronic charge, and m its mass. The calculations in columns 5 and 6 are based on the theory of anomalous skin effect in metals developed by Reuter and Sondheimer [4]. The values in column 5 are computed from figure 1 of their paper which represents their results if relaxation effects are assumed negligible. The figures in column 6 are obtained by interpolation from figure 2 of their paper, which represents their results for the optical region where relaxation effects play an important part in determining the surface resistance. In all these calculations n, the number of free electrons per atom has been assumed to be 1; the numerical values are not much changed if n is taken as ½ or 2.

The following features in the table may be noted: (1) The absorptions in column 5 are in good agreement with the experimental values, (2) the calculations in other columns, for most cases, lead to absorptions lower than the observed, this discrepancy being more marked in the case of the pure metals, (3) the experimental values for alloys show good agreement with those of classical theory except for Sn+1% In where the resistivity is still low enough to produce the anomalous skin effect and the Bi-Sn eutectic where the internal photoelectric effect may be responsible for the high absorption, (4) finally, the high value of absorption for a mechanically polished surface of copper [3] brings out the importance of using electrolytically polished surfaces for such optical measurements, as Chambers [5] has shown that a layer of high resistivity is produced at the surface of a mechanically polished metal.

[1] J. G. Daunt, T. C. Keeley, and K. Mendelssohn, Phil. Mag. **23,** 264 (1937).
[2] H. London, Proc. Roy. Soc. [A] **176,** 522 (1940).
[3] A. B. Pippard, Proc. Roy. Soc. [A] **191,** 370 (1947).
[4] G. E. H. Reuter and E. H. Sondheimer, Proc. Roy. Soc. [A] **195,** 336 (1948).
[5] R. G. Chambers, Nature **165,** 239 (1950).
[6] A. Wexler, Westinghouse Research Laboratories, Scientific Paper 1558 (1951).

---

[3] This measurement was made after I had heard of the investigation by Wexler [6], on the absorption of mechanically polished copper. The value given in the table is not very different from that obtained by Wexler (1.29%) for the same mean wavelength $\lambda = 14\ \mu$.

53. The de Haas-van Alphen Effect

by D. Shoenberg [1]

During the last 18 months experiments on the de Haas-van Alphen effect (periodic field-dependence of magnetic susceptibility of metal single crystals) have been extended to higher fields (up to 15,800 gauss), to lower temperatures (down to 1.1° K), and to other metals [1].[2] The effect, which was already known to occur in bismuth, zinc, gallium, tin, and graphite, has now also been found to occur in cadmium, indium, antimony, and aluminium. Verkin, Lazarev, and Rudenko [2] have independently observed the effect in tin, cadmium, and indium, and also in magnesium and beryllium. It now appears clear that the effect is one that should be found in every metal at sufficiently high fields and sufficiently low temperatures, but that it is most easily observed in metals where the Fermi surface crosses Brillouin zone boundaries, presumably because under such circumstances abnormally low effective numbers of electrons and abnormally low effective masses may be expected.

In cadmium the effect occurs along the hexagonal axis and in indium, perpendicular to the tetragonal axis. For both metals the period of oscillation is very small (at 15,300 gauss, about 43 gauss for cadmium and 48 gauss for indium). The amplitude is scarcely measurable except at the highest fields and lowest temperatures, so it is not surprising that the effect was not observed in the earlier experiments. In aluminium and antimony the effect depends in a complicated way on the direction of the magnetic field; typical values of the period at 15,000 gauss are 900 gauss in aluminium and 270 gauss in antimony; the amplitude in both metals increases by a factor of the order of 4 when the temperature is reduced from 4.2° to 1.5° K. It may be mentioned that aluminium is the first metal of cubic symmetry in which the effect has been found.

More thorough experiments on a pure gallium crystal have shown that the effect is more marked and its character more complicated than the previous observations [3] on a less pure crystal had suggested. The characteristics of the effect are different for each of the three principal axes. One interesting feature (which occurs also for tin and graphite) is the existence of beats in the oscillations, that is, periodic modulation of the envelope of the oscillations (see figs. 53.1,a, and 53.1,b). The beat period and the depth of modulation vary in a complicated manner with field direction, and the amplitude increases rapidly as the temperature is lowered. For certain directions in gallium at the lowest temperatures there is evidence also for a "fine structure" of the oscillations, that is, superposition of a frequency several times higher than the fundamental. In very recent experiments [3] this fine structure has shown up particularly strikingly in aluminium (fig. 53.2). Presumably such features are at least partly associated with the coexistence of several groups of electrons with different effective masses.

---

[1] Royal Society Mond Laboratory, Cambridge, England.
[2] Figures in brackets indicate the literature references on p. 264.
[3] Since this paper was read at the NBS Symposium.

In parallel with the experimental work, R. B. Dingle has been reconsidering the theoretical position. The main theoretical advance has been the consideration of the influence of collision broadening of the energy levels in a magnetic field. This has been shown to diminish

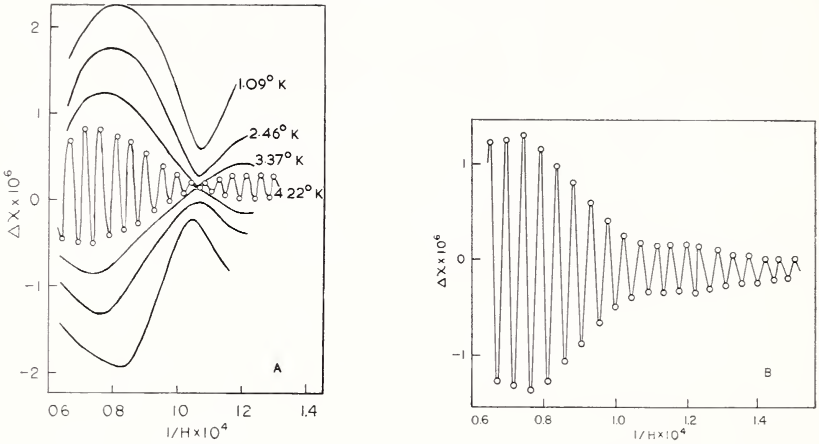

FIGURES 53.1. *Variation of $\Delta\chi$ (anisotropy of mass susceptibility) with $1/H$ in the AC and BC planes of a gallium single crystal.*

ψ is the angle between H and the C axis. The expermimental points are maxima and minima of the oscillations. The full curves are rough envelopes of the oscillations at the temperatures indicated and illustrate the growth of the effect as the temperature is lowered. A, Gallium AC plane $\psi=10°$; B, gallium BC plane $\psi=10°$; T=4.2° K.

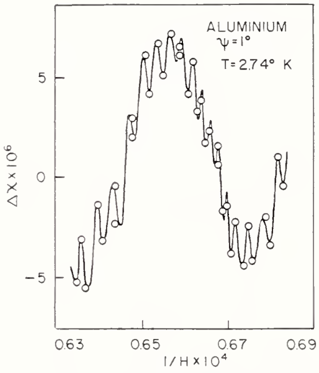

FIGURE 53.2. *Variation of $\Delta\chi$ with $1/H$ for the 100 plane of an aluminium single crystal.*

Only one main period is shown in order to illustrate the fine structure of the oscillations. The experimental points are intended to be maxima and minima of the higher frequency oscillations, but owing to the difficulty of controlling the field sufficiently precisely their exact positions are not very accurate, and the full curve has been sketched in rather schematically.

amplitude of the leading term in Landau's theoretical formula [4] for the periodic field-dependence by a factor $\exp(-h/\tau\beta H)$, where τ is the appropriate collision time, β is $eh/2\pi mc$ (m being an effective electronic mass), and the other symbols have their usual meanings; thus the amplitude becomes proportional to $\exp[-(2\pi^2kT+h/\tau)/\beta H]$. In other words, the influence of collision-broadening is as if the temperature were increased by x, where $x=h/2\pi^2k\tau$, and x should be independent of temperature, since at the temperatures concerned the electric resistance, and hence τ, is independent of temperature. This modification of Landau's formula provides a possible explanation of a number of experimental features that did not previously fit the theory.

1. In all the metals studied, the amplitude of the de Haas-van Alphen effect decays more rapidly with field at a given temperature than is to be expected, on the basis of Landau's formula, from the temperature-dependence at a given field. With suitable choice of x (usually of order a few degrees), the addition of the new exponential factor brings all the data into reasonable accord. It should be noted that if this is done, the effective electronic masses and degeneracy temperatures previously estimated from Landau's formula require some revision (although the orders of magnitude are unchanged).

2. As the direction of the magnetic field departs from a principal axis, the amplitude of the de Haas-van Alphen effect decays more rapidly than is to be expected from the variation of the relevant effective mass. This can be accounted for by supposing that x increases with ψ, the angle between the field and the principal axis. In graphite, where conductivity is practically confined to the hexagonal plane, the circumstances are particularly simple, and the plausible result is found that x varies roughly as $\sec^2 \psi$, that is, τ varies as $\cos^2 \psi$. For the other metals the angular variation of x has not yet been fully studied.

3. The decrease of amplitude of the de Haas-van Alphen effect with increasing impurity content [5] finds an immediate explanation, since x should be proportional to residual resistance, which increases with impurity content. In order to test this interpretation, some new experiments have been made on the influence of adding small amounts of mercury and indium to tin. It turns out that the value of the parameter x increases linearly with the increase in residual resistance of the alloy. From the slope of this linear relation it is possible to deduce that the collision time τ_0 of the electrons at room temperature is of order 1.5×10^{-14} sec, which agrees well with the collision time estimated from the anomalous skin effect [6] and the size dependence of resistivity [7]. Although this provides confirmation for the theory of collision broadening effects, the linear plot of x against residual resistance (fig. 53.3) does not pass through the origin, that is, there must be some other effect that produces a value of x that is not associated with collision broadening. A possible cause for this residual value of x in tin is the removal by the periodic lattice

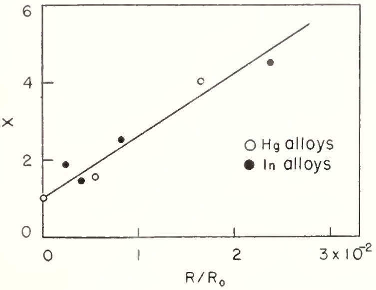

FIGURE 53.3. *Variation of the parameter x with R/R_0 (ratio of the residual resistance to the room temperature resistance of a piece of the same crystal.*

The value of x has been calculated assuming that the factor in Landau's formula is $H^{-3/2}$; the alternative assumption increases all the values of x by approximately the same amount (about 1). The slope of the straight line is given by $h/2\pi^2 k\tau_0$.

field of the degeneracy of the electronic states quantized in a magnetic field. This removal leads effectively to a broadening of the relevant energy levels, even in a completely pure metal.

Another puzzling discrepancy between the results for bismuth and zinc and Landau's formula has been the wrong phase of the oscillations [4, 8] (available magnetic fields are too small to allow estimation of the phase for the other metals). Landau's theory assumes constancy with field of the number of electrons effective for the de Haas-van Alphen effect; but detailed considerations suggest that usually it is rather the thermodynamic potential per electron which should be constant, because only a very small fraction of the conduction electrons contributes to the effect. This leads to a phase change of $\frac{1}{2}\pi$ in the theoretical formula, which then agrees better with experiment, but it is possible that other effects not yet fully considered (for example, influence of the lattice field) may further change the phase and modify the situation. The assumption of a constant thermodynamic potential also modifies the field variation of the envelope of the de Haas-van Alphen effect, changing a factor $H^{-3/2}$ that appears in Landau's formula to $H^{-5/2}$.[4] Because of the dominant exponential factor, however, the experimental data cannot as yet decide between these two powers of H.

[1] R. B. Dingle and D. Shoenberg, Nature **166,** 652 (1950); D. Shoenberg, Nature **167,** 646 (1951) Phil. Trans. Roy. Soc. [A] **245,** 1 (1952).
[2] B. I. Verkin, B. G. Lazarev, and N. S. Rudenko, J. Exptl. Theoret. Phys. (USSR) **20,** 93 (1950).
[3] D. Shoenberg, Nature **164,** 225 (1949).
[4] See appendix to D. Shoenberg, Proc. Roy. Soc. [A] **170,** 341 (1939).
[5] D. Shoenberg and M. Zaki Uddin, Proc. Roy. Soc. [A] **156,** 701 (1936); J. Marcus, Phys. Rev. **77,** 750 (1950).
[6] A. B. Pippard, Physica **15,** 45 (1949).
[7] E. R. Andrew, Proc. Phys. Soc. [A] **62,** 77 (1949).
[8] L. Mackinnon, Proc. Phys. Soc. [B] **62,** 170 (1949).

---

[4] *Note added in proof.* Prof. L. Onsager has recently pointed out a fallacy in Dingle's argument regarding the phase and power of H. For the correct argument, see Dingle, Proc. Roy. Soc. [A] **211,** 500 (1952).

54. Approximate Calculations of the Surface Impedance of a Metal in the Anomalous Region

by P. M. Marcus [1]

Anomalous Skin Effect

The long mean free paths of the electrons in a metal at low temperatures greatly modify the high-frequency behavior of the metal. This idea, first proposed by H. London [1] [2] and used by Pippard [2] in explanation of his observations, was developed on an exact mathematical basis by Reuter and Sondheimer [3], using a free-electron model and a relaxation time. Reasonable experimental verification of the general predictions of the theory was provided by Pippard's work, but some quantitative discrepancies were removed by later work of Chambers [4], so that the theory may now be regarded as a reliable description of the main features of metal behavior under these conditions.

The behavior of a metal in the anomalous region (i. e., the region in which occur deviations from the behavior predicted by classical skin effect theory) is of general interest for several reasons. It is an example of the violation of the point relationship between electric current and electric-field strength. Hence one can no longer strictly speak of a conductivity, but to describe the phenomena in the metal one must consider the current and field separately as functions of position. The behavior toward external fields, however, is conveniently described by the surface impedance defined below.

In addition, the effect provides a direct measurement of the electron mean free path by comparing this with the classical skin depth, and it may lead to values of the relaxation time as well. One should also point out that the anomalous behavior is a fairly universal phenomenon that will occur in any reasonably good conductor at low temperatures and high frequencies.

The exact theory is a considerable achievement, but it is complicated and conceals the nature of the physical processes taking place in the metal. It leans heavily on the particular form of the integrodifferential equation to be solved and solves this only for two special values of the parameter, p, describing the reflection of electrons at the metal surface. An approximate approach that yields the main results will give increased insight into the physical behavior and will make possible extensions to more complex physical situations where an exact theory would be difficult. Such an approximate approach will be described below. It starts by considering the kinetics of the motion of electrons in a field decreasing exponentially from the surface and then improves the results by introducing various refinements of this idea. Of course, the exact theory is a valuable guide and check throughout the calculations.

---

[1] University of Illinois, Urbana, Ill.
[2] Figures in brackets indicate the literature references on p. 272.

Physical Background

Figure 54.1 illustrates the physical background of this phenomenon and explains why it has been called the anomalous skin effect. Three characteristic lengths associated with the electromagnetic behavior of a metal are plotted here as a function of temperature, T, for a pure tin specimen over the range from room temperature (290° K) to liquid helium temperature (4° K). (1) The electron mean free path, l, (obtained from the theory and Pippard's measurements) increases from 10^{-6} cm to 5×10^{-3} cm over the temperature range, reflecting a factor of 5,000 in the d–c conductivity, σ; l levels off in the residual region and is proportional to $1/T$ at higher T. (2) The classical skin depth, δ, (obtained from σ) is plotted at two frequencies. At the lower frequency of 1,200 Mc/s,δ decreases from 5×10^{-4}cm to 7×10^{-6}cm. Thus at about 25° K, $\delta = l$, and here the anomalous region begins. (3) The effective skin-depth, δ_e, is essentially the actual penetration depth of the field into the metal, although it is defined precisely in terms of the surface resistance. δ_e coincides with δ at higher T but becomes greater than δ when the anomalous region is entered and characteristically becomes quickly independent of T. This occurs at temperatures where δ, l and σ are still changing, much above the residual resistance region. δ_e is finally $\simeq 5\delta \simeq (1/150)l$.

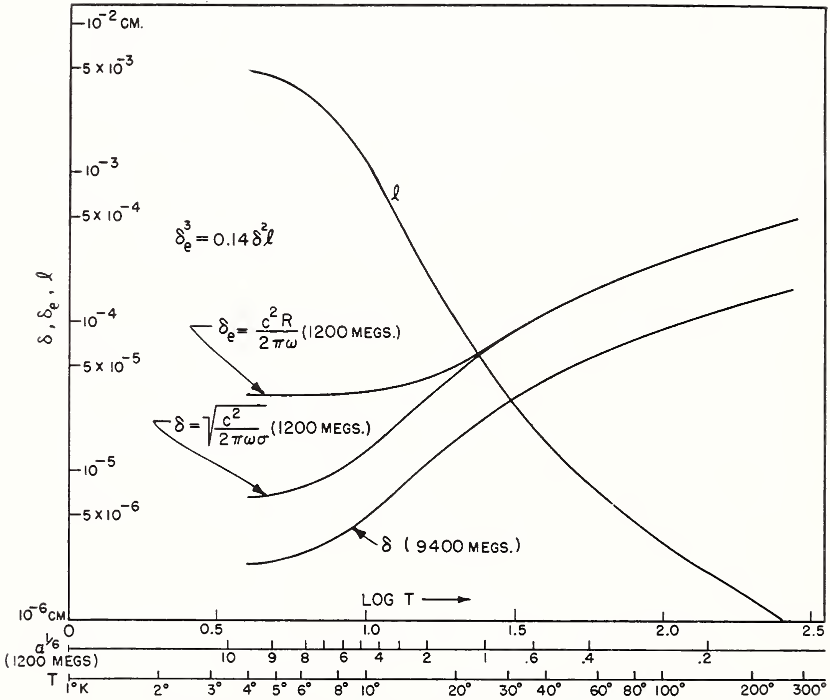

FIGURE 54.1. *Behavior of mean free path l, classical skin depth, δ, and effective skin depth, δ_e, as a function of temperature, T, in tin.*

The progress of anomalous conditions is conveniently indicated by the values of the dimensionless parameter $\alpha = (3/2)l^2/\delta^2$, whose sixth root covers the range from about 0 to 10. α is greater than unity in the anomalous region.

The basis for a first approximation to the theory and an illustration of the meaning of the effective skin depth are shown in figure 54.2 by a plot of the (absolute value of the) exact field in the metal in the extreme anomalous region ($\alpha = 3 \times 10^5$) obtained from a power-series expansion of the field in the case $p=1$. Comparison of the exact field with an exponential with the same initial slope shows the former to be well approximated by the exponential to a depth approximately equal to the penetration depth of the exponential field (where the amplitude is $1/e$ of its initial value). This depth is also essentially δ_e (it actually ranges between δ_e and 1.15 δ_e). At greater depths than δ_e the exact field falls more slowly than the exponential, and the exact theory shows the asymptotic field to be proportional to $e^{-z/l}/z^2$. For comparison, the steeply falling exponential field predicted by classical skin-effect theory, and the slowly falling exponential, $e^{-z/l}$, are also plotted.

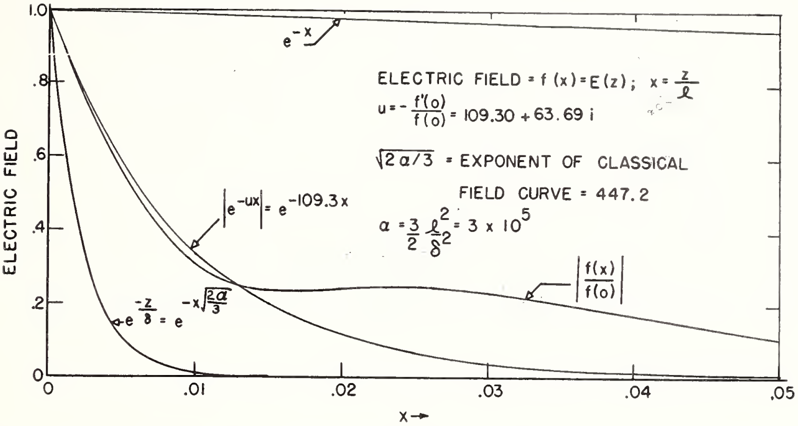

FIGURE 54.2. *Magnitudes of exact field,* $|f(x)/f(0)|$, *at* $p=1$, *exponential approximation field,* $|e^{-ux}|$, *and classical skin depth field,* $\exp\left(-\sqrt{(2\alpha/3)}x\right)$, *as functions of depth in the extreme anomalous region,* $\alpha = 3 \times 10^5$.

The first approximation used for the field will therefore be a complex exponential, and it is assumed that the predominant physical processes take place in the penetration depth defined by this exponential, where it is a good representation of the actual field. Under less anomalous conditions, the actual field must approach the exponential field of classical theory, hence this approximation should hold even better.

Refinement of the Ineffectiveness Concept

A simple picture of the effect may now be obtained by considering the kinetics of electrons that move and acquire drift velocity in an electric field, $E(z)e^{i\omega t}$, decreasing exponentially with z in a depth δ_e but pointing in the x-direction, as illustrated in figure 54.3. The electrons are schematically shown as converging from all directions on a point at the surface of the metal, after starting about a distance l

away. The electrons and field at negative z values are a device for taking account of the electrons reflected at the metal surface with no loss of drift velocity. If p is the fraction of such electrons (the rest are scattered diffusely), then the electron density in the region $z<0$ may be considered to be reduced by a factor p, but to move in a field symmetrical to that for $z>0$.

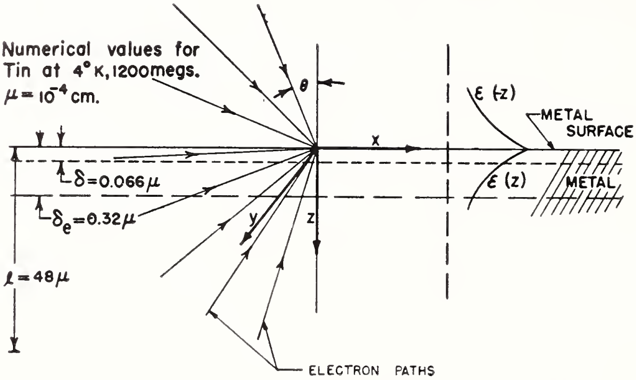

Figure 54.3. *Schematic picture of kinetics of electrons accelerating in an exponentially decreasing field under anomalous conditions with coordinate designations.*

A simple but crude procedure for calculating the surface impedance Z in extreme anomalous conditions such as in figure 54.3 has been called by Pippard the ineffectiveness concept [2]. Only electrons moving in a skin layer of depth δ_e (i. e., which spend an entire free path there) are considered to be effective in producing the current, and these electrons are treated as if they move in constant field. This is equivalent to introducing an effective conductivity, σ_e, smaller than the d-c conductivity by a solid angle factor, δ_e/l and then applying ordinary skin-effect theory. This yields a dimensionally correct expression of the proper order of magnitude which is independent of T, as required by observations.

Thus if $\sigma_e=(\delta_e/l)\sigma$, then skin-effect theory gives

$$\delta_e=\sqrt{\frac{c^2}{2\pi\omega\sigma_e}}=\left[\frac{c^2 l}{2\pi\omega\sigma}\right]^{1/3}.$$

Hence defining

$$Z=R+iX=\frac{4\pi}{c}\frac{E(0)}{H(0)}=\frac{2\pi\omega\delta_e}{c^2}(1+i). \tag{1}$$

Therefore,

$$\frac{1}{R}=\frac{1}{X}=\left(\frac{c^2}{2\pi\omega}\right)^{2/3}\left(\frac{\sigma}{l}\right)^{1/3}. \tag{2}$$

A refinement of this procedure can be made which introduces new physical detail and remedies certain objections, namely, that the electrons may not be considered to travel in constant field, that the dominant contribution to the current does not come from the electrons in the skin layer, and that the surface-reflection factor is neglected. All electrons in the solid angle about a point are considered to contribute effectively to the current in proportion to the length of their path in the skin layer where they acquire drift velocity, thus reducing each contribution by the same factor δ_e/l that appears above through the restriction of the group of electrons considered. The variation of the field over the electron path is taken into account, and the beginning of the path is assumed to be at a position where the field is negligible, thus using the assumption $l >> \delta_e$. Then we write for the current at z (in the x-direction)

$$I(z) \cong -n\epsilon \int^{z} \left(-\frac{\epsilon E(z)}{m}\right) \frac{dz}{v\,\overline{\cos\theta}} \frac{(1+p)}{2}, \tag{3}$$

where $-n\epsilon$ is the total charge, $-\epsilon E(z)/m$ the drift acceleration, v, the thermal (Fermi) velocity, and $dz/v\,\overline{\cos\theta}$ a time differential, where $\overline{\cos\theta}$ is some average over the angles of approach to take account of the greater contribution of electrons more nearly parallel to the surface (the contributions at some angle must actually be cut off by limiting the length of acceleration path to a mean free path). The factor $(1+p)/2$ takes account of reflected electrons by reducing the current contribution from reflected electrons by a factor p.

Putting $E(z) = e^{-i\kappa|z|}$, where κ is a complex propagation constant and (rather arbitrarily) $\overline{\cos\theta} = \frac{1}{2}$ gives

$$I(z) \cong \frac{n\epsilon^2}{mv} \frac{E(z)\,(1+p)}{i\kappa} = \frac{\sigma\,(1+p)}{i\kappa l} E(z). \tag{4}$$

From the electromagnetic equations, however,

$$I(z) = \frac{c^2}{4\pi i\omega} \frac{\partial^2 E(z)}{\partial z^2} = \frac{-c^2\kappa^2}{4\pi i\omega} E(z). \tag{5}$$

Hence

$$i\kappa = \left[\frac{4\pi i\omega}{c^2}\,(1+p)\,\frac{\sigma}{l}\right]^{1/3} \tag{6}$$

and using $Z = 4\pi\omega/c^2\kappa$,

$$\frac{1}{R} = \frac{\sqrt{3}}{X} = (2(1+p))^{1/3} \left(\frac{c^2}{2\pi\omega}\right)^{2/3} \left(\frac{\sigma}{l}\right)^{1/3}. \tag{7}$$

This formula gives the correct ratio $(\sqrt{3})$ of surface reactance, X, to surface resistant, R, predicted asymptotically by the exact theory, as well as the correct dimensional factors. The numerical factor $(2(1+p))^{1/3} = 1.6$ at $p=1$ and 1.3 at $p=0$, to be compared with exact values 2.18 and 1.94, respectively.

More Exact Kinetic Considerations

The kinetic approach used above when carried out precisely leads to the following integral formula for the current in terms of an arbitrary electric field:

$$I(z) = \frac{3}{4}\frac{\sigma}{l}\left[\int_0^{\frac{\pi}{2}} d\theta \frac{\sin^3\theta}{\cos\theta} \left\{\int_0^{z} dz_0 e^{-\left(\frac{z-z_0}{l\cos\theta}\right)} E(z_0) + p\int_{-\infty}^{0} dz_0 e^{-\left(\frac{z-z_0}{l\cos\theta}\right)} E(z_0)\right\} + \int_{\frac{\pi}{2}}^{\pi} d\theta \frac{\sin^3\theta}{\cos\theta} \int_{\infty}^{z} dz_0 e^{-\frac{(z-z_0)}{v\cos\theta}} E(z_0)\right], \tag{8}$$

where the first two integrals give the contribution to the current of electrons coming from $z_0 < z$—the two terms arising from the drift velocity acquired between the surface and z, and from $z < 0$ (reflected electrons), respectively. The third integral is the contribution from $z_0 > z$. The Fermi distribution is distinguished from a one-velocity distribution by the presence of the factor $\sin^3 \theta$ rather than $\sin \theta$.

If this expression for I is used with eq (5), the integrodifferential equation of the exact theory is now obtained (eq (11)). An exponential field, $E(z) = E_0 e^{-i\kappa|z|}$, may be used to satisfy this equation approximately by several procedures. The two sides of the equation may be matched at the surface $z=0$, which is physically the most important point as the current and field are largest there, yielding an equation for κ of the following form:

$$u^3 = i\alpha(1+p)\left[\left(1-\frac{1}{u^2}\right)\ln(1+u) - \frac{1}{2} + \frac{1}{u}\right], \tag{9}$$

where $u = i\kappa l$ and $\alpha = 3l^2/2\delta^2$.

The equation may also be multiplied through by the exponential $E(z)$ and integrated over all z, thus matching the two sides in an average way weighted essentially by the power at each point. The equation obtained for κ is

$$u^3 = 2i\alpha\left[\left(1+p-\frac{1+3p}{u^2}\right)\ln(1+u) - \frac{1+3p}{2} + \frac{1+3p}{u}\right]. \tag{10}$$

Solving (9) and (10) for the complex quantity κ as a function of α, for p=0, 1 which is easily done by iteration procedures, leads to ap-

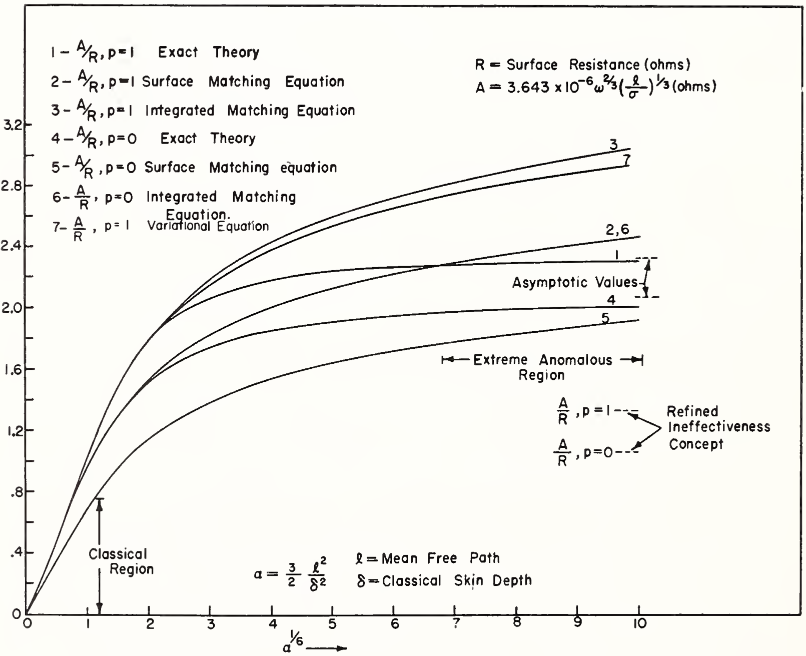

FIGURE 54.4. *Values of surface resistance calculated from various approximations compared with exact theory.*

proximate values of R and X over the entire range of α from classical to extreme anamalous conditions. Values of R relative to a characteristic quantity A with the dimensions of an impedance, but independent of temperature, are plotted in figure 54.4, together with values of the exact theory. The results of the average matching procedure are seen to be considerably better (in fact, for $p=0$ the surface matching equation does not approach the correct classical limit, since half the current is removed at the surface by the scattering, although this is not physically significant in the classical region where l is small). A/R is given to better than 10 percent for $\alpha<4\times10^3$ and better than 20 percent at $\alpha=5\times10^4$.

A Variational Formulation

The most effective use of an exponential field approximation is obtained, however, by combining it with a variational expression [5] for the surface impedance. In dimensionless variables the exact equation for the field is

$$\left.\begin{aligned} f''(x)&=i\alpha\int_0^\infty K(x,y)f(y)dy\\ K(x,y)&=k(x-y)+pk(x+y)\\ k(x)&=E_1(x)-E_3(x)=\int_1^\infty \frac{e^{-t|x|}}{t}\,dt-\int_1^\infty \frac{e^{-t|x|}}{t^3}\,dt\\ x&=z/l;\ f(x)=E(z). \end{aligned}\right\} \qquad (11)$$

Multiplication of (11) by $f(x)$ and integration from 0 to ∞ leads to the form for Z:

$$\frac{4\pi i\omega l}{c^2}\,\frac{1}{Z}=i\sqrt{\frac{8}{3}}\,\alpha^{1/3}\,\frac{A}{Z}=-\frac{f'(0)}{f(0)}$$

$$=\frac{\int_0^\infty [f'(x)]^2dx+i\alpha\int_0^\infty\int_0^\infty f(x)K(x,y)f(y)dxdy}{[f(0)]^2} \qquad (12)$$

which is stationary for small variations of $f(x)$ about the exact field. Putting $f(x)=e^{-ux}$ in (12) yields an expression for Z of the form

$$i\sqrt{\frac{8}{3}}\,\alpha^{1/3}\frac{A}{Z}=\frac{u}{2}+\frac{i\alpha}{u^2}\left[\left(1+p-\frac{1+3p}{u^2}\right)\ln\,(u+1)-\frac{1+3p}{2}+\frac{1+3p}{u}\right]. \qquad (13)$$

The parameter, u, is determined by the condition that (13) be stationary, yielding the equation:

$$u^3=4i\alpha\left[\left(1+p-\frac{2(1+3p)}{u^2}\right)\ln\,(u+1)-(1+2p)+\frac{2(1+3p)}{u}-\frac{p}{u+1}\right]. \qquad (14)$$

Solving (14) for u as a function of α and p and substituting in (13) gives values of A/R and A/X a few percent better than eq (10). Thus for $\alpha < 4\times 10^3$, A/R is given within 8 percent, and at $\alpha = 5\times 10^4$ within 16 percent.

The variational formulation has the great advantage that it may be improved by use of more elaborate trial functions. A new trial function of the form

$$f(x) = e^{-ux} + aE_4(x); \quad E_4(x) = \int_1^\infty e^{-tx} t^{-4} dt \tag{15}$$

is reasonable because it is more nearly asymptotically correct, which the exponential is not, and can be integrated. The nth order exponential integrals, $E_n(x)$, occur also in the theory of diffusion of neutrons of one velocity, which bears many points of analogy to the present problem. In fact, a variational formulation of the neutron problem leads to many of the same integrals [6]. The present problem is more complicated, however, because the kernel is more complicated, a second derivative of the unknown function appears in the equation, and all functions are complex. The new trial function may be expected to give substantial improvement in the values of Z, and calculations are in progress now.

Extension to More Complicated Physical Situations

Only one extension will be mentioned here that can definitely be carried through, namely, transmission through a thin film of metal in the anomalous region. The integral equation (for $p=0$) now has the form

$$f''(x) = i\alpha \int_0^d K(x,y) f(y) dy, \tag{16}$$

where d is the thickness of the film and $K(x,y)$ is the same as in (11) with $p=0$. An exact solution is probably not feasible, but variational calculations are quite possible to the accuracy mentioned above.

Measurements of the transmission through such a film would be of considerable interest as they would provide a direct measure of the behavior of the field in the metal, whereas present measurements give only the surface impedance. Appreciable transmission should occur for much greater thickness of film than classical theory would predict because of the greater penetration depth; also the long, slowly falling tail on the field should affect the transmission.

References

[1] H. London, Proc. Roy. Soc. [A] **176,** 522 (1940).
[2] A. B. Pippard, Proc. Roy. Soc. [A] **191,** 385 (1947).
[3] G. E. H. Reuter and E. H. Sondheimer, Proc. Roy. Soc. [A] **195,** 336 (1948).
[4] R. G. Chambers, Nature **165,** 239 (Feb. 11, 1950).
[5] The use of a variational principle in this connection was first suggested by H. Levine in a private communication.
[6] J. LeCaine, Phys. Rev. **72,** 564 (1947); A table of integrals involving the functions $E_n(x)$ (National Research Council of Canada, No. 1553).

55. Magneto-resistance of Superconducting Mercury

by T. G. Berlincourt and C. T. Lane [1]

Abstract

The change of resistance in a magnetic field for mercury (average mass number 200.6) has been determined for temperatures below the normal superconductive (zero field) transition and for fields above critical.

Defining R_c as the resistance at the critical field, and R as the change in resistance for a field of 8 kilogauss, we have

$$T=3.5°\text{K} \quad \frac{\Delta R}{R_c}\sim 2$$

$$T=1.2°\text{K} \quad \frac{R}{R_c}\sim 200.$$

Measurements to determine whether or not the above effect depends on the nuclear mass are now in progress.

---

[1] Yale University, assisted by the Office of Naval Research.

56. Magnetic Susceptibility of Liquid Nitric Oxide and the Heat of Dissociation of $(NO)_2$

by A. Lee Smith and Herrick L. Johnston [1]

Abstract

Infrared and Raman spectra studies made previously in this laboratory show that liquid nitric oxide is almost completely dimerized. As NO is paramagnetic, and $(NO)_2$ is only weakly magnetic, magnetic susceptibility studies were undertaken in order to find the extent of the dimerization as a function of temperature.

The very sensitive Faraday test-body method was used, and the degree of association of the liquid was found to be 97.4 percent at 110° K and 94.8 percent at the boiling point (121.36° K).

Equilibrium constants for the dissociation reaction were computed and a plot of $-R \ln K$ against the reciprocal of the temperature showed the heat of dissociation of the dimer to be 3,300 cal/mole.

---

[1] Ohio State University, Columbus, Ohio.

57. Heat Capacity of Solid Deuterium from 1.3° to 12° K

by O. D. Gonzales, David White, and Herrick L. Johnston [1]

Abstract

The heat capacities of 66.7 percent (normal) and 98 percent orthodeuterium have been measured from 1.3° to 12° K. The heat capacity for normal deuterium displayed an anomaly similar to that for normal hydrogen [2] with no observed maximum down to 1.3° K; the entropy loss amounted to 0.29 entropy units at this temperature.

The heat capacity of the 98 percent orthodeuterium decreased rapidly with temperature. No appreciable anomalous contribution from the 2 percent paradeuterium was observed. However, further investigation is needed to determine unambiguously whether this effect was caused by conversion of the para form or by suppression of the anomaly by dilution. At the form or by suppression of the anomaly by dilution. At the higher temperature the heat capacities of both mixtures agreed with values previously obtained in our laboratory.[3]

Preliminary experiments below 1° K indicate that the heat capacity for the normal mixture rises sharply to approximately 0.8 cal/mole^{-1} degree^{-1} in the vicinity of 0.7 to 0.8° K.

---

[1] Ohio State University, Columbus, Ohio.

[2] K. Mendelssohn, M. Ruhemann, and F. Simon, Z. physik. Chem. [B] **15**, 121 (1931).

[3] Kerr, Rifkin, H. L. Johnston, and Clark, J. Am. Chem. Soc. **73**, 282 (1951).

58. Compressibility of Liquid Normal Hydrogen from the Boiling Point to the Critical Point at Pressures up to 100 Atmospheres

by Wm. E. Keller, Abraham S. Friedman, and Herrick L. Johnston [1]

Abstract

An apparatus has been constructed to determine compressibility isotherms of low-boiling liquids at pressures up to 100 atmospheres and at temperatures up to the critical point. The isotherms of hydrogen between the boiling point and critical points have been determined. The derived isochores are linear and their slopes are linear functions of the density. Thus $P=A(v)+B(v)T$ . . . and $B(v)=(P/T)_v=-7.11+(437/V)$. The experimental data are compared with the liquid densities predicted by the Lennard-Jones and Devonshire theory of very dense fluids. The theory is not in good agreement with the experiments.

---

[1] Ohio State University, Columbus, Ohio.

59. Elastic Constants of Rock Salt

by W. C. Overton, Jr., and R. T. Swim [1]

Introduction

The familiar ultransonic pulse technique used to measure velocity and attenuation in solids has been employed in the determination of the velocity of 10-Mc/sec sound waves in single crystals of NaCl, over the temperature range from 65° to 300° K. From a knowledge of the velocity of propagation of longitudinal and transverse waves in the medium, the elastic constants c_{11}, c_{44}, and c_{12} have been calculated.

Experimental Procedure

The principles of the ultrasonic-pluse technique have been described by Huntington [1][2], Galt [2], Roth [3], and others. The electronic apparatus used in the present experiment is essentially the same as that discussed by Overton [4], with the omission of attenuation measurements. In the temperature range 160° K to 300° K the binding agent between the quartz-crystal transducer and the rock salt was different from the binder used at liquid-nitrogen temperatures. For the higher temperatures the binding agent was stopcock grease, but below 160° K the differential thermal contraction between the quartz, the binder, and the rock salt may result in effects that make measurements impossible. These effects are, first, that the binder cracks away leaving the quartz free from the salt, and second, that stresses introduced in the quartz crystal by thermal contraction may deform it and hence change its piezoelectric properties so that sound energy can not be produced. Both effects have been observed, and because of these, no measurements have been obtained below 60° K, even with the low-temperature binding agent composed of alcohol, ether, and isopentane. Stresses in the rock salt due to the differential contraction have been large enough to cleave the specimen slightly. Care was taken to avoid these effects.

At a particular temperature within the experimental chamber, the velocity of propagation of the 10-Mc/sec sound waves in the rock salt is calculated from a knowledge of the length of the specimen and of the time necessary for a sound pulse to travel the length of the specimen, be reflected, and return to the face from which it started. These round-trip travel times may be determined to an accuracy of ±0.02 μsec with the oscilloscope (DuMont type 256–D). Good single crystals of rock salt gave multiple echoes that were quite clean and allowed high precision of measurement.

In order accurately to determine the length of the specimen, it is necessary to know the behavior of the linear coefficient of thermal expansion of rock salt. This coefficient has not been located in the literature by us over the temperature range under consideration. We have calculated the expansion coefficient in two ways and get

---

[1] The Rice Institute, Houston, Tex.

[2] Figures in brackets indicate the literature references on p. 278.

good agreement. Gruneisen [5] and others have shown that the ratio α/c_p, where α is the linear coefficient of thermal expansion, and c_p, the specific heat at constant pressure, is quite independent of temperature for most solids. Using published values of α and of c_p at 273° K, and using the temperature variation of c_p as given in the International Critical Tables, we have computed α as a function of temperature. The second method employs the empirical relation between density and temperature [6]:

$$\rho = \rho_0(1 - at - bt^2),$$

where the values of the coefficients are given in the International Critical Tables. Thus, from a unit cube of rock salt at 0° C, the volume coefficient, and hence the linear coefficient of thermal expansion, may be calculated. The values of α obtained in these two independent ways agree very well, and in the calculation of lengths an average of the two was used. The actual specimen lengths are obtained by numerical integration of the relationship

$$L(T) = L(T_0)\left\{1 + \int_{T_0}^{T} \alpha(T)\,dT\right\}.$$

Measurements were made on two separate single crystals of rock salt, one having as end faces the (0,0,1) plane, the other the (0,1,1) plane. The piezoelectric quartz crystals were both of the X-cut, giving compressional vibrations and of the Y-cut, giving transverse vibrations. It can be shown [7] that the following relations hold for rock salt, where ρ is the density in grams per cubic centimeter, and v is the wave velocity in centimeters per second:

Longitudinal waves normal to (0,0,1) plane:

$$\rho v^2 = {}_{11}. \tag{1}$$

Transverse waves normal to (0,0,1) plane:

$$\rho v^2 = {}_{44}. \tag{2}$$

Longitudinal waves normal to (0,1,1) plane:

$$\rho v^2 = \frac{1}{2}\,(c_{11} + 2c_{44} + c_{12}). \tag{3}$$

Experimental Results

Figures 59.1, 59.2, and 59.3 show the elastic constants computed from these equations. The precision in the measurements of c_{11} and c_{44} is about 0.4 percent and of c_{12} is about 2 percent. The greater uncertainty in c_{12} is of course due to the contributions of uncertainties in c_{11} and c_{44} in eq (3) above. The low temperature cryogenic technique and the experimental results are discussed in greater detail in a recent paper [9] by the authors.

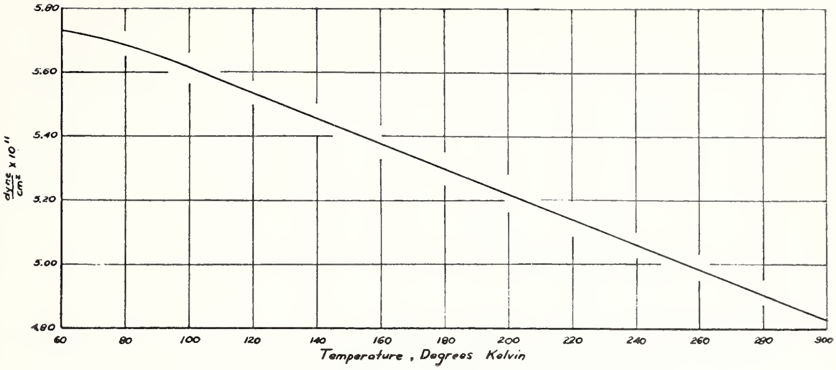

FIGURE 59.1 *Elastic constant C_{11} of rock salt.*

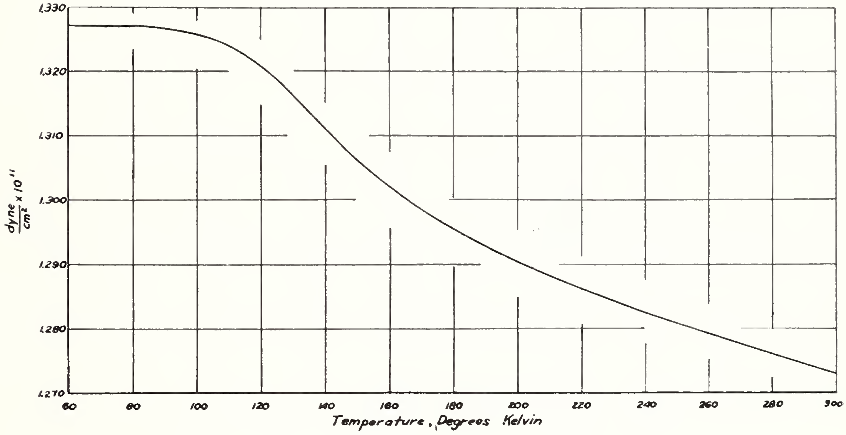

FIGURE 59.2. *Elastic constant C_{44} of rock salt.*

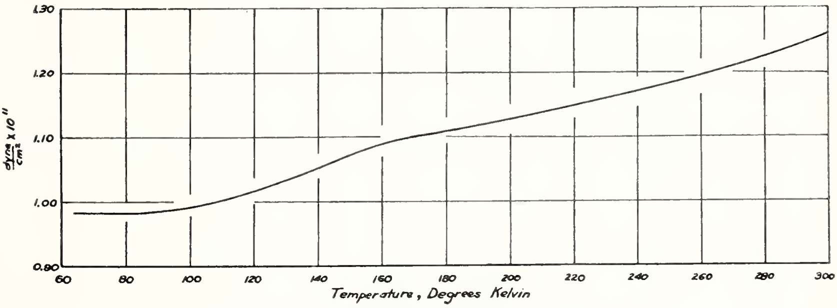

FIGURE 59.3. *Elastic constant C_{12} of rock salt.*

Discussion of Results

There is some disagreement between our results and those of Rose [8] on the elastic constants of rock salt, which we quote for comparison:

T	c_{11}	c_{44}	c_{12}
°*K*	*Dyne/cm*^{2}	*Dyne/cm*^{2}	*Dyne/cm*^{2}
80	5.76x10^{-11}	1.332x10^{-11}	1.17x10^{-11}
270	5.06	1.278	1.30

The values reported by us in figures 59.1, 59.2, and 59.3 agree with the room-temperature values of Huntington [1].

Of considerable interest is the temperature at which the slope of the curves becomes zero, which is about 80° K for c_{44} and c_{12}, and perhaps 50° K for c_{11}. This latter temperature is approximately that at which the curve of c_{11} assumed zero slope for KBr measured by Galt [2].

References

[1] H. B. Huntington, Phys. Rev. **72,** 321 (1947).
[2] J. K. Galt, Phys. Rev. **73,** 1460 (1948).
[3] W. Roth, J. Applied Phys. **19,** 901 (1948).
[4] W. C. Overton, Jr., J. Chem. Phys. **18,** 113 (1950)and Annual Progress Report, Low Temperature Physics, Rice Institute (1949).
[5] E. Gruneisen, Ann. Physik **26,** 211 (1908).
[6] Int. Crit. Tables **3,** 43 (McGraw-Hill Book Co., New York, N. Y., 1928).
[7] A. E. H. Love, The mathematical theory of elasticity (Dover Pub. 1944).
[8] F. C. Rose, Phys. Rev. **49,** 50 (1936).
[9] W. C. Overton, Jr., and R. T. Swim, Phys. Rev. **84,** 758 (1951).

60. Specific Heat of Silicon Below 100° K

by P. H. Keesom and N. Pearlman [1]

Introduction

Previous measurements of the specific heat of Si, reported by Nernst and Schwers [1] [2] and Anderson [2] have covered the temperature range above 20° K. In view of the recent theoretical work by Blackman [3] and others on the role of the lattice in determining the vibration spectrum in crystalline solids, which in turn determines the specific heat, it was considered important to extend the measurements on Si, which has a diamond lattice, below 20° K. It is in this temperature region that comparisons can most easily be made between the predictions of the Debye [4] continuum theory of specific heat and the newer lattice calculations. Also, as Si is a semiconductor, the electronic contribution is negligible, and hence need not be corrected for in comparing the observed heat capacity with that calculated as the contribution of the lattice.

Experimental Method

A modification of the Nernst-Eucken method was used to measure the heat capacity of the sample, which weighed about 40 g. and contained 0.0015 percent of B. The sample was in the form of a disk 42 mm in diameter with both faces highly polished. It was suspended by cotton threads in a brass "radiation shield" (so-called, although, of course, at these temperatures radiation plays only a minor part in the total heat transfer). The radiation shield had a heater attached by means of which the temperature of the sample could be brought above that of the bath, and in this way the temperature range between the boiling point of hydrogen and the lowest temperatures attainable with nitrogen was covered, and also temperatures above the boiling point of nitrogen. Above 160° K, however, it was no longer possible to maintain steady conditions in this way. The radiation shield was surrounded by a brass vacuum can. Electric leads to the sample were made through a copper-to-glass seal in the top of the vacuum can. Silk-insulated constantan wire was used for the heater and bare phosphor bronze and lead wires, insulated from the sample by means of a piece of cigarette paper, used as thermometers. These were all glued to the sample with glyptal, after various other materials were tried, but found to peel off the polished faces of the sample at the lowest temperatures.

The lead thermometer was calibrated against vapor pressures of liquid and solid nitrogen and hydrogen, and the phosphor-bronze thermometer, against the vapor pressure of liquid helium. Above about 25° K, the resistance versus temperature relation for the Pb was linear, which was also checked with a He gas thermometer. The entire range of the phosphor bronze could be fitted with a parab-

---

[1] Purdue University, Lafayette, Ind. This work was carried out under a contract between the Purdue Research Foundation and the U. S. Signal Corps.

[2] Figures in brackets indicate the literature references on p. 283.

ola, to an accuracy of about 0.1 percent. This parabola was extrapolated to about 5° K for measurements above the boiling point of helium. Resistances were measured by comparing the voltages across the thermometers with that across a standard 10-ohm resistor, using a Wenner potentiometer.

The heat input was measured by measuring the voltage across the heater with a millivoltmeter and the current with a milliammeter. Both meters were calibrated against the 10-ohm standard with the potentiometer. A timing circuit, photoelectrically activated by the pendulum of a clock that was checked against the timing signals broadcast by WWV, was arranged so that current could be supplied to the heater in multiples of 10 seconds. The over-all error introduced by the timing circuit was probably not larger than 0.01 percent.

The first measurements gave the heat capacity of the sample, plus that of the heater and thermometer wires, plus that of the glyptal (0.2 g). The calculated heat capacity of the wires was found to be negligible, but as nothing was known of the heat capacity of the glyptal, an identical set of heater and thermometer wires was glued to a copper disk weighing 3.3 g, using 0.3 g of glyptal, and the heat capacity measured. The correction found in this way was rather large (about 30 percent at 10° K), so as a check on the purity of the copper in the disk, the duplicate set of wires was mounted directly on the Si sample, using an additional 0.2 g of glyptal, and the heat capacity measured. The correction found from this set of measurements agreed with that calculated from the measurements on the Cu disk. This indicated that the heat capacity of the wires was indeed negligible, and that therefore the excess heat capacity was due essentially to the glyptal. As a final check on this, an additional 0.6 g of glyptal was added, making a total of 1.0 g of glyptal, and the heat capacity remeasured. The four sets of measurements are summarized below:

(1) 40 g of Si, plus 1 set of heater and thermometer wires, plus 0.2 g of glyptal.
(2) 3.3 g of Cu, plus 1 set of heater and thermometer wires, plus 0.3 g of glyptal.
(3) 40 g of Si, plus 2 sets of heater and thermometer wires, plus 0.4 g of glyptal.
(4) 40 g of Si, plus 2 sets of heater and thermometer wires, plus 1.0 g of glyptal.

Results

The heat-capacity values of the Si sample, as calculated from the four series of measurements tabulated above, agreed with one another at temperatures down to 10° K, where the discrepancy was a maximum, and equal to about 2 percent. In the neighborhood of 4° K, the various values were no longer in agreement, and so are not reported. In this temperature region, the glyptal, with about ½ percent of the total mass, contributed about 50 percent of the total heat capacity in measurement (1). Its specific heat was calculated to be 3 to 4×10^{-3} j/g °K; that of Si is about 10^{-5} j/g °K. That these values are respectively large and small can be seen from the fact that Cu, for instance, has at 4° K a specific heat of about 10^{-4} j/g °K. Figure 60.1 shows the values of the heat capacity of Si at constant volume, per mole, from 10° to 100° K. The measurements give the heat capacity at constant pressure, C_p, but C_v differs from C_p by less than 0.4 percent below 100° K. Experimental points are shown above 20°K; between 10 and 20° K a smooth curve has been drawn through the values calculated from the four separate runs. Also plotted are the values found by

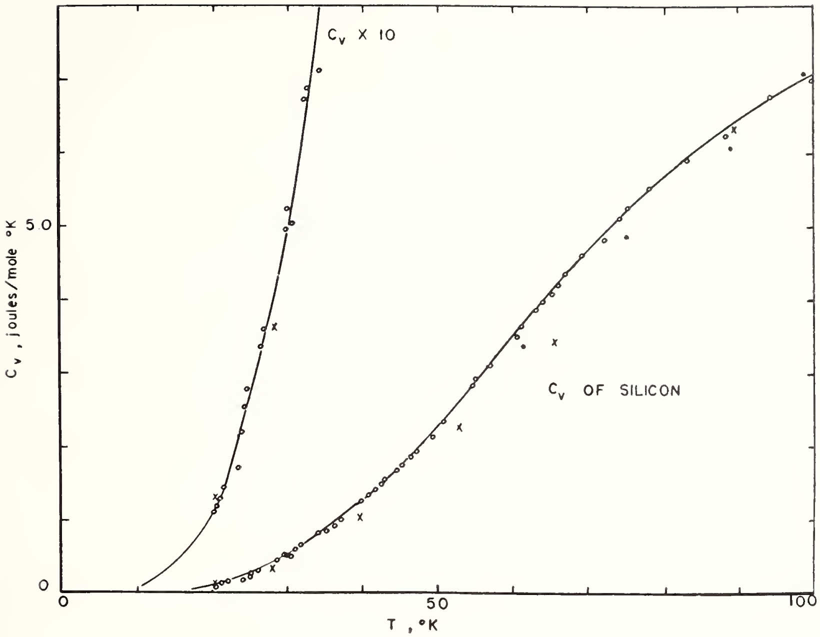

FIGURE 60.1. *Molar heat capacity of silicon, 10° to 100° K.*

×, Nernst; ○, Anderson

Nernst and Schwers [1] and Anderson [2]. Our curve is seen to be somewhat higher than these values, between 40° and 90° K.

Figure 60.2 shows the Debye θ_D values, calculated from C_v values taken from the smooth curve drawn through the experimental points. It is evident that θ_D is not constant over the temperature range investigated, as predicted by the Debye theory, so that in particular, C_v is not proportional to T^3 below $\theta_D/12$ (about 40° K). The two points drawn at about 4° K are calculated from the average of the

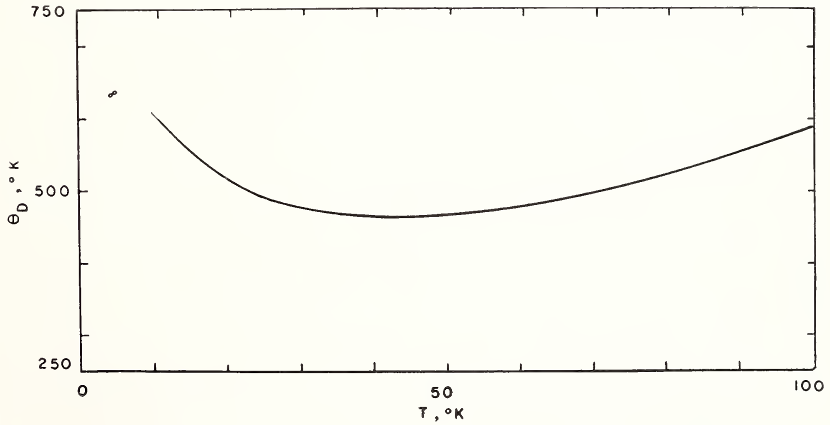

FIGURE 60.2. *Debye characteristic temperature, θ_D, of silicon.*

C_v values at that temperature. As $C_v^{1/3}$ enters into the calculation, these θ_D values are probably good to about 5 percent.

Discussion

In order to calculate the specific heat at constant volume, C_v, the internal energy of the substance must be known. This is calculated as the sum of the energies of the normal modes of vibration of the substance, each normal mode behaving as a Planck oscillator. In the first application of this method, Einstein [5] used only one oscillator, the frequency of which was estimated from infrared absorption data. This method gave an exponential decrease of C_v with temperature, which is too rapid to fit the data. Nernst and Lindemann [6] improved the agreement with experiment by introducing a second frequency equal to half of Einstein's single frequency. Debye [4] introduced a continuum of frequencies, up to a maximum in the neighborhood of Einstein's frequency, by calculating the normal modes of vibration of a continuum. The density of modes, or vibration spectrum, he found, was proportional to the square of the frequency. A consequence of this spectrum is that C_v is proportional to T^3 at low temperatures, the temperature region in which this relation is expected to hold varying with the substance. It may be stated as being below $\theta_D/12$, where θ_D is a temperature that may be calculated from the proportionality constant between C_v and T^3, and also independently from optical and elastic data.

A much more complicated procedure for calculating the modes of vibration, and therefore the frequency spectrum, was independently developed by Born and von Karman [7]. In principle, this involves taking into account explicitly the forces between nearest and the next nearest neighbors, but the complexity of the problem is so great that not until about 1935 was Blackman [3] able to carry out the calculations and derive the form of the spectrum for a real lattice. Since then, he and others have calculated the spectra for a variety of lattices, and, in particular, Smith [10], using methods developed by Born [8] and Begbie and Born [9], has published the spectrum of the diamond lattice, the form in which Si crystallizes. It turns out that while the spectrum starts off with the density of modes proportional to the square of the frequency, thereafter the relation is not so simple, and, in general, one or more peaks in the spectrum are observed. It seems to be a general feature of the spectra that have so far been calculated, that following the initial square-law region, the density of modes rises faster than the square of the frequency. Hence at very low temperatures, at which only the very long waves are of importance in determining the specific heat, C_v will be proportional to T^3 and θ_D will be constant. This temperature region will have as its upper limit, depending on the particular shape of the spectrum, a temperature in the neighborhood of $\theta_D/50$ or $\theta_D/100$. Following this "true" T^3 region, C_v rises faster than T^3 and so θ_D falls from its low-temperature constant value. It therefore appears to be unnecsary to postulate the existence of special mechanisms to explain deviations from the Debye theory. This has been done, for instance, by Simon [11], who explains the deviations in the earlier data for Si in terms of a Schottky jump between two levels with a separation of 0.021 ev. This provides an additional source of heat capacity, with a maximum at about 103° K. It is evident from figure 60.2

that we have not yet reached the "true" low-temperature T^3 region, although the two points at about 4° K could be the beginning of this constant θ_D region. Measurements are now underway with a larger sample of Si (both this new sample, weighing about 260 g, and the original sample, were kindly provided by the Bell Telephone Laboratories). We hope to extend the measurements to lower temperatures so as to be able to determine the low-temperature constant value of θ_D.

References

[1] W. Nernst and F. Schwers, Sitzber. Preuss. Akad. Wiss. 355 (1914).
[2] C. T. Anderson, J. Am. Chem. Soc. **52,** 2301 (1930).
[3] M. Blackman, Proc. Roy. Soc. [A] **148,** 365, 384; **149,** 117, 126 (1935). Reports on Progress in Physics **8,** 11 (1941).
[4] P. Debye, Ann. Phys. **39,** 789 (1912).
[5] A. Einstein, Ann. Phys. **22,** 180, 800 (1907).
[6] W. Nernst and F. Lindemann, Z. Elektrochem. **17,** 817 (1911).
[7] M. Born and T. von Karman, Phys. Z. **13,** 297 (1912); **14,** 15 (1913).
[8] M. Born, Reports on Progress in Physics **9,** 294 (1942).
[9] G. H. Begbie and M. Born, Proc. Roy. Soc. [A] **188,** 179 (1947)
[10] H. M. J. Smith, Phil. Trans. Roy. Soc. [A] **241,** 105 (1948).
[11] F. Simon, Erg. Exakt. Naturwiss. **9,** 222, 253 to 262 (1930).

61. Optical Properties of *F*-Centers at Liquid-Helium Temperatures

by E. Burstein and J. J. Oberly [1]

Electrons trapped at negative-ion vacancies in the alkali halides (*F*-centers) exhibit characteristic absorption bands that are fairly broad at room temperature. With decreasing temperature, the bands narrow and shift toward shorter wavelengths. At liquid-helium temperatures the band widths, however, are still quite appreciable. In KCl, for example, the band width at liquid-helium temperatures (0.17 ev) does not differ greatly from that at room temperature (0.35 ev). The temperature dependence of the *F*-bands can be explained in terms of a simple model in which the trapped electron is treated as a particle in a box. Temperature broadening of the band is attributed to vibrations of the ions that make up the walls of the box. The residual band width at low temperatures is, on this basis, due to the zero-point vibrations of the ions. The position of the band, on the other hand, is determined by the equilibrium configuration of the ions.

When electrons are trapped by lattice defects in alkali halides, they exhibit optical absorption bands that are characteristic of the trapped electron center and of the particular alkali halide (fig. 61.1)[1].[2] The nature of the centers responsible for the various bands has not yet been established except for the *F*-band, whose center consists of an electron trapped at a single negative-ion vacancy [2]. The bell-

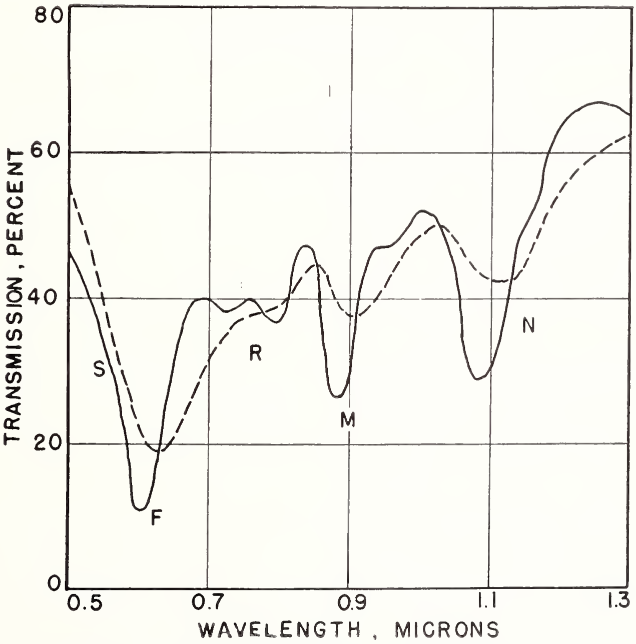

FIGURE 61.1. *Trapped-electron color-center bands in KBr.*

— — — — —, +20°C; ————, −190°C.

---

[1] Crystal Branch, Metallurgy Division, Naval Research Laboratory, Washington, D. C.

[2] Figures in brackets indicate literature references and notes on p. 291.

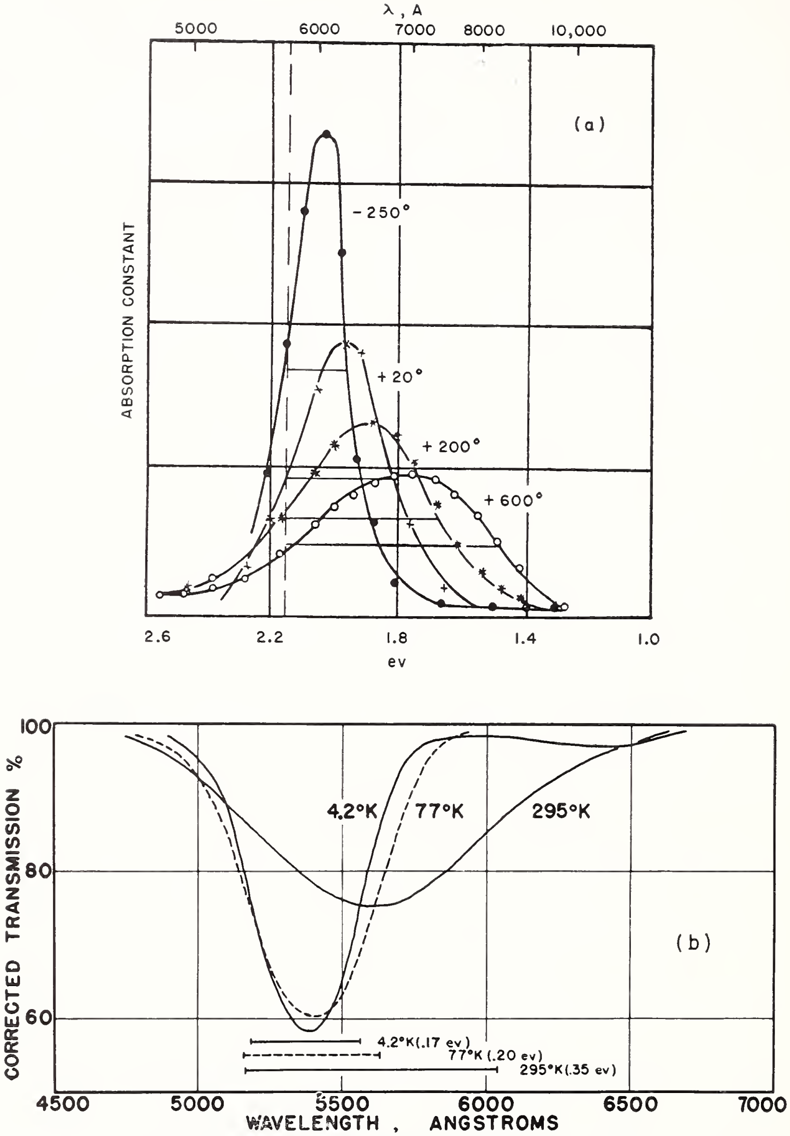

Figure 61.2. *Effect of temperature on the F-band.*

(a) KBr (Mollwo); (b) KCl (NRL).

shaped *F*-band arises from the absorption of a quantum of light by the trapped electron that raises it from a 1*s* ground state to a 2*p* excited state, from which it either returns to the ground state by a nonradiative transition or is thermally excited into the conduction band [3].

The effect of temperature on the *F*-band has been extensively investigated by Flechsig [4] and Mollwo [5], who found that the *F*-band narrowed and shifted to shorter wavelengths with decreasing temperature (fig. 61.2,a). However, the bands did not narrow indefinitely, but rather exhibited a considerable residual band width, which was tentatively ascribed by these investigators to lattice distortions or to zero-point energy. In order to establish definitely the nature of the residual band width, experiments were carried out at this laboratory on the effect of thermal and mechanical history and of impurity content of the crystal on the width of the *F*-band formed by *x*-irradiation. For this purpose, band width measurements were obtained at temperatures down to that of liquid helium for annealed, quenched, and mechanically deformed KCl crystals and for a crystal of KCl containing 0.05 percent of Ag^+. Data were also obtained for mixed crystals (solid solutions) of KCl-KBr and KCl-RbCl and for pure KBr[3]. An A. D. Little liquid-helium specimen holder [6] equipped with quartz windows was used in these experiments to maintain the specimen at liquid-nitrogen and liquid-helium temperatures. Typical-transmission curves for the *F*-band in KCl are given in figure 61.2, b, and the band widths obtained for the various crystals under different conditions are summarized in table 61.1.

TABLE 61.1. *Transmission band widths*

T °*K*	KCl (A)[a]	KCl (Q)	KCl (P)	KCl plus Ag^+ (.05%)	KCl (40%) plus KBr (60%)	KBr	KCl (70%) plus RbCl (30%)
295	0.35	0.35	0.34	0.34	0.36	0.35	0.37
77	.20	.20	.20	.19	.22	.19	.25
4.2	.17	.17	--------	--------	.20	--------	--------

[a] (A)=annealed; (Q)=quenched from a temperature 50° C below the melting point; (P)=plastically deformed.

The results may be briefly stated as follows:

1. The width of the *F*-band is not appreciably affected by thermal and mechanical treatment or by the presence of impurities.

2. The band width at low temperatures is somewhat greater in the mixed crystal of KCl-KBr, where there is a statistical variation in second nearest neighbors, than in the pure components, and it is still greater in KCl-RbCl, where there is a statistical variation in nearest neighbors. The *F*-band in the mixed alkali halides is otherwise similar to that in the pure crystals, and its position is linearly dependent on composition.

3. The bands do not narrow indefinitely but approach a residual width that is considerable at liquid-helium temperatures. Thus in KCl the band width at liquid-helium temperature (0.17 ev) does not differ greatly from that at room temperature (0.35 ev).

We may conclude from these results that the large residual band width at low temperatures does not arise from lattice distortion or impurity effects. It must therefore be attributed either to the superposition of a large number of narrow absorption bands whose frequency distribution arises from other causes or to the interaction between the *F*-center and the zero-point vibrations of the lattice. We show by means of a simple model for the *F*-center, in which the trapped electron is treated as a particle in a box, that the residual band width

---

[3] The authors are indebted to L. R. Johnson and W. Zimmerman, III, of the Crystal Growing Section of the Crystal Branch for samples of the mixed crystals of KCl-KBr and KCl-RbCl and to R. J. Ginther of the Luminescence Section of the Crystal Branch for samples of the impurity crystal KCl+.05 percent of Ag^+.

can be accounted for by interactions of the *F*-center with zero-point vibrations [7].

The applicability of the "particle-in-a-box" model to the *F*-center is indicated by the fact that the position of the *F*-band (in electron volts) in different alkali halides is, to a good approximation, inversely proportional to the square of the distance a_0 between adjacent ions (fig. 6.3, a),

$$h\nu = E_{2p} - E_{1s} = \frac{k}{a^2} \tag{1}$$

where k, the proportionality constant, equals 20 when a_0 is given in *A* and $h\nu$ is given in electron volts. In terms of the model, temperature broadening of the *F*-band is attributed to the vibrations of the alkali-metal ions that make up the walls of the box, whereas the position of the *F*-band is determined by the size of the box, and therefore by the equilibrium positions of the nearest-neighbor alkali-metal ions. The residual band width at low temperature is accordingly due to zero-point vibrations of the adjacent alkali-metal ions. In making use of this approximate model for the *F*-center, it is assumed that more distant ions do not affect the energy levels of the trapped electron, except indirectly by determining the configuration of the nearest-neighbor alkali-metal ions.

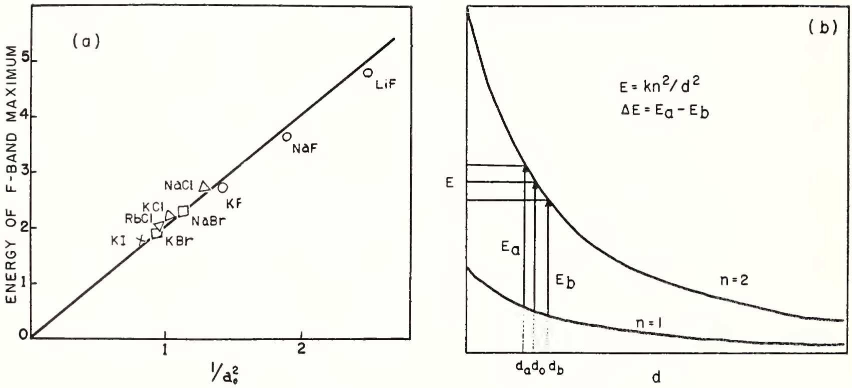

FIGURE 61.3.

(a) Dependence of *F*-band position, in electron volts, on the inverse square of the distance between adjacent ions.

○, F; △, Cl; □, Br; ×, I.

(b) Dependence of the energy of the ground level and first excited level of the particle-in-a-box electron on the box dimension.

The width of the *F*-band can be calculated by means of an adiabatic approximation in which it is assumed that the instantaneous energies of the electron in its normal and excited states are determined only by the dimensions of the box. In calculating the band width we need only consider the energy of the electron and its dependence on the dimensions of the box, which is shown schematically in figure 61.3, b. In accordance with the Franck-Condon principle, we consider optical transitions from the ground state to the first excited state to occur without change in the configuration of the ions. Broadening of the band accordingly occurs as a result of the variation in the dimensions of the box caused by thermal vibrations. Thus if $\Delta d=(d_b-d_a)$ is the change in box dimensions, as shown in figure 61.3, b, the band width $\Delta E=(E_a-E_b)$ is given by

$$\Delta E=\frac{2E_0}{d_0}\Delta d, \tag{2}$$

where d_0 is the equilibrium dimension of the box, and E_0 is the position of the band in electron volts. The band width at a given temperature can be calculated from the vibration amplitudes of the alkali-metal ions and the experimental values of E_0 and d_0.

$$\Delta E=\frac{2Ec}{d_0}\sqrt{\overline{\mu^2}}, \tag{3}$$

where $\overline{\mu^2}$ is the mean-squared amplitude of vibration of the ions, and c is a proportionality factor that includes the extent to which the vibrations of the alkali-metal ions making up the walls of the box are correlated. The vibration amplitudes can be obtained either experimentally from X-ray scattering data or theoretically from the approximate "isotropic" equation [8]

$$\overline{\mu^2}=\frac{4.364\times10^{-14}}{A\theta}\left(\frac{\phi(x)}{(x)}+\frac{1}{4}\right), \tag{4}$$

where A is the molecular weight divided by two for diatomic crystals, θ is the Debye temperature, T is the absolute temperature, $x=\theta/T$, and $\phi(x)$ is the Debye function

$$\phi(x)=\frac{1}{x}\int_0^x\frac{x\,dx}{e^x-1}. \tag{5}$$

The contribution from zero-point energy is represented by the term 1/4 in eq (4). At low temperatures $(T<\theta)$, eq (3) takes the approximate form

$$\Delta E=\frac{2Ec}{d_0}\left\{\frac{4.364\times10^{-14}}{A\theta}\left[\frac{\pi^2}{6}\left(\frac{T}{\theta}\right)^2+\frac{1}{4}\right]\right\}^{\frac{1}{2}}, \tag{6}$$

whereas at high temperatures $(T>\theta)$ it takes the form

$$\Delta E=\frac{2Ec}{d_0}\left\{\frac{4.364\times10^{-14}}{A\theta}\frac{T}{\theta}\right\}^{\frac{1}{2}}. \tag{7}$$

The width of the F-band in KCl, calculated from eq (3) and (4), is plotted against temperature in figure 61.4, together with experimental values obtained at this laboratory. In these calculations, the box dimensions, d_0, was taken as $2a_0$, and an empirical value of c was used, which was obtained by adjusting the theoretical band width to the experimental value at room temperature. The agreement between calculated and experimental values at liquid-helium temperatures clearly shows that the zero-point vibrations do account for the large residual band width. It demonstrates further that the interaction between lattice vibrations and F-centers is large, even at absolute zero, which undoubtedly accounts for the fact that the return of the electron from the excited state to the ground state is nonradiative, even at liquid-helium temperatures [9].

The equilibrium positions of the nearest-neighbor alkali-metal ions that make up the walls of the box are given only to a rough approximation by their normal positions in the lattice. Actually, the alkali-metal ions adjacent to the electron trapped in a negative-ion vacancy are displaced toward the trapped electron. This results from the fact that the electron trapped in a negative-ion vacancy exerts a considerably smaller repulsion than the halogen ion it replaces. The effective radius of the alkali-metal ion also plays a role in determining the dimensions of the box and must be taken into consideration.

An interesting property of the F-band, which also can be interpreted readily by the particle-in-a-box model, is the fact that the wavelength at which the absorption coefficient is one-half of its maximum value on the short-wavelength side of the band remains fixed as the temperature changes (fig. 61.2, a). According to the model, this wavelength corresponds to the "closest approach" of the alkali-metal ion neighbors to the trapped electron during vibration. This closest approach is determined primarily by the mutual repulsion of the alkali-metal ions and is essentially independent of their equilibrium positions at different temperatures.

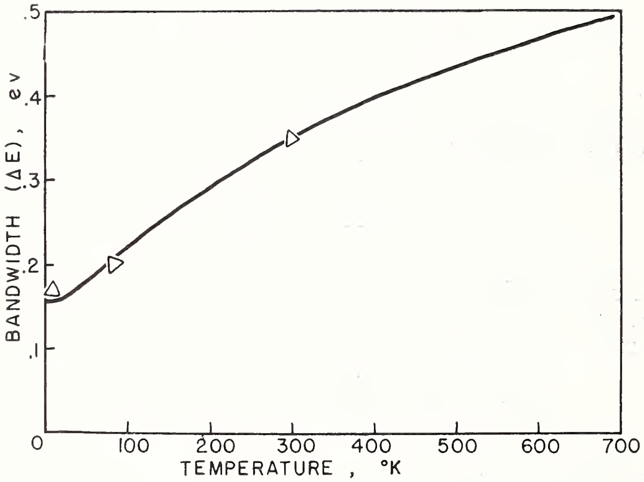

FIGURE 61.4. *Comparison of the observed widths of the F-band in* KCl *at various temperatures with the theoretical values determined from the particle-in-a box model.*

———, Theoretical; △, experimental (NRL).

The shift in position of the F-band with temperature can also be calculated from eq (2). The observed shift in the position of the F-band in KCl is approximately twice that calculated from this equation, assuming that the expansion coefficient of the box is equal to the expansion coefficient of the lattice. It appears, therefore, that the coefficient of expansion of the box is roughly twice as large as that of the lattice. A similar result has recently been obtained at this laboratory for the effect of pressure on the position of the F-band, the observed shift being about twice that calculated from the compressibility of the crystal. Calculations based on the Born-Mayer treatment [10] are now being carried out in order to obtain more exact information on the positions of the nearest-neighbor alkali metal ions as a function of temperature and pressure for a more rigorous application of the particle-in-a-box model of the *F*-center.

---

[1] E. Burstein and J. J. Oberly, Phys. Rev. **79,** 903 (1950).

[2] F. Seitz, Rev. Modern Phys. **18,** 384 (1946).

[3] R. W. Gurney and N. F. Mott, Trans. Faraday Soc. **34,** 506 (1938).

[4] W. Flechsig, Z. Phys. **46,** 788 (1928).

[5] E. Mollwo, Z. Phys. **85,** 56 (1933).

[6] H. O. McMahon, R. M. Hainer, and G. W. King, J. Opt. Soc. Am. **39,** 786 (1949).

[7] A theoretical analysis of a somewhat similar model has recently been carried out by T. Innui and Y. Uemura, Progress Theor. Phys. **5,** 395 (1950). See also, the papers of K. Huang, Proc. Roy. Soc. (London) [A] **204,** 406 (1951) and T. Muto, Progress Theor. Phys. **4,** 181 (1949), who treat the interactions of the *F*-center with lattice vibrations without resorting to an explicit formulation of the electronic energy levels of the *F*-center and their dependence on the interatomic distance.

[8] K. Lonsdale, Acta Cryst. **1,** 142 (1948).

[9] C. C. Klick, Phys. Rev. **79,** 894 (1950).

[10] M. Born and J. Mayer, Z. Phys. **75,** 1 (1932).

U. S. GOVERNMENT PRINTING OFFICE: 1952